

**TOXICOLOGY AND PHARMACOLOGY  
INVESTIGATION OF  
2-PHENYLAMINOPHENYLACETIC ACID  
DERIVED NSAIDS: IMPLICATION OF CHEMICAL  
STRUCTURE ON BIOLOGICAL OUTCOMES**

**PANG YI YUN**  
*(B.A.Sc. Food Sci. & Tech. (Hons.), NUS)*

**A THESIS SUBMITTED FOR THE DEGREE OF  
DOCTOR OF PHILOSOPHY**

**DEPARTMENT OF PHARMACY  
NATIONAL UNIVERSITY OF SINGAPORE  
2014**

## **DECLARATION**

I hereby declare that the thesis is my original work and it has been written by me in its entirety.

I have duly acknowledged all the sources of information which have been used in the thesis.

This thesis has also not been submitted for any degree in any university previously.



---

**Pang Yi Yun**

**20 January 2014**

## **Acknowledgements**

First and foremost, I want to thank my supervisor, Dr. Ho Han Kiat for his guidance, encouragement and support throughout these years. The course of my research had been an invaluable and enjoyable experience and I thank him for making it so. This thesis would not had been be possible without his advice and insights into the research topic.

I would also like to thank my co-supervisor, Assoc. Prof. Go Mei Lin for her advice and support, especially during the synthesis part of my project. Without her encouragement and help, I would not had been able to complete the synthesis of my compounds successfully.

I want to extend special thanks to several people who have helped me immensely during the course of my research. Firstly, I would like to thank Dr. Yeo Wee Kiang for his help in the *in silico* experimental parts of the project. Many thanks to Dr. Yang Tianming and Dr. Wee Xi Kai for their patience in teaching me essential synthetic skills. I want to thank Ms. Winnie Wong for her guidance in biological assays. Also, many thanks to Ms. Yap Siew Qi and Ms. Tan Yee Min for their guidance on mass spectroscopy techniques. Last but not least, I would like to thank Assoc. Prof. Christina Chai and Assoc. Prof. Seng Han Ming for their advice and guidance as part of my thesis committee.

Many thanks to the current and past members of the Laboratory of Liver Cancer and Drug-Induced Liver Research for their friendship, support and sharing of knowledge and research: Ms. Phua Lee Cheng, Ms. Tan Cheau Yih,

Ms. Angie Yeo, Ms. Zhao Chunyan, Ms. Chew Yun Shan and Ms. Sheela David Packiaraj. I would also like to extend my thanks to past and present members of Prof. Go's laboratory: Ms. Tan Kheng Lin, Ms. Chen Xiao and Dr. Pandy Murgappan Ramanujulu. To other fellow students and friends from the Department of Pharmacy, thank you for all the help and support you have provided throughout these years! Appreciation goes to my final year student, Mr. Loh Kep Yong for his dedication and help in my project. Gratitude goes to Mr. Johannes Murti Jaya, Ms. Ng Sek Eng, Mdm Oh Tang Booy and the rest of the technical staff at the Department of Pharmacy for making research easier with their help in purchasing of consumables and trouble-shooting of machines.

I would like to acknowledge the financial support for my graduate studies from the National University of Singapore Research Scholarship.

Many thanks to all my friends and relatives throughout the world. Their support and encouragement has enabled me to carry on with my research. Last but not least, I would like to give my heartfelt thanks and gratitude to my dad, my mom and my sister. This journey would not had been possible without their constant support, encouragement and cheering.

## **Table of Contents**

<b>Summary</b> .....	<b>viii</b>
<b>List of Tables</b> .....	<b>x</b>
<b>List of Figures</b> .....	<b>xiii</b>
<b>List of Schemes</b> .....	<b>xviii</b>
<b>List of Abbreviations</b> .....	<b>xix</b>
<b>Chapter 1. Introduction</b> .....	<b>1</b>
1.1. Adverse drug reactions – drug-induced liver injury (DILI).....	1
1.2. Metabolism and its role in DILI.....	4
1.3. NSAIDs – Mechanism of action and induced liver injury .....	12
1.4. Comparison of non-selective NSAID (Diclofenac) and COX-2 selective NSAID (Lumiracoxib) .....	14
1.5. Statement of purpose.....	19
<b>Chapter 2. Design and Synthesis of 2-Phenylaminophenylacetic Acid Derived Compounds</b> .....	<b>22</b>
2.1. Introduction .....	22
2.2. Experimental methods.....	23
2.2.1. Extraction of diclofenac ( <b>3</b> ) from Voltaren tablets.....	24
2.2.2. Synthesis of compounds <b>1</b> , <b>2</b> and <b>4</b> .....	25
2.2.2.1. Synthesis of 2-iodophenyl- <i>N,N</i> -dimethylacetamide ( <b>25</b> ).....	25
2.2.2.2. General procedure for the synthesis of 2-[(2,6-disubstituted phenyl)amino]phenyl- <i>N,N</i> -diethylacetamides ( <b>26 - 28</b> ) .....	26
2.2.2.3. General procedure for hydrolysis of acetamide to free acid ( <b>1</b> , <b>2</b> and <b>4</b> ).....	26
2.2.3. Synthesis of compounds <b>5 – 8</b> .....	27
2.2.3.1. General procedure for the syntheses of 2,6-disubstituted- <i>N</i> -( <i>p</i> -alkyl)anilines ( <b>29 – 48</b> ).....	28

2.2.3.2. General procedure for the syntheses of N-acetylated 2,6-disubstituted-N-(p-tolyl)anilines ( <b>49 – 52</b> ).....	28
2.2.3.3. General procedure for the syntheses of 1-(2,6-disubstituted)-5-methylindolin-2-ones ( <b>53 – 56</b> ) .....	29
2.2.3.4. General procedure for the syntheses of 2-(2-(2,6-disubstitutedphenyl)amino)-5-methylphenyl)acetic acid ( <b>5 – 8</b> ) .....	29
2.2.4. Synthesis of compounds <b>9 – 24</b> .....	30
2.2.4.1. General method for the synthesis of 1-(2,6-disubstituted phenyl)-5-ethylindoline-2,3-diones ( <b>57 - 72</b> ).....	30
2.2.4.2. General method for the syntheses of 2-(2-(2,6-disubstitutedphenyl)amino)-5-alkylphenyl)acetic acid ( <b>9 – 24</b> ).....	31
2.2.5. Purity determination by HPLC .....	32
2.3. Discussion .....	32
2.4. Conclusion.....	41
<b>Chapter 3. <i>In vitro</i> toxicity of 2-Phenylaminophenylacetic Acid derived Compounds in Liver Cell Lines: Effect of Substituents on Toxicity and Derivation of Quantitative Structure-Toxicity Relationships (QSTR).....</b>	<b>42</b>
3.1. Introduction .....	42
3.2. Experimental methods.....	43
3.2.1. Cell culture .....	43
3.2.2. Determination of key cytochrome P450 enzyme activities.....	44
3.2.3. MTT assay to determine cytotoxicity.....	45
3.2.4. Calculation of molecular descriptors.....	45
3.2.5. Selection of relevant molecular descriptors .....	46
3.2.6. QSTR models: Multiple linear regression and validation .....	46
3.2.7. Partial order ranking.....	47
3.2.8. Hasse diagram technique.....	48
3.2.9. Statistical Analysis .....	49
3.3. Results .....	49

3.3.1. Determination of key cytochrome P450 activities .....	49
3.3.2. Effect of structural changes on toxicity .....	50
3.3.3. Effect of cell lines with varying metabolic competencies.....	55
3.3.4. QSTR models: Multiple linear regression and validation .....	56
3.4. Discussion .....	60
3.4.1. Comparison of cell lines.....	61
3.4.2. Effect of substituents on toxicity – relationship with lipophilicity.. .....	63
3.4.3. Halogen substituents and their role in drug design .....	66
3.5. Conclusion.....	68

**Chapter 4. Inhibitory Effects of Synthesized Compounds on COX  
Expressing Cell Lines: Potency, Selectivity and Elucidation of Structure-  
Activity-Toxicity Relationships..... 70**

4.1. Introduction .....	70
4.2. Experimental methods.....	71
4.2.1. Cell culture .....	71
4.2.2. Western blot to determine expression of COX enzymes in cell lines .....	72
4.2.2.1. Cell harvesting and lysis.....	72
4.2.2.2. SDS-PAGE and Transfer.....	72
4.2.2.3. Detection.....	73
4.2.3. Cell-based COX-1 inhibition assay .....	73
4.2.4. Cell-based COX-2 inhibition assay .....	73
4.2.5. <i>In silico</i> docking of compounds to crystallized COX isoforms .....	74
4.3. Results .....	75
4.3.1. Expression of COX enzymes in cell lines .....	75
4.3.2. Activity and selectivity of synthesized compounds .....	76

4.3.3. <i>In silico</i> docking scores .....	82
4.3.4. Lipophilicity and effect on inhibitory potency of the compounds .	86
4.4. Discussion .....	87
4.4.1. Effect of substituents on inhibitory effect and safety of the compounds .....	87
4.4.2. Lipophilicity and its effect on inhibitory potency .....	94
4.5. Conclusion.....	96
<b>Chapter 5. Investigations of the Role of Metabolism in the Toxicity of the Synthesized compounds: Effect of Substituents on Metabolic Stability and Metabolite Reactivity, and the Relationships between Metabolic Stability, Metabolite Reactivity and Toxicity .....</b>	<b>99</b>
5.1. Introduction .....	99
5.2. Experimental methods.....	101
5.2.1. Microsomal incubation for Phase I metabolic stability assay .....	101
5.2.2. Microsomal incubation for Phase II metabolic stability assay .....	102
5.2.3. Microsomal incubation for AG reactivity .....	102
5.2.3.1. Incubation for AG formation.....	102
5.2.3.2. AG-Phe-Lys formation with biosynthesized AGs.....	103
5.2.4. LC-MS/MS analysis .....	103
5.2.4.1. LC-MS/MS analysis for metabolic stability assays.....	103
5.2.4.2. LC-MS/MS analysis for AG reactivity.....	105
5.2.5. Cell-based GSH depletion assay using TAMH cells.....	106
5.2.6. Linear regression for relationship investigation of metabolic stability, reactivity and toxicity .....	107
5.3. Results .....	108
5.3.1. Metabolic stability of compounds towards Phase I and Phase II metabolism .....	108



5.3.1.1. Effect of changes in substituents on Phase I metabolic stability .....	109
5.3.1.2. Effect of changes in substituents on Phase II metabolic stability .....	111
5.3.1.3. Inter-comparison between Phase I and Phase II metabolic stability and their relationship with lipophilicity .....	114
5.3.2. <i>In vitro</i> GSH depletion of the compounds in TAMH cells .....	115
5.3.3. Reactivity of AGs of the compounds towards Phe-Lys .....	119
5.3.4. Relationship between metabolic stability and metabolite reactivity .....	122
5.3.5. Relationship between metabolic stability and toxicity .....	125
5.3.6. Relationship between reactivity and toxicity .....	127
5.4. Discussion .....	129
5.4.1. Phase I and Phase II metabolic stability .....	129
5.4.2. Reactivity of metabolites generated via metabolism .....	136
5.4.3. Role of metabolic stability and metabolite reactivity in toxicity of the compounds .....	143
5.5. Conclusion .....	145
<b>Chapter 6. Investigations of the Role of Metabolism in the Toxicity of the Synthesized Compounds: Structure Elucidation of Trapped Reactive Metabolites and Proposition of Possible Bioactivation Pathways .....</b>	<b>149</b>
6.1. Introduction .....	149
6.2 Experimental methods .....	151
6.2.1. Microsomal incubation for Phase I reactive metabolites trapping with GSH .....	151
6.2.2. Microsomal incubation for Phase II reactive metabolites trapping with Phe-Lys .....	151
6.2.3. LC-MS/MS for identification of Phase I GSH trapped metabolites .....	152
6.2.3.1. LC-MS/MS for identification of Phase II Phe-Lys trapped metabolites .....	154

6.3. Results .....	155
6.3.1. Structure elucidation of Phase I GSH trapped reactive metabolites for selected compounds .....	155
6.3.2. Structure elucidation of Phase II Phe-Lys trapped reactive metabolites for selected compounds.....	178
6.4. Discussion .....	185
6.4.1. Structure elucidation and possible bioactivation pathways of Phase I GSH trapped reactive metabolites for selected compounds.....	185
6.4.2. Structure elucidation and possible bioactivation pathways of Phase II Phe-Lys trapped reactive metabolites for selected compounds .....	192
6.5. Conclusion.....	195
<b>Chapter 7. Conclusion and Future Work .....</b>	<b>199</b>
<b>Bibliography .....</b>	<b>209</b>
<b>Appendix.....</b>	<b>222</b>
<b>Appendix 2-1:</b> Complete structures of all twenty-four synthesized compounds .....	222
<b>Appendix 2-2:</b> Characterization of synthesized compounds ( <b>1 – 24</b> ) and intermediates ( <b>25 – 72</b> ).....	223
<b>Appendix 2-3:</b> Purities of compounds 1 – 24 as determined by HPLC at 280 nm (two gradients) .....	236
<b>Appendix 3-1a:</b> Partial ranking (Hasse diagram) of the twenty-four compounds in TAMH cells .....	237
<b>Appendix 3-1b:</b> Partial ranking (Hasse diagram) of the twenty-four compounds in HuH-7 cells.....	238
<b>Appendix 3-2a:</b> QSTR regression statistics for TAMH cells.....	239
<b>Appendix 3-2b:</b> QSTR regression statistics for HuH-7 cells .....	240
<b>Appendix 4-1:</b> Recipes for Western-Blot buffers and gels .....	241
<b>Appendix 4-2:</b> Docking poses of all twenty-four compounds in COX-1 and COX-2 .....	243

<b>Appendix 4-3:</b> Log D(o/w) value calculated using online ACD/I-Lab prediction engine .....	248
<b>Appendix 5-1:</b> Precursor and product ions utilized for MRM analysis in determination of Phase I and Phase II metabolic stability .....	249
<b>Appendix 5-2:</b> List of masses used for SIM analysis. Selection was based on nominal mass and tailored for negative ESI mode.....	251
<b>Appendix 5-3:</b> Representative mass spectrum and linear regression model for determination of Phase I and Phase II metabolic stability.....	252
<b>Appendix 5-4:</b> Linear regression models for metabolite reactivity and metabolic stability relationships for Phase I and Phase II metabolism .....	253
<b>Appendix 5-5:</b> Linear regression models for toxicity and metabolic stability relationships for Phase I and Phase II metabolism .....	254
<b>Appendix 5-6:</b> Linear regression models for toxicity and metabolite reactivity relationships for Phase I and Phase II metabolism.....	255
<b>Appendix 6-1:</b> Phase II reactive metabolite trapping - XIC traces of selected compounds .....	256

## **Summary**

The aim of this thesis was to test the hypothesis that varying substituents on the 2-phenylaminophenylacetic acid scaffold, of which diclofenac and lumiracoxib were derived from, will affect bioactivation and subsequently, toxicity to a significant degree. We also aimed to study how these subtle changes to substituents on the given chemical scaffold affect the intricate link between toxicity and pharmacology, providing an opportunity to optimize drug safety and efficacy.

Twenty-four 2-phenylaminophenylacetic acid derived compounds with varying substituents at three critical pharmacophores were synthesized. The compounds were subjected to *in vitro* cytotoxicity testing on two liver cell lines of contrasting metabolic competencies. We observed higher toxicity in the more metabolically competent cell line. We have also shown that structural changes on the chemical scaffold exerted pronounced effect on liver cytotoxicity. Thereafter, we developed a quantitative-structure-toxicity relationship (QSTR) model which unveils the trend of increasing lipophilicity in the cellular manifestation of toxicity. A concurrent determination of their pharmacological activity using COX inhibition assays allowed us to derive a safety profile, which showed that selectivity towards COX-2 negatively affected activity and in some cases, toxicity.

In order to probe further into the toxicity caused by bioactivation, we carried out a series of metabolic assays. We measured the Phase I and Phase II metabolic stability of the compounds separately. We observed that the most

toxic compound was not the least stable compound. In fact, the toxicity of the compounds is not intricately linked to their metabolic stabilities. Given this interesting observation, we decided to determine the reactivity of the Phase I and Phase II metabolites formed from the compounds. We observed that the more toxic compounds produced more reactive metabolites regardless of the compound's metabolic stability, especially in the case of Phase I metabolism.

Last but not least, we carried out trapping assays to elucidate possible structures of the reactive metabolites via LC-MS/MS and to investigate possible bioactivation pathways. We elucidated several possible structures of the Phase I and Phase II reactive metabolites and their possible bioactivation pathways. In addition, we observed that the varying substituents do affect the structures and amount of reactive metabolites formed but further experiments need to be carried out. On the other hand, we observed that substituents have no effect on the structures of Phase II reactive metabolites.

In conclusion, the findings of this thesis supported our hypothesis that varying substituents on the 2-phenylaminophenylacetic acid scaffold, will affect bioactivation and subsequently, toxicity to a significant degree. In addition, we also elucidated a possible relationship between toxicity and pharmacology, which provided a better understanding in the balance between toxicity and activity and presents the possibility to associate the two biological outcomes.

*(437 words)*

## **List of Tables**

<b>Table 1-1</b> Routes of elimination of marketed drugs.....	<b>4</b>
<b>Table 1-2</b> Examples of hard and soft electrophiles and hard and soft nucleophiles .....	<b>6</b>
<b>Table 1-3</b> Abundance of CYP enzymes in the human liver and their possible substrates.....	<b>7</b>
<b>Table 3-1</b> LC <sub>50</sub> values and calculated descriptors of the twenty-four compounds .....	<b>51</b>
<b>Table 3-2</b> Ratios of LC <sub>50</sub> values between substitutions at R <sub>1</sub> : H and R <sub>1</sub> : <i>tert</i> -butyl .....	<b>55</b>
<b>Table 3-3</b> The predicted and the experimental -log(TAMH LC <sub>50</sub> ) and -log(HuH-7 LC <sub>50</sub> ) values of the twenty-four compounds .....	<b>58</b>
<b>Table 4-1</b> COX median inhibitory concentration (IC <sub>50</sub> ), selectivity index and safety index of the twenty-four synthesized compounds.....	<b>77</b>
<b>Table 4-2</b> Comparison of potency ranking of compounds with literature data .....	<b>80</b>
<b>Table 4-3</b> <i>In silico</i> docking scores for the synthesized twenty-four compounds .....	<b>83</b>
<b>Table 5-1</b> LC conditions for Agilent 1290 Infinity LC system + Agilent 6430 Triple Quadrupole MS and Agilent 1290 Infinity LC system + AB Sciex Qtrap ® 5500 .....	<b>104</b>
<b>Table 5-2</b> MS source parameters for Agilent 6430 Triple Quadrupole MS and AB Sciex Qtrap ® 5500 .....	<b>105</b>
<b>Table 5-3</b> LC conditions for AG reactivity analysis .....	<b>106</b>

<b>Table 5-4</b> MS source parameters for AG reactivity analysis .....	<b>105</b>
<b>Table 5-5</b> Phase I and Phase II microsomal metabolic $t_{1/2}$ of the twenty-four compounds .....	<b>108</b>
<b>Table 5-6</b> <i>In vitro</i> GSH depletion (%) for the twenty-four compounds in TAMH cells .....	<b>116</b>
<b>Table 5-7</b> Reactivity of AGs of the twenty-four compounds toward Phe-Lys in a 24 h incubation.....	<b>120</b>
<b>Table 5-8</b> Physicochemical parameters of halogen substituents employed in our study.....	<b>132</b>
<b>Table 5-9</b> Physicochemical parameters of alkyl substituents employed in our study .....	<b>133</b>
<b>Table 6-1</b> LC conditions for Phase I GSH trapped metabolites identification .....	<b>153</b>
<b>Table 6-2</b> MS source parameters for Phase I GSH trapped metabolites identification .....	<b>153</b>
<b>Table 6-3</b> LC conditions for Phase II Phe-Lys trapped metabolites identification .....	<b>154</b>
<b>Table 6-4</b> MS source parameters for Phase II Phe-Lys trapped metabolites identification .....	<b>155</b>
<b>Table 6-5</b> Proposed structures and fragmentation pathways for GSH-trapped metabolites of compound <b>1</b> .....	<b>165</b>
<b>Table 6-6</b> Proposed structures and fragmentation pathways for GSH-trapped metabolites of compound <b>3</b> (diclofenac).....	<b>166</b>
<b>Table 6-7</b> Proposed structures and fragmentation pathways for GSH-trapped metabolites of compound <b>5</b> (lumiracoxib).....	<b>168</b>

<b>Table 6-8</b> Proposed structures and fragmentation pathways for GSH-trapped metabolites of compound <b>6</b> .....	<b>170</b>
<b>Table 6-9</b> Proposed structures and fragmentation pathways for GSH-trapped metabolites of compound <b>7</b> .....	<b>171</b>
<b>Table 6-10</b> Proposed structures and fragmentation pathways for GSH-trapped metabolites of compound <b>8</b> .....	<b>172</b>
<b>Table 6-11</b> Proposed structures and fragmentation pathways for GSH-trapped metabolites of compound <b>9</b> .....	<b>173</b>
<b>Table 6-12</b> Proposed structures and fragmentation pathways for GSH-trapped metabolites of compound <b>13</b> .....	<b>174</b>
<b>Table 6-13</b> Proposed structures and fragmentation pathways for GSH-trapped metabolites of compound <b>17</b> .....	<b>175</b>
<b>Table 6-14</b> Proposed structures and fragmentation pathways for GSH-trapped metabolites of compound <b>21</b> .....	<b>176</b>
<b>Table 6-15</b> Proposed structures and fragmentation pathways for GSH-trapped metabolites of compound <b>23</b> .....	<b>177</b>
<b>Table 6-16</b> Proposed structures and fragmentation pathways for GSH-trapped metabolites of compound <b>24</b> .....	<b>178</b>
<b>Table 6-17</b> Proposed structures and fragmentation pathways for Phe-Lys-trapped metabolites of five selected compounds .....	<b>183</b>



## **List of Figures**

<b>Figure 1-1</b> Six mechanisms of liver injury.....	<b>3</b>
<b>Figure 1-2</b> Hydroxylated aromatic rings can undergo a further two electron oxidation to reactive electrophiles .....	<b>8</b>
<b>Figure 1-3</b> Redox cycling of benzoquinones produces ROS which causes oxidative damage .....	<b>9</b>
<b>Figure 1-4</b> AGs can undergo transacylation or acyl migration (2- $\beta$ -O-, 3- $\beta$ -O-, 4- $\beta$ -O-) followed by glycation .....	<b>11</b>
<b>Figure 1-5</b> Production of prostanoids by COX-1 and COX-2 from arachidonic acid and their respective target tissue/organ .....	<b>13</b>
<b>Figure 1-6</b> Phase I metabolic pathway of diclofenac by CYP2C9 and CYP3A4 and subsequent possible bioactivation .....	<b>15</b>
<b>Figure 1-7</b> Formation of covalent adducts by diclofenac-1- $\beta$ -O-acyl glucuronide through transacylation or acyl migration .....	<b>16</b>
<b>Figure 1-8</b> Numbering of aromatic rings of lumiracoxib.....	<b>17</b>
<b>Figure 1-9</b> Phase I metabolism pathway and subsequent bioactivation and conjugation of nucleophiles for lumiracoxib .....	<b>18</b>
<b>Figure 2-1</b> Structures of target compounds synthesized with position R <sub>1</sub> on ring A and positions R <sub>2</sub> and R <sub>3</sub> on ring B .....	<b>22</b>
<b>Figure 2-2</b> Mechanism of the formation of an amide via formation of an acid chloride .....	<b>33</b>
<b>Figure 2-3</b> Mechanism of Ullmann condensation.....	<b>34</b>
<b>Figure 2-4</b> Mechanism of Buchwald-Hartwig coupling (X: Br, I) .....	<b>36</b>

<b>Figure 2-5</b> Mechanism for intramolecular Friedel-Crafts alkylation.....	<b>37</b>
<b>Figure 2-6</b> Mechanism of Friedel-Crafts acylation.....	<b>38</b>
<b>Figure 2-7</b> (a) H <sup>1</sup> NMR spectrum of compound <b>10</b> acetamide; (b) H <sup>1</sup> NMR spectrum of compound <b>10</b> oxindole; (c) [M+H] <sup>+</sup> of compound <b>10</b> oxindole ..	<b>39</b>
<b>Figure 2-8</b> Mechanism of reverse Friedel-Crafts .....	<b>40</b>
<b>Figure 2-9</b> Mechanism of a modified Wolff-Kishner reduction .....	<b>41</b>
<b>Figure 3-1</b> Comparison between the relative luminescence units (RLU) obtained for HuH-7 and TAMH for (a) CYP2C9 and (b) CYP3As .....	<b>50</b>
<b>Figure 3-2</b> The Hasse diagram of the twenty-four compounds investigated in this study .....	<b>53</b>
<b>Figure 3-3</b> Plot of LC <sub>50</sub> values of HuH-7 against TAMH for all compounds	<b>56</b>
<b>Figure 3-4</b> Predicted -log(LC <sub>50</sub> ) versus experimental -log(LC <sub>50</sub> ) for (a) TAMH (R <sup>2</sup> = 0.6641) and (b) HuH-7 (R <sup>2</sup> = 0.458) .....	<b>59</b>
<b>Figure 3-5</b> (a) Plot of -log(LC <sub>50</sub> ) against log P(o/w) for TAMH and (b) Plot of -log(LC <sub>50</sub> ) against FASA_H for HuH-7 .....	<b>60</b>
<b>Figure 4-1</b> Western blot of HEL92.1.7 and RAW264.7 .....	<b>75</b>
<b>Figure 4-2</b> Comparison plots for IC <sub>50</sub> values for COX-1 and COX-2 obtained from cell-based COX inhibition assays for (a) F-Cl series; (b) F-F series; (c) Cl-Cl series and (d) Br-Br series.....	<b>78</b>
<b>Figure 4-3</b> Docking pose of diclofenac and compound <b>7</b> in COX-1 co-crystallized with acclufenac as ligand.....	<b>84</b>
<b>Figure 4-4</b> Docking pose of diclofenac and compound <b>7</b> in COX-2 co-crystallized with diclofenac ligand .....	<b>85</b>

<b>Figure 4-5</b> Plot of Log IC <sub>50</sub> (nM) against log P(o/w) of the compounds for COX-1 and COX-2 for compound series (a) F-Cl; (b) F-F; (c) Cl-Cl and (d) Br-Br .....	<b>86</b>
<b>Figure 5-1</b> Comparison plot for Phase I metabolic stability between halogen substituents at R <sub>2</sub> and R <sub>3</sub> grouped by R <sub>1</sub> substituents .....	<b>109</b>
<b>Figure 5-2</b> Comparison plot for Phase I metabolic stability between alkyl substituents at R <sub>1</sub> and grouped by R <sub>2</sub> and R <sub>3</sub> substituents .....	<b>110</b>
<b>Figure 5-3</b> Comparison plot for Phase II metabolic stability between halogen substituents at R <sub>2</sub> and R <sub>3</sub> and grouped by R <sub>1</sub> substituents .....	<b>111</b>
<b>Figure 5-4</b> Comparison plot for Phase II metabolic stability between alkyl substituents at R <sub>1</sub> and grouped by R <sub>2</sub> and R <sub>3</sub> substituents .....	<b>112</b>
<b>Figure 5-5</b> Comparison of Phase I (orange) and Phase II (blue) metabolic t <sub>1/2</sub> . .....	<b>114</b>
<b>Figure 5-6</b> Comparison plot for GSH depletion between halogen substituents at R <sub>2</sub> and R <sub>3</sub> grouped by R <sub>1</sub> substituents .....	<b>117</b>
<b>Figure 5-7</b> Comparison plot for GSH depletion between alkyl substituents at R <sub>1</sub> and grouped by R <sub>2</sub> and R <sub>3</sub> substituents .....	<b>118</b>
<b>Figure 5-8</b> Comparison plot for AG reactivity between halogen substituents at R <sub>2</sub> and R <sub>3</sub> and grouped by R <sub>1</sub> substituents .....	<b>120</b>
<b>Figure 5-9</b> Comparison plot for AG reactivity between alkyl substituents at R <sub>1</sub> and grouped by R <sub>2</sub> and R <sub>3</sub> substituents .....	<b>121</b>
<b>Figure 5-10</b> Comparison of Phase I average metabolic t <sub>1/2</sub> and <i>in vitro</i> GSH depletion .....	<b>123</b>
<b>Figure 5-11</b> Comparison of Phase II average metabolic t <sub>1/2</sub> and AG reactivity (24 h) .....	<b>124</b>

<b>Figure 5-12</b> Comparison of Phase I average metabolic $t_{1/2}$ and <i>in vitro</i> toxicity in TAMH.....	<b>125</b>
<b>Figure 5-13</b> Comparison of Phase II average metabolic $t_{1/2}$ and <i>in vitro</i> toxicity in TAMH .....	<b>126</b>
<b>Figure 5-14</b> Comparison of <i>in vitro</i> GSH depletion and corresponding <i>in vitro</i> toxicity in TAMH .....	<b>128</b>
<b>Figure 5-15</b> Comparison of AG reactivity and <i>in vitro</i> toxicity in TAMH...	<b>128</b>
<b>Figure 5-16</b> Hydroxylation at 4'-position and subsequent oxidation to a quinone imine.....	<b>137</b>
<b>Figure 5-17</b> Formation of an imine methide when R <sub>1</sub> is an alkyl group.....	<b>139</b>
<b>Figure 5-18</b> Hydroxylation at 5-position and subsequent oxidation to a quinone imine.....	<b>142</b>
<b>Figure 6-1</b> TIC of negative PI scan of m/z 272 and the subsequent XIC trace of the trapped metabolites for compound <b>3</b> (diclofenac).....	<b>156</b>
<b>Figure 6-2</b> XIC trace of GSH trapped metabolites of (a) compound <b>5</b> ; (b) compound <b>6</b> ; (c) compound <b>7</b> and (d) compound <b>8</b> of the methyl series .....	<b>157</b>
<b>Figure 6-3</b> XIC trace of GSH trapped metabolites of (a) compound <b>1</b> ; (b) compound <b>9</b> ; (c) compound <b>13</b> and (d) compound <b>17</b> .....	<b>158</b>
<b>Figure 6-4</b> XIC trace of GSH trapped metabolites of (a) compound <b>21</b> ; (b) compound <b>23</b> and (c) compound <b>24</b> .....	<b>159</b>
<b>Figure 6-5</b> EPI spectra for <b>3</b> -RM2 (m/z 583).....	<b>160</b>
<b>Figure 6-6</b> Spectras of negative EMS full scan of compound <b>3</b> (diclofenac) reactive AGs trapped with Phe-Lys .....	<b>180</b>

<b>Figure 6-7</b> Spectras of negative EMS full scan of compound <b>5</b> (lumiracoxib) reactive AGs trapped with Phe-Lys .....	<b>182</b>
<b>Figure 6-8</b> Possible pathways for dehalogenation of quinone imines formed with subsequent conjugation of GSH via (a) direct attack on chlorinated atom or (b) <i>ipso</i> GSH addition.....	<b>186</b>
<b>Figure 6-9</b> Possible pathways for GSH adduct formation from quinone imines formed from the phenylacetic acid (Ring A) or the aniline ring (Ring B) ....	<b>189</b>
<b>Figure 6-10</b> Possible pathways for GSH adduct formation from imine methides formed from alkyl groups with an extractable hydrogen .....	<b>190</b>
<b>Figure 6-11</b> Possible pathways for GSH adduct formation from <i>ortho</i> -imine methides formed oxidative decarboxylation.....	<b>190</b>
<b>Figure 6-12</b> Possible pathway for formation of <b>23</b> -RM2 from dechlorination followed by direct GSH conjugation via an <i>ipso</i> GSH addition mechanism.	<b>191</b>
<b>Figure 6-13</b> Pathways involved in formation of AG adducts for the synthesized compounds .....	<b>193</b>
<b>Figure 6-14</b> Possible reactive metabolites and their GSH conjugates proposed for our synthesized compounds .....	<b>197</b>
<b>Figure 7-1</b> Possible reactive metabolites and their trapped conjugates proposed for our synthesized compounds for both Phase I and Phase II metabolism.....	<b>204</b>

## **List of Schemes**

**Scheme 2-1** Synthetic scheme for synthesis of **1, 2** and **4**.....**25**

**Scheme 2-2** Synthetic scheme for synthesis of **5 – 8** .....**27**

**Scheme 2-3** Synthetic scheme for synthesis of **9 – 24** .....**30**

## **List of Abbreviations**

<sup>1</sup> H NMR	Proton nuclear magnetic resonance spectrum
<sup>13</sup> C NMR	Carbon-13 nuclear magnetic resonance spectrum
(±)-BINAP	(±)-2,2'-Bis(diphenylphosphino)-1,1'-binaphthalene
ADRs	Adverse drug reactions
AGs	Acyl glucuronides
ANOVA	Analysis of variance
BCA	Bicinchoninic acid
CDCl <sub>3</sub>	Chloroform, deuterated
CE	Collision energy
COX	Cyclooxygenase
CXP	Collision cell exit potential
DCM	Dichloromethane
DILI	Drug-Induced Liver Injury
DMEM	Dulbecco's Modified Eagle's Medium
DMEM/F12	Dulbecco's modified Eagle's medium/Ham's F12
DMSO	Dimethyl sulfoxide
DP	Declustering potential
ELISA	Enzyme-linked immunosorbent assay
EMS	Enhanced mass scan
EP	Entrance potential
EPI	Enhanced product ion
ESI	Electrospray ionization
EtOAc	Ethyl acetate
FASA_H	Fractional accessible surface area_hydrophobic

FBS	Fetal bovine serum
FDA	U.S. Food and Drug administration
GSH	Glutathione
HLM	Human liver microsomes
HPLC	High-performance liquid chromatography
IC <sub>50</sub>	Median inhibitory concentration
IDA	Information-dependent acquisition
LC <sub>50</sub>	Median lethal concentration
LC-MS/MS	Liquid chromatography-tandem mass spectroscopy
Log D(o/w)	Calculated partition coefficient in water/octanol, pH 7.4
Log P(o/w)	Calculated partition coefficient in water/octanol
LPS	Lipopolysaccharides
MCB	Monochlorobimane
MOE	Molecular Operating Environment
MRM	Multiple reaction monitoring
MTT	3-(4,5-Dimethylthiazol-2-yl)-2,5-diphenyltetrazolium bromide
NAC	N-acetylcysteine
NADP <sup>+</sup>	Nicotinamide adenine dinucleotide phosphate
NAPQI	N-acetyl- <i>p</i> -benzoquinone imine
NSAIDs	Non-steroidal anti-inflammatory drugs
P450s	Cytochrome P450 enzymes
PBS-T	Phosphate buffered saline Tween-20
PDB	Protein Data Bank
PGE <sub>2</sub>	Prostaglandin E <sub>2</sub>
Phe-Lys	Phenylalanine-lysine dipeptide



PI	Precursor ion
QSTR	Quantitative structure-toxicity relationship
RLU	Relative luminescence units
ROS	Reactive oxygen species
SAR	Structure-activity relationship
SDS-PAGE	Sodium dodecyl sulfate polyacrylamide gel electrophoresis
SIM	Single ion mode
$t_{1/2}$	Metabolic half-lives
TIC	Total ion chromatogram
TLC	Thin layer chromatography
TXB <sub>2</sub>	Thromboxane-B <sub>2</sub>
UDPGA	Uridine diphosphoglucuronic acid
UGTs	Uridine disphosphate glucuronosyltransferases
WHO	World Health Organization
XIC	Extracted ion chromatogram

## **Chapter 1. Introduction**

### 1.1. Adverse drug reactions – Drug-induced liver injury (DILI)

Adverse drug reactions (ADRs), as defined by the World Health Organization (WHO), are “any responses to a drug which are noxious and unintended, and which occur at doses used in man for prophylaxis, diagnosis or treatment”. It is estimated that ADRs are the sixth leading cause of death worldwide, and the financial cost to society can range from \$75 to \$180 billion each year (Hacker, 2009). Mechanistically, there are four types of ADRs; Type A (pharmacological), Type B (idiosyncratic), Type C (chemical) and Type D (delayed) (Williams *et al.*, 2002). Such classification of ADRs facilitates swift identification and intervention should a patient encounter such an episode, as well as a basis for re-designing a drug to achieve a better safety profile. Type A reactions are an extension of the desired pharmacological effect of the drug administered and is often predictable and preventable. Type B reactions, which include drug allergies, idiosyncratic responses and intolerance, are difficult or impossible to predict from the known pharmacology of the drug. Type B reactions often surface after a period of usage of newly approved drugs by a large population of patients. Thus, often than not, type B reactions are the underlying cause of withdrawals of newly approved drugs. Type C reactions result from the formation of certain chemical features after metabolism. Certain chemical features predispose the molecule to greater toxicity than others. Type D reactions are delayed toxicities such as carcinogenicity and teratogenicity that arise from long-term drug treatment.

These toxicities are often observed in bioassays or during preclinical trials and may be prevented from occurring in patients.

ADRs that involve the liver are known as drug-induced liver injuries (DILIs). The impact of DILI on drug development is very significant, being the most common reason, among all forms of drug-induced toxicities, for the restriction or withdrawal of a drug from the market and cessation of drug testing in clinical trials (Tran and Lee, 2013). Most DILIs fall under type B and type C reactions and are classified as idiosyncratic responses. Idiosyncratic responses are individual-based and can be affected by several internal and external factors. Even though incidence rates are relatively low, with estimates at 1 per 10 000 to 1 per 100 000 treated patients (Stirnemann *et al.*, 2010), DILI accounts for 5% of hospital admissions and 50% of acute liver failures in the USA, with paracetamol being the lead cause of such events (Russo *et al.*, 2004).

The liver is highly susceptible to drug-induced injury as it is the site of detoxification. Blood from the gastrointestinal system and spleen arrives directly via the portal vein and hepatic artery respectively to the liver in a unidirectional flow, bringing drugs and xenobiotics in concentrated forms and in large volumes per unit time (Giri *et al.*, 2010). Liver injury can range from mild elevations in serum transaminases (alanine aminotransferase, ALT and aspartate aminotransferase, AST) to life-threatening fulminant hepatic failure. Although classified as an idiosyncratic response, DILI is not independent of dose. It has been shown that a number of liver transplants carried out for

hepatic failure due to an oral prescription drug was the lowest for patients assigned the lowest daily drug dosage (Stirnemann *et al.*, 2010). Other than dose, DILI can also depend on both intrinsic and environmental factors, such as age, sex, nutritional factors, physiological changes, genotype, duration, drug-drug interactions, drug-enzyme induction/inhibition and metabolic conditions (Giri *et al.*, 2010).

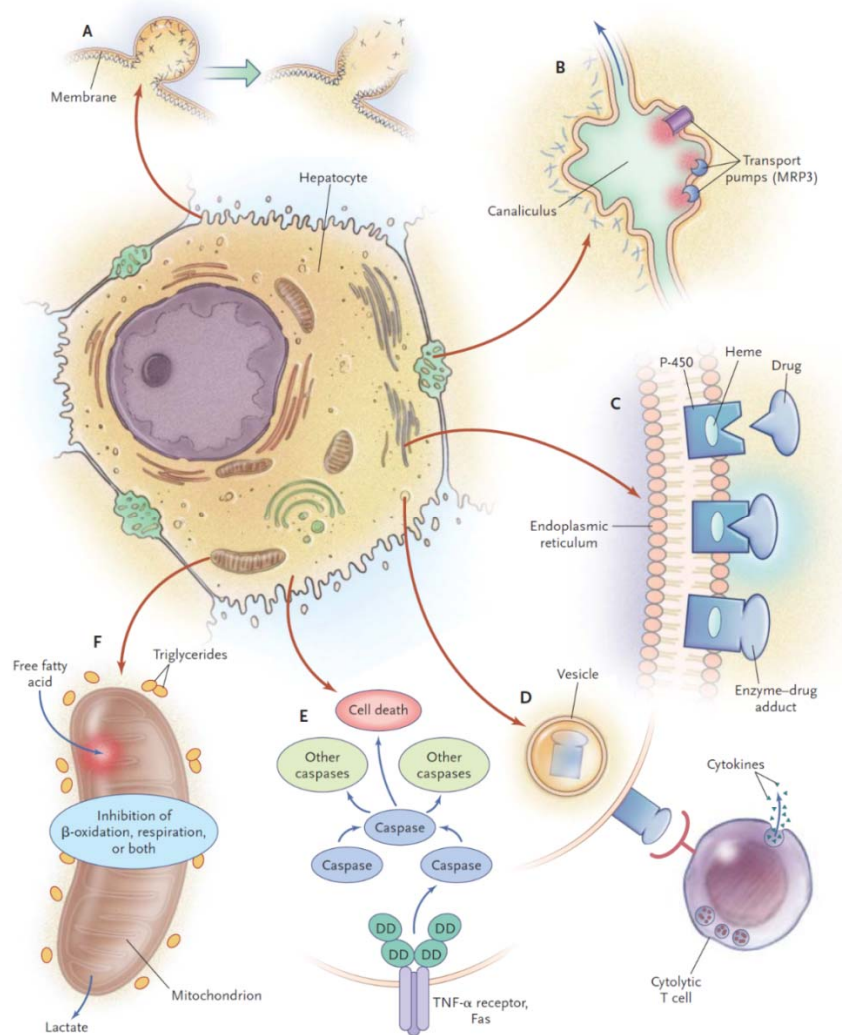


**Figure 1-1** Six mechanisms of liver injury: A) Disruption of cellular calcium homeostasis results in cell membrane disruption, leading to rupture and lysis; B) Injury to the cannaliculus, the portion responsible for bile excretion; C) Bioactivation to reactive metabolites by cytochrome P450 system; D) Enzyme-drug adducts causes immune responses; E) Activation of apoptosis and F) Inhibition of  $\beta$ -oxidation of free fatty acids and respiration, resulting in mitochondrial injury. Reproduced with permission from Lee (2003), Copyright Massachusetts Medical Society.

At the cellular and molecular level, there are several ways a drug can induce injury to the liver. To date, there are six proposed mechanisms of DILI (Figure 1-1): A) disruption of calcium homeostasis leading to cell blebbing and lysis; B) canaliculular injury; C) metabolic bioactivation; D) stimulation of autoimmunity; E) activation of apoptosis and F) inhibition of mitochondrial function (Lee, 2003). These six mechanisms are not mutually exclusive. The onset of these mechanisms of toxicity requires an initial interaction between the administered drug and the biological target. Oftentimes, the metabolic activation of the parent drug is the initiating event for these other events to occur.

## 1.2. Metabolism and its role in DILI

Biotransformation of the parent drug via metabolism is a means by the body to aid in excretion of the lipophilic parent drug. In this process, the lipophilic parent drug is converted to a more water-soluble form, which is more readily excreted in the bile, urine or feces. It is estimated that 70% of marketed drugs undergo metabolism prior to excretion, while the remaining are excreted in their parent form (Table 1-1).

**Table 1-1** Routes of elimination of marketed drugs (Williams *et al.*, 2004).

Route of elimination	Percentage of marketed drugs
Metabolism	70% (50% P450, 12% UGT, 5% esterases, 3% others) <sup>a</sup>
Urine	20%
Bile	10%

<sup>a</sup> Percentage contribution of different enzymes based on 70% metabolism of a molecule

While the goal of drug metabolism is “detoxification”, “intoxication” can occur as an unintended outcome. Occasionally, bioactivation of the parent drug can result in the formation of reactive metabolites. These reactive metabolites can present as either electrophiles or free radicals (Williams *et al.*, 2002). Electrophiles are electron deficient and they readily form covalent adducts with cellular nucleophiles such as proteins and DNA. Adduct formation, if irreversible, leads to the loss of function of the original biological molecules and induces cellular toxicity. For example, N-acetyl-*p*-benzoquinone imine (NAPQI), a quinone imine derived from the oxidative metabolism of paracetamol, can form adducts with critical thiol groups in calcium channels in hepatic mitochondria, causing increased cytosolic calcium concentrations and adverse effects (Monks and Jones, 2002). Electrophiles are classified into two categories: hard (high positive charge density at the electrophilic center) and soft (lower positive charge density at the electrophilic center) (Srivastava *et al.*, 2010). Hard and soft electrophiles differ in their selective binding to target nucleophiles in the body. Generally, hard electrophiles like aldehydes bind to hard nucleophiles such as DNA and amino groups on amino acid residues while soft electrophiles like quinone imines bind to soft nucleophiles such as protein thiol groups (Table 1-2). Another type of reactive metabolites is free radicals, such as reactive oxygen species (ROS) generated from redox cycling. Free radicals possess unpaired electrons which can self-propagate and induce oxidative stress, causing oxidative damage to proteins, DNA and lipids (Williams *et al.*, 2002).

**Table 1-2** Examples of hard and soft electrophiles and hard and soft nucleophiles (Attia, 2010; Srivastava *et al.*, 2010).

Type	Electrophiles	Nucleophiles
Hard	Alkyl carbonium ions	Oxygen atoms of purine/ pyrimidine bases in DNA
	Benzylic carbonium ions	Endocyclic nitrogens of purine bases in DNA
	Iminium ions	Primary/ secondary amino groups
Soft	Aldehydes	Protein thiol groups
	Epoxides	
	Enones	Sulfhydryl groups of glutathione (GSH)
	Quinone imines	Alkenes
	Quinone methides	Selenium groups
	Michael acceptors	

Drugs carrying certain physicochemical features can be predisposed to the formation of reactive and toxic metabolites through specific metabolic pathways. Broadly, xenobiotics can undergo two phases of metabolism, namely Phase I and/or Phase II. Each phase is carried out by a different family of enzymes and results in formation of different metabolites. Phase I metabolism is defined by changes in functionality and involves oxidation, reduction, and/or hydrolysis while Phase II metabolism involves conjugate formation (Khojasteh *et al.*, 2010).

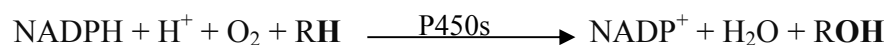
The major family of enzymes involved in Phase I metabolism is the cytochrome P450 enzymes (P450s). P450s are found in many organs, with the highest concentration in the liver (1.5-3% of the total microsomal protein in human livers) (Khojasteh *et al.*, 2010). P450s are bound to the membrane of the cytoplasmic side of the endoplasmic reticulum (ER). There are several different P450 isoforms. Expression levels and substrates of each isoform differ from one another (Table 1-3). Genetic polymorphism of P450s can exist for each isoform. Such polymorphism has significant effects on the

metabolism of a drug by the P450 isoform, resulting in differences in drug responses and possibly a higher risk of ADRs (Zhou *et al.*, 2009).

**Table 1-3** Abundance of CYP enzymes in the human liver and their possible substrates (Khojasteh *et al.*, 2010).

Isoform	Mean abundance in human liver (% total)	Basic, acidic or neutral substrates	Substrate characteristics
CYP1A2	11%	B, N	Planar polyaromatic, one hydrogen bond donor, may contain amines or amides
CYP2A6	8.6%	B, N	Small size, nonplanar, at least one aromatic ring
CYP2B6	2.1%	B, N	Medium size, angular, 1–2 H-bond donors or acceptors
CYP2C8	5.7%	A, N	Large size, elongated
CYP2C9	18%	A	Medium size, 1–2 H-bond donors, lipophilic
CYP2C19	2.7%	B	2–3 H-bond acceptors, moderately lipophilic
CYP2D6	2.1%	B	Medium size, 5–7 Å distance between basic nitrogen and site of oxidation
CYP2E1	15%	N	Small size, hydrophilic, relatively planar
CYP3A4/5	40%	B, A, N	Large size, lipophilic

P450s are mainly involved in oxidative reactions. Polar functionalities are introduced into the parent drug molecules. A simplified P450-catalysed reaction is:



where RH represents an oxidizable drug substrate and ROH, the hydroxylated metabolite (Ionescu and Cairns, 2005a). One oxygen atom is incorporated into the substrate while the other is reduced to water. P450s are also involved in N-dealkylation, O-dealkylation and S-dealkylation, which can be considered a



special form of oxidative reaction as the initial event is a hydroxylation followed by elimination.

At times, hydroxylation can become the precursor for reactive metabolite formation. Some hydroxylated aromatic rings have the ability to be further oxidized into reactive metabolites via a further two electron oxidation to generate benzoquinones, quinone imines, quinone methides and imine methides by monooxygenase and peroxidase enzymes, metal ions and molecular oxygen (Figure 1-2) (Bolton *et al.*, 2000; Leung *et al.*, 2011). These reactive metabolites are electrophilic in nature and are able to form covalent adducts with nucleophiles. For example, benzene can be metabolized to benzoquinones and conjugate to nucleophiles in bone marrow, causing aplastic anemia and acute myelogenic leukemia (Bolton *et al.*, 2000).

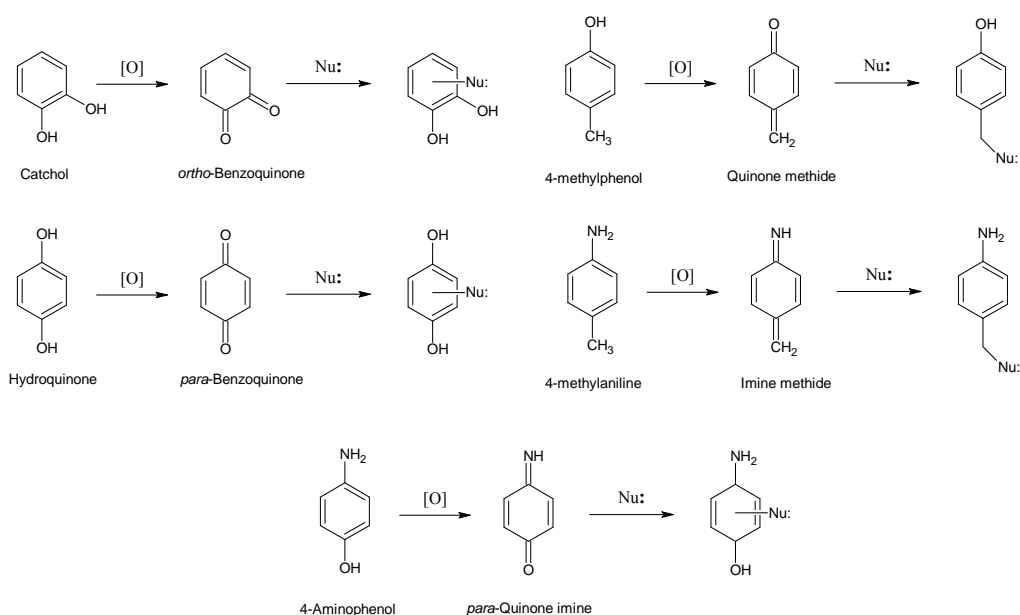


**Figure 1-2** Hydroxylated aromatic rings can undergo a further two electron oxidation to reactive electrophiles such as benzoquinones, quinone imines, quinone methides and imine methides.

Besides the generation of electrophilic intermediates, quinones can undergo enzymatic or non-enzymatic redox cycling, yielding reactive free radicals such as ROS which causes oxidative damage to biological macromolecules (Figure 1-3) (Bolton *et al.*, 2000; Monks and Jones, 2002). For example, doxorubicin is an extensively used chemotherapy agent. However, it is known to cause cardiomyotoxicity due to formation of ROS via redox cycling of its quinone nucleus (Ganey *et al.*, 1988). Quinone imines, due to the substitution of one oxygen atom with a nitrogen atom are less likely to undergo redox cycling as compared to benzoquinones as the redox potential of quinone imines is lower. Nevertheless, it is still possible for quinone imines to undergo redox cycling to produce free radicals (Monks and Jones, 2002), contributing to their significance in drug toxicology. One example is primaquine, an anti-malarial drug known to cause hemolysis. The hydroxylated metabolites are aminophenols, which can undergo redox cycling to produce ROS that damages erythrocytes (Vasquezvivar and Augusto, 1992).

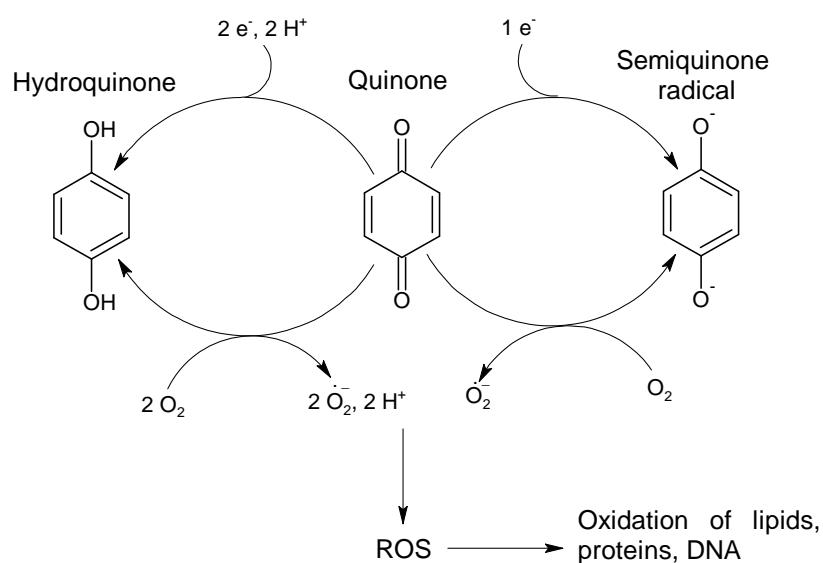


**Figure 1-3** Redox cycling of benzoquinones produces ROS which causes oxidative damage (Bolton *et al.*, 2000).

Metabolites formed after Phase I metabolism or the parent drug can undergo Phase II conjugation reactions to form more hydrophilic molecules that are more readily excreted (Ionescu and Caira, 2005a; Khojasteh *et al.*, 2010). Major Phase II conjugation reactions include glucuronidation, sulfation and acetylation (Ionescu and Caira, 2005b). Of all the Phase II reactions, glucuronidation, which involves conjugation of the parent aglycone to a  $\alpha$ -D-glucuronic acid sugar moiety, is the major route of conjugation and mainly occurs in the liver (Ionescu and Caira, 2005b). Glucuronidation is catalyzed by the enzyme uridine diphosphate glucuronosyltransferases (UGTs) and requires the presence of cofactor, uridine diphosphoglucuronic acid (UDPGA) (Khojasteh *et al.*, 2010).

While most glucuronides are readily excreted from the system, some toxicity of glucuronides can arise from the formation of 1- $\beta$ -O-acyl glucuronides (1- $\beta$ -O-AGs). 1- $\beta$ -O-AGs are formed from glucuronidation of a carboxylic acid moiety. Covalent modification of proteins may occur through transacylation, whereby the glucuronic acid moiety is displaced and the parent drug conjugates to the protein (Figure 1-4). 1- $\beta$ -O-AGs have the ability to undergo a process known as acyl migration, which is the intramolecular migration of the acyl group. The pyranose ring of the acyl migration products (2- $\beta$ -O-, 3- $\beta$ -O-, 4- $\beta$ -O-) can open up to form an aldehyde (Figure 1-4). Aldehydes are reactive in nature and will bind to amine groups in proteins or DNA via an imine (Schiff base) linkage through a process known as glycation (Regan *et al.*, 2010). Imines are hydrolyzable and the bound protein can be released from the aldehyde. In the case of 3- $\beta$ -O- and 4- $\beta$ -O-AGs, imine adducts can undergo

acid-catalyzed Amadori rearrangement whereby a more stable 1-amino-keto product is formed, rendering the glycation irreversible (Figure 1-4) (Smith *et al.*, 1990). A classic example of transacylation and acyl migration of Phase II acyl glucuronides is diclofenac, which will be further illustrated in the next section.

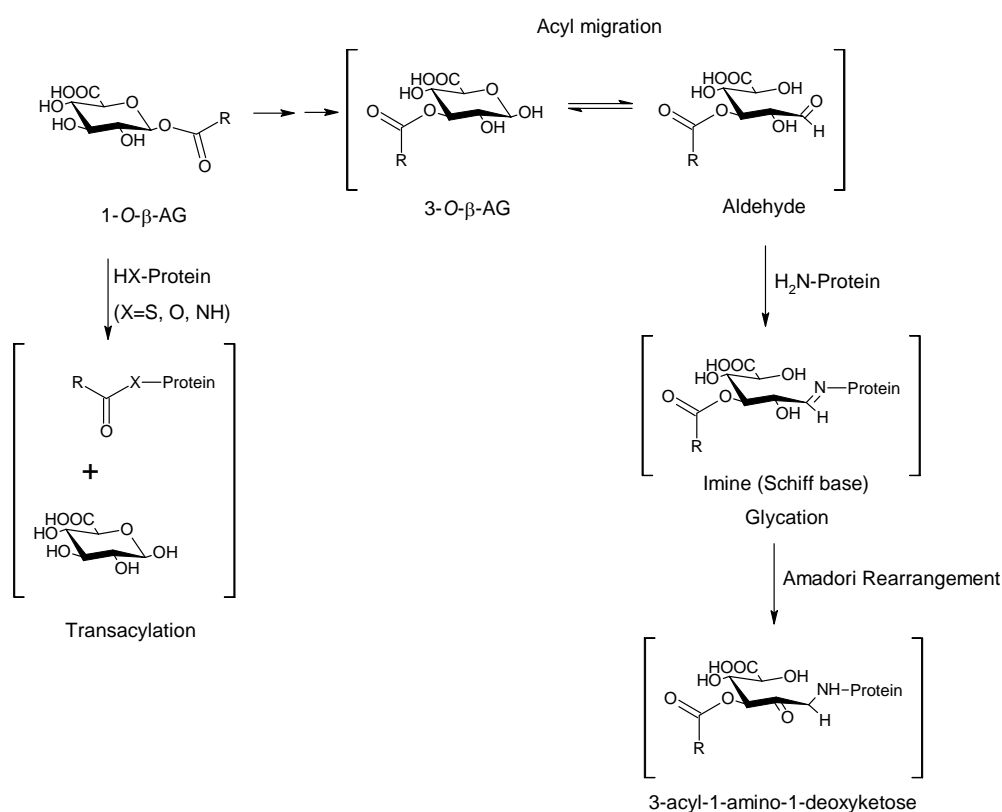


**Figure 1-4** AGs can undergo transacylation or acyl migration (2- $\beta$ -O-, 3- $\beta$ -O-, 4- $\beta$ -O-) followed by glycation. A 3- $\beta$ -O-AG is shown here as an example whereby the resulting aldehyde from ring opening can undergo glycation to form an imine. Acid-catalyzed Amadori rearrangement of the imine can occur to give the more stable 1-amino-keto product.

Clearly, Phase I and Phase II metabolism are important contributors to DILI via the possible generation of reactive metabolites. A better understanding of the drug property that alters this tendency will go a long way towards addressing this problem. One such class of drugs with a highly manifested

DILI due to metabolism that might benefit from an improved understanding is the non-steroidal anti-inflammatory drugs (NSAIDs).

### 1.3. NSAIDs - Mechanism of action and induced liver injury

NSAIDs are drugs with analgesic, antipyretic and anti-inflammatory properties. They act by blocking cyclooxygenase (COX) enzymes, which inhibit the production of prostanoids, thereby giving rise to their therapeutic properties (Vonkeman and van de Laar, 2010). Prostanoids are a collective group of bioactive lipids that consist of prostaglandins, prostacyclins and thromboxanes which play an important role in inflammatory and resolution responses. Prostanoids are produced by COX from arachidonic acid when trauma or tissue damage occurs, giving rise to inflammatory responses (Figure 1-5) (FitzGerald and Patrono, 2001). There are two isoforms of COX, the constitutive COX-1 and the inducible COX-2, of which COX-2 had been indicated as the COX isoform responsible for the main production of prostanoids involved in inflammation (Masferrer *et al.*, 1990).

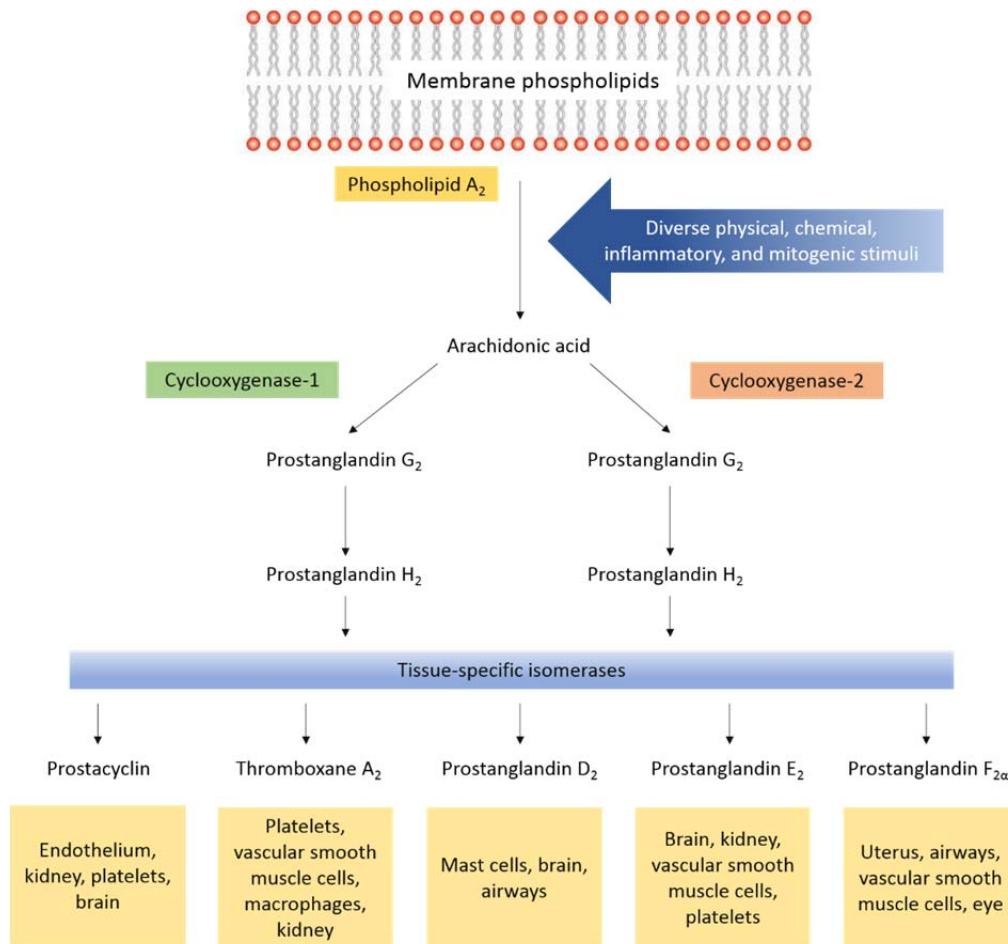


**Figure 1-5** Production of prostanoids by COX-1 and COX-2 from arachidonic acid and their respective target tissue/organ. Reproduced with permission from FitzGerald and Patrono (2001), Copyright Massachusetts Medical Society.

In recent years, the focus of NSAIDs have been on the development of COX-2 selective inhibitors to reduce the side-effects such as gastrointestinal toxicity associated with inhibition of COX-1 by non-selective COX inhibitors (Chakraborti *et al.*, 2010). The ability of COX-2 inhibitors to selectively inhibit COX-2 arises from the presence of a hydrophobic pocket in COX-2 which allows accommodation of side chains. The same pocket is not available in COX-1 due to bulky amino acid residues which restrict the insertion of a side chain on the drug molecule and thus lowering the binding affinity of the molecule (Grosser, 2006).

Besides toxicity arising from COX-1 inhibition, liver toxicity continues to remain as the bane of NSAID therapeutics. It is estimated that roughly 10% of total DILI is NSAIDs-related and 50% of fulminant hepatic failure is due to DILI (Bessone, 2010). This is a significant clinical challenge that has sidelined many of the promising drugs in this class. The most common route of elimination for NSAIDs is via hepatic biotransformation by Phase I and Phase II metabolism (Davies and Skjodt, 2000). It has been proposed that NSAID-induced hepatotoxicity is a result of drug bioactivation by Phase I and Phase II metabolic enzymes (Agundez *et al.*, 2011; Lee *et al.*, 2011). Many NSAIDs, for example, nimesulide and ibuprofen, possess aromatic structures and carboxylic acid moieties that can potentially be metabolized to reactive metabolites and contribute to the onset of liver injury.

#### 1.4. Comparison of non-selective NSAID (Diclofenac) and COX-2 selective NSAID (Lumiracoxib)

One commonly used NSAID, diclofenac (Voltaren®, Norvatis) is a reversible non-selective COX inhibitor. The established mechanism of action of diclofenac has been attributed to its extremely good ability to block the synthesis of prostaglandin E<sub>2</sub> (PGE<sub>2</sub>) in COX (Gan, 2010). However, a potent effect on COX-1 besides COX-2, resulted in gastrointestinal toxicity. Diclofenac has also been attributed to cause approximately 34.1% of NSAID-induced hepatotoxicity via bioactivation by metabolism (Agundez *et al.*, 2011). The bioactivation process of diclofenac has been extensively studied and its hepatotoxicity could be attributed to the formation of reactive quinone imines, arene oxides and 1-β-O-AGs. Diclofenac can be hydroxylated at two positions:

5-position to form 5-hydroxy (OH) diclofenac by CYP3A4 (Shen *et al.*, 1999) and 4'-position to form 4'-OH-diclofenac by CYP2C9 (Figure 1-6) (Leemann *et al.*, 1993). *In vivo* studies involving rats and humans have found two different hydroxyl-diclofenac conjugates in urine samples; 5-OH-4-N-acetylcysteine (NAC) diclofenac and 4'-OH-3'-NAC-diclofenac (Poon *et al.*, 2001). These conjugates were proposed to be N-acetylated degradation products of S-glutathionyl (GS) adducts derived from both 5-OH and 4'-OH-diclofenac. Additional *in vivo* studies involving bile samples from rats and *in vitro* studies involving human hepatocytes and human liver microsomes identified two additional conjugates; 5-OH-6-GS-diclofenac (Tang *et al.*, 1999a) and 4'-OH-2'-GS-diclofenac (Yu *et al.*, 2005).

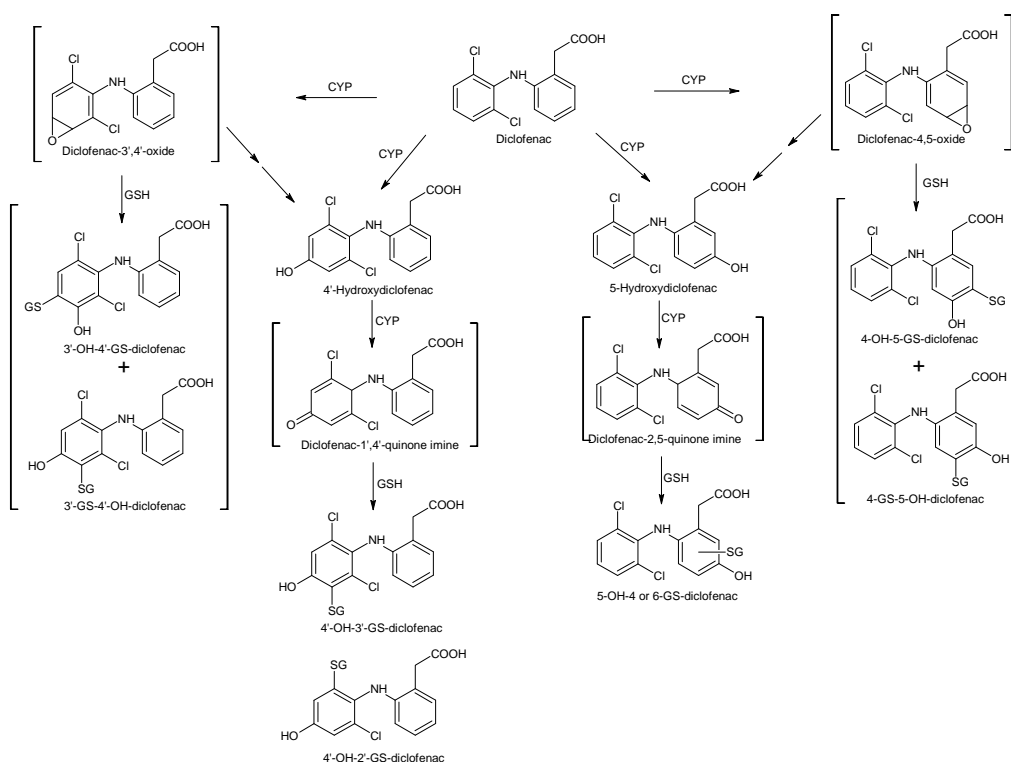


**Figure 1-6** Phase I metabolic pathway of diclofenac by CYP2C9 and CYP3A4 and subsequent possible bioactivation and conjugation of cellular nucleophiles (Kretzrommel and Boelsterli, 1994b; Tang *et al.*, 1999a).



Diclofenac possesses an acetic acid moiety that can undergo Phase II metabolism to form 1- $\beta$ -O-AG. Both *in vivo* studies in rats and *in vitro* studies utilizing hepatocytes and liver microsomes have detected GSH or protein adducts of diclofenac-1- $\beta$ -O-AG and have shown that such adduct formation induces toxicity (Kretzrommel and Boelsterli, 1993; Kretzrommel and Boelsterli, 1994b; Kretzrommel and Boelsterli, 1994a; Grillo *et al.*, 2003). As shown in Figure 1-7, diclofenac-1- $\beta$ -O-AG can undergo two conjugation pathways; direct transacylation whereby the glucuronic acid moiety is lost (Grillo *et al.*, 2003), or by acyl migration followed by glycation whereby the glucuronic acid moiety is retained (Kretzrommel and Boelsterli, 1994a). Despite its ability to form reactive metabolites and its high percentage contribution to NSAID-induced hepatotoxicity, only a very small percentage had fatal outcomes or required hospitalizations and liver transplants (Bessone, 2010). Nonetheless, the incidence of such adverse events remains appreciable.

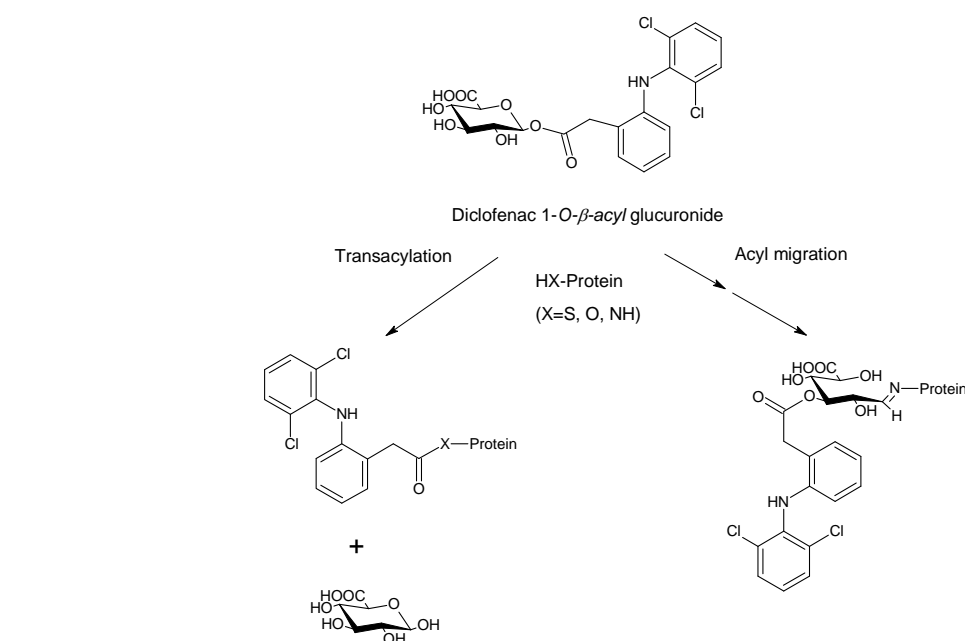


**Figure 1-7** Formation of covalent adducts by diclofenac-1- $\beta$ -O-AG through transacylation or acyl migration (Boelsterli, 2003).

A drug with a similar structure, lumiracoxib (Prexige®), was developed by Novartis as a reversible COX-2 selective inhibitor to counteract the undesirable gastrointestinal effects associated with non-COX selective NSAIDs and was first approved in 2006. Instead of having two chlorine atoms at the positions 2' and 6' as with diclofenac, a chlorine atom was substituted with fluorine and a methyl group was substituted at position 5 (Figure 1-8).

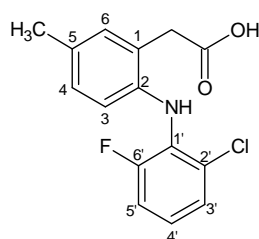


**Figure 1-8** Numbering of aromatic rings of lumiracoxib. A methyl group is substituted at position 5 and a fluorine replaces chlorine at position 6'.

A structure-activity relationship (SAR) study done on analogs of lumiracoxib has shown that the methyl group at position 5 confers COX-2 selectivity to the drug (Blobaum and Marnett, 2007). However, within a year of approval in Canada, Oceanic and European countries, lumiracoxib was withdrawn from the market due to eight cases of severe hepatotoxicity, resulting in two deaths and two liver transplants in Australia in the span of 2006 to 2007 (Li *et al.*, 2008). An *in vivo* study in human subjects has identified that lumiracoxib is extensively metabolized by CYP2C9 to form 4'-OH-lumiracoxib, a metabolite that can possibly undergo further oxidation to a reactive quinone imine (Mangold *et al.*, 2004). Additional *in vitro* bioactivation studies were done using human and rat liver microsomes. These studies utilized GSH and NAC as trapping agents to trap reactive metabolites formed. Similar to the *in vivo*

study, 4'-OH-lumiracoxib was detected and was shown to further oxidize to a quinone imine, which was trapped with NAC to form 4'-OH-3'-NAC-lumiracoxib (Li *et al.*, 2008). It should be noted with interest that the conjugation occurred at the position *ortho* to chlorine and not at the position *ortho* to fluorine. 4'-OH-6'-NAC-lumiracoxib and 4'-OH-6'-GS-lumiracoxib were identified in two studies, whereby a selective displacement of fluorine occurred (Li *et al.*, 2008; Kang *et al.*, 2009). Lumiracoxib was also proposed to be able to form an imine methide, 5-methyl-GS-lumiracoxib, which was detected in a trapping study with GSH (Kang *et al.*, 2009). In addition to mono-conjugated adducts, di-, tri- and tetra-GSH adducts were identified, which indicates that re-oxidation of the mono-GSH adduct is possible (Kang *et al.*, 2009).

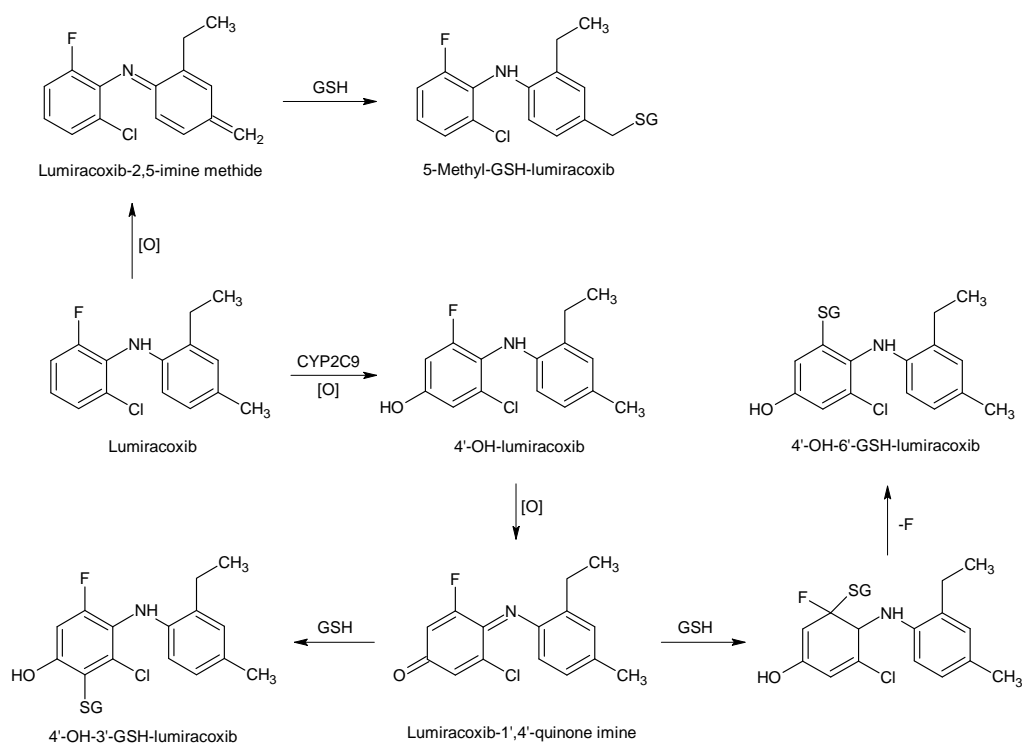


**Figure 1-9** Phase I metabolism pathway and subsequent bioactivation and conjugation of nucleophiles for lumiracoxib (Li *et al.*, 2008; Kang *et al.*, 2009)

### 1.5. Statement of purpose

Individual bioactivation studies of drugs give mechanistic insights into how drugs induce toxicity through formation of reactive metabolites. In the case of diclofenac and lumiracoxib, which are structurally-similar NSAIDs possessing the 2-phenylaminophenylacetic acid backbone, individual studies have noted that both drugs form reactive metabolites that are highly reactive electrophiles. However, there are few studies to compare the toxic effects due to bioactivation of such structurally similar drugs. Given that diclofenac and lumiracoxib are so similar structurally yet so different in their toxic effects and pharmacological properties, we propose to study how subtle changes to substituents on the 2-phenylaminophenylacetic acid backbone affect 1) the toxicity induced through bioactivation and 2) their pharmacological properties in order to elucidate the structure-toxicity relationship for a given chemical backbone. This study could provide better mechanistic insights on how substituents on a given chemical backbone affect its bioactivation to reactive metabolites and their subsequent reactivity and toxicity. It will also provide better understanding in the balance between toxicity and activity for further drug design.

In order to investigate the effects of substituents on toxicity and pharmacology, we designed and synthesized 2-phenylaminophenylacetic acid analogs that were structurally similar to diclofenac and lumiracoxib with varying substituents at three positions on the said backbone. The *in vitro* toxicity of the synthesized compounds was determined on two liver cell-lines with different

metabolic capabilities using MTT assay. With the data obtained, further comparative structure-toxicity relationships could be elucidated.

However, with only the *in vitro* cell toxicity data in hand, we could not determine if toxicity was caused by formation of reactive metabolites or via other mechanisms. Thus, we carried out *in vitro* bioactivation assays such as GSH depletion assay, AG reactivity determination, metabolic stability assays and reactive metabolite identification. These investigations provide an insight into the role of metabolism and bioactivation in affecting the toxicity of the compounds. Furthermore, the effect of subtle changes on the chemical backbone on metabolic stability, metabolite reactivity and the structures of reactive metabolites formed could be elucidated.

In addition to the toxicity and metabolic studies, pharmacological studies involving cell-based COX inhibition assays were carried out to determine the efficacy and selectivity of the synthesized compounds. These assays allowed elucidation of SARs for the compounds. In addition, with the combined pharmacology and toxicity data, activity-selectivity-toxicity relationships could be deduced for the synthesized compounds.

In summary, this thesis is organized into five experimental chapters. Chapter 2 illustrates the chemical structures and synthetic schemes of the compounds. With the synthesized compounds available, Chapter 3 compiles the *in vitro* toxicity data together with subsequently generated structure-toxicity relationship models. Chapter 4 looks into the pharmacological properties and

the activity-selectivity-toxicity relationships of the synthesized compounds. Moving on, we looked into the role of metabolism in the toxicity of the compounds. Chapter 5 involves investigating the metabolic stability and reactivity of the compounds for both Phase I and Phase II metabolism. Last but not least, the identification and proposal of mechanistic pathways involved in the formation of Phase I and Phase II reactive metabolites of the compounds were investigated in Chapter 6.

## Chapter 2. Design and Synthesis of 2-Phenylaminophenylacetic Acid

### Derived Compounds

#### 2.1. Introduction

Twenty-four compounds, including diclofenac and lumiracoxib were proposed for this study. The basis of analog design was to change the substitutions at R<sub>1</sub>, R<sub>2</sub> and R<sub>3</sub> so as to evaluate the influence of these positions to the observed toxicities (Figure 2-1). Lumiracoxib differs from diclofenac in having a methyl group at R<sub>1</sub> on ring A and a fluorine at R<sub>2</sub> on ring B. Thus, the focus was placed on these three positions.

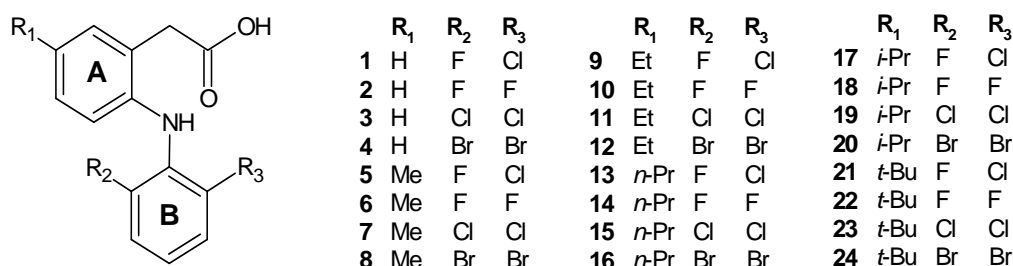


**Figure 2-1** Structures of target compounds synthesized with position R<sub>1</sub> on ring A and positions R<sub>2</sub> and R<sub>3</sub> on ring B. Diclofenac and lumiracoxib are compounds 3 and 5 respectively. Full structures are listed in Appendix 2-1.

The selectivity of lumiracoxib for COX-2 arises from the addition of a methyl group at R<sub>1</sub>. It was observed that the addition of the methyl group reduces potency in addition to conferring selectivity (Blobaum and Marnett, 2007). Thus far, SAR studies of 2-phenylaminophenylacetic acids were carried out only for and up to methyl substitution at R<sub>1</sub> (Blobaum and Marnett, 2007). Further increase in alkyl group size was not determined. Thus, a change in alkyl groups at position R<sub>1</sub> was proposed to investigate if the size of the substituent will affect the toxicity and pharmacology of the compound.

Hydrogen, methyl, ethyl, *n*-propyl, *iso*-propyl and *tert*-butyl were chosen as the substituents at R<sub>1</sub>.

R<sub>2</sub> and R<sub>3</sub> were proposed as changes in halogen substituents. A SAR-study on 2-phenylaminophenylacetic acids observed that substituting chlorine for fluorine increased potency of the analog. It was proposed that larger halogens contribute to an increased angle of twist between the two phenyl rings, which affects the potency of the compound (Moser *et al.*, 1990).

The selection of substituents at these positions allow us to probe specific physicochemical contributors to toxicity because homologous alkyl groups on ring A differ in size, lipophilicity and extent of branching, while the halogens on ring B differ in size, lipophilicity and electronegativity. These physicochemical parameters can in turn affect the metabolism and disposition to effect varying biological responses.

## 2.2. Experimental methods

Merck silica 60 F254 sheets and Merck silica gel (0.040-0.063 mm) (Merck KGaA, Darmstadt, Germany) were used for thin layer chromatography (TLC) and flash chromatography respectively. HPLC/spectro grade acetonitrile and methanol were purchased from Tedia (Fairfield, OH). All other chemicals and reagents were obtained from Sigma Aldrich (St. Louis, MO) or Alfa Aesar (Ward Hill, MA) unless otherwise mentioned. Final compounds characterized by <sup>1</sup>H and <sup>13</sup>C nuclear magnetic resonance (NMR) spectra were recorded on a Bruker DPX 300 or Bruker ADVIII 400 spectrometer (Billerica, MA).

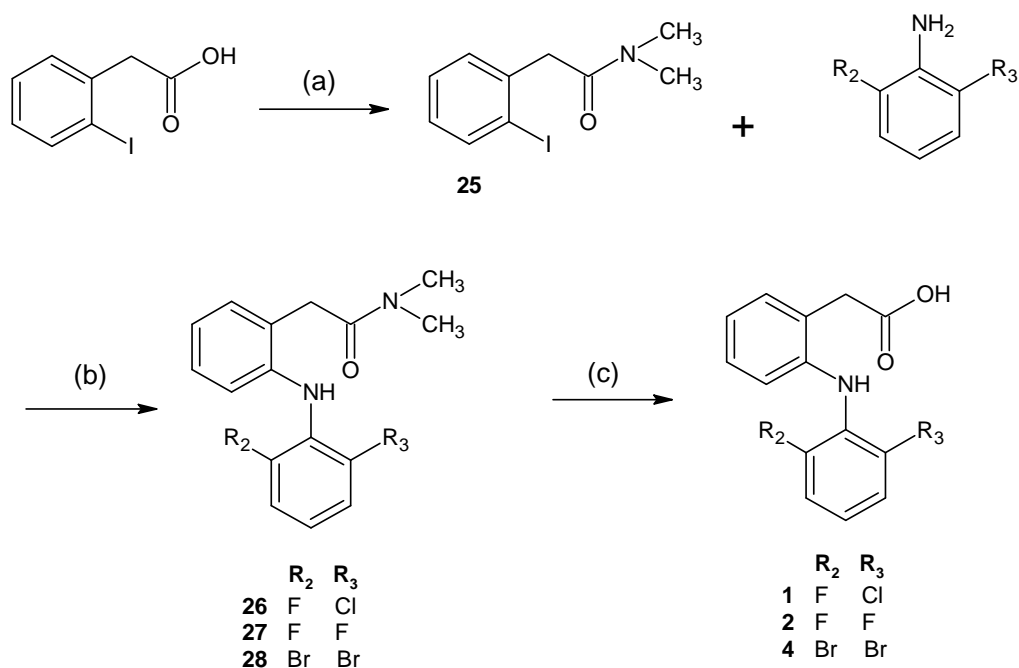


Chemical shifts were reported in parts per million (ppm,  $\delta$ ) and referenced to residual solvents, deuterated chloroform ( $\text{CDCl}_3$ ) ( $\delta$  77.260) or deuterated dimethyl sulfoxide ( $\text{DMSO-}d_6$ ) ( $\delta$  2.500) for  $^1\text{H}$  spectra and  $\text{DMSO-}d_6$  ( $\delta$  39.43) for proton decoupled  $^{13}\text{C}$  NMR. Coupling constants ( $J$ ) were reported in Hertz (Hz). Proton coupling patterns were described as singlet (s), doublet (d), triplet (t), quartet (q), sextet (sext), septet (sept), doublet of doublets (dd), doublet of doublet of doublets (ddd), doublet of triplets (dt), triplet of doublets (td), triplet of triplets (tt) and multiplet (m). Mass spectra were captured on a Sciex API 3000 Qtrap (AB Sciex, Framingham, MA) equipped with an electrospray ionization (ESI) probe. Accurate mass was determined on a Bruker MicroOTOF-QII (Billerica, MA) equipped with an ESI probe. Masses of the compounds were reported in  $m/z$  values for the molecular ion detected. Melting point was acquired on a Gallenkamp melting point apparatus (Weiss Technik UK, United Kingdom). All characterization data of intermediates and final compounds are listed in Appendix 2-2.

#### 2.2.1. Extraction of diclofenac (3) from Voltaren tablets

The enteric coating of six Voltaren® tablets (50 mg diclofenac per tablet, Novartis, Switzerland) was removed. The tablets were then powdered with a pestle and mortar. To the powdered tablets (1.66 g), methanol (30 mL) and glacial acetic acid (1 mL) were added and the mixture sonicated for 5 min. The mixture was then shaken gently for 1 min and filtered. Water (30 mL) was added to the filtrate and the residue was removed by filtration under reduced pressure, after which it was washed with cold water (5 mL x 4). The residue (**A3**) was allowed to dry in an oven (50°C) overnight.

### 2.2.2. Synthesis of compounds **1**, **2** and **4**



**Scheme 2-1** Synthetic scheme for synthesis of **1**, **2** and **4**: (a) SOCl<sub>2</sub>, NH(CH<sub>3</sub>)<sub>2</sub>, DCM, 0°C; (b) Anhydrous K<sub>2</sub>CO<sub>3</sub>, CuI, Cu, toluene, reflux, 96 h; (c) Ethanolic KOH, reflux, overnight.

#### 2.2.2.1. Synthesis of 2-iodophenyl-*N,N*-dimethylacetamide (**25**)

The method reported by Kenny, *et al.* (Kenny *et al.*, 2004) was followed with some modifications. 2-Iodophenylacetic acid (0.53 g, 1.98 mmol) was dissolved in 12 mL of dichloromethane (DCM). To this solution, thionyl chloride (0.5 mL, 6.88 mmol) was added drop-wise with stirring at 0°C. DMF (1 drop) was added and the solution stirred at room temperature for 2 h, then evaporated to dryness. DCM was added, the mixture evaporated and the evaporating procedure was repeated again. The product was re-dissolved in DCM (5 mL) and added drop-wise to a two-phase system of 40% w/w aqueous dimethylamine (12 mL) in water (35 mL) and DCM (50 mL), which was stirred vigorously at 0°C. After 1 h, the organic layer was separated, washed with 1 M HCl, 10% aqueous Na<sub>2</sub>CO<sub>3</sub>, and water, and dried over

anhydrous Na<sub>2</sub>SO<sub>4</sub> before evaporating to dryness. Purification by chromatography (eluting with ethyl acetate (EtOAc):hexane, 1:3) afforded **25** as a colorless oil.

#### 2.2.2.2. General procedure for the synthesis of 2-[(2,6-disubstituted phenyl)amino]phenyl-N,N,-diethylacetamides (**26 - 28**)

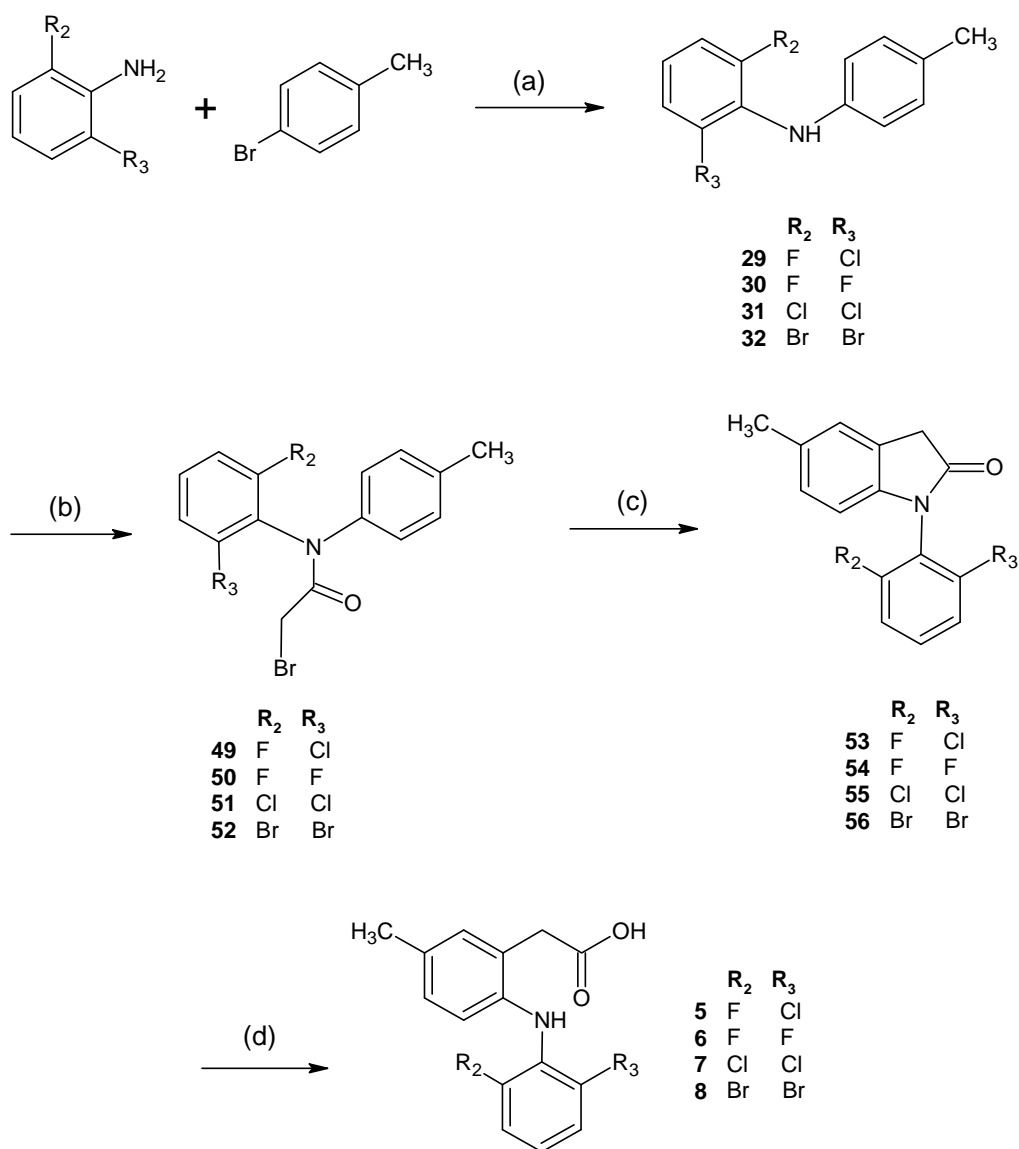
A mixture of **25** (0.24 g, 0.83 mmol), 2,6-disubstituted aniline (1.90 mmol), anhydrous K<sub>2</sub>CO<sub>3</sub> (0.11 g, 0.76 mmol), CuI (0.011 g, 0.052 mmol) and freshly activated Cu(Vogel, 1989) (0.035 g) in toluene (5 mL) in a Dean-Stark apparatus filled with 4 Å molecular sieves was stirred and refluxed for 96 h. The mixture was filtered while still warm over celite, concentrated, and re-dissolved in EtOAc, then washed with water, dried over anhydrous Na<sub>2</sub>SO<sub>4</sub> and evaporated. Purification by chromatography (eluting with EtOAc:hexane, 1:4 followed by 2:3) afforded the product as crystals.

#### 2.2.2.3. General procedure for hydrolysis of acetamide to free acid (**1, 2 and 4**)

The 2-[(2,6-disubstituted phenyl)amino]phenyl-N,N,-diethylacetamide (**26 - 28**) (0.16 M) was dissolved in ethanolic KOH (0.67 M) and refluxed overnight in an inert N<sub>2</sub> atmosphere. The solution was cooled to room temperature, concentrated and then re-dissolved in water (10 mL). The aqueous solution was extracted with EtOAc (2 x 30 mL) and the organic layer discarded. The aqueous solution was acidified with 1 M HCl to pH 3 and extracted with EtOAc (2 x 30 mL), washed with water, dried over Na<sub>2</sub>SO<sub>4</sub> and evaporated to dryness. Purification by chromatography (eluting with EtOAc:hexane/1%

acetic acid, 1:4 to 2:3), followed by recrystallization from EtOAc/hexane afforded the product as powder.

### 2.2.3. Synthesis of compounds **5 – 8**



**Scheme 2-2** Synthetic scheme for synthesis of **5 - 8**: (a) Pd(OAc)<sub>2</sub>, (±) BINAP, NaOC(CH<sub>3</sub>)<sub>3</sub>, toluene, reflux, 24-48 h; (b) BrCH<sub>2</sub>COBr, 80°C, neat; (c) AlCl<sub>3</sub>, chlorobenzene, 155-160°C, 5 h; (d) NaOH, ethanol, reflux, 4-5 h.

#### 2.2.3.1. General procedure for the syntheses of 2,6-disubstituted-N-(p-alkyl)anilines (**29 - 48**)

The reaction was carried out as previously reported (Wolfe and Buchwald, 2000). Toluene (2 mL) and ( $\pm$ )-2,2'-bis(diphenylphosphino)-1,1'-binaphthalene (( $\pm$ )-BINAP) (9.3 mg, 1.5 mol%) were stirred under argon at 80°C for 1 min. Pd(OAc)<sub>2</sub> (2.2 mg, 1 mol%) was added to the mixture, purged with argon for approximately 30 s and stirred at room temperature for 1 min. 1-Bromo-4-alkylbenzene or 1-iodo-4-alkylbenzene (2 mmol) and the 2,6-disubstituted aniline (2 mmol) were added to the mixture, followed by addition of NaOC(CH<sub>3</sub>)<sub>3</sub> (0.270 g, 2.8 mmol) and toluene (1.6 mL). The mixture was stirred and refluxed under argon for 24-48 h (reaction progress was checked by TLC and halted when aniline spot was faint or not visible). The mixture was cooled to room temperature, 5 M HCl (4 mL) and activated charcoal (0.5 g) was added and stirred for an additional 1 h. The organic layer was separated, washed with water, dried over Na<sub>2</sub>SO<sub>4</sub> and evaporated. The product was used with minimal purification (filtration through silica gel to reduce color) or removal of remaining aniline (by, chromatography, eluting with hexane) for the next step. It should be noted that the product obtained and used for the next step is not pure as the only concern here is the removal of color and aniline.

#### 2.2.3.2. General procedure for the syntheses of N-acetylated 2,6-disubstituted-N-(p-tolyl)anilines (49 – 52)

The 2,6-disubstituted-N-(p-tolyl)aniline (**29 – 32**) (~1 mmol) was heated, neat, to 80°C and bromoacetyl bromide (1.2 mmol, 0.1 mL) was added drop-wise with stirring. The mixture was heated at 80°C for 2-3 h. After the mixture was cooled to room temperature, water (5 mL) and toluene (5 mL) was added. The organic layer was separated, washed with water, dried over anhydrous Na<sub>2</sub>SO<sub>4</sub>

and evaporated. Purification by chromatography (eluting with EtOAc:hexane, 1:3) afforded the N-acetylated 2,6-disubstituted-N-(p-tolyl)anilines (**49** - **52**).

#### 2.2.3.3. General procedure for the syntheses of 1-(2,6-disubstituted)-5-methylindolin-2-ones (**53** - **56**)

The reaction was carried out as previously reported (Acemoglu *et al.*, 2004). A mixture of the N-acetylated 2,6-disubstituted-N-(p-tolyl)aniline (1 mmol), AlCl<sub>3</sub> (1.5 mmol) and chlorobenzene (2 mL) was stirred and heated to 155-160°C and maintained at this temperature for 5 h. The reaction mixture was then cooled to room temperature and water (5 mL) and toluene (5 mL) were added. The organic layer was separated, washed with 2 M HCl and water, dried over anhydrous Na<sub>2</sub>SO<sub>4</sub> and evaporated. The residue was re-dissolved in ethanol, stirred with activated charcoal (0.2 g) for 30 min, filtered over celite and evaporated. Purification by recrystallization from 2-propanol afforded the product as crystals.

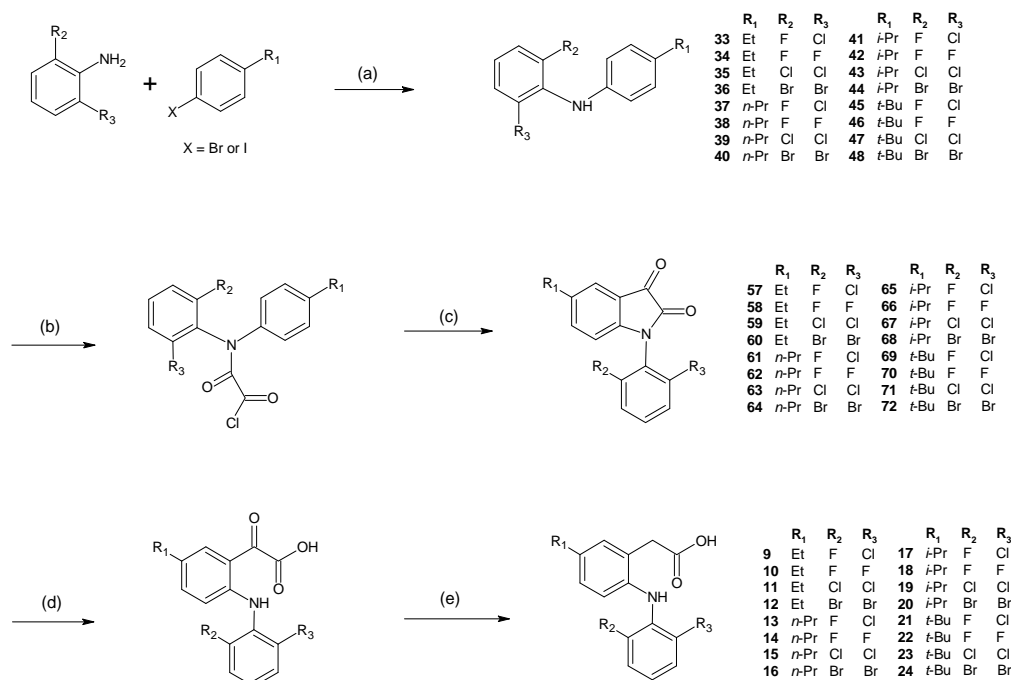
#### 2.2.3.4. General procedure for the syntheses of 2-(2-(2,6-disubstitutedphenyl)amino)-5-methylphenyl)acetic acid (**5** - **8**)

A solution of the indolinone (**53** - **56**) (1 mmol), in ethanol (3.7 mL) and water (0.2 mL) was heated to reflux under nitrogen. NaOH solution (0.39 g of a 30% w/w solution) was slowly added and refluxing was continued for 4-5 h. The solution was cooled, evaporated to remove ethanol, re-dissolved in water, acidified with 5 M HCl to pH 3, extracted with EtOAc, washed with water and dried over anhydrous Na<sub>2</sub>SO<sub>4</sub>. The residue was dissolved in ethanol, stirred

with activated charcoal (0.2 g) for 30 min, filtered over celite and evaporated.

Recrystallization from DCM/hexane twice gave the product as crystals.

#### 2.2.4. Synthesis of compounds **9** – **24**



**Scheme 2-3** Synthetic scheme for synthesis of **9** - **24**: (a) Pd(OAc)<sub>2</sub>, (±) BINAP, NaOC(CH<sub>3</sub>)<sub>3</sub>, toluene, reflux, 24-48 h; (b) Oxalyl chloride, DCM, 2h, rt.; (c) AlCl<sub>3</sub>, DCM, 2h, rt.; (d) NaOH, ethanol, reflux, 10-15 min; (e) H<sub>2</sub>NNH<sub>2</sub>•H<sub>2</sub>O, NaOCH<sub>3</sub>, 2-methoxyethanol, 150°C, 2 h.

##### 2.2.4.1. General method for the synthesis of 1-(2,6-disubstituted phenyl)-5-ethylindoline-2,3-diones (**57** - **72**)

To a mixture of the 2,6-disubstituted-N-(4-alkyl)aniline (**33** - **48**) (2 mmol) in DCM (2 mL), oxalyl chloride (0.5 mL, 4 mmol) was added drop-wise with stirring at 0°C. The mixture was stirred for 2 h at room temperature, evaporated to dryness and twice evaporated from DCM. The resulting oxoacid chloride was re-dissolved in DCM (4 mL), cooled to 0°C and anhydrous AlCl<sub>3</sub> (0.54 g, 4 mmol) was added portion wise with stirring. The mixture was flushed with argon, allowed to stir at room temperature for 2 h and poured

over crushed ice and 2 M HCl (5 mL). The mixture was extracted with DCM and the organic layer separated, washed with 2 M HCl and water, dried over anhydrous Na<sub>2</sub>SO<sub>4</sub> and evaporated. Purification by chromatography (eluting with EtOAc:hexane, 1:9 to 1:4) afforded the product as a semi-crystalline residue.

#### 2.2.4.2. General method for the syntheses of 2-(2-(2,6-disubstitutedphenyl)amino)-5-alkylphenyl)acetic acid (9 - 24)

The reaction was carried out as previously reported (Moser *et al.*, 1990). A mixture of the indoline-diones (**57 - 72**) (1 mmol) and NaOH solution (0.39 g of a 30% w/w solution) (0.39 g) in ethanol (4.3 mL) was refluxed for 10-15 min, cooled and evaporated. The residue was re-dissolved in water and acidified with 5 M HCl to pH 3 to form a fine suspension. The acidified mixture was extracted with EtOAc, the organic layer washed with water, dried over anhydrous Na<sub>2</sub>SO<sub>4</sub> and evaporated. The resulting oxoacetic acid, without purification, was re-dissolved in 2-methoxyethanol (4.3 mL) and hydrazine hydrate (0.28 mL, 5 mmol) was added. The mixture was warmed to 60°C with stirring and NaOCH<sub>3</sub> (0.53 g, 10 mmol) was added portion-wise. The mixture was slowly heated to 150°C, held at that temperature for 2 h, cooled to room temperature and poured over crushed ice. The mixture was acidified with 5 M HCl to pH 3 and extracted with EtOAc. The organic layer was separated, washed with water, dried over anhydrous Na<sub>2</sub>SO<sub>4</sub> and evaporated. Purification by chromatography (eluting with EtOAc:hexane/0.5% acetic acid, 1:9 to 1:4) followed by recrystallization from DCM/hexane twice to afford the product as a crystalline solid.



### 2.2.5. Purity determination by HPLC

Purities of final compounds were verified by high performance liquid chromatography (HPLC) using an Agilent 1100 series system (Santa Clara, CA) coupled with a diode array detector using a reverse phase Phenomenex Luna® 5 µm C18(2) 100 Å 250 × 4.6 mm column (Torrance, CA). The solvents used were acetonitrile (A), methanol (B) and water with 0.1% trifluoroacetic acid (C). For **1 - 4**, gradient A was run from 5:95 A:C to 95:5 A:C over 10 min and held at 95:5 A:C for 3 min. Gradient B was run from 5:95 B:C to 95:5 B:C over 10 min and held at 95:5 B:C for 3 min. For **5 - 8**, gradient A was run from 5:95 A:C to 95:5 A:C over 10 min and held at 95:5 A:C for 3 min. Gradient B was run from 15:95 B:C to 95:5 B:C over 8 min and held at 95:5 B:C for 5 min. For **9 - 24**, gradient A was run from 15:95 A:C to 95:5 A:C over 8 min and held at 95:5 A:C for 5 min. Gradient B was run from 15:95 B:C to 95:5 B:C over 8 min and held at 95:5 B:C for 5 min. The compounds were analyzed at a wavelength of 280 nm. Purities of all twenty-four compounds are listed in Appendix 2-3.

### 2.3. Discussion

The structures of the test compounds are presented in Figure 2-1. The compounds possess a common 2-phenylamino-phenylacetic acid scaffold but with varying alkyl substituents (methyl, ethyl, *n*-propyl, *iso*-propyl, *tert*-butyl) at position R<sub>1</sub> on ring A and different halogens (fluoro, bromo, chloro and combinations thereof) at positions R<sub>2</sub> and R<sub>3</sub> on ring B. Compounds **3** and **5** are diclofenac and lumiracoxib respectively.

Compounds **1**, **2** and **4** are structurally related to diclofenac (**3**), differing only in the halogens substituted on ring B. Their reaction scheme is shown in Scheme 2-1. The carboxylic acid present in 2-iodophenylacetic acid was first converted to the tertiary amide by reaction with thionyl chloride and dimethylamine via a nucleophilic acyl substitution pathway. Amide formation via acid chlorides is faster and requires milder conditions as compared to direct synthesis from the carboxylic acid. The acid chloride reacts with dimethylamine by a nucleophilic acyl substitution process to form the 2-(2-iodophenyl)-*N,N*-dimethylacetamide (Figure 2-2). The acid to amide conversion was necessary to ensure that the Ullman condensation between the *ortho*-disubstituted aniline and the iodo functionality in phenylacetamide **25** was not impeded by the presence of the free acid.

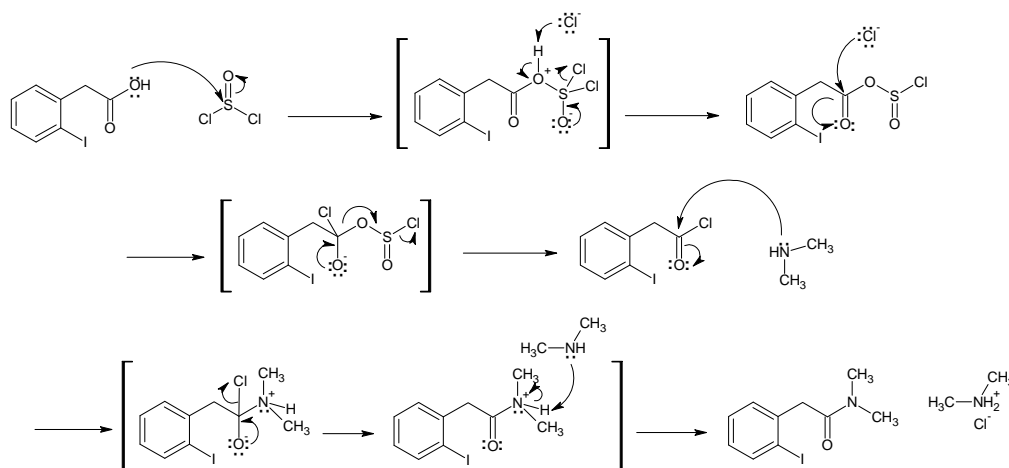


**Figure 2-2** Mechanism of the formation of an amide via formation of an acid chloride (Li, 2009).

Ullman condensation was carried out by between the *ortho*-disubstituted aniline and the iodo functionality in phenylacetamide **25**. Ullmann condensation occurs by the formation of a copper (III) complex. The aniline

first forms a complex with the copper (I) iodide (CuI) catalyst. 2-(2-iodophenyl)-*N,N*-dimethylacetamide adds to the complex via oxidative addition. The copper (III) complex then undergoes reductive elimination to form the 2-phenylaminophenylacetic acid product (Figure 2-3). The CuI catalyst is regenerated.

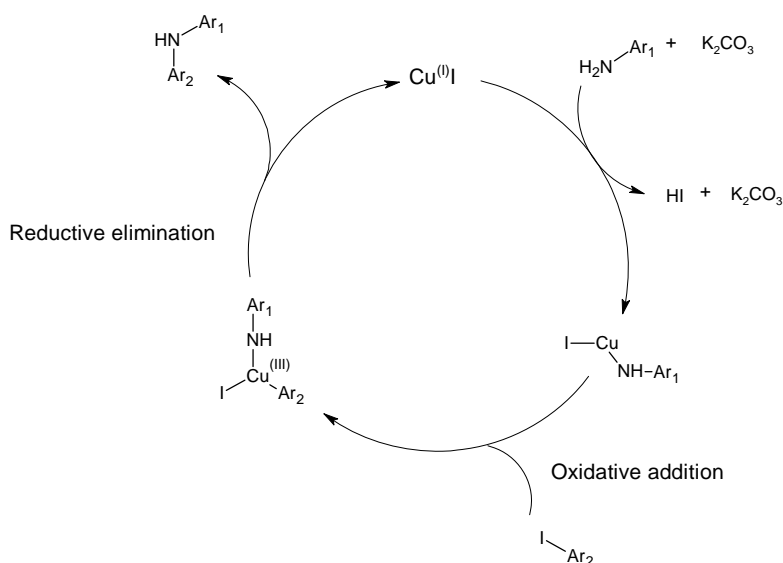


**Figure 2-3** Mechanism of Ullmann condensation (Li, 2009).

On completion of the reaction, the amide (**26**, **27** or **28**) was hydrolyzed to regenerate the free acid. The size of the halogens on ring B did not affect the rate of the Ullman condensation reaction but it was observed that the yield decreased for the dibromo-substituted compound (**4**) after hydrolysis. For this compound, the aqueous solution after hydrolysis was washed with EtOAc in order to facilitate the purification process after acidification. It is possible that the dibromo-substituted compound (**4**), although present in its ionized anionic state, was sufficiently lipophilic to be partitioned into the discarded organic phase.

Compounds **6 - 8** are analogs of lumiracoxib (**5**), differing only in the *ortho*-halogens present on ring B. Scheme 2-2 illustrates the reaction sequences involved in their syntheses. The first step in the synthesis involves formation of a diarylamine via Buchwald-Hartwig coupling from the respective aniline and halo-alkylbenzene. For bromo-substituted analogs at R<sub>2</sub> and R<sub>3</sub> positions, iodo-alkylbenzene is required instead of bromo-alkylbenzene as the reaction could not proceed with a bromo-alkylbenzene. Palladium (II) acetate (Pd(OAc)<sub>2</sub>) was used as the catalyst and can be reduced to the required palladium (0) upon contact with the hindered base sodium *tert*-butoxide (NaOtBu) used (Wolfe and Buchwald, 2000). The mechanism behind Buchwald-Hartwig coupling starts with addition of 13a to the Pd<sup>(0)</sup>-ligand complex via oxidative addition. This is followed by displacement of the halide by NaOtBu, which is in turn displaced by the aniline. Finally, the diarylamine is formed by reductive elimination and the catalyst is regenerated (Figure 2-4).

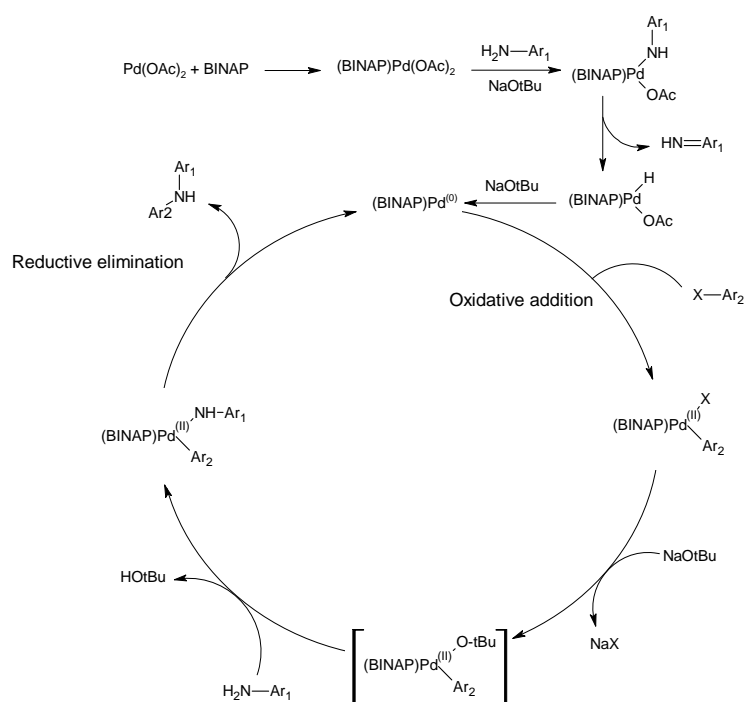


**Figure 2-4** Mechanism of Buchwald-Hartwig coupling (X: Br, I) (Li, 2009).

The aniline nitrogen of the product (**29 - 32**) was acetylated by reacting with bromoacetyl bromide to give *N,N*-disubstituted bromoacetamide (**49 - 52**). The next step involved an intramolecular Friedel-Crafts alkylation to give the oxindole (**53 - 56**). Friedel-Crafts alkylation occurs by formation of a carbocation, which acts as the electrophile in an electrophilic aromatic substitution, forming an oxindole (Figure 2-5). Hydrolysis of the oxindole under alkaline conditions gave the desired free acids (**5 - 8**).

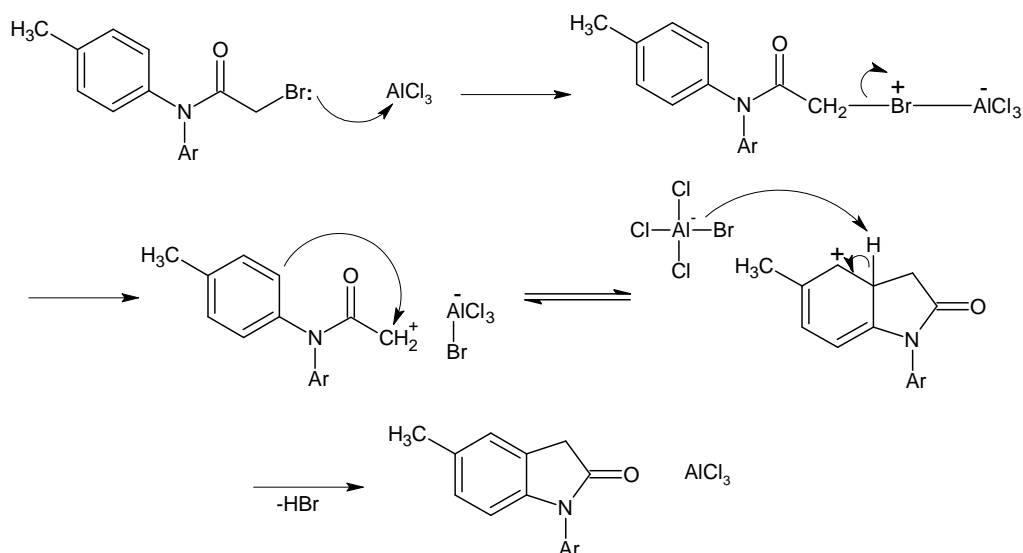


**Figure 2-5** Mechanism for intramolecular Friedel-Crafts alkylation (Li, 2009).

Compounds **9 - 24** have ethyl, *n*-propyl, *iso*-propyl or *tert*-butyl at  $\text{R}_1$  on ring A. The syntheses of these compounds are similar to the ring A methyl analogs **5 - 8**. Scheme 2-3 illustrates the reactions involved in the synthesis. The Buchwald-Hartwig reaction was employed to give the diarylamine (**33 - 48**). The removal of any remaining disubstituted aniline was crucial as the acid chloride obtained in the next step cannot be purified. However, it was found that the diarylamine could be used in spite of impurities as long as the disubstituted aniline was not present. Thus, disubstituted aniline was the only

impurity removed as elution with hexane made separation of other impurities difficult. The aniline nitrogen was then acylated with oxalyl chloride to form an acyl chloride. An acyl cation is generated from the reaction between the acyl chloride and  $\text{AlCl}_3$ , which attacks the upper aromatic ring (Figure 2-6). *N*-substituted isatin (**57** – **72**) were formed via this intramolecular Friedel-Crafts acylation.

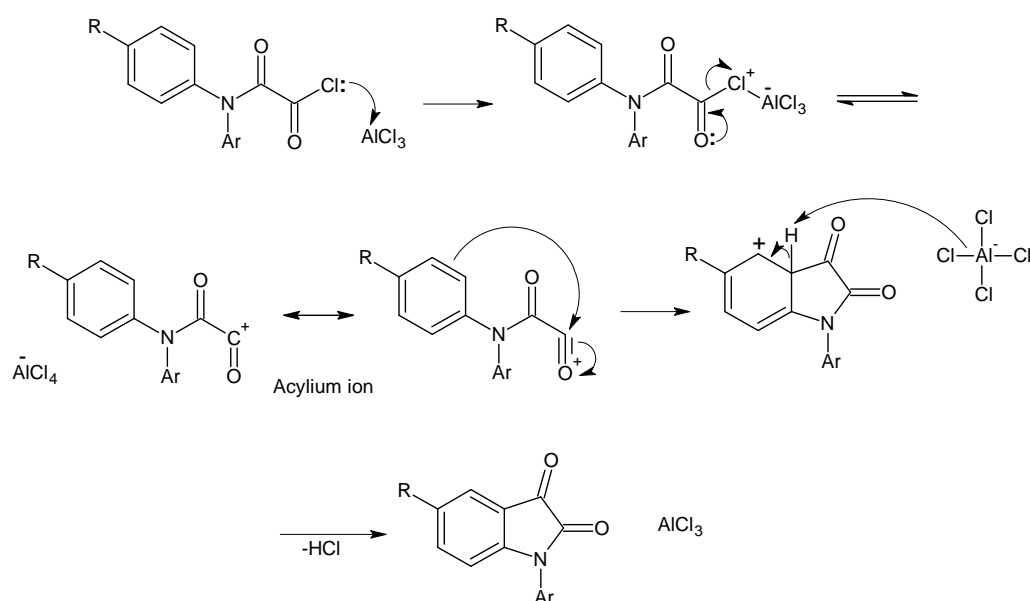


**Figure 2-6** Mechanism of Friedel-Crafts acylation (Li, 2009).

A Friedel-Crafts acylation was required as previous attempts at Friedel-Crafts alkylation resulted in the loss of the alkyl group on ring A. As seen from Figure 2-7a, an ethyl group ( $\delta$  ppm 2.66 (q,  $J = 7.6$  Hz, 2H), 1.25 (t,  $J = 7.6$  Hz, 3H)) is present in the NMR spectrum of 2-bromo-*N*-(2,6-difluorophenyl)-*N*-(4-ethylphenyl)acetamide. After Friedel-Crafts alkylation, the peaks corresponding to an ethyl group is absent from the NMR spectrum of the reaction product (Figure 2-7b). Determination of mass by mass spectroscopy



The loss of the ethyl group was most probably due to reverse Friedel-Crafts reaction. This reaction is actually Friedel-Crafts reaction occurring backwards and occurs in the presence of an acid and a Lewis acid. The acid in this instance was the hydrobromic acid (HBr) formed from the forward Friedel-Crafts alkylation. The acid forms a complex with aluminum (III) chloride ( $\text{AlCl}_3$ ), allowing the proton to protonate the aromatic ring of the oxindole to form an aromatic carbocation. The alkyl group is then expelled and is trapped by the solvent (chlorobenzene) used (Figure 2-8). The resulting product is a dealkylated oxindole.

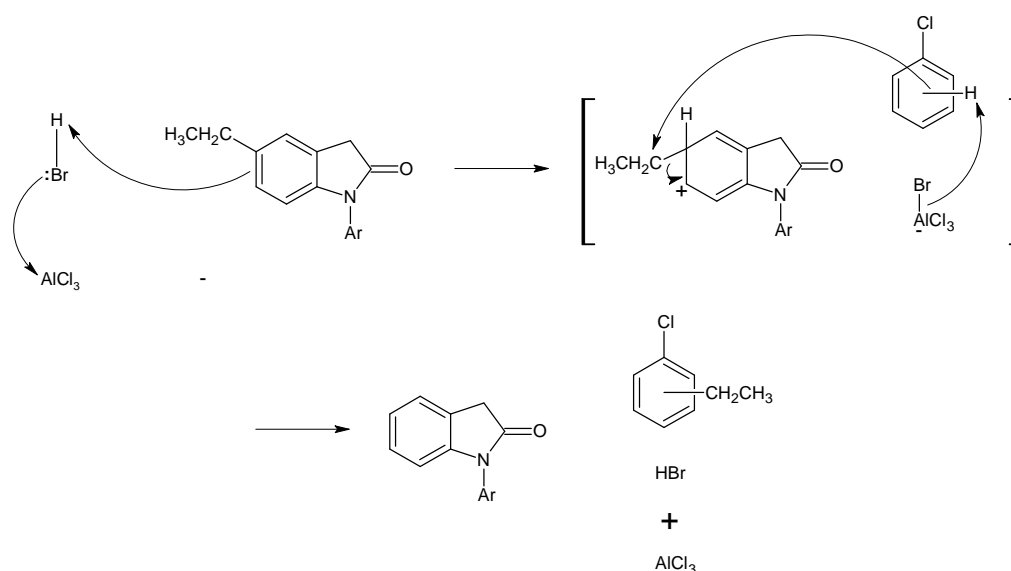


**Figure 2-8** Mechanism of reverse Friedel-Crafts (Li, 2009).

Ring opening was effected by alkaline hydrolysis to give the oxoacetic acid. The oxoacetic acid was not purified before use as it degraded rapidly to the starting N-substituted isatin. The ketone carbonyl was reduced in a Wolff-Kishner reaction with hydrazine hydrate and sodium methoxide as base. The oxoacetic acid reacts with hydrazine ( $\text{H}_2\text{NNH}_2$ ) at the ketone oxygen to form a hydrazone which is subsequently deprotonated, with the release of nitrogen



gas (Figure 2-9). The ketone is reduced to an alkane, forming the 2-phenylaminophenylacetic acid product (9 – 24).

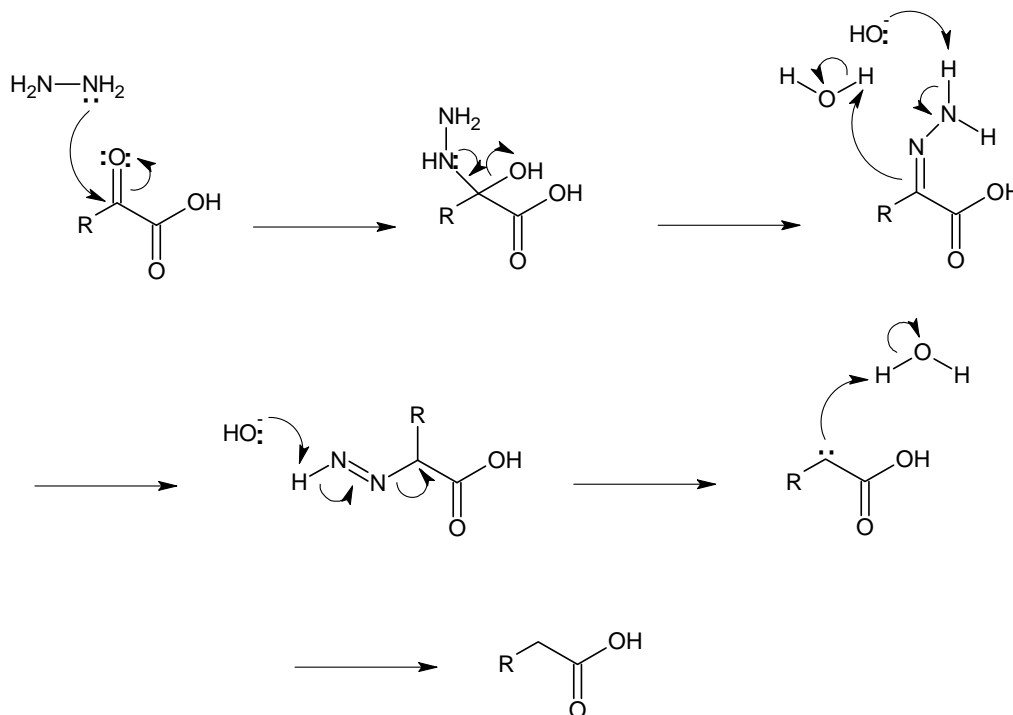


**Figure 2-9** Mechanism of a modified Wolff-Kishner reduction (Li, 2009).

#### 2.4. Conclusion

In conclusion, twenty-four analogs were synthesized via three schemes. The obtained yields of the analogs ranged from 25% to 89%. They were characterized via NMR, mass spectroscopy and melting point (Appendix 2-2). Their purities were determined via HPLC and were ascertained to be acceptable (Appendix 2-3).

**Chapter 3. *In vitro* toxicity of 2-Phenylaminophenylacetic Acid derived Compounds in Liver Cell Lines: Effect of Substituents on Toxicity and Derivation of Quantitative Structure-Toxicity Relationships (QSTR)**

**3.1. Introduction**

Diclofenac and lumiracoxib toxicities are mainly associated with the liver. Extensive research has revealed that their liver toxicities were primarily due to the formation of reactive metabolites via Phase I and Phase II metabolism in the liver (Kretzrommel and Boelsterli, 1994a; Tang *et al.*, 1999b; Tang, 2003; Li *et al.*, 2008; Kang *et al.*, 2009). Thus, in order to determine the effect of substituents on the 2-phenylaminophenylacetic acid chemical scaffold on its toxicity, we have decided to test the twenty-four synthesized compounds on liver cell lines. To further ascertain the role of bioactivation in such toxicities, we intentionally selected liver cell lines of contrasting metabolic capacity for toxicity profiling of the compounds. HuH-7 and TAMH were used to carry out the 3-(4,5-Dimethylthiazol-2-yl)-2,5-diphenyltetrazolium bromide (MTT) assay in order to determine the effect of the compounds on cell viability. In addition, we carried out an enzyme functionality test on the two key cytochrome P450 enzymes involved in the metabolism of diclofenac and lumiracoxib to validate the contrasting metabolic potential of our experimental models.

We decided to look at the possible relationships between physicochemical properties of the compounds and their *in vitro* cytotoxicity. In addition to a qualitative analysis, we performed a quantitative structure-toxicity relationship

(QSTR) modelling which led to the creation of regression models depicting the relationship between physicochemical properties in terms of molecular descriptors and experimental data.

### 3.2. Experimental methods

Dulbecco's modified Eagle's medium/Ham's F12 (DMEM/F12) and soybean trypsin inhibitor were obtained from Gibco® (Life Technologies, Carlsbad, CA). ITS Universal Culture Supplement Premix containing 5 mg/mL insulin, 5 mg/mL transferrin and 5 ng/mL selenium was obtained from BD Bioscience (Belford, MA). Fetal bovine serum (FBS) was obtained from Hyclone (Thermo Scientific, Waltham, MA). MTT was obtained from Duchefa Biochemie (Haarlem, Netherlands). Luciferin-H and Luciferin-PFBE P450-Glo assay kits were obtained from Promega (Fitchburg, WI). All other chemicals and reagents were obtained from Sigma Aldrich (St. Louis, MO) unless otherwise mentioned.

#### 3.2.1. Cell culture

All cultures were maintained in a humidified incubator with 5% carbon dioxide at 37°C unless otherwise stated. TAMH cells were a gift from Professor Nelson Fausto (University of Washington, USA). The cells were grown in serum free DMEM/F12 supplemented with ITS Universal Culture Supplement Premix, 100 nM dexamethasone, 10 mM nicotinamide and 0.01% (v/v) gentamicin (Pierce *et al.*, 2002). Trypsin was used to passage cells at 80-90% confluence, and was inhibited with 0.5 mg/mL soybean trypsin inhibitor. HuH-7 cells were obtained from *Health Science Research Resources Bank*

(HSRRB, Japan). The cells were grown in Dulbecco's Modified Eagle's Medium (DMEM) supplemented with 10% FBS. Trypsin was used to passage cells at 80-90% confluence, and was inhibited with 10% FBS supplemented DMEM. Cultures were maintained in a humidified incubator with 5% carbon dioxide at 37 °C.

### 3.2.2. Determination of key cytochrome P450 enzyme activities

TAMH and HuH-7 cells seeded at a density of  $5.0 \times 10^4$  cells/ well. The activity of two classes of cytochrome P450s, CYP2C9 and CYP3As, were determined using the Luciferin-H and Luciferin-PFBE P450-Glo assay respectively. The P450-Glo assay was carried out in accordance to manufacturer's instruction. Briefly, medium was aspirated 48 h after seeding of cells. Luciferin substrates were dissolved in the respective growth medium and 50  $\mu$ L was added to each well. The plates were incubated for 4 h in the dark at 37°C. The medium in each well were then transferred to a 96-well opaque white plate and 50  $\mu$ L of Luciferin Detection Reagent was added. The plate was incubated at room temperature for 20 min. Luminescence was read on a Tecan M200 Pro plate reader (Männedorf, Switzerland) and the readout was expressed in relative luminescence units (RLU). Net signals were calculated by subtracting away the background luminescence values. MTT assay was carried out on the same cells to normalize the net luminescence signals to cell viability.

### 3.2.3. MTT assay to determine cytotoxicity

MTT assay was carried out as reported elsewhere (Plumb *et al.*, 1989). Briefly, TAMH cells were seeded at a density of  $1.2 \times 10^4$  cells/ well. HuH-7 cells were seeded at a density of  $1 \times 10^4$  cells/ well. Test compounds were dissolved in DMSO and the final DMSO concentration for all treatments was synchronized at 0.5% v/v in the growth medium. The treatment duration was 24 h, after which the medium was aspirated from the wells. MTT dye (50  $\mu$ L of 2 mg/mL in PBS) and growth medium (200  $\mu$ L) were added per well and incubated at 37°C in the dark for 3 h. The MTT containing medium was then aspirated and Sorenson's buffer (25  $\mu$ L of 0.1 M glycine and 0.1 M sodium chloride equilibrated to pH 10.5 with 0.1 M sodium hydroxide) and DMSO (200  $\mu$ L) were added to each well. The plates were read at 560 nm using a Tecan M200 plate reader. Cell viability was expressed as the percentage ratio of treated cells normalized over DMSO controls. Median lethal concentrations (LC<sub>50</sub>) values were obtained from the dose-response curve using Graphpad Prism 5 (Graphpad Software Inc., San Diego, CA).

### 3.2.4. Calculation of molecular descriptors

The chemical structures of the twenty-four compounds were drawn and energy-minimized using the MMFF94x force field in the Molecular Operating Environment (MOE) 2008.10 software (Chemical Computing Group, Montreal, Canada) with the root-mean-square (RMS) gradient set to 0.00001. All available 327 molecular descriptors were calculated with MOE. In addition, log D(o/w) values were calculated using the online ACD/I-Lab prediction engine (ACD/Labs, Canada). These descriptors were put through a

descriptor selection procedure in order to remove unsuitable descriptors (as described in the next section).

### 3.2.5. Selection of relevant molecular descriptors

Molecular descriptors with constant values were eliminated. The respective  $LC_{50}$  values were converted to  $pLC_{50}$  or  $-\log(LC_{50})$  values. Thereafter, all the remaining descriptors were first sorted in descending order based on the Pearson's correlation coefficients between TAMH  $pLC_{50}$  values and the individual descriptors. In the next step, the descriptor possessing the highest correlation coefficient to the TAMH  $pLC_{50}$  values was retained. All other descriptors with correlation coefficients of more than or equal to 0.60 to the retained descriptor were discarded. This was carried out to ensure the absence of collinearity in the selected set of descriptors. Of the remaining descriptors, the descriptor with the next highest correlation coefficient to TAMH  $pLC_{50}$  was retained. Similarly, as mentioned above, the descriptors found to be correlated to the second retained descriptor were discarded. This procedure was repeated until all the descriptors were processed. The same procedure was repeated using the HuH-7  $pLC_{50}$  values.

### 3.2.6. QSTR models: Multiple linear regression and validation

For each set of the assay data from the TAMH and HuH-7 cell lines, a QSTR model was built using multiple linear regression based on the remaining molecular descriptors that were passed through the descriptor selection step. Prior to building the QSTR models, the respective  $LC_{50}$  values were converted to  $pLC_{50}$  or  $-\log(LC_{50})$  values so as to facilitate the regression process. The

step-wise multiple linear regression was carried out using the IBM SPSS Statistics for Windows, Version 21.0 (IBM, Armonk, NY). In order to ensure statistical rigor, the ratio of the number of compounds to the number of descriptors is recommended to be  $\geq 5$ . Therefore, with twenty-four compounds in this study, the maximum number of descriptors that can be included in each of the QSAR regression models is 4.

In order to validate the QSAR models generated, leave-one-out cross-validation and 100 rounds of y-scrambling were conducted for each of the models (Wold *et al.*, 1995). In leave-one-out cross-validation, each compound was left out of the inputs during the regression model building stage and the model obtained was used to predict the corresponding pLC<sub>50</sub> value for that left-out compound. The predicted pLC<sub>50</sub> values were then compared to the experimental pLC<sub>50</sub> and the cross-validated  $R^2$  or  $q^2$  value was calculated. Furthermore, in order to eliminate the possibility that the regression models were generated by chance, the y-scrambling procedure was carried out. In this procedure, models are fitted for randomly re-ordered pLC<sub>50</sub> values and compared with the model obtained for the actual pLC<sub>50</sub> values. This was conducted for 100 iterations.

### 3.2.7. Partial order ranking

In order to get an overview of the toxicity of the compounds in this study, one of the possible ways is to rank them according to the LC<sub>50</sub> values obtained using the two cell lines. However, the LC<sub>50</sub> values from each of the cell lines are not in total agreement for some of the compounds. In other words, if the

compounds are ranked according to each of the cell line  $LC_{50}$  values, then the rankings obtained will be different. This is because the separate rankings are not able to reconcile contradictions in the assay results. Therefore, in order to take those contradictions from both cell lines into account, the compounds need to be ranked using a method known as partial order ranking. Partial order ranking is a vectorial approach that not only ranks elements but also identifies contradictions in the criteria used for ranking (Lerche *et al.*, 2002; Carlsen, 2008). It helps to circumvent the lack of comparability with some compounds. Such incomparability is due to contradictory attributes; for each incomparable pair of compounds there must be  $LC_{50}$  values from different cell lines that are counteracting. In order to visualize the partial order rankings, the Hasse diagram technique can be applied.

### 3.2.8. Hasse diagram technique

In the Hasse diagram, the compound that is at the apex is called the maximal (Halfon and Reggiani, 1986; Bruggemann and Bartel, 1999; Bruggemann *et al.*, 1999). On the other hand, the compound at the bottom of the diagram without any compounds below it is called the minimal.

When the Hasse diagram technique was first applied, the criteria describe the elements in terms of environmental hazard. The main assumption is that the lower the numerical value the lower the hazard. Since a high numerical value of cell line  $LC_{50}$  values corresponds to low toxicity, the values must be multiplied by -1 to invert their order. Based on this convention, the maximal elements are the most toxic and top priority should be assigned to them. In this



study, the partial order ranking and the Hass diagram were generated using the Data Analysis by Ranking Techniques (DART) version 2.0.5 software.

### 3.2.9. Statistical Analysis

Unpaired t-test (one-tailed) was used to analyze the expression of P450 enzymes in the cell-lines using GraphPad Prism 5. LC<sub>50</sub> values were calculated from triplicates and expressed as mean and standard deviation. One-way analysis of variance (ANOVA) was used to determine the statistical significant difference between the MTT results using GraphPad Prism 5.

## 3.3. Results

### 3.3.1. Determination of key cytochrome P450 activities

To determine if the difference in toxicity could be due to the contrasting metabolic capacity between the two cell lines, TAMH and HuH-7, cytochrome P450 activities were evaluated. Two key enzymes important in the metabolism of phenylaminophenylacetic acid were considered, namely CYP2C9 and CYP3As (CYP3A4, CYP3A5 and CYP3A7). These P450 enzymes were previously shown to be involved in the metabolism of diclofenac and lumiracoxib (Leemann *et al.*, 1993; Shen *et al.*, 1999; Mangold *et al.*, 2004). The activity was evaluated using luminogenic P450 substrates incubated in the respective cell lines. Unpaired one-tailed t-tests showed that the differences in CYP activity between the two cell lines are significant (Figure 3-1). The activity of CYP2C9 and CYP3As in TAMH are approximately 5.7 and 6.2 fold respectively of that of HuH-7. Based on the RLU measured, both cell

lines have more CYP3As activity as compared to CYP2C9, consistent with the predominance of CYP3A4/5 also seen in humans.

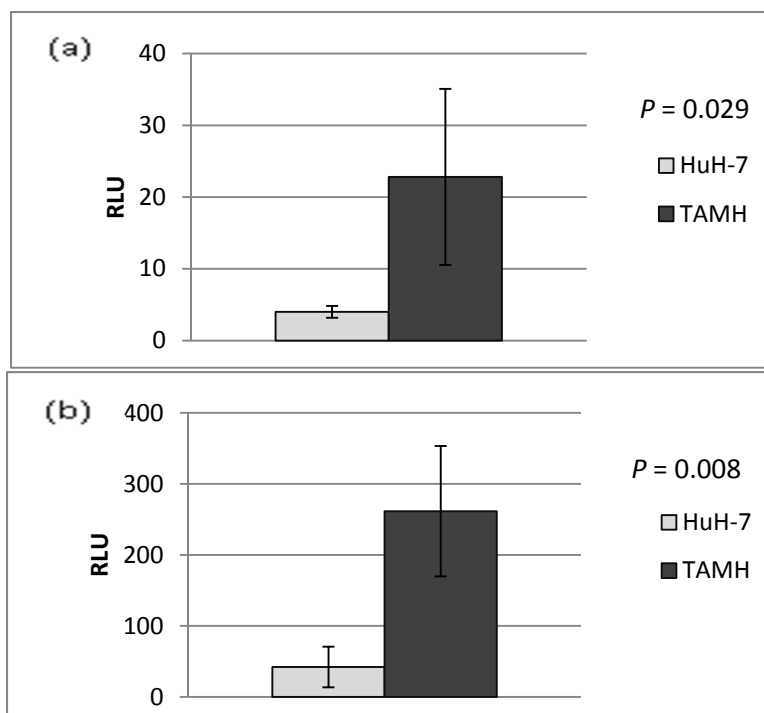


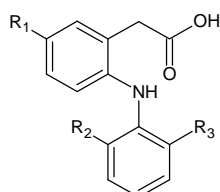
**Figure 3-1** Comparison between the relative luminescence units (RLU) obtained for HuH-7 and TAMH for (a) CYP2C9 and (b) CYP3As. Values were generated from three biological replicates. Unpaired *t*-test (one-tailed) of results with calculated *P* values. Statistically significant only when *P* < 0.05.

### 3.3.2. Effect of structural changes on toxicity

The cytotoxicity of synthesized compounds were evaluated on two liver cell lines, namely TAMH, which is a TGF- $\alpha$  overexpressing mouse hepatocyte cell line derived from transgenic MT42 male mice (Wu *et al.*, 1994) and HuH-7, a human hepatocellular carcinoma cell line. Test compounds were tested up to a concentration of 1000  $\mu$ M, which is close to the limit of solubility. The calculated LC<sub>50</sub> values range from approximately 3  $\mu$ M to 500  $\mu$ M for TAMH and 140  $\mu$ M to 1900  $\mu$ M for HuH-7 as shown in Table 3-1. It was observed

that the most cytotoxic compound on both cell lines was compound **24** while compound **2** was identified as the least.

**Table 3-1** LC<sub>50</sub> values and calculated descriptors of the twenty-four compounds.



Compound	R <sub>1</sub>	R <sub>2</sub>	R <sub>3</sub>	Calculated Descriptors		LC <sub>50</sub> (μM) <sup>a</sup>	
				Log P(o/w) <sup>f</sup>	FASA_H <sup>g</sup>	TAMH <sup>b,c</sup>	HuH-7 <sup>d,e</sup>
<b>1</b>	H	F	Cl	3.913	0.835	232.7 ± 9.2	639.6 ± 77.5
<b>2</b>	H	F	F	3.474	0.826	513.1 ± 34.2	1959 ± 477.8 <sup>h</sup>
<b>3 (Diclofenac)</b>	H	Cl	Cl	4.352	0.851	94.2 ± 2.9	341.1 ± 23.8
<b>4</b>	H	Br	Br	4.764	0.860	36.7 ± 3.7	231.7 ± 9.8
<b>5 (Lumiracoxib)</b>	Me	F	Cl	4.248	0.842	111.1 ± 6.1	424.6 ± 39.3
<b>6</b>	Me	F	F	3.809	0.836	323.9 ± 7.9	659.9 ± 88.3
<b>7</b>	Me	Cl	Cl	4.687	0.861	48.7 ± 4.0	311.6 ± 50.0
<b>8</b>	Me	Br	Br	5.099	0.874	15.9 ± 1.6	213.8 ± 10.7
<b>9</b>	Et	F	Cl	4.723	0.849	46.8 ± 5.1	323.3 ± 19.9
<b>10</b>	Et	F	F	4.284	0.844	106.6 ± 11.3	472.4 ± 50.5
<b>11</b>	Et	Cl	Cl	5.162	0.866	21.1 ± 1.3	235.5 ± 11.4
<b>12</b>	Et	Br	Br	5.574	0.874	11.3 ± 0.7	247.6 ± 2.2
<b>13</b>	<i>n</i> -Pr	F	Cl	5.165	0.859	17.0 ± 1.4	241.1 ± 22.1
<b>14</b>	<i>n</i> -Pr	F	F	4.726	0.854	32.8 ± 1.0	310.2 ± 12.6
<b>15</b>	<i>n</i> -Pr	Cl	Cl	5.604	0.876	8.0 ± 1.1	195.2 ± 19.6
<b>16</b>	<i>n</i> -Pr	Br	Br	6.016	0.871	4.0 ± 0.4	192.1 ± 5.2
<b>17</b>	<i>i</i> -Pr	F	Cl	5.093	0.856	22.2 ± 1.8	261.3 ± 9.0
<b>18</b>	<i>i</i> -Pr	F	F	4.654	0.854	36.9 ± 0.6	360.8 ± 33.8
<b>19</b>	<i>i</i> -Pr	Cl	Cl	5.532	0.870	8.9 ± 0.7	207.0 ± 12.8
<b>20</b>	<i>i</i> -Pr	Br	Br	5.944	0.880	5.8 ± 0.5	171.1 ± 16.7
<b>21</b>	<i>t</i> -Bu	F	Cl	5.449	0.860	10.4 ± 0.4	213.2 ± 12.8
<b>22</b>	<i>t</i> -Bu	F	F	5.010	0.857	23.3 ± 1.1	260.8 ± 15.1
<b>23</b>	<i>t</i> -Bu	Cl	Cl	5.888	0.877	5.5 ± 0.8	173.0 ± 12.7
<b>24</b>	<i>t</i> -Bu	Br	Br	6.300	0.883	3.7 ± 0.4	143.4 ± 5.6

<sup>a</sup> LC<sub>50</sub> values were determined after an incubation period of 24 h, 37°C from three biological replicates and expressed as mean ± standard error.

<sup>b</sup> TGF-α transfected mouse hepatocyte cell line.

<sup>c</sup> One-way ANOVA: P < 0.05, indicating average IC<sub>50</sub> values for TAMH are statistically different.

<sup>d</sup> Human hepatocellular carcinoma cell line.

<sup>e</sup> One-way ANOVA: P < 0.05, indicating average IC<sub>50</sub> values for HuH-7 are statistically different.

<sup>f</sup> Calculated partition coefficient in water/octanol.

<sup>g</sup> Fractional accessible surface area\_hydrophobic (FASA\_H) is calculated as ASA\_H / ASA. ASA\_H is the water accessible surface area of all hydrophobic atoms. ASA is the water accessible surface area calculated using a radius of 1.4 Å for the water molecule.

<sup>h</sup> Extrapolated from plot to generate an LC<sub>50</sub> value using GraphPad Prism 5.

There was however some variability in the toxicity ranking of the other compounds. To obtain a comprehensive overview of the standing of the series on both cell lines, and thus the structure toxicity relationship, we employed the approach described in the Hasse diagram (Halfon and Reggiani, 1986; Bruggemann and Bartel, 1999; Bruggemann *et al.*, 1999). In the Hasse diagram (Figure 3-2), the compounds are arranged into 16 levels based on the cytotoxicity results from both cell lines. Accordingly, the levels in the Hasse diagram indicates the level of toxicity in descending order, i.e. compounds assigned to Level 16 are the most toxic and those at Level 1 are the least toxic. As mentioned earlier, these were compounds **24** and **2** respectively. By convention, compounds that were not comparable are placed on the same level. At level 15, compounds **16**, **20** and **23** can be said to be incomparable according to the partial order concept (Lerche *et al.*, 2002; Carlsen, 2008). Incomparability is due to contradictory attributes: for each incomparable pair of compounds there must be LC<sub>50</sub> values that are counteracting. For example, the LC<sub>50</sub> of compound **16**, **20** and **23** were ranked as level 23, 21 and 22 respectively in TAMH but level 21, 23 and 22 respectively in HuH-7. In short, compounds with similar LC<sub>50</sub> values were ranked at the same level due to incomparability and cannot be said to be more toxic than the other. The levels with the most number of compounds are Levels 15, 10 and 6.

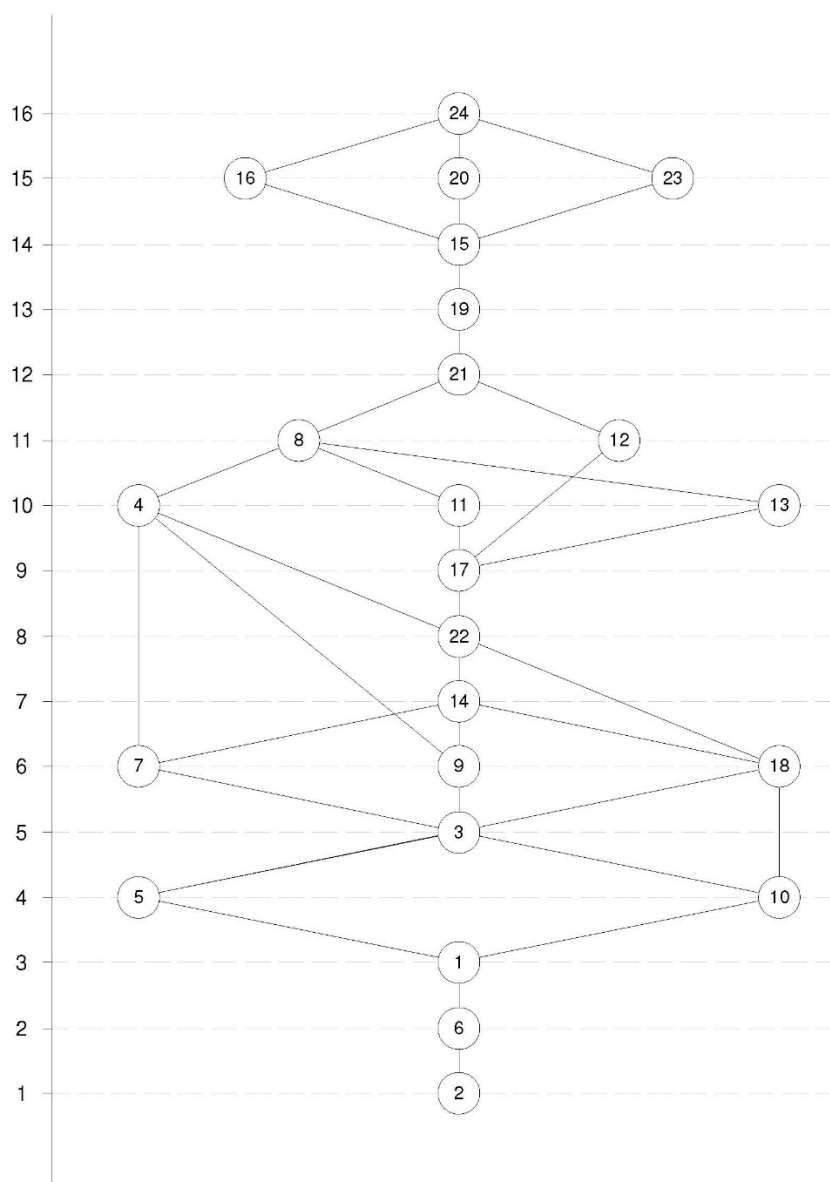


**Figure 3-2** The Hasse diagram of the twenty-four compounds investigated in this study. The numbers in the circles are the compound numbers. The numbers in the left margin are the levels that the compounds are assigned to according to partial order ranking based on both cell lines. The toxicity is ranked in ascending order, with level 1 being the least toxic.

Broadly, the  $LC_{50}$  values obtained for the twenty-four compounds decreased with respect to both increase in size of alkyl group at  $R_1$  of ring A and the size of the halogens at  $R_2$  and  $R_3$  on ring B. In general, the contribution to toxicity by the alkyl substituents are  $H < \text{methyl} < \text{ethyl} < \text{iso-propyl} \leq n\text{-propyl} < \text{tert-butyl}$ , of which H contributing the least to toxicity. For halogen substituents,

the contributions are fluorine < chlorine < bromine, with fluorine contributing the least to toxicity. We examined the effect of alkyl substituents for a given set of halogen substituents on ring B. As an example, we compared compounds **1**, **5**, **9**, **13**, **17** and **21** where substitutions at R<sub>2</sub> and R<sub>3</sub> are fluorine and chlorine and with alkyl substitution increasing from H to *tert*-butyl at R<sub>1</sub>. Here, the LC<sub>50</sub> values decreased from compounds **1** to **21**. This decrease is clearly shown in the Hasse diagram (Figure 3-2) whereby each subsequent compound is ranked at higher levels. The LC<sub>50</sub> values of compounds with *n*-propyl substitution at R<sub>1</sub> were slightly lower than that of a branched *iso*-propyl substitution but were ranked at a higher level (except in the case of **16** and **20**). This indicates that branching of the alkyl side chain affected the toxicity of the compounds, albeit to a small degree.

On the other hand, with respect to the influence of halogen on toxicity, we examined the halogen series while keeping the alkyl substituents constant. For example, compounds **5** to **8** possess a methyl group at R<sub>1</sub> but the halogen substituents at R<sub>2</sub> and R<sub>3</sub> were varied. The LC<sub>50</sub> values within this group of four compounds decreased as the substitutions changed from fluorine to bromine (**6** > **5** > **7** > **8**), in agreement to the rankings proposed in the Hasse diagram. A replacement of fluorine with either chlorine or bromine caused a more dramatic change in LC<sub>50</sub> values as compared to a substitution of chlorine with bromine or vice versa. To further illustrate the potential benefit of fluorine, compounds **5** and **10** (Figure 3-2, Level 4) were compared. It is shown that a change in R<sub>1</sub> from methyl (compound **5**) to ethyl (compound **9**) caused a dramatic drop in LC<sub>50</sub> value. However, substituting fluorine at R<sub>2</sub> or

R<sub>3</sub>, with R<sub>1</sub> as ethyl (compound **10**) gave a LC<sub>50</sub> value similar to that of compound **5**, indicating that fluorine substitutions decreases toxicity.

Another observation made was that for bigger halogen groups, the effect of increasing the size of the alkyl group is less significant. As seen in Table 3-2, the ratio between LC<sub>50</sub> values of the H-substituted compound and the *tert*-butyl-substituted compound at R<sub>1</sub> is the greatest for difluoro-substituted compounds (**1** : **21**) and the least for dibromo-substituted compounds (**4** : **24**).

**Table 3-2** Ratios of LC<sub>50</sub> values between substitutions at R<sub>1</sub>: H and R<sub>1</sub>: *tert*-butyl. Compound names are bracketed.

	HuH-7	TAMH
R <sub>2</sub> : F, R <sub>3</sub> :Cl ( <b>1</b> : <b>21</b> )	3.0	22.4
R <sub>2</sub> : F, R <sub>3</sub> : F ( <b>2</b> : <b>22</b> )	7.5	22.0
R <sub>2</sub> : Cl, R <sub>3</sub> : Cl ( <b>3</b> : <b>23</b> )	2.0	17.1
R <sub>2</sub> : Br, R <sub>3</sub> : Br ( <b>4</b> : <b>24</b> )	1.6	9.9

### 3.3.3. Effect of cell lines with varying metabolic competencies

Toxicity profiles of the compounds were compared across two liver cell lines: TAMH and HuH-7. Consistent between them, the least toxic compound is observed to be **2** and the most toxic compound is **24**. Compound **2** possesses the combination of the least toxic substituents observed, which are hydrogen at R<sub>1</sub> and fluorine at R<sub>2</sub> and R<sub>3</sub>. On the other hand, compound **24** possesses the most toxic substituents observed, which are *tert*-butyl at R<sub>1</sub> and bromines at R<sub>2</sub> and R<sub>3</sub>.

However, the LC<sub>50</sub> values obtained for TAMH are consistently lower than that for HuH-7 (Figure 3-3). The LC<sub>50</sub> of the most toxic compound (**24**) for TAMH (3.7 μM) is very much lower than that of HuH-7 (143.4 μM). Furthermore, as the size of the alkyl and halogen substituents increases, the decrease in LC<sub>50</sub> values for HuH-7 is less pronounced as compared to the corresponding values for TAMH. The LC<sub>50</sub> of the least toxic compound (**2**) is approximately 139 times higher than that of the most toxic compound (**24**) for TAMH, while for HuH-7, the difference between the extremes is only 14 times.

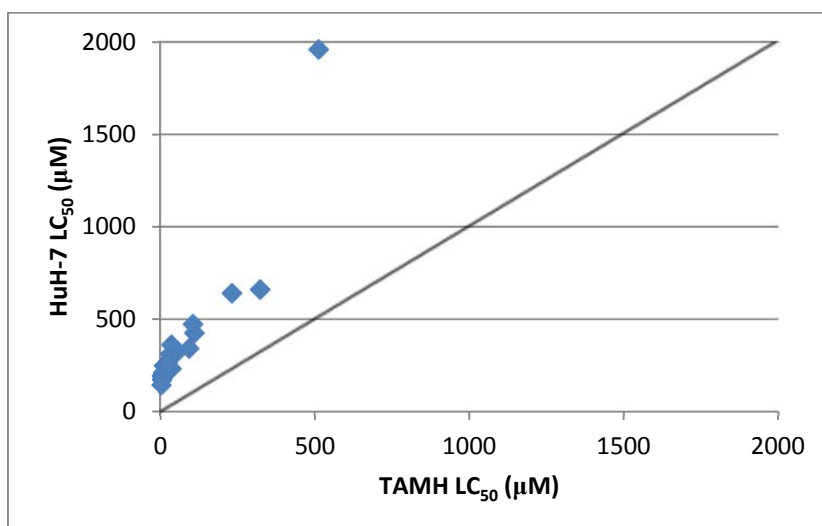


**Figure 3-3** Plot of LC<sub>50</sub> values of HuH-7 against TAMH for all compounds. Point lying above the intersection line indicates that LC<sub>50</sub> value is higher for HuH-7 for that compound.

### 3.3.4. QSTR models: Multiple linear regression and validation

To define the relationship between structural changes and toxicity more explicitly to support subsequent structural modifications, a QSTR model was generated using cytotoxicity results from each cell line. The QSTR regression model obtained for the TAMH cell line using  $-\log(\text{TAMH LC}_{50})$  and  $\log P(o/w)$  (partition coefficient) was:

$$-\log(\text{TAMH LC}_{50}) = 0.801 \times \log P(o/w) - 0.568, \quad (\text{Eq. 1})$$



$R = 0.991$ ,  $q^2 = 0.978$ ,  $F = 1161.020$ ,  $S = 0.083$ ,  $N = 24$ , where  $R$  is the correlation coefficient,  $q^2$  is the cross-validated  $R^2$ ,  $F$  is the Fisher test for significance of the equation,  $S$  denotes the standard error, and  $N$  is the number of compounds. The predicted  $-\log(\text{TAMH LC}_{50})$  and experimental  $-\log(\text{TAMH LC}_{50})$  are listed in Table 3-3.  $\log P(\text{o/w})$  is the calculated partition coefficient in water/octanol, which indicates the lipophilicity of the compounds.

Correspondingly, the QSTR regression model obtained for the HuH-7 cell line using  $-\log(\text{HuH-7 LC}_{50})$  and FASA\_H was:

$$-\log(\text{HuH-7 LC}_{50}) = 14.485 \times \text{FASA\_H} - 8.913 \quad (\text{Eq. 2})$$

$R = 0.910$ ,  $q^2 = 0.770$ ,  $F = 106.636$ ,  $S = 0.103$ ,  $N = 24$ .

The predicted  $-\log(\text{HuH-7 LC}_{50})$  and experimental  $-\log(\text{HuH-7 LC}_{50})$  are listed in Table 3-3. FASA\_H is calculated as  $\text{ASA\_H} / \text{ASA}$ . ASA\_H is the water accessible surface area of all hydrophobic ( $|q_i| < 0.2$ ) atoms. The  $q_i$  value denotes the partial charge of atom  $i$ . ASA is the water accessible surface area calculated using a radius of 1.4 Å for the water molecule. A polyhedral representation is used for each atom in calculating the surface area. FASA\_H is an indicator of the total hydrophobic area in a molecule of the compound, which is related to the lipophilicity of the compounds.

**Table 3-3** The predicted and the experimental  $-\log(\text{TAMH } LC_{50})$  and  $-\log(\text{HuH-7 } LC_{50})$  values of the twenty-four compounds.

Compound	TAMH		HuH-7	
	Predicted $-\log(LC_{50})$	Experimental $-\log(LC_{50})$	Predicted $-\log(LC_{50})$	Experimental $-\log(LC_{50})$
<b>1</b>	4.05	3.63	3.41	3.19
<b>2</b>	3.70	3.29	3.18	2.71
<b>3 (Diclofenac)</b>	3.62	4.03	3.55	3.47
<b>4</b>	4.00	4.44	3.71	3.64
<b>5 (Lumiracoxib)</b>	4.38	3.95	3.28	3.37
<b>6</b>	3.35	3.49	3.05	3.18
<b>7</b>	4.32	4.31	3.38	3.51
<b>8</b>	5.39	4.80	3.49	3.67
<b>9</b>	4.65	4.33	3.75	3.49
<b>10</b>	3.97	3.97	3.54	3.33
<b>11</b>	4.35	4.68	3.77	3.63
<b>12</b>	4.65	4.95	3.53	3.61
<b>13</b>	5.06	4.77	3.46	3.62
<b>14</b>	4.70	4.48	3.31	3.51
<b>15</b>	5.33	5.10	3.84	3.71
<b>16</b>	5.28	5.40	3.55	3.72
<b>17</b>	4.70	4.65	3.63	3.58
<b>18</b>	4.35	4.43	3.20	3.44
<b>19</b>	5.00	5.05	3.68	3.68
<b>20</b>	4.93	5.24	3.80	3.77
<b>21</b>	4.29	4.98	3.45	3.67
<b>22</b>	5.03	4.63	3.75	3.58
<b>23</b>	4.58	5.26	3.49	3.76
<b>24</b>	5.61	5.43	3.88	3.84

In the y-scrambling procedure, the average correlation coefficient ( $R$ ) values obtained for TAMH and HuH-7 were 0.368 and 0.333 respectively. The values obtained were low, indicating that the derived regression models did not arise by chance. The QSTR model for TAMH gave better predicted  $LC_{50}$  values compared to experimental  $LC_{50}$  values than the model for HuH-7 as seen from Figure 3-4. Interestingly, both the QSTR models obtained were single-descriptor ( $\log P(o/w)$  and FASA\_H respectively) models. The high correlation coefficients obtained for both models indicate that the toxicity of the twenty-four compounds investigated in this study were strongly dependent

on the lipophilicity of the compounds, which is consistent and affirms our qualitative analysis. It was also observed that the relationship between  $\log P(o/w)$  or FASA\_H and  $\log LC_{50}$  values is linear in both the QSTR model and plots of the two descriptors (Figures 3-5a and 3-5b).

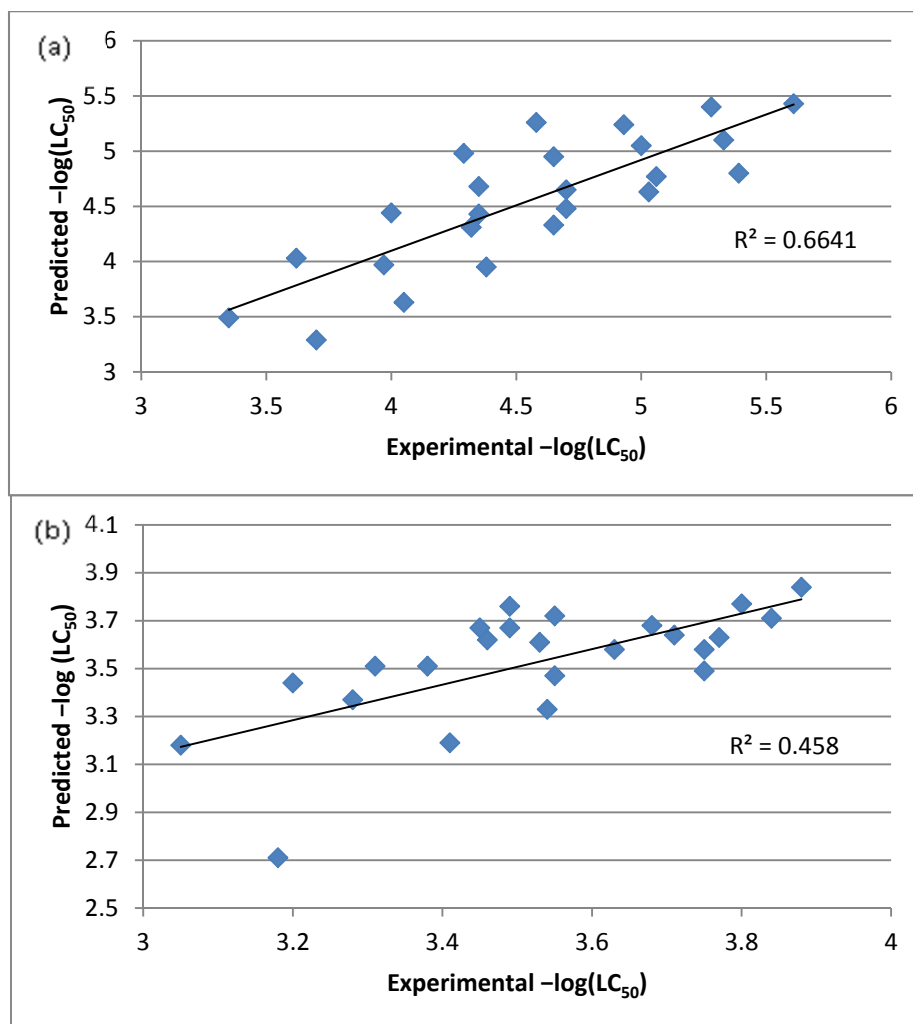


**Figure 3-4** Predicted  $-\log(LC_{50})$  versus experimental  $-\log(LC_{50})$  for (a) TAMH ( $R^2 = 0.6641$ ) and (b) HuH-7 ( $R^2 = 0.458$ ). TAMH is observed to give better predicted values from the QSTR model as compared to HuH-7.

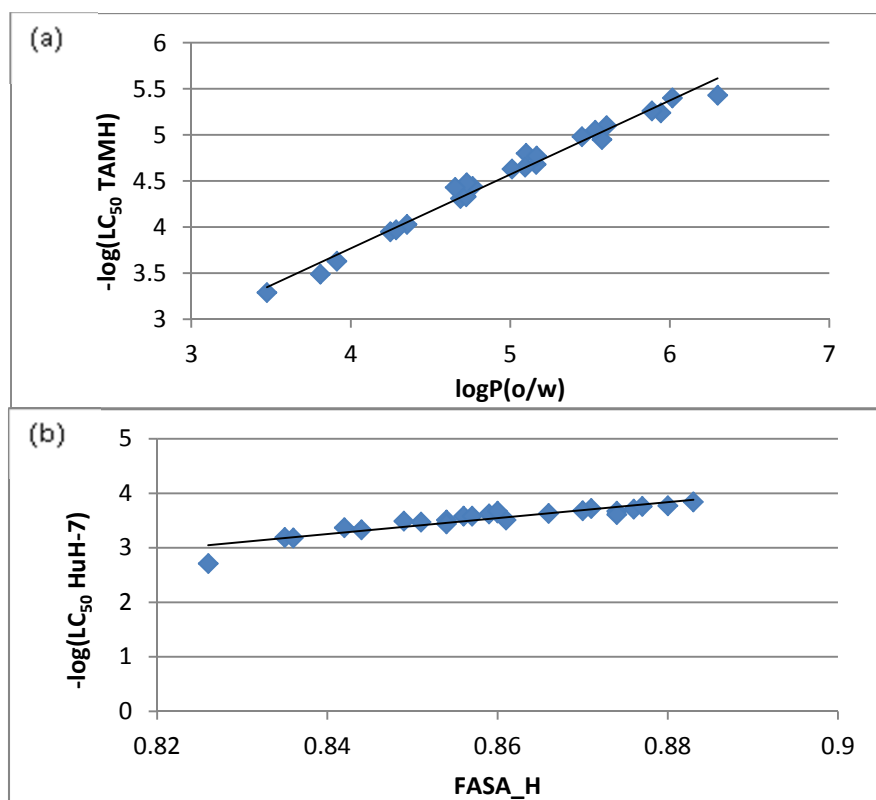


**Figure 3-5** (a) Plot of  $-\log(\text{LC}_{50})$  against  $\log P(\text{o/w})$  for TAMH. A linear relationship was observed with an  $R^2 = 0.9816$ ; (b) Plot of  $-\log(\text{LC}_{50})$  against FASA\_H for HuH-7. A linear relationship was observed with an  $R^2 = 0.8331$ .

### 3.4. Discussion

The subtle structural difference between diclofenac and lumiracoxib and the dramatic differences in both their pharmacology and toxicity alluded to a profound influence of chemical contributors that remains incompletely understood. In this study, we aimed to define a structure-toxicity relationship by exploiting the three positions where analogs of diclofenac are often investigated. Twenty-four compounds were synthesized; their cytotoxicity tested *in vitro* and a QSTR model was generated to investigate structure-toxicity relationship of the compounds. In addition, the activity and selectivity of the compounds were determined *in vitro* and a cross-comparison between toxicity and activity was done.

### 3.4.1. Comparison of cell lines

We performed the cytotoxicity assays of the synthesized compounds on two cell-lines for two reasons: first, to eliminate cell-line specific phenomena, and second, to qualitatively determine the impact of the hosts' metabolic capacities on the onset of toxicity. Two liver cell lines, TAMH and HuH-7 were chosen as cell models for the cytotoxicity studies. TAMH is an immortalized murine hepatocyte cell line derived from transgenic MT42 male mice. Due to the over-expression of TGF- $\alpha$ , TAMH is able to proliferate continuously as a stable monolayer culture (Wu *et al.*, 1994). In addition, TAMH is able to express adult differentiated hepatocytic markers (Wu *et al.*, 1994), unlike liver cancer cell lines. There have been studies which have successfully used TAMH as an *in vitro* model to investigate drug-induced liver toxicity and have shown that this cell line expresses considerable levels of CYP2e1 and CYP3a11 enzymes, which are homologous to human CYP2E1 and CYP3A4 respectively (Pierce *et al.*, 2002; Coe *et al.*, 2007). The Phase I P450s of interest in this study is CYP2C9 and CYP3A4. The mice orthologs to CYP2C9 and CYP3A4 are Cyp2c29 and Cyp3a11 respectively. These orthologs have been shown to carry approximately 80% similarity in both protein sequence and function (McLaughlin *et al.*, 2008).

HuH-7, a representative liver cell line, is widely used. It is a human hepatoma cell line derived from a liver tumor in a Japanese male. Metabolic enzyme profiling of HuH-7 has shown that this cell line expresses considerably low levels of Phase I and Phase II enzymes as compared to primary hepatocytes (Sivertsson *et al.*, 2010; Guo *et al.*, 2011). In addition, the ability of HuH-7 to

metabolize P450s specific substrates was shown to be lower as compared to primary hepatocytes. Given that this cell line has significantly lower metabolic capability, HuH-7 can be used as a comparison to a metabolically active cell line to determine the role of metabolism and reactive metabolite formation in inducing toxicity.

TAMH was utilized as the liver cell line exhibiting greater metabolic capacities. This difference in metabolic capacities was shown in our results obtained whereby key enzymatic activities in TAMH are 5 to 6 folds higher than in HuH-7 (Figure 3-1). Despite a huge difference in metabolic capacities, toxicity of the compounds in TAMH and HuH-7 displayed similar trends. Yet, LC<sub>50</sub> values are consistently much lower in TAMH than HuH-7 (Figure 3-3). It was hypothesized that metabolism to reactive metabolites is one of main reasons behind the toxicity induced by 2-phenylaminophenylacetic acid derivatives. The lower metabolic capability of HuH-7 reduces the propensity of forming reactive metabolites responsible for cytotoxicity. The lower metabolic capability of HuH-7 could mean that the amount of metabolic enzyme sites present in the cells is lower and thus, the highest rate of metabolism in HuH-7 is fixed at a lower level as compared to TAMH at any given time. The results suggest a greater susceptibility of TAMH to the toxicity of the compounds, which undergird the role of bioactivation as a driving mechanism.

### 3.4.2. Effect of substituents on toxicity – relationship with lipophilicity

The substituents on the three positions on both rings A and B affected the lipophilicity of the compounds, with increase in size of alkyl substituents at R<sub>1</sub> and halogen substituents on R<sub>2</sub> and R<sub>3</sub> leading to an increase in cytotoxicity. Increase in toxicity with increase in alkyl substituent size was also observed in other studies on substituted anilines and phenols (Schultz *et al.*, 1989; Cronin and Schultz, 1996). The Hansch ( $\pi$ ) values of alkyl substituents show an increase from hydrogen (0.00) to methyl (0.56), ethyl (1.02), *n*-propyl (1.55), *iso*-propyl (1.53) and finally to *tert*-butyl (1.98) (Selassie, 2003), indicating an increase in lipophilicity of the substituent. Similarly for halogen substituents,  $\pi$  values increase from fluorine (0.14) to chlorine (0.71) and to bromine (0.86) (Selassie, 2003). *iso*-Propyl has a slightly lower  $\pi$  value as compared to *n*-propyl but the effect of that difference on toxicity can be seen clearly from the Hasse diagram. *iso*-Propyl compounds are ranked lower in toxicity as compared to *n*-propyl compounds (Figure 3-2). Looking more broadly at the overall lipophilicity of the compounds, the increase in lipophilicity coupled with increase in toxicity is observed in our study as seen from the linear relationship between log P(o/w) or FASA\_H and log LC<sub>50</sub> values (Figures 3-5a and 3-5b). Both log P(o/w) and FASA\_H are molecular descriptors related to lipophilicity. However, FASA\_H depended on the partial charge and conformation of the molecules while log P(o/w) did not take that into account during calculation. It was also observed that the gradient of the plot for TAMH is steeper than for HuH-7. This could indicate that lipophilicity has a greater effect on toxicity of the compounds in TAMH than in HuH-7. From the QSTR model, TAMH gave better predicted values as compared to HuH-7 (Figure 3-

4). This could be due to the better metabolic capabilities of TAMH. HuH-7 is less sensitive towards the toxicity induced by the compounds as mentioned in section 3.3.3 whereby the difference between the least and most toxic compounds in HuH-7 is much lower than in TAMH. The QSTR model of HuH-7 will thus give a less accurate prediction as the experimental values used to create the model did not truly reflect the actual toxicity of the compounds due to low metabolic capabilities.

Lipophilicity is an important physicochemical property that can affect pharmacological and toxicological effects of drugs in many ways. Lipophilic compounds are generally metabolized to a larger extent in order to increase their hydrophilicity to aid in excretion. The more lipophilic the compound, the rate of metabolism of the compound will be higher. For example, studies done to investigate the relationship between lipophilicity and metabolism rates showed that metabolism rates generally increase with increase in lipophilicity for both Phase I and Phase II (Siraki *et al.*, 2005; Smith *et al.*, 2006). This is because lipophilic compounds are more likely to interact with Phase I and Phase II metabolic enzymes such as cytochrome P450s and UGTs (Little and Ryan, 1982; Lewis *et al.*, 1995; Vashishtha *et al.*, 2001). A possible consequence of increased metabolism would be the generation of reactive metabolites, if such a structural predisposition exists for the given compound. Independent groups found that  $\log P(o/w)$  was an important descriptor in the QSAR models generated from data obtained from *in vitro* cell assays for halogenated benzene ring series and observed that an increase in  $\log P(o/w)$



lead to increased cytotoxicity (Fratello *et al.*, 1997; Chan *et al.*, 2007). This trend was similarly observed in our study.

More lipophilic compounds may have greater binding affinities or higher abilities to disrupt cellular sites, thus causing a direct toxic effect. Absorption also plays a part in effecting toxicity as the compound needs to be absorbed by the cells to exert any toxic effects or to be metabolized. It is interesting to note that while the relationship between toxicity and log P(o/w) values usually follows a bell-shaped trend, we observed a linear proportionality between the two parameters. In situations where cell permeation is a limiting factor for drug accumulation, lipophilicity can alter the extent of toxicity in significant ways. In an *in vitro* cell setting, permeability is chiefly represented by compounds diffusing through the lipid bilayer of the cell membrane. Compounds of greater lipophilicity can diffuse through the lipid bilayer more easily as compared to compounds of lower lipophilicity. The log P(o/w) values of the compounds tested range from 3.5 to 6.3. Presumably, compounds with log P(o/w) values closer to the upper range will be able to cross the lipid bilayer of the cells more easily as compared with those at the lower range. This causes greater accumulation of compounds in the cells, which will increase the magnitude of toxicity induced by the compounds. It is anticipated that at even higher log P(o/w) values, we may be able to observe a trend reversal where solubility and the sequestration of the drugs within the membrane will limit toxicity, hence re-establishing a bell-shaped relationship. Alternatively, it is possible that the proportional increase in toxicity with lipophilicity could be due to a direct toxicant effect. The toxicity caused by the

compounds could be a physical association with off-target cellular sites such as receptors, disruption of cellular sites such as the cell membrane or accumulation within the cells.

#### 3.4.3. Halogen substituents and their role in drug design

Compounds with fluorine substituents at R<sub>2</sub> and R<sub>3</sub> were observed to be the least toxic among the series of compounds in this study. Using the Hasse diagram (Figure 3-2), it was shown that fluorine has the greatest effect on toxicity, namely its ability to decrease toxicity. Not surprisingly, fluorinated drugs (57%) form a huge proportion of drugs approved by the U.S. Food and Drug administration (FDA) as compared to chlorinated (38%) or brominated drugs (4%) (Hernandes *et al.*, 2010). The high proportion of fluorinated drugs may underscore their contribution to better efficacy and absorption, or lowered toxicities as exemplified by the relationship between the halogen groups and toxicity seen in this study. Fluorinated compounds are generally metabolically more stable than the larger sized halogens. Prior studies suggested that fluorine substitution can block metabolic sites or decrease the susceptibility of neighboring moieties to cytochrome P450 enzyme metabolism, which in turn could lead to reduced formation of reactive metabolites (Park *et al.*, 2001). It was found that introduction of fluorine substitutions into the aromatic ring of paracetamol increased the oxidative potential of the parent molecule and subsequently decreased the chances of the metabolite being oxidized to a cytotoxic quinone imine (Barnard *et al.*, 1993). Another classic example of fluorine improving metabolic stability is the addition of a fluorine at the 4-position of the aminophenol ring to block the metabolic site of amodiaquine,

which resulted in the abolishment of bioactivation with said compound (Oneill *et al.*, 1994).

The low proportion of brominated drugs could be due to the common occurrence of elevated toxicity. Brominated compounds were often susceptible to P450-mediated metabolism. Several studies have shown that aromatic compounds carrying bromine substitution were metabolized into reactive species and these were proposed as the mechanisms involved in their toxicities (Monks *et al.*, 1982; McDonald and Rettie, 2007). For example, the hepatotoxicity of benzbromarone was linked to the formation of reactive species via metabolic hydroxylation to catechols (McDonald and Rettie, 2007). Anecdotally, the usage of several brominated drugs such as zimelidine, bromfenac and benzbromarone were curtailed (United-Nations, 2005b; United-Nations, 2005a), thus causing this substituent to be flagged out as a potential toxicophoric group (Nelson, 2001). Mechanistically, this tendency could also have arisen from an intrinsic chemical inactivity due to a shorter and stronger C-F bond as compared to either C-Cl or C-Br. In addition, Cl<sup>-</sup> and Br<sup>-</sup> are weaker bases than F<sup>-</sup>, which make chlorine and bromine better leaving groups as compared to fluorine. Defluorination is thus much less likely to occur than dechlorination and debromination. The relationship reflected in this study is also consistent with several structure-toxicity relationship investigations of halogenated compounds in different biological systems (Schultz *et al.*, 1989; Cronin and Schultz, 1996; Fratello *et al.*, 1997; Warne *et al.*, 1999; Chan *et al.*, 2007). For example, in a study on the toxicity of substituted phenols, it was found that fluoro-substitution generally had the

lowest toxicity and bromo-substitution had the highest toxicity (Cronin and Schultz, 1996). However, it is important to note that the effect of halogen substitution and toxicity is dependent on the overall molecular structure and the substitution positions. Yet, it is interesting to note that in some studies such as structure-toxicity relationships of (bis)aziridinyl-benzoquinones (Prins *et al.*, 1994) and paracetamol analogs (Bessems *et al.*, 1995), the reverse was observed whereby fluoro-substituted compounds are the most toxic. Hence, the exact influence of halogens to toxicity must be contextualized and investigated separately in the light of different chemical scaffolds being used for drug design.

### 3.5. Conclusion

In summary, from the cytotoxicity profile of the synthesized twenty-four 2-phenylaminophenylacetic acid compounds, metabolism could be postulated as an important factor in the toxic effects of the compounds. These compounds were subjected to cytotoxicity studies using MTT assay to determine their cytotoxicity on liver cells. Two liver cell lines, TAMH and HuH-7, were used as a comparison to determine the role of metabolism in the toxicity induced by the compounds. Metabolic enzyme activities were determined for both cell lines and TAMH was shown to be the more metabolically competent one. From experimental results, it was shown that metabolism could be an important factor in the toxic effects of the compounds as the toxic effects were more prominent in TAMH as compared to HuH-7. However, metabolism to reactive metabolites cannot be attributed as the sole cause as direct toxicant effects of the compounds could also be a contributor. Further studies are

required to determine whether metabolism or direct toxicant effects is the more important contributor to the toxicity induced by the compounds.

Substituents on both phenyl rings are crucial in affecting the toxicity of the compounds. As seen from the results obtained, increasing the alkyl group size at R<sub>1</sub> resulted in an increase in toxicity (indicated by a decrease in LC<sub>50</sub> values). Increasing the halogen group size at R<sub>2</sub> and R<sub>3</sub> increased the toxicity. Taken together, difluoro-substituted compounds are the least toxic while dibromo-substituted compounds are the most toxic. The contribution of the changes in substituents to toxicity could be an increase in lipophilic properties of the parent compounds. A QSTR model generated with experimental data clearly showed a linear relationship between lipophilicity and toxicity. Toxicity was shown to increase with increase in lipophilicity.

**Chapter 4. Inhibitory Effects of Synthesized Compounds on COX**  
**Expressing Cell Lines: Potency, Selectivity and Elucidation of Structure-Activity-Toxicity Relationships**

**4.1. Introduction**

Diclofenac and lumiracoxib are NSAIDs that inhibit the prostaglandin synthesis in COX enzymes. Diclofenac is a non-selective COX inhibitor. On the other hand, lumiracoxib is selective towards COX-2. The twenty-four compounds synthesized vary in their alkyl and halogen substituents where many of which were not previously investigated for pharmacological activity. These include those with alkyl groups such as *n*-propyl, *iso*-propyl and *tert*-butyl and bromine. Thus, we would like to investigate the potency and the selectivity towards COX-2, and how the pharmacophore may differ from the toxicophore.

In order to investigate the potency of the compounds, a cell-based assay involving two cell lines that expresses either exclusively COX-1 or COX-2 was used. Enzyme-linked immunosorbent assay (ELISA) was carried out to detect the eicosanoids produced by the cells as a surrogate for COX activities. In the previous chapter, we have evaluated the toxicity of the compounds in liver cell lines. A safety profile was then generated using the toxicity and pharmacological data obtained in order to determine the relationship between activity, selectivity and toxicity.

## 4.2. Experimental methods

COX-1 antibody, rabbit polyclonal IgG and COX-2 antibody, rabbit polyclonal IgG were purchased from Santa Cruz Biotechnology (Dallas, TX).  $\beta$ -actin antibody, mouse monoclonal IgG was purchased from Abcam (Cambridge, UK). Bicinchoninic acid (BCA) Protein Assay Kit and SuperSignal West Chemiluminescent Substrate were purchased from Thermo Scientific Pierce (Waltham, MA). Thromboxane-B<sub>2</sub> (TXB<sub>2</sub>) and prostaglandin-E<sub>2</sub> (PGE<sub>2</sub>) ELISA kits were purchased from Cayman Chemical Company (Ann Arbor, MI). All other chemicals and reagents were obtained from Sigma Aldrich (St. Louis, MO) unless otherwise mentioned.

### 4.2.1. Cell culture

All cultures were maintained in a humidified incubator with 5% carbon dioxide at 37°C unless otherwise stated. COX-1 expressing HEL92.1.7 cells and COX-2 inducible RAW264.7 were obtained from ATCC (Manassas, VA). HEL92.1.7 cells were grown in Roswell Park Memorial Institute Medium 1640 (RPMI 1640) supplemented with 10% FBS, 2 mM glutamine and 1 mM sodium pyruvate. Cells were maintained between  $1 \times 10^5$  and  $1 \times 10^6$  cells/mL. RAW264.7 cells were grown in DMEM supplemented with 10% FBS, 2 mM glutamine and 1 mM sodium pyruvate. Cells were passaged at 80-90% confluence by scraping with a rubber scrapper.

#### 4.2.2. Western blot to determine expression of COX enzymes in cell lines

##### 4.2.2.1. Cell harvesting and lysis

Five million RAW264.7 cells were seeded onto petri dishes and incubated at 37°C, 5% CO<sub>2</sub> for 24 h. Following which, the culture medium was aspirated from each petri dish and replaced with 10 mL medium containing 500 ng/mL or no lipopolysaccharides (LPS) respectively. The cells were incubated at 37°C, 5% CO<sub>2</sub> for 20 h. Likewise, 5 x 10<sup>6</sup> HEL92.1.7 cells were seeded onto petri dishes and incubated at 37°C, 5% CO<sub>2</sub> for 24 h. The cells were harvested and washed with cold 1X PBS, centrifuged at 5000 rpm for 1 min and the supernatant removed. 80 µL of complete cell lysis buffer was added to each cell pellet and incubated in ice for 30 min. The lysates were centrifuged at 4°C, 13,000 rpm for 20 min. The supernatant was collected and protein concentration of each supernatant was determined using BCA Protein Assay Kit. Readouts of sample absorbance in the assay were measured at 560nm by a Tecan M200 Pro plate reader (Männedorf, Switzerland).

##### 4.2.2.2. SDS-PAGE and Transfer

6X Laemmli SDS protein sample buffer (Appendix 4-1) with 6% beta-mercaptoethanol was added to each sample to achieve a final concentration of 1X Laemmli SDS protein sample buffer. Samples were then vortexed and heated at 95°C for 15 min. Samples were subjected to electrophoresis on 5% sodium dodecyl sulfate polyacrylamide gel electrophoresis (SDS-PAGE) stacking and 10% SDS-PAGE resolving gels for 3 h at 60V. Proteins were transferred from gels onto nitrocellulose membranes by electroblotting at 40V and 4°C overnight.



#### 4.2.2.3. Detection

Membranes were blocked with 5% milk in 1X phosphate buffered saline Tween-20 (PBS-T) (Appendix 4-1) for 1 h at room temperature. The membranes were incubated in their respective primary antibodies diluted in 10 mL of 5% milk overnight at 4°C. The membranes were then washed with 1X PBS-T and were subsequently incubated in their respective secondary antibodies diluted in 10 mL of 5% milk at room temperature for 1 h. The membranes were washed with 1X PBS-T, incubated in SuperSignal West Chemiluminescent Substrate and exposed to film in a dark room for development.

#### 4.2.3. Cell-based COX-1 inhibition assay

The assay was carried out as reported elsewhere (Berg *et al.*, 1997). Briefly, HEL92.1.7 cells were seeded at  $1 \times 10^5$  cells/ well in a 96-well plate. Test compounds were dissolved in DMSO and the final DMSO concentration was 0.5% in medium. The cells were incubated for 30 min at 37°C, 5% CO<sub>2</sub> with varying concentrations of test compounds. Arachidonic acid was added to a final concentration of 30 µM and further incubated for 15 min at 37°C, 5% CO<sub>2</sub>. The reaction was stopped by centrifugation (4000 rpm) for 5 min at 4°C. The levels of TXB<sub>2</sub> were measured using the ELISA method.

#### 4.2.4. Cell-based COX-2 inhibition assay

RAW264.7 cells were seeded at a density of  $1 \times 10^5$  cells/ well a 96-well plate and incubated at 37°C, 5% CO<sub>2</sub> for 24 h. The culture medium from each well was then aspirated and replaced with 200 µL of medium containing 500

ng/mL LPS. The cells were incubated at 37°C, 5% CO<sub>2</sub> for a further 20 h. Thereafter, the assaying procedures are similar to the COX-1 inhibition assay. The levels of PGE<sub>2</sub> were measured using the ELISA method.

#### 4.2.5. *In silico* docking of compounds to crystallized COX-isoforms

AutoDock Vina version 1.1.2 (Trott and Olson, 2010) was used to conduct the docking of the compounds into the respective ligand sites of the Protein Data Bank (PDB) structures 1HT8 (COX-1) and 1PXX (COX-2).

For the COX-1 docking, the PDB structure 1HT8 (Chain A) was protonated using the Protonate3D module of the Molecular Operating Environment (MOE) version 2008.10. Thereafter, the coordinates of the geometric center of the co-crystallized ligand acclufenac was determined using MOE. This served as the center of the docking box in AutoDock Vina version 1.1.2. The box was defined by the space within 22 Å in the x-y-z directions from the previously mentioned center. After the docking was completed, the docking scores for each compound were sorted and the best-scoring pose was taken as the putative pose for the compound. The spatial orientation of the docked pose was then compared visually to that of the co-crystallized ligand in order to appreciate any similarities in the interactions with the binding pocket.

The PDB structure 1PXX (Chain A) was used for the COX-2 docking. The protein structure was similarly protonated as previously mentioned. The coordinates of the geometric center of the co-crystallized ligand diclofenac was also determined using MOE. However, the docking box was defined by

the space within 20 Å in the x-y-z directions from the geometric center. AutoDock Vina was also used for the docking of the compounds into COX-2 protein. The best-scoring pose of each compound was also taken as the putative pose in COX-2. Visual inspection against the co-crystallized ligand was also conducted for the docked poses.

### 4.3. Results

#### 4.3.1. Expression of COX enzymes in cell lines

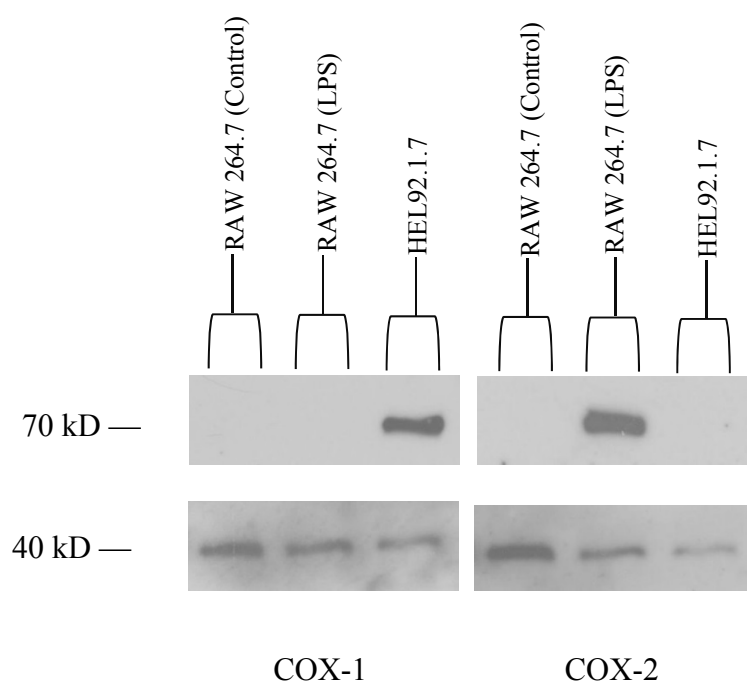


**Figure 4-1** Western blot of HEL92.1.7 and RAW264.7. HEL92.1.7 was shown to express only COX-1 and RAW264.7 was shown to only express COX-2 when induced with LPS.

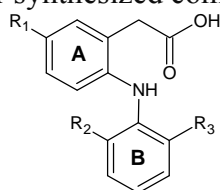
In literature, HEL92.1.7 was shown to only express COX-1 constitutively and RAW264.7 was shown to only express COX-2 when induced with LPS (Berg *et al.*, 1997; Patel *et al.*, 1999). As seen from Figure 4-1, HEL92.1.7 cells were shown to only express COX-1 under normal conditions. RAW264.7 cells did not express any COX-1 or COX-2 under normal conditions. When induced

with LPS, RAW264.7 was shown to express only COX-2. Therefore, we have confirmed and optimized the conditions needed to utilize these cells effectively for the determination of cell-based COX-1 and COX-2 activities.

#### 4.3.2. Activity and selectivity of synthesized compounds

Cell-based COX inhibition assay was used to determine the inhibitory effects of the compounds on the two enzyme isoforms. From Table 4-1, it can be observed that adding an alkyl group at R<sub>1</sub> seemed to have a negative effect on the inhibition potency of the compounds. In general, the larger the alkyl group, the higher the IC<sub>50</sub> values of the compounds in COX-2. For COX-1, the effect of alkyl chain size on the IC<sub>50</sub> values depended on the halogen substituents.

**Table 4-1** COX median inhibitory concentrations (IC<sub>50</sub>), selectivity index and safety index of the twenty-four synthesized compounds.



Compound	R <sub>1</sub>	R <sub>2</sub>	R <sub>3</sub>	IC <sub>50</sub> (nM) <sup>a</sup>		Selectivity Index (COX-1 /COX-2) <sup>c</sup>	Safety Index <sup>d</sup>
				COX-1	COX-2		
<b>1</b>	H	F	Cl	222.2	34.2	6.5	6804
<b>2</b>	H	F	F	3311	152.1	21.8	3373
<b>3 (Diclofenac)</b>	H	Cl	Cl	2.279	10.4	0.2	9058
<b>4</b>	H	Br	Br	9558 <sup>a</sup>	247.8	38.6	148
<b>5 (Lumiracoxib)</b>	Me	F	Cl	2034	46.1	44.1	2410
<b>6</b>	Me	F	F	5172 <sup>a</sup>	432.5	12.0	749
<b>7</b>	Me	Cl	Cl	1364	177.9	7.7	274
<b>8</b>	Me	Br	Br	7414 <sup>a</sup>	2214	3.4	7
<b>9</b>	Et	F	Cl	1945	220.5	8.8	212
<b>10</b>	Et	F	F	13720 <sup>a</sup>	635.5	21.6	168
<b>11</b>	Et	Cl	Cl	91.4	36.8	2.5	573
<b>12</b>	Et	Br	Br	469.8	149.8	3.1	75
<b>13</b>	<i>n</i> -Pr	F	Cl	439.2	238.5	1.8	71
<b>14</b>	<i>n</i> -Pr	F	F	324.9	36860 <sup>b</sup>	0.01	1
<b>15</b>	<i>n</i> -Pr	Cl	Cl	443.7	5041	0.1	2
<b>16</b>	<i>n</i> -Pr	Br	Br	1980	4171	0.5	1
<b>17</b>	<i>i</i> -Pr	F	Cl	1963	2581	0.8	9
<b>18</b>	<i>i</i> -Pr	F	F	815	16290 <sup>a</sup>	0.1	2
<b>19</b>	<i>i</i> -Pr	Cl	Cl	643.4	329.9	2.0	27
<b>20</b>	<i>i</i> -Pr	Br	Br	1234	1056	1.2	5
<b>21</b>	<i>t</i> -Bu	F	Cl	336	3473	0.1	3
<b>22</b>	<i>t</i> -Bu	F	F	148.5	15850	0.01	1
<b>23</b>	<i>t</i> -Bu	Cl	Cl	1495	542.2	2.8	10
<b>24</b>	<i>t</i> -Bu	Br	Br	3002	1863	1.6	2

<sup>a</sup> Each IC<sub>50</sub> value was generated from dose response curve using three technical replicates.

<sup>b</sup> IC<sub>50</sub> value extrapolated from dose response curve using Graphpad Prism 5.

<sup>c</sup> Selectivity Index calculated by ratio of IC<sub>50</sub> value of COX-1 to IC<sub>50</sub> value of COX-2 for each compound.

<sup>d</sup> Safety Index is calculated by toxicity/activity ratio using LC<sub>50</sub> of TAMH and IC<sub>50</sub> of COX-2.

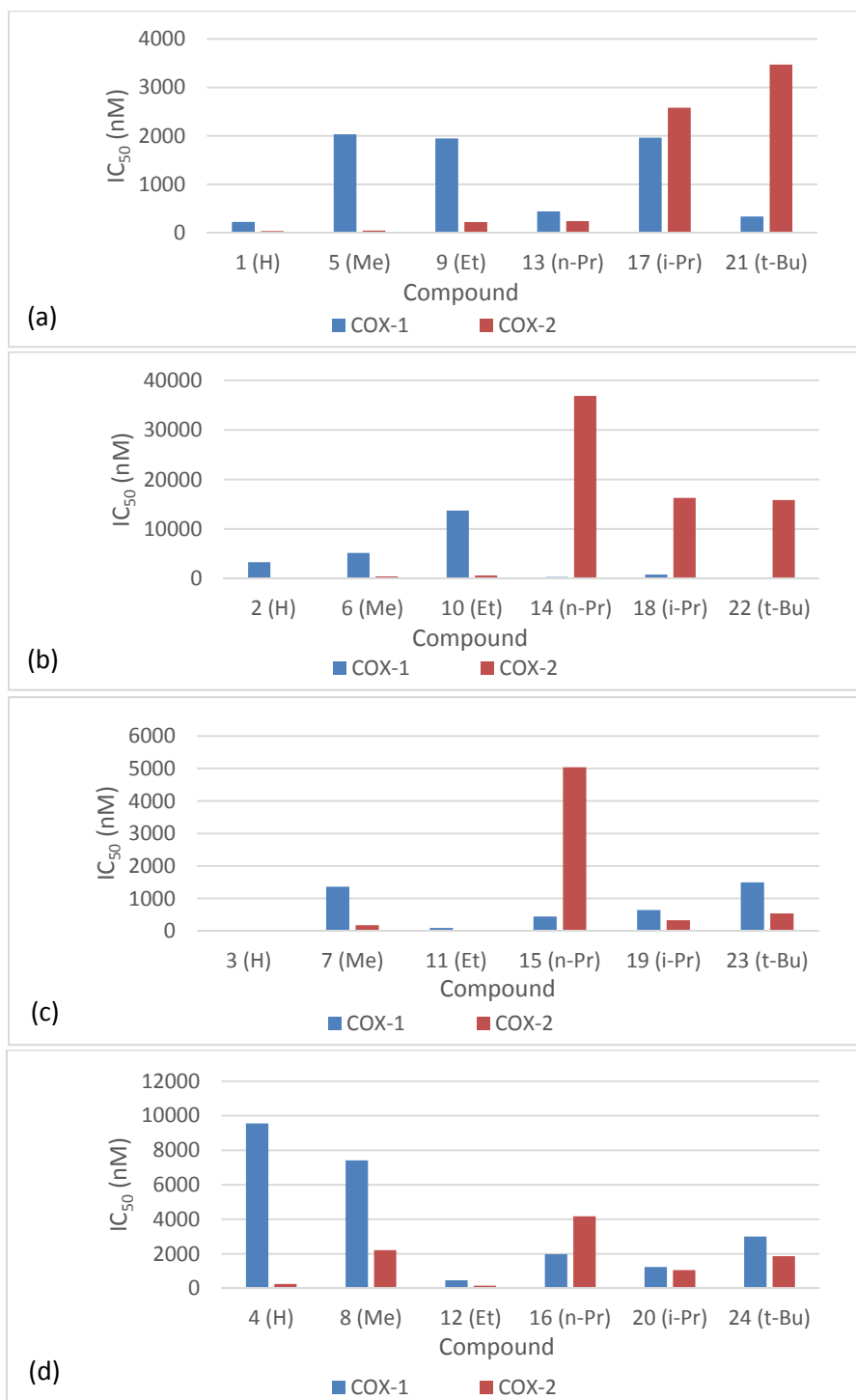


**Figure 4-2** Comparison plots for IC<sub>50</sub> values for COX-1 and COX-2 obtained from cell-based COX inhibition assays for (a) F-Cl series; (b) F-F series; (c) Cl-Cl series and (d) Br-Br series.

Comparing each halogen series, some observations can be made. For the F-Cl series (Figure 4-2a), IC<sub>50</sub> values were observed to increase when alkyl chain sizes increased for both COX isoforms. The effect of adding an alkyl chain to

R<sub>1</sub> (for example, a methyl group) was much more pronounced in COX-1 (approximately 10 times increment) than in COX-2 (approximately 1.3 times increment) as seen from Table 4-1. For the F-F series (Figure 4-2b), IC<sub>50</sub> for COX-1 inhibition increased initially followed by a decrement with increase in alkyl chain. A more consistent trend was observed for COX-2, whereby increases in alkyl chain size increased the IC<sub>50</sub> values. For the Cl-Cl series (Figure 4-2c), a dramatic increase in IC<sub>50</sub> values for both COX isoforms was observed with increase in alkyl chain size. The only exception was compound **11** whereby a decrease in IC<sub>50</sub> values was observed for both COX isoforms as compared to other alkyl chain lengths. For Br-Br series (Figure 4-2d), increase in alkyl chain size overall decreased IC<sub>50</sub> values for COX-1 while an increase in IC<sub>50</sub> values was observed for COX-2. The ethyl substituted compound **12** (COX-1: 469.8 nM and COX-2: 149.8 nM) was observed to be the most potent among the Br-Br series. Overall, we observed that the potency of these series was very poor as compared to diclofenac or lumiracoxib.

Besides the influence of alkyl substitution to the COX inhibiting pharmacophore, the halogen substituents had profound effect on the activity too. It was observed that chlorine substituent at R<sub>2</sub> or R<sub>3</sub> improved the inhibitory effects of the compounds in both COX enzymes. Having at least one chlorine substituent on ring B gave better inhibitory effects on both COX isoforms. Cl-Cl compounds in general possess the highest inhibitory effect in each alkyl series. Fluorine and bromine substituents dramatically decrease the inhibitory effect of the compounds on both COX isoforms. It was noted that replacement of a fluorine substituent with a chlorine substituent improved the

inhibitory effects as seen from hydrogen series compounds **1** and **3** and ethyl series compounds **9** and **11** (Table 4-1). In terms of absolute inhibitory effect, diclofenac (**3**) is the most potent compound out of all the synthesized compounds for both COX isoforms and our reported IC<sub>50</sub> is consistent with literature findings (Moser *et al.*, 1990; Blobaum and Marnett, 2007).

Selectivity was calculated based on the ratio of the activities of the compounds in COX-1 to that in COX-2. A selectivity ratio of 6.5 (Table 4-1, compound **1**) indicates the compound is 6.5 times more selective towards COX-2 than COX-1. From Table 4-1, lumiracoxib (**5**) was the most selective towards COX-2 as compared to other compounds. Adding an alkyl substituent at R<sub>1</sub> did not improve selectivity towards COX-2 by much except in the case of lumiracoxib. For most of the compounds, the improvement in selectivity was only marginal and in some cases, no selectivity was observed. Thus, improved selectivity may arise from the optimal combination of substituents at all three pharmacophoric positions.

**Table 4-2** Comparison of potency ranking of compounds with literature data.

Ranking	COX-1 (Compounds)		COX-2 (Compounds)	
	Our study	Literature	Our study	Literature
Most potent	<b>1</b> <sup>a</sup>	<b>7</b>	<b>1</b>	<b>7</b>
↓	<b>7</b> <sup>c</sup>	<b>1</b>	<b>5</b>	<b>5</b>
Least potent	<b>5</b> <sup>b</sup>	<b>5</b>	<b>7</b>	<b>1</b>

<sup>a</sup> Literature values of compound **1** IC<sub>50</sub>: 30% inhibition at 4 μM (COX-1) and 25% inhibition at 4 μM (COX-2).

<sup>b</sup> Literature values of compound **5** IC<sub>50</sub>: < 20% inhibition at 4 μM (COX-1) and 107 nM (COX-2).

<sup>c</sup> Literature values of compound **7** IC<sub>50</sub>: 40% inhibition at 4 μM (COX-1) and 63 nM (COX-1)



Comparisons between literature findings and our data revealed some discrepancies (Table 4-2). Compounds **1**, **5** and **7** were reported in literature and were tested for both COX-1 and COX-2. Against COX-2, our data showed that Compound **1** (34.2 nM) was the most potent compound of the F-Cl series, followed by compound **5** (46.1 nM). Our data also showed that compound **5** was more potent than compound **7** (177.9nM). In contrast, literature data showed that compound **5** was more potent than compound **1**. Also, compound **7** was shown to be superior to compound **5** (Blobaum and Marnett, 2007). In COX-1, our results showed that compound **1** was more potent than both compounds **5** and **7**. In literature, it was shown that compound **7** was more potent than both compounds **5** and **1** in COX-1 (Blobaum and Marnett, 2007).

A safety index was calculated by dividing the LC<sub>50</sub> of the compound in TAMH by the IC<sub>50</sub> of the compound for COX-2. The safety index indicated that diclofenac (**3**) is the compound with the highest activity and least toxic effects. Interestingly, lumiracoxib (**5**), which has been withdrawn from the market, has a safety index that is approximately 3.8 times lower than diclofenac (**3**). The non-alkylated compounds **1**, **2** and **3** with the exception of compounds **4** were observed to give the highest safety indices. Compounds with ethyl, *n*-propyl, *iso*-propyl or *tert*-butyl substituents at R<sub>1</sub> have very low safety indices. It would seem that inclusion of an alkyl substituent on R<sub>1</sub> added some selectivity but decreased the safety index as shown in Table 4-1. Compounds with bromine or fluorine at both R<sub>1</sub> and R<sub>2</sub> also exhibited low safety indices. It can be concluded that both alkyl substituent at R<sub>1</sub> and

halogen substituents at R<sub>2</sub> and R<sub>3</sub> exert significant impact on the safety of the compounds.

#### 4.3.3. *In silico* docking scores

Docking was carried out to determine the affinity of each compound to each of the two COX isoforms. Crystallized COX-1 bound to an acclufenac ligand and crystallized COX-2 bound to diclofenac were used for the docking studies. The results obtained are summarized in Table 4-3. Docking score is an arbitrary parameter generated by the model where a more negative score indicates greater affinity to the enzyme. It was observed that the compounds in general have higher affinities to COX-2 as compared to COX-1, especially compounds with alkyl substituents at R<sub>1</sub>. While there was general agreement between the *in silico* and *in vitro* data, there were some contradiction between our experimental data and docking scores. Specifically, this occurred with compounds with propyl and butyl substituents at R<sub>1</sub>. For example, **15 – 18, 21** and **22** were observed to have lower IC<sub>50</sub> values for COX-1 but were shown to have higher affinity for COX-2 via docking.

**Table 4-3** *In silico* docking scores for the synthesized twenty-four compounds.

Compound	Docking Scores (Affinity)	
	COX-1	COX-2
<b>1</b>	-8.0	-8.4
<b>2</b>	-8.0	-8.3
<b>3 (Diclofenac)</b>	-7.4	-8.5
<b>4</b>	-7.4	-8.2
<b>5 (Lumiracoxib)</b>	-8.2	-8.7
<b>6</b>	-8.3	-8.8
<b>7</b>	-8.2	-8.6
<b>8</b>	-7.3	-8.1
<b>9</b>	-7.6	-8.6
<b>10</b>	-8.7	-8.5
<b>11</b>	-7.8	-8.4
<b>12</b>	-7.1	-8.1
<b>13</b>	-8.3	-8.9
<b>14</b>	-8.0	-9
<b>15</b>	-7.8	-8.5
<b>16</b>	-7.1	-7.9
<b>17</b>	-8.5	-9.1
<b>18</b>	-8.3	-9.0
<b>19</b>	-8.0	-8.8
<b>20</b>	-7.4	-7.8
<b>21</b>	-7.3	-8.8
<b>22</b>	-7.5	-9.1
<b>23</b>	-6.9	-8.3
<b>24</b>	-6.4	-8.2

The docking poses of diclofenac in both crystallized COX isoforms showed that the carboxylic acid moiety on ring A interacts with Try-385 and Ser-530. We also observed that the chlorine substituent on the compounds shown in Figures 4-3 and 4-4 interacts with four amino acid residues, Ala-527, Ser-530, Val-349 and Leu-531 in COX-1 (Figure 4-3) and two amino acid residues Ser-530 and Ala-527 in COX-2 (Val-349 and Leu-531 not shown on Figure 4-4).

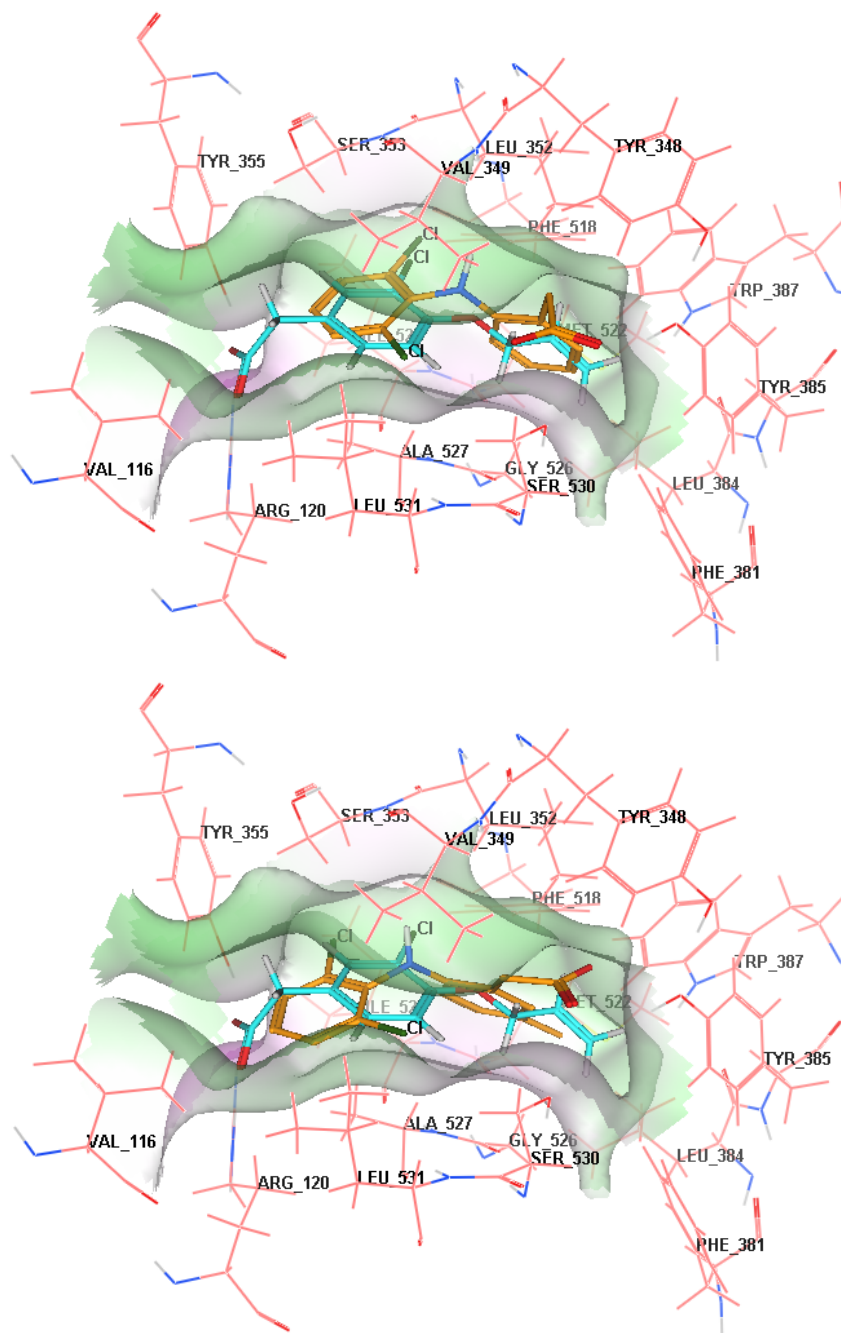


**Figure 4-3** Docking pose of diclofenac (orange, top) and compound **7** (orange, bottom) in COX-1 co-crystallized with acclufenac (blue) as ligand.

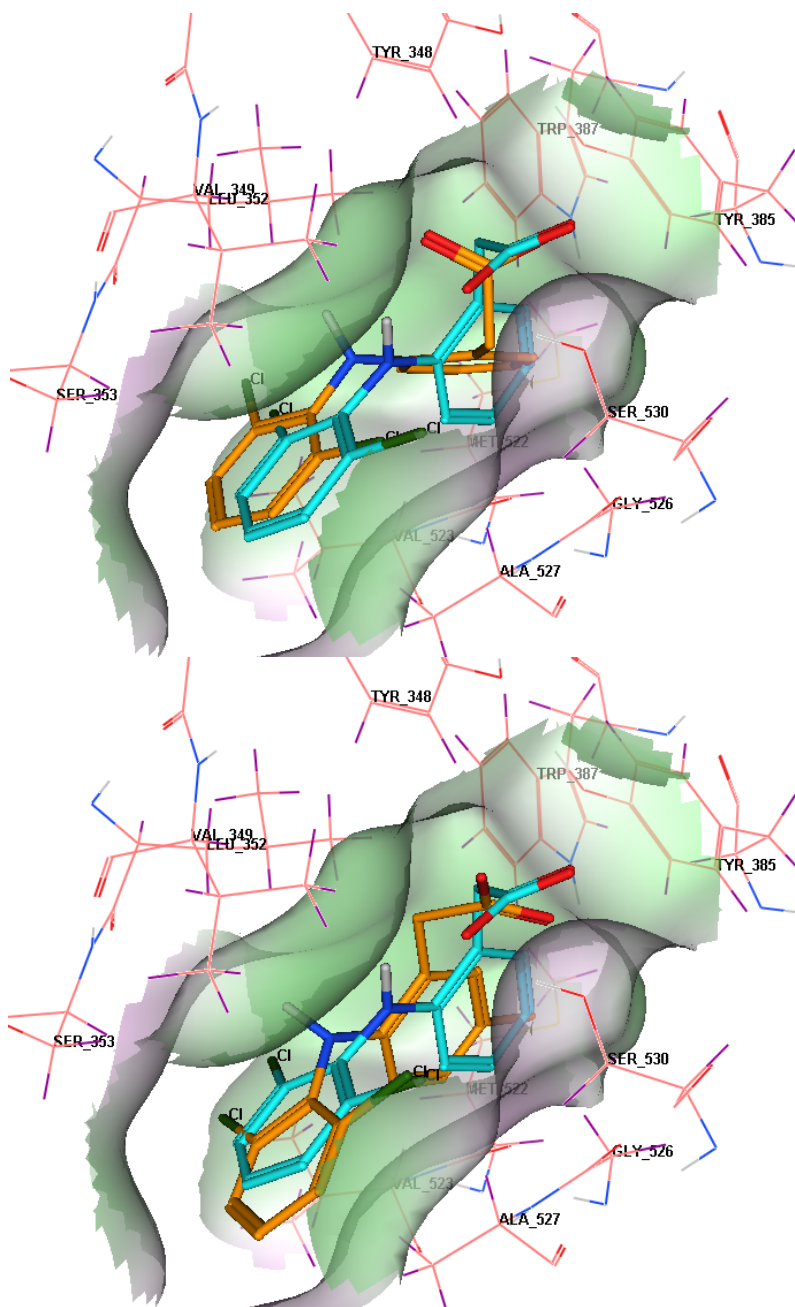


**Figure 4-4** Docking pose of diclofenac (orange, left) and compound 7 (orange, right) in COX-2 co-crystallized with diclofenac (blue) ligand.

#### 4.3.4. Lipophilicity and effect on inhibitory potency of the compounds

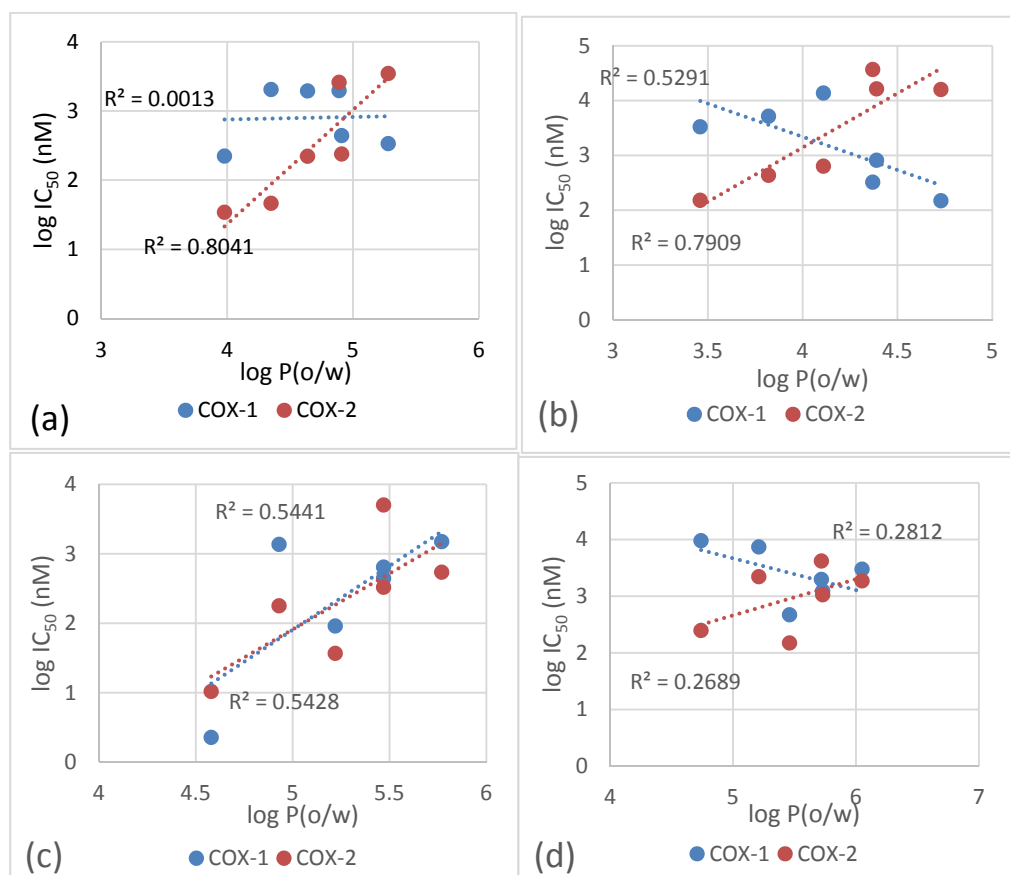


**Figure 4-5** Plot of  $\log IC_{50}$  (nM) against  $\log P(o/w)$  of the compounds for COX-1 (blue) and COX-2 (red) for compound series (a) F-Cl; (b) F-F; (c) Cl-Cl and (d) Br-Br.

In Chapter 3, we observed that lipophilicity and toxicity had a positive relationship. Thus, there was interest to evaluate the influence of lipophilicity on the pharmacological activity. We compared the  $\log P(o/w)$  of the compounds to their COX  $IC_{50}$  values for each of the halogen series. From Figure 4-5, it was observed that lipophilicity played a role in the inhibitory effect of the compounds for COX-2. As whole cell assay was carried, the penetration of the compounds into the cells will be affected by the size and lipophilicity of the compounds. In this instance, lipophilicity of the compounds were measured in terms of  $\log P(o/w)$ . It can be observed that for COX-1, an increase in  $\log P(o/w)$  increased  $IC_{50}$  values only for the Cl-Cl

series. For the F-Cl series, the increase in log P(o/w) across the compounds had little effect on IC<sub>50</sub> values. On the other hand, F-F and Br-Br series showed an opposite trend whereby increase in log P(o/w) decreased IC<sub>50</sub> values and improved inhibitory effects of the compounds. The F-F and Cl-Cl series were observed to give more linear relationships between lipophilicity and inhibitory effect.

As observed from Figure 4-5, a much more consistent trend was observed between lipophilicity and COX-2, especially for F-Cl and Cl-Cl compounds. For all the series, a consistent increase in IC<sub>50</sub> values was observed with increase in log P(o/w) values of the compounds. A more linear relationship was observed for F-Cl and F-F series as seen from Figures 4-5a and 4-5b ( $R^2 = 0.8401$  and  $0.7909$  respectively). The Br-Br series gave the least linear relationship between inhibitory effect and lipophilicity as seen from Figure 4-5d ( $R^2 = 0.2689$ ). This indicated that the correlation between lipophilicity and COX-2 inhibitory activities is weak for Cl-Cl and Br-Br compounds.

#### 4.4. Discussion

##### 4.4.1. Effect of substituents on inhibitory effect and safety of the compounds

The pharmacological properties of the compounds were evaluated using a cell-based assay. A cell-based assay was chosen over conventional enzyme-based assays as whole cells will mimic an environment where absorption and intracellular metabolism occur. The substituents on R<sub>1</sub>, R<sub>2</sub> and R<sub>3</sub> were shown to affect the selectivity and activity of the synthesized compounds in this study as mentioned earlier in section 4.3.2. This is in line with literature whereby it

was found that the methyl group at R<sub>1</sub> was postulated to give rise to the selectivity of the lumiracoxib towards COX-2 (Blobaum and Marnett, 2007). It was hypothesized that an amino acid residue, Leu-384 in the COX isoforms determines the selectivity of lumiracoxib. COX-2 possesses a more flexible Leu-384 due to less steric hindrance between the amino acid residues as compared to COX-1 which allows the methyl group to insert into the small groove created by movement of Leu-384. Our study gave an insight into the possibility of larger alkyl chain lengths to selectively inhibit COX-2. However, with that said, the most selective compound seen in this study was lumiracoxib (Selectivity Index of 44.1). As the alkyl group size at R<sub>1</sub> increased, selectivity was seen to decrease. This could be a restriction on the size on the groove created by movement of Leu-384. It was observed that any alkyl group size bigger than an ethyl group (*n*-propyl, *iso*-propyl and *tert*-butyl) was detrimental to the selectivity towards COX-2.

Compounds that contain at least one chlorine substituent on ring B in general were more potent in the series as compared to other halogen substituents. Both COX isoforms have a hydrophobic pocket made up by four amino acid residues; Ala-527, Val-349, Ser-530 and Leu-531. It was postulated in literature that the substituents on ring B make important binding interactions with this hydrophobic pocket and is crucial in the interaction between compound and enzyme (Blobaum and Marnett, 2007). Chlorine was found to be the best substituent to interact with this hydrophobic pocket via halogen bonds. Fluorine is unable to make halogen bonds which disallow it to form any substantial interactions with the hydrophobic pocket (Wilcken *et al.*,



2013). Although bromine is able to form stronger halogen bonds as compared to chlorine, it may be too big in size to fit into this hydrophobic pocket.

In addition to interaction with the hydrophobic pocket in COX, the angle of twist between the two phenyl rings can affect the potency of the compounds. It was reported that the substituent at R<sub>2</sub> and R<sub>3</sub> affected the angle of twist between the two phenyl rings of the compound and larger substituents contributed to a larger angle of twist, which in turn increased the activity (Moser *et al.*, 1990). Moser *et al.* also indicated that compounds with increasing substituent size at R<sub>2</sub> and R<sub>3</sub> (F-F < Cl-F < Cl-Cl < Cl-Br < Cl-I) improved the potency of the compounds. Given that Cl-Br compound gave better potency than the Cl-Cl compound, we expected the Br-Br compound in our series to have improved potency. However, this was not the case with Br-Br compounds often having lower potency on the COX isoforms. Chlorine is perhaps the best sized substituent to constrain the angle of twist to achieve an optimum spatial relationship between the two rings for interaction with the active site and at least one is needed for potency. The fluorine and bromine may be too small or too large respectively to exert the correct angle of twist between the two phenyl rings. In addition, the need for at least one chlorine substituent to be present could be due to the important interaction with the hydrophobic pocket in the COX enzymes as mentioned in the previous paragraph. It was also reported in literature that potency also arises from the carboxylate group on diclofenac interacting with amino acid residues Ser-530 and Tyr-385 via hydrogen bonding at the top of the active site of both COX isoforms (Rowlinson *et al.*, 2003). The angle of twist of the two phenyl rings

could be necessary to rotate the carboxylate group on ring A to the right conformation to interact with Ser-530 and Try-385. In addition, interaction of chlorine with the hydrophobic pocket mentioned could also be crucial to anchor down the molecule to the right conformation for optimal interactions of the carboxylate group to interact with the two amino acid residues.

The inhibitory effect of the compounds with alkyl substituents at R<sub>1</sub> (**5 – 24**) are lower than of the compounds without substituents at R<sub>1</sub> (**1 – 4**) in both COX isoforms. It was reported in literature that inclusion of the methyl group at R<sub>1</sub> in lumiracoxib decreased the potency of the compound in COX-2 (Blobaum and Marnett, 2007). From our docking results, we observed that the addition of an alkyl substituent at R<sub>1</sub> improved affinity of the compound towards COX-2 as compared to COX-1. This indicates that the compounds should in general be more potent towards COX-2 than COX-1 and thus be selective. However, the docking results showed some contradictions, particularly for compounds with propyl and butyl substituents at R<sub>1</sub> in terms of selectivity. It should be noted that the activity assay used in this study was a cell-based assay while docking is a direct compound-enzyme interaction. Cell-based assays involve other factors such cell penetration, possibility of metabolism and effect on cell viability by the compounds which could affect the activity of the compound towards the COX enzymes. Taking diclofenac (**3**) as an example, in a cell-based assay, diclofenac was shown to be more active towards COX-1 (0.6 nM) than COX-2 (20 nM) (Berg *et al.*, 1997). However, in an enzyme-based assay, the reverse was observed whereby diclofenac is

more active towards COX-2 (28 nM) than COX-1 (67 nM) (Blobaum and Marnett, 2007).

The interactions with the hydrophobic pocket and two amino acid residues at the top of the active site and angle of twist between the two phenyl rings of the compound could be essential in determining the potency of the compound. Adding an alkyl group to R<sub>1</sub> could essentially change the conformation of the compound in the COX active site from an optimal conformation that gives the highest binding interaction to one that is less optimal, thus decreasing the potency of the compound. As seen from Figures 4-3 and 4-4, the docking pose of diclofenac and compound **7** showed the interaction between the chlorine substituent on ring B with the hydrophobic pocket consisting of Ala-527, Val-349, Ser-530 and Leu-531. Also, it can be seen from both figures that the carboxylate group of the two compounds interacted with the two amino acid residues Ser-530 and Tyr-385 at the top of the active site. However, not all of the compounds conform to this binding confirmation. Several compounds have very different docking poses (Appendix 4-2), which could be due to the inflexibility of the crystallized protein structure or the inability of the compounds to conform to the binding conformation of diclofenac due to size issues. This could have affected the docking scores and gave rise to experimental-*in silico* contradictions.

We mentioned previously that with increase in alkyl chain length, we noted a decrease in potency. The exception was compound **11** and **12** whereby the increase of the alkyl chain size at R<sub>1</sub> from methyl to ethyl improved the

potency of the compounds in both COX isoforms. The improvement in potency with the presence of an ethyl group at R<sub>1</sub> towards COX-2 inhibitory potency could be due to the further insertion of the longer ethyl group into the small pocket exposed by the movement of Leu-384. For COX-1, it could simply be due to a larger molecule being fit into the active site. The conformation of the molecule could have changed by further pushing the chlorine or bromine substituent on ring B closer to the hydrophobic pocket consisting of Ala-527, Val-349, Ser-530 and Leu-531. The carboxylate group on ring A could also be pushed closer to Ser-530 and Tyr-385. The increased proximity could translate to stronger halogen or hydrogen bonding to the amino acid residues, which increases the inhibitory potency of compounds **11** and **12** over compounds **7** and **8**.

While some of our findings may not entirely agree with literature findings for a few of the similar compounds, this discrepancy could be due to the differences in experimental methods used. Literature findings were based on a purified enzyme inhibitory assay using purified COX-1 and COX-2 enzymes. On the other hand, we carried out a whole cell assay using cell-lines that expresses one isoform of COX. Additional factors such as cell permeation and cell metabolism can come into play. Thus, differences in the inhibitory effects of the compounds can be expected due to methodology differences. We reasoned that using a cell-based assay over an enzyme-based assay could factor in the effect of cell permeation and metabolism to obtain more broad and comprehensive data on the potency and selectivity of the compounds.

A safety index was calculated using the ratio of LC<sub>50</sub> values in TAMH to the IC<sub>50</sub> values of COX-2 inhibition assay. Diclofenac (compound **3**) possesses the highest safety index out of the twenty-four compounds. It is interesting to note that the other non-alkylated compounds **1** and **2** also possess high safety indices than alkylated compounds. The exception is compound **4**, a dibrominated analog. The safety index is affected by both changes in IC<sub>50</sub> and LC<sub>50</sub> values. The decrease of the safety indices of the compound across the series was due to a significant decrease in LC<sub>50</sub> values due to elevated toxicity (Chapter 3) and a notable increase in IC<sub>50</sub> values due to reduced potency. The ethyl substituent was shown to be favorable towards compound potency for compounds **11** and **12** previously. However, compounds **11** and **12** have rather low LC<sub>50</sub> values (Chapter 3), which indicates that they are rather toxic in nature. Thus, even though they exhibit good inhibition potency towards COX-2, their toxicity negates all beneficial potency effects which resulted in low safety indices. On the other hand, F-F compounds general have low toxicity as seen from their high LC<sub>50</sub> values (Chapter 3). However, the low potency of F-F compounds negates any beneficial effect of their low toxicity, resulting in their low safety indices. It can be concluded that increasing the size of the compound either via addition of alkyl groups on R<sub>1</sub> or swapping out smaller halogens for larger ones at R<sub>2</sub> and R<sub>3</sub> (fluorine to chlorine to bromine) can adversely affect the safety of the compounds *in vitro*.

It is interesting to note that in terms of absolute toxicity, diclofenac (**3**) is shown to be slightly more toxic than lumiracoxib (**5**) (Chapter 3, Table 3-1). This is surprising considering that lumiracoxib was withdrawn from the

market but diclofenac is still widely available. However, taking into account the dose required to achieve the desired pharmacological activity and the safety index calculated for both drugs, lumiracoxib was demonstrated to be less safe than diclofenac. From our findings, diclofenac is only 1.2 times more toxic than lumiracoxib but is 4.4 times more active to achieve the intended COX inhibition. Clinically, lumiracoxib was dosed at high dosages (100 mg to 400 mg) in one sitting while diclofenac is usually dosed at lower dosages (50 mg to 100 mg) two to three times a day or with an extended release formulation (Bannwarth and Berenbaum, 2007; Gan, 2010). This heightened exposure could have been a contributing factor to lumiracoxib's severe toxicity observed in patients (Stepan *et al.*, 2011).

#### 4.4.2. Lipophilicity and its effect on inhibitory potency

It was reported previously that the penetration of the cell membrane by NSAIDs plays a significant role in their activity (Mitchell *et al.*, 1993). Since a cell-based assay was used in our study, lipophilicity can affect the potency via affecting the rate of permeation across the cell membrane into the whole cells. In general, a lipophilic compound of a certain degree can diffuse more easily across the cell membrane. From Figure 4-5, it can be observed that lipophilicity and potency have a linear relationship in COX-2. Consistent across all the series, it was observed that increasing log P(o/w) negatively affects the potency of the compounds. This can be attributed to Lipinski's "Rule of 5" whereby there is a higher probability of poor permeation associated with compounds with log P(o/w) more than 5 (Lipinski, 2000; Lipinski *et al.*, 2001). Poor permeation results in decreased concentration of

compounds within the cell and could potentially affect the inhibition of the compounds on COX enzymes.

On the other hand, the trend for COX-1 was not as consistent as COX-2. In fact opposite trends were observed for the F-F and Br-Br series. It is rather puzzling as in the case of these two series, an increase in log P(o/w) increased the potency of the compounds in COX-1. It was previously reported in a QSAR study of acidic NSAIDs that membrane affinity was only a prerequisite required for COX-2 inhibition and no such relationship was observed for COX-1 (Barbato *et al.*, 1997). The inconsistent trend between lipophilicity and COX-1 observed in our study could thus be explained by the absence of a membrane affinity-COX-1 relationship. Also, the substituents on the compound itself could have exerted more effect on the pharmacology of the compound in COX-1 than the lipophilicity of the compound. F-F and Br-Br may not be favorable substituents for binding into the COX-1 active site; thus, an increase in lipophilicity may not confer significant gains beyond the weak interactions possibly associated with these two series of compounds.

The compounds have an ionizable carboxylic acid. Diclofenac possess a  $pK_a$  of 4.15 (Sangster, 2006) and will exist in its ionizable form at physiological pH. Given the high degree of similarity across the compounds, their  $pK_a$  are not expected to differ dramatically and they should also be significantly ionized under our experimental conditions. Thus, log D(o/w) at pH 7.4 will be a better measurement of the lipophilicity of the compounds. The log D(o/w) at pH 7.4 of the compounds ranges from 0.46 to 3.03 (Appendix 4-3), which is

lower than the Lipinski's "Rule of 5". However, since the compounds are charged, permeation through the cell membrane is often hindered. Thus, overall lipophilicity of the compound could have a less important role in affecting the potency of the compounds. On the other hand, the substituent combinations on the molecule could have a greater effect on the potency of the compounds. We mentioned earlier in section 4.4.1 that interaction of substituents with the hydrophobic pocket in COX enzymes was important in determining the potency of the compound. Previous QSAR studies have further proposed that the lipophilicity of the individual substituents on the chemical backbone of the compound played significant roles in the determining the potency of the compounds (Wilkerson *et al.*, 1995; Prasanna *et al.*, 2005). Thus, the interplay of these factors (for example, overall lipophilicity, substituent lipophilicity, substituent positioning) on overall efficacy would be a better estimate than relying only on a single factor.

#### 4.5. Conclusion

The pharmacological aspect of the compounds in terms of their inhibitory effects on COX-1 and COX-2 was determined using whole cell assay. Two cell lines, HEL92.1.7 and RAW264.7, which expresses COX-1 constitutively and COX-2 when induced respectively were used in the study. In terms of absolute activity, diclofenac (compound **3**) was found to be the most potent in both COX isoforms. In general, the addition of an alkyl group at R<sub>1</sub> on ring A of the compound was observed to decrease potency. The increase in the alkyl group size was also observed to decrease the potency of the compounds. The halogen substituents at R<sub>2</sub> and R<sub>3</sub> on ring B were found to affect the activity in



addition to the alkyl group at R<sub>1</sub>. It was observed that the presence of at least one chlorine substituent improved the potency of the compounds. In general, fluorine or bromine substituents decreased the potency of the compounds.

The selectivity of the compounds was determined by the ratio of the IC<sub>50</sub> values obtained for COX-1 inhibition to the IC<sub>50</sub> values obtained for COX-2 inhibition. Lumiracoxib (compound **5**) was found to be the most selective of all the compounds. The selectivity arises from the addition of the methyl group at R<sub>1</sub>. It was observed that further increase in alkyl chain length decreased selectivity in general. Changes in halogen substituents also affected selectivity for some compounds. An increase in selectivity was observed to occur with a decrease in absolute potency. Thus, it can be concluded that the right combination of substituents at R<sub>1</sub>, R<sub>2</sub> and R<sub>3</sub> are required for good selectivity and potency.

With the pharmacology data obtained, we generated a safety index to link toxicity to pharmacology. Diclofenac (compound **3**) was found to be the safest among all the compounds but is not selective towards COX-2. Lumiracoxib (compounds **5**), which is selective towards COX-2 had a 3.8 times lower safety index as compared to diclofenac. For many of the other compounds, safety indices were low due to increased toxicity and lowered potency. From this we can conclude that selectivity may come at the expense of compound safety when a larger dose is required due to decreased activity that accompanied increased selectivity.

We also carried out *in silico* docking in order to better understand the interaction of the compounds with both COX isoforms. However, in reconciling these biological findings with *in silico* docking experiments, we experienced contradictions particularly for compounds with propyl and butyl substituents at R<sub>1</sub> in terms of selectivity. It was postulated that the contradictions could be due to the cell-based experimental methodology we used, whereby docking is a direct enzyme-compound interaction. Also, the contradictions could be due to receptor or ligand inflexibility during docking.

Another source of variability we have yet to consider is whether the compounds themselves are biotransformed to generate metabolites of varying affinity to COX enzymes and potential for toxicity. This important property will be the emphasis for the next chapter.

**Chapter 5. Investigations of the Role of Metabolism in the Toxicity of the synthesized compounds: Effect of Substituents on Metabolic Stability Metabolite Reactivity, and Potential Implications on Toxicity**

**5.1. Introduction**

In Chapter 3, we explored the *in vitro* toxicity of the twenty-four compounds in two cell-lines; HuH-7 and TAMH, which exhibit contrasting metabolic capabilities. The outcome led us to postulate that metabolism to reactive metabolites could be a factor that contributes to the toxicity of the compounds. This chapter will expound on the mechanistic details of such metabolism.

In order for reactive metabolites to be formed, the compounds requires a bioactivation process mediated by cellular metabolism. An *in vitro* metabolic stability assessment is a preliminary determination of susceptibility for metabolism. Thus, we carried out metabolic stability assays to determine the metabolic half-lives ( $t_{1/2}$ ) of the compounds in presence of metabolic enzymes. A microsomal incubation system was used to mimic the metabolic system and analysis was carried via liquid chromatography-tandem mass spectroscopy (LC-MS/MS). Both Phase I and Phase II metabolic  $t_{1/2}$  were determined separately.

The metabolites formed can exhibit different reactivity and toxicity. Therefore, a necessary follow-up would be to evaluate the reactivity of the metabolites. The reactive metabolites of toxicological significance are often electrophiles that can conjugate to cellular nucleophiles (Williams *et al.*, 2002). Thus,

depletion of cellular nucleophiles can be a surrogate marker of the reactivity of the reactive metabolites formed from the compounds. In this work, we consider the use of GSH, a tri-peptide consisting of glutamic acid, glycine and cysteine. The sulfhydryl group on the cysteine moiety presents a soft nucleophilic site for attack by soft electrophiles such as quinone imines generated via Phase I metabolism. Thus, the depletion of GSH is often used as an indicator of cellular toxicity. We performed a cell-based GSH depletion assay in TAMH cells and used the GSH-binding fluorescence probe, monochlorobimane (MCB), to detect GSH remaining in the cells after exposure to the compounds (Rice *et al.*, 1986).

Acyl glucuronides (AGs) generated by Phase II metabolism of diclofenac had been linked to the hepatotoxicity caused by the drug via formation of reactive metabolites from transacylation and acyl migration (Kretzrommel and Boelsterli, 1994a; Grillo *et al.*, 2003). Since our synthesized analogues preserve the carboxylic acid moiety which is required for the formation of AGs by UGTs, we cannot occlude the possibility that AGs can contribute to the toxicity of the compounds. Yet, the effect of different substituents on the change in metabolism and reactivity of the glucuronides has not been studied. Thus, we investigated the reactivity of AGs by biosynthesizing said AGs in a microsomal incubation system. As opposed to Phase I reactive metabolites, AGs are hard electrophiles, they require hard nucleophiles to trap (Srivastava *et al.*, 2010). Hence, we used a dipeptide consisting of phenylalanine and lysine (Phe-Lys) as the nucleophilic trap. The un-trapped and trapped AGs were quantified by LC-MS/MS to determine their reactivity.

The studies done in this chapter will allow us to improve our understanding of the role of metabolism and bioactivation in the toxicity observed with the compounds. Given the changes in toxicity associated with changes in substituents, we hypothesize that metabolic stability and metabolite reactivity will change with different substituents. In addition, highly toxic compounds were expected to be metabolically unstable and form highly reactive metabolites.

## 5.2. Experimental methods

Pooled human liver microsomes (HLM) (20 mg/mL) were purchased from XenoTech (Lenexa, KS). *Nicotinamide adenine dinucleotide phosphate* (NADP<sup>+</sup>) was from ENZO (Farmingdale, NY). UDPGA was from Nacalai Tesque (Kyoto, Japan). Phe-Lys hydrochloride and 3-phenylpropionic acid were from MP Biomedicals (Santa Ana, CA). Bio-Rad Protein Assay Kit was purchased from Bio-Rad Laboratories (Hercules, CA). HPLC/spectro grade acetonitrile and methanol were from Tedia Company (Fairfield, OH). All other reagents and chemicals were from Sigma-Aldrich (St. Louis, MO) unless otherwise stated.

### 5.2.1. Microsomal incubation for Phase I metabolic stability assay

Stock solutions of compounds in acetonitrile were prepared individually. Each compound (1  $\mu$ M) was incubated with shaking at 37°C in an incubation system consisting of 100 mM potassium phosphate buffer (pH 7.4), 0.5 mg/mL HLM, 1.3 mM NADP<sup>+</sup>, 3.3 mM glucose-6-phosphate, 0.4 U/mL glucose-6-phosphate dehydrogenase, 3.3 mM magnesium chloride and 0.05

mM sodium citrate. The final organic solvent concentration was 0.25% v/v. Aliquots of the incubation mixture were transferred out and quenched in ice cold acetonitrile containing an internal standard (indomethacin or compound **23**) at time points of 0, 5, 10, 15, 20, 30 and 60 min. Each aliquot was vortexed for 30 s and centrifuged down at 13,000 rpm for 20 min at 4°C. The supernatant was collected and injected into LC-MS/MS for analysis.

#### 5.2.2. Microsomal incubation for Phase II metabolic stability assay

Stock solutions of compounds in acetonitrile were prepared individually. HLM (0.5 mg/mL) and alamethicin (25 ug/mg protein) in 100 mM potassium phosphate buffer were incubated in ice for 15 min. After which, each compound (1 µM), 1 mM magnesium chloride and 4 mM UDPGA were added and the mixture incubated with shaking at 37°C. The final organic solvent concentration was 0.25% v/v. Aliquots of the incubation mixture were transferred out and quenched in ice cold acetonitrile containing an internal standard (indomethacin or compound **23**) at time points of 0, 5, 15, 30, 45 and 60 min. Each aliquot was vortexed for 30 s and centrifuged down at 13,000 rpm for 20 min at 4°C. The supernatant was collected and injected into LC-MS/MS for analysis.

#### 5.2.3. Microsomal incubation for AG reactivity

##### 5.2.3.1. Incubation for AG formation

The incubation method from elsewhere was carried out with modifications (Wang *et al.*, 2004). Stock solutions of compounds were prepared in DMSO individually. HLM (1.0 mg/mL) and alamethicin (25 ug/mg protein) in 100

mM potassium phosphate buffer were incubated in ice for 15 min. After which, each compound (300  $\mu$ M), 1 mM magnesium chloride and 4 mM UDPGA were added and the mixture incubated with shaking at 37°C for 1.5 h. The final organic solvent concentration was 0.5% v/v. A half aliquot of microsomal incubation mixture was transferred to an equal volume of 50/50 water/acetonitrile (v/v). The pH was adjusted to 3.5 using 10% acetic acid. An equal volume of acetonitrile containing 10  $\mu$ g/mL 3-phenylpropionic acid was added to the incubation mixture, followed by vortexing for 1 min. The mixture was centrifuged at 13,000 rpm for 20 min at 4°C. The supernatant was collected and injected into LC-MS/MS for analysis.

#### 5.2.3.2. AG-Phe-Lys formation with biosynthesized AGs

A half aliquot of microsomal incubation mixture from section 5.2.3.1 was centrifuged at 13,000 rpm and 4°C for 15 min. The supernatant was transferred to an equal volume of 20 mM Phe-Lys in 100 mM potassium phosphate buffer. The mixture was incubated with shaking at 37°C for 24 h. An equal volume of acetonitrile containing 10  $\mu$ g/mL 3-phenylproponoic acid was added to the incubation mixture, followed by vortexing for 1 min. The mixture was centrifuged at 13,000 rpm for 20 min at 4°C. The supernatant was collected and injected into LC-MS/MS for analysis.

#### 5.2.4. LC-MS/MS analysis

##### 5.2.4.1. LC-MS/MS analysis for metabolic stability assays

Samples generated in incubation experiments were analyzed using LC-MS/MS. Quantitative LC-MS/MS was performed on either an Agilent 1290 Infinity LC

system (Agilent Technologies, Santa Clara, CA) connected to an Agilent 6430 Triple Quadrupole MS (Agilent Technologies, Santa Clara, CA) or an Agilent 1290 Infinity LC system connected to a AB Sciex Qtrap® 5500 (AB Sciex, Framingham, MA). The column used was a Waters AQUITY UPLC BEH C18 120Å, 1.7 µm, 2.1 mm × 100 mm column (Waters Corporation, Milford, MA). The flow rate used was 400 uL/min and the column temperature was set at 40°C. Gradient elution was used to separate the compounds and internal standards. Total run time was 5.1 min and 5.5 min for each sample for Agilent 6430 Triple Quadrupole MS and AB Sciex Qtrap® 5500 respectively. The LC conditions are summarized in Table 5-1.

**Table 5-1** LC conditions for Agilent 1290 Infinity LC system + Agilent 6430 Triple Quadrupole MS (left) and Agilent 1290 Infinity LC system + AB Sciex Qtrap® 5500 (right).

Agilent 1290 Infinity LC system + Agilent 6430 Triple Quadrupole MS			Agilent 1290 Infinity LC system + AB Sciex Qtrap® 5500		
Mobile Phase	A: 0.2% formic acid, aqueous		Mobile Phase	A: 0.1% formic acid, 5 mM ammonium formate, aqueous	
	B: Acetonitrile			B: Acetonitrile	
Time (min)	% B	Flow (µL/min)	Time	% B	Flow (µL/min)
0.0	20.0	500	0.0	20.0	400
0.2	20.0	500	0.2	20.0	400
3.2	95.0	500	3.2	95.0	400
3.9	95.0	500	3.9	95.0	400
4.1	20.0	500	4.1	20.0	400
5.1	20.0	500	5.5	20.0	400

Negative ion ESI LC-MS/MS was carried out to quantify the amount of compound in each sample. The LC effluent was introduced directly into the MS. The multiple reaction monitoring (MRM) mode was applied to each sample analysis. Compound dependent parameters such as declustering



potential (DP), entrance potential (EP), collision energy (CE) and collision cell exit potential (CXP) were optimized for each individual compound. Operation parameters for each LC-MS/MS system are summarized in Table 5-2. Precursor and product ions utilized for MRM analysis are listed in Appendix 5-1. Evaluation of loss of parent compound with time against internal standard was carried out using MassHunter Workstation Quantitative Analysis (Agilent Technologies, Santa Clara, CA) or Analyst® Software version 1.5.2 (AB Sciex, Framingham, MA). Linear regression models for calculation of metabolic  $t_{1/2}$  are listed in Appendix 5-3.

**Table 5-2** MS source parameters for Agilent 6430 Triple Quadrupole MS (left) and AB Sciex Qtrap® 5500 (right).

Agilent 6430 Triple Quadrupole MS		AB Sciex Qtrap® 5500	
Source parameters		Source parameters	
Temperature (°C)	325	Temperature (°C)	500
Gas flow (L/min)	10.0	Curtain gas (psi)	25.0
Nebulizer pressure (psi)	40.0	Gas 1 (psi)	50.0
Capillary voltage (V)	-3500	Gas 2 (psi)	60.0
		Collision gas (psi)	Medium
		IonSpray voltage (V)	-4500

#### 5.2.4.2. LC-MS/MS analysis for AG reactivity

Samples generated in incubations experiments were analyzed using LC-MS/MS. Quantitative LC-MS/MS was performed on an Agilent 1290 Infinity LC system connected to a AB Sciex Qtrap® 5500. The column used was a Waters AQUITY UPLC BEH C18 120Å, 1.7 µm, 2.1 mm × 100 mm column. The flow rate used was 400 uL/min and the column temperature was set at 35°C. The mobile phase consisted of 5 mM aqueous ammonium formate, pH 5.0 (A) and acetonitrile (B). Gradient elution was used to separate the

compounds and internal standards. Total run time was 15 min for each sample.

The LC conditions are summarized in Table 5-3.

**Table 5-3** LC conditions for AG reactivity analysis.

Mobile Phase	A: 5 mM ammonium formate, pH 5.0	B: Acetonitrile
Time (min)	% B	Flow ( $\mu\text{L}/\text{min}$ )
0.0	20.0	500
2.0	20.0	500
10.0	95.0	500
12.0	95.0	500
13.0	20.0	500
15.0	20.0	500

Negative ion ESI LC-MS/MS was carried out to analyze the analyte in each sample. The LC effluent was introduced directly into the MS. Single ion mode (SIM) mode was applied to individual sample analysis. Operation parameters for the LC-MS/MS system are summarized in Table 5-4. Masses used for SIM analysis are listed in Appendix 5-2. Evaluation of analytes relative to internal standard was carried out using Analyst® Software version 1.5.2.

**Table 5-4** MS source parameters for AG reactivity analysis.

Source parameters	
Temperature ( $^{\circ}\text{C}$ )	400
Curtain gas (psi)	25.0
Gas 1 (psi)	50.0
Gas 2 (psi)	60.0
IonSpray voltage (V)	-3500
DP (V)	-90.0
EP (V)	-10.0

#### 5.2.5. Cell-based GSH depletion assay using TAMH cells

TAMH cells were cultured as described in Chapter 3. TAMH cells were seeded at  $3.5 \times 10^4$  cells per well in a 12-well plate. Test compounds were dissolved in DMSO and the final DMSO concentration was 0.5% v/v in

medium. The cells were treated with compounds at a concentration of 20  $\mu\text{M}$  or 10  $\mu\text{M}$ . Diethyl maleate was used as a positive control at concentrations of 0.5  $\mu\text{M}$  and 1.0  $\mu\text{M}$ . The exposure period was 6 h at 37°C, 5%  $\text{CO}_2$ . 100  $\mu\text{M}$  of MCB in medium was added and further incubated in the dark at 37°C, 5%  $\text{CO}_2$  for 3 h. The cells were harvested by scraping and centrifuged at 5000 rpm and 4°C for 1 min. The cell pellet was washed with 1X PBS and lysed in 0.1% Triton-X in 1M Tris-HCL, pH 7.4. The lysate was sonicated in a water sonicator for 1 min, incubated in ice for 30 min, followed by centrifugation at 13,000 rpm for 20 min. The fluorescence signal of the supernatant was read at an excitation wavelength of 380 nm and emission wavelength of 485 nm using a Tecan M200 Pro plate reader (Männedorf, Switzerland). To prepare a standard calibration curve, GSH at varying concentrations were incubated with 1 U/mL glutathione-S-transferase, 100  $\mu\text{M}$  of MCB and 1X PBS with shaking in the dark at 37°C. Protein quantification was carried out using the Bio-Rad Protein Assay.

#### 5.2.6. Linear regression for relationship investigation of metabolic stability, reactivity and toxicity

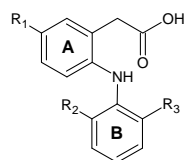
Linear regression was carried out for the following three relationships: metabolic stability and metabolic reactivity; metabolic stability and toxicity; metabolic reactivity and toxicity using Graphpad Prism 5 (Graphpad Software Inc., San Diego, CA).

### 5.3. Results

#### 5.3.1. Metabolic stability of compounds towards Phase I and Phase II metabolism

The metabolic stability of the compounds for both Phase I and Phase II metabolism was investigated by microsomal incubation assays followed by LC-MS/MS analysis. Both phases of metabolism were carried out separately by using the appropriate co-factors required by the metabolic enzymes.

**Table 5-5** Phase I and Phase II microsomal metabolic  $t_{1/2}$  of the twenty-four compounds.



Compound	R <sub>1</sub>	R <sub>2</sub>	R <sub>3</sub>	Phase I Metabolic $t_{1/2}$ (min) <sup>a</sup>	Phase II Metabolic $t_{1/2}$ (min) <sup>a</sup>
<b>1</b>	H	F	Cl	9.9 ± 2.4	22.9 ± 3.3
<b>2</b>	H	F	F	10.9 ± 1.6	43.1 ± 9.6
<b>3 (Diclofenac)</b>	H	Cl	Cl	10.7 ± 1.5	16.9 ± 2.3
<b>4</b>	H	Br	Br	25.7 ± 3.1	10.5 ± 1.1
<b>5 (Lumiracoxib)</b>	Me	F	Cl	13.8 ± 2.1	38.4 ± 6.4
<b>6</b>	Me	F	F	9.8 ± 1.8	60.6 ± 9.7
<b>7</b>	Me	Cl	Cl	27.1 ± 1.5	9.2 ± 0.7
<b>8</b>	Me	Br	Br	39.6 ± 1.1	7.9 ± 2.1
<b>9</b>	Et	F	Cl	44.6 ± 3.2	12.9 ± 3.0
<b>10</b>	Et	F	F	50.7 ± 3.9	16.8 ± 3.7
<b>11</b>	Et	Cl	Cl	35.6 ± 7.5	9.9 ± 4.0
<b>12</b>	Et	Br	Br	47.1 ± 9.1	6.9 ± 2.6
<b>13</b>	<i>n</i> -Pr	F	Cl	11.1 ± 1.4	12.0 ± 2.6
<b>14</b>	<i>n</i> -Pr	F	F	19.6 ± 1.4	24.7 ± 4.8
<b>15</b>	<i>n</i> -Pr	Cl	Cl	8.2 ± 0.7	19.6 ± 6.3
<b>16</b>	<i>n</i> -Pr	Br	Br	4.6 ± 1.1	11.9 ± 4.1
<b>17</b>	<i>i</i> -Pr	F	Cl	22.4 ± 1.6	15.8 ± 1.8
<b>18</b>	<i>i</i> -Pr	F	F	43.5 ± 5.7	24.3 ± 5.0
<b>19</b>	<i>i</i> -Pr	Cl	Cl	20.0 ± 1.7	12.3 ± 4.4
<b>20</b>	<i>i</i> -Pr	Br	Br	15.5 ± 1.0	16.5 ± 4.9
<b>21</b>	<i>t</i> -Bu	F	Cl	20.3 ± 2.6	33.0 ± 6.3
<b>22</b>	<i>t</i> -Bu	F	F	59.4 ± 6.3	47.9 ± 1.8
<b>23</b>	<i>t</i> -Bu	Cl	Cl	14.9 ± 1.7	28.4 ± 7.5
<b>24</b>	<i>t</i> -Bu	Br	Br	25.7 ± 3.1	18.4 ± 1.1

<sup>a</sup> Metabolic  $t_{1/2}$  was determined from triplicates and is expressed as mean ± standard deviation.

Metabolic  $t_{1/2}$  was calculated as 50% decrease in peak area ratio of compound relative to internal standard over time against the peak area ratio of compound relative to internal standard at the 0 min time point. The metabolic  $t_{1/2}$  of the compounds are listed in Table 5-5. For Phase I metabolic  $t_{1/2}$ , the values ranged from 4.6 min (lowest) to 59.4 min (highest). For Phase II metabolic  $t_{1/2}$ , the values ranged from 6.9 min (lowest) to 60.6 min (highest). The Phase I metabolic  $t_{1/2}$  value obtained for diclofenac in our experiment ( $10.7 \pm 1.5$  min, 0.5 mg/mL HLM) was similar to previous literature findings ( $11 \pm 3$  min, 0.3 mg/mL HLM) despite having used a higher concentration of HLM (Obach, 1999). On the other hand, the Phase II metabolic  $t_{1/2}$  value obtained for diclofenac ( $16.9 \pm 2.3$  min, 0.5 mg/mL HLM) was much shorter as compared to literature findings (32 min, 1.0 mg/mL HLM) (Perloft *et al.*, 2006).

### 5.3.1.1. Effect of changes in substituents on Phase I metabolic stability

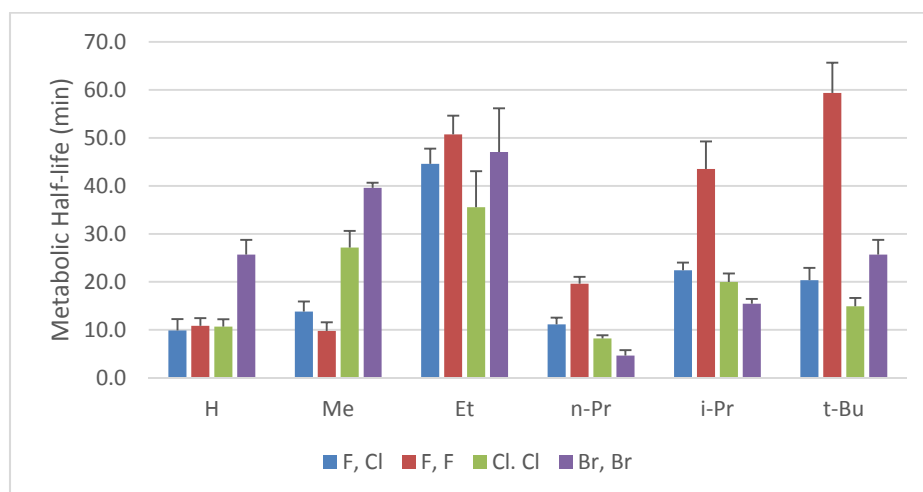


**Figure 5-1** Comparison plot for Phase I metabolic stability between halogen substituents at R<sub>2</sub> and R<sub>3</sub> grouped by R<sub>1</sub> substituents.

Figure 5-1 shows a comparison between halogen substituents at R<sub>2</sub> and R<sub>3</sub> grouped by alkyl group at R<sub>1</sub>. The comparison plot showed that for Phase I metabolic  $t_{1/2}$  values, halogen substituents have significant effects on the

metabolic stability of the compounds. The Cl-Cl compounds in general possess relatively shorter  $t_{1/2}$  values as compared to other halogen substituents when alkyl group is kept constant. The only exception was when  $R_1$  was substituted with a methyl group (compound 7) whereby a longer  $t_{1/2}$  value was observed as compared to F-Cl or F-F compounds. F-F compounds were observed to have relatively longer  $t_{1/2}$  than other halogens when alkyl group sizes are bigger than methyl. Similar to F-F compounds, F-Cl compounds were observed to have longer  $t_{1/2}$  values as compared to Cl-Cl compounds but not Br-Br compounds when alkyl group size at  $R_1$  increases beyond methyl. For Br-Br compounds, we observed that the compounds were generally more stable as compared to other halogen substituents except in the case where  $R_1$  was a propyl substituent (*n*-propyl or *iso*-propyl).

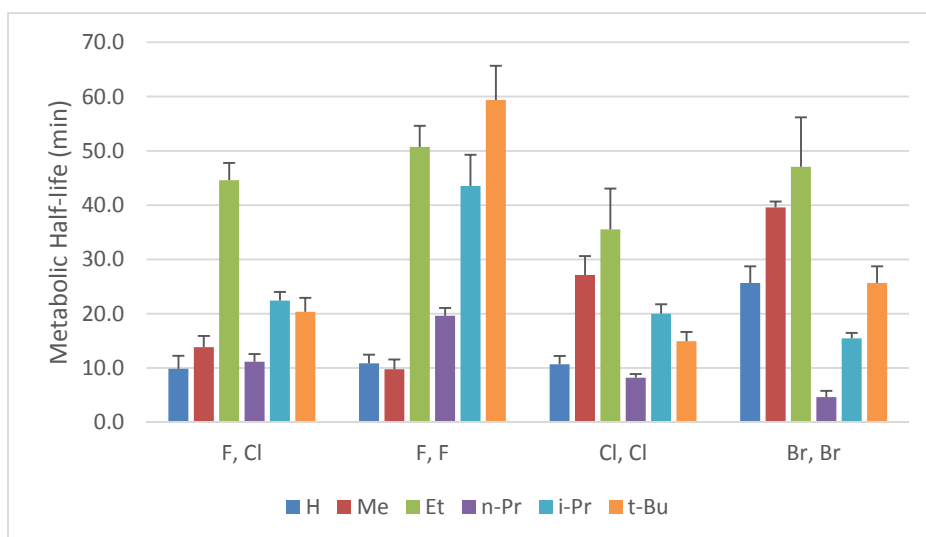


**Figure 5-2** Comparison plot for Phase I metabolic stability between alkyl substituents at  $R_1$  and grouped by  $R_2$  and  $R_3$  substituents.

In addition to the effect of halogen substituents, the alkyl substituent at  $R_1$  had an effect on the metabolic stability of the compounds. Notably, the compounds with ethyl at  $R_1$  showed relatively high metabolic stability across all halogen

combinations at R<sub>2</sub> and R<sub>3</sub>, a trend not seen in other alkyl series (Figure 5-2). We observed that with no alkyl group substituent at R<sub>1</sub>, t<sub>1/2</sub> values were generally short except in the case of Br-Br compounds where a notable increase in t<sub>1/2</sub> was observed. For methyl substituents, compounds with at least one fluorine substituent were observed to have low t<sub>1/2</sub> values while the notable increase in t<sub>1/2</sub> were observed for Cl-Cl and Br-Br compounds. The branched alkyl substituents, *iso*-propyl and *tert*-butyl were observed to have similar trends. F-F compounds of these alkyl series were observed to have much longer t<sub>1/2</sub> values as compared to other halogen substituents at R<sub>2</sub> and R<sub>3</sub>. The alkyl substituent that was constantly observed to result in relatively short t<sub>1/2</sub> values was *n*-propyl. Compound **16** (*n*-propyl, Br-Br) was observed to possess the shortest t<sub>1/2</sub> value of all compounds. On the other hand, compound **22** (*tert*-butyl, F-F) was observed to be the most stable compound with the longest t<sub>1/2</sub> value.

### 5.3.1.2. Effect of changes in substituents on Phase II metabolic stability

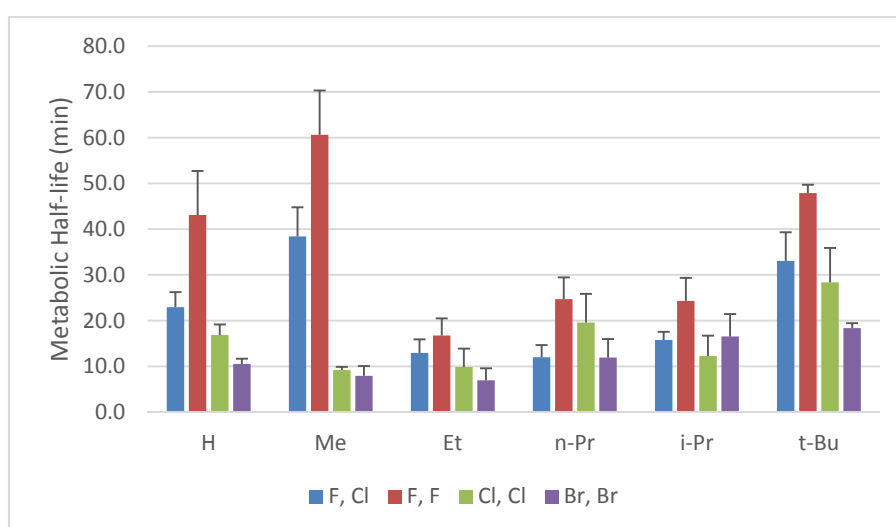


**Figure 5-3** Comparison plot for Phase II metabolic stability between halogen substituents at R<sub>2</sub> and R<sub>3</sub> and grouped by R<sub>1</sub> substituents.

Figure 5-3 shows the comparison between halogen substituents while keeping alkyl substituent at R<sub>1</sub> constant for Phase II metabolic stability. We observed that for Phase II metabolic stability, regardless of the substituent at R<sub>1</sub>, F-F compounds were the most metabolically stable with longer t<sub>1/2</sub> values as compared to other halogen combinations. On the other hand, Br-Br compounds were observed to have relatively shorter t<sub>1/2</sub> values as compared to other halogen combinations. The only exception was compound **20** (*iso*-propyl, Br-Br) where the t<sub>1/2</sub> value was slightly longer than compound **19** (*iso*-propyl, Cl-Cl) and compound **17** (*iso*-propyl, F-Cl). Similar to Br-Br compounds, Cl-Cl compounds were observed to have short t<sub>1/2</sub> values as compared to other halogen combinations but not to Br-Br compounds when alkyl substituent was kept constant. F-Cl compounds were observed to be less metabolically stable as compared to F-F compounds but were mostly found to be significantly more stable than Cl-Cl and Br-Br compounds, especially when alkyl substituent at R<sub>1</sub> is small in size.

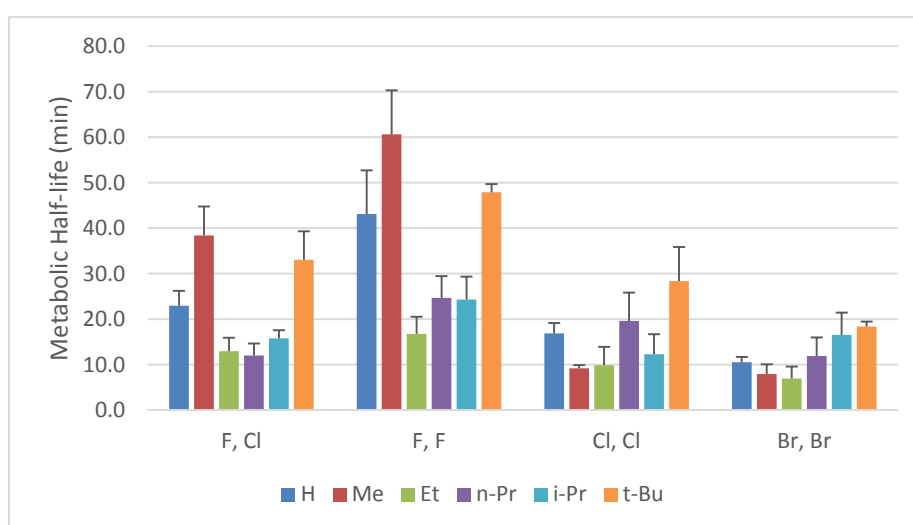


**Figure 5-4** Comparison plot for Phase II metabolic stability between alkyl substituents at R<sub>1</sub> and grouped by R<sub>2</sub> and R<sub>3</sub> substituents.



Figure 5-4 shows the comparison between different alkyl substituents at R<sub>1</sub> while keeping halogen substituents at R<sub>2</sub> and R<sub>3</sub> constant. We observed that ethyl substituent at R<sub>1</sub> resulted in reduced metabolic stability across all halogen combinations. This observation was reverse of what was observed in Phase I metabolic stability whereby ethyl substituted compounds were observed to be more metabolically stable as compared to other alkyl substituted or un-substituted compounds (section 5.3.1.1.). The propyl substituents, *n*-propyl and *iso*-propyl were observed to be similar in t<sub>1/2</sub> values across halogen combinations. Their t<sub>1/2</sub> values were relatively shorter as compared to other alkyl substituents (with the exception of ethyl substituents) for F-F and F-Cl compounds but were observed to be relatively longer for Cl-Cl and Br-Br compounds. The reverse was observed for non-alkylated (H) and methyl substituted compounds where F-Cl and F-F compounds had comparably much longer t<sub>1/2</sub> values as compared to other alkyl substituents, especially in the case of methyl substitution. On the other hand, the non-alkylated or methyl substituted Cl-Cl and Br-Br compounds were shown to have comparably shorter t<sub>1/2</sub> values. *tert*-Butyl substituted compounds were observed to have long t<sub>1/2</sub> values as compared to other alkyl substituents regardless of halogen combinations at R<sub>2</sub> and R<sub>3</sub>. Compound **12** (*tert*-butyl, Br-Br) was found to be the least metabolically stable for Phase II metabolism while compound **6** (methyl, F-F) was found to be the most metabolically stable.

### 5.3.1.3. Inter-comparison between Phase I and Phase II metabolic stability and their relationship with lipophilicity

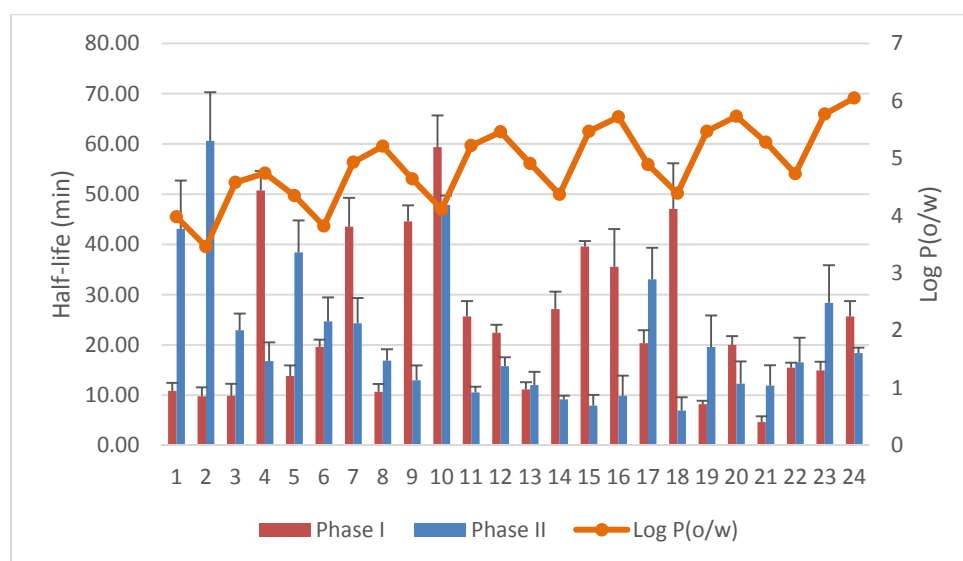


**Figure 5-5** Comparison of Phase I (orange) and Phase II (blue) metabolic  $t_{1/2}$ . Comparison with log P(o/w) (green) with metabolic  $t_{1/2}$  of both metabolic phases.

Comparing between the two phases of metabolism, some interesting observations can be made. As seen from Figure 5-5, some compounds that are more susceptible to Phase I metabolism were less prone to Phase II metabolism, vice versa. A good example will be compound **6**, which was the least stable for Phase I metabolism but is the most stable for Phase II metabolism. Compounds **7** to **12** were observed to be very metabolically stable for Phase I metabolism but were observed to be metabolically unstable for Phase II metabolism. On the other hand, the reverse was seen for compounds **1** to **6** (exception of compound **4**) where the compounds were metabolically unstable for Phase I but metabolically stable for Phase II.

A comparison of the metabolic stability to the lipophilicity of the compounds (indicated by log P(o/w)) showed no apparent relationship. Compounds that

were less lipophilic can possess either low or high metabolic stability for both phases of metabolism. Even with increase in the lipophilicity of the compounds as indicated by the increase in log P(o/w), the metabolic stability of the compounds for both phases fluctuated up and down. It would seem that the actual substituents on the compound scaffold affect the metabolic stability more than the resulting physicochemical properties that arose from the changes in substituent.

### 5.3.2. *In vitro* GSH depletion of the compounds in TAMH

GSH is a cellular nucleophile that is often used as an indicator of cellular toxicity and is usually depleted via conjugation to reactive metabolites and oxidative stress. We performed a cell-based GSH depletion assay in TAMH cells to investigate the extent by which the compounds deplete cellular GSH as a measurement of the reactivity of Phase I metabolites formed from the compounds. Phase I metabolism tend to generate reactive metabolites that are amenable to conjugate soft nucleophiles like GSH, whereas Phase II metabolites preferably conjugate to hard nucleophiles. MCB was used as the probe for cellular GSH. MCB when conjugated to GSH, forms a MCB-GSH adduct which is fluorescent in nature and can be easily detected with a fluorescence detector.

From Table 5-6, the percentage GSH depletion ranged from 6.8% to 71.4%. Compounds **13** to **24**, with the exception of compounds **14**, **18** and **22**, were tested at a lowered concentration of 10  $\mu$ M instead of 20  $\mu$ M. This was due to the extensive cell death caused by the compounds when tested at 20  $\mu$ M,

which made it impossible to obtain measurable turnover and readings from the samples.

**Table 5-6** *In vitro* GSH depletion (%) for the twenty compounds in TAMH cells.

Compound	R <sub>1</sub>	R <sub>2</sub>	R <sub>3</sub>	GSH Depletion (%) <sup>a</sup>
<b>1</b>	H	F	Cl	12.5 ± 4.7
<b>2</b>	H	F	F	12.2 ± 2.7
<b>3 (Diclofenac)</b>	H	Cl	Cl	20.7 ± 9.6
<b>4</b>	H	Br	Br	20.1 ± 9.2
<b>5 (Lumiracoxib)</b>	Me	F	Cl	15.8 ± 6.4
<b>6</b>	Me	F	F	11.8 ± 3.6
<b>7</b>	Me	Cl	Cl	10.2 ± 4.5
<b>8</b>	Me	Br	Br	9.6 ± 5.6
<b>9</b>	Et	F	Cl	14.6 ± 4.5
<b>10</b>	Et	F	F	10.8 ± 6.1
<b>11</b>	Et	Cl	Cl	8.1 ± 5.7
<b>12</b>	Et	Br	Br	71.4 ± 12.2
<b>13</b>	<i>n</i> -Pr	F	Cl	10.2 ± 4.4 <sup>b</sup>
<b>14</b>	<i>n</i> -Pr	F	F	6.8 ± 3.8
<b>15</b>	<i>n</i> -Pr	Cl	Cl	11.7 ± 3.9 <sup>b</sup>
<b>16</b>	<i>n</i> -Pr	Br	Br	44.4 ± 9.0 <sup>b</sup>
<b>17</b>	<i>i</i> -Pr	F	Cl	16.4 ± 6.4 <sup>b</sup>
<b>18</b>	<i>i</i> -Pr	F	F	7.8 ± 3.8
<b>19</b>	<i>i</i> -Pr	Cl	Cl	12.7 ± 4.1 <sup>b</sup>
<b>20</b>	<i>i</i> -Pr	Br	Br	48.6 ± 9.7 <sup>b</sup>
<b>21</b>	<i>t</i> -Bu	F	Cl	10.5 ± 4.1 <sup>b</sup>
<b>22</b>	<i>t</i> -Bu	F	F	17.1 ± 4.9
<b>23</b>	<i>t</i> -Bu	Cl	Cl	45.8 ± 11.1 <sup>b</sup>
<b>24</b>	<i>t</i> -Bu	Br	Br	64.9 ± 19.1 <sup>b</sup>

<sup>a</sup> GSH depletion (%) was determined from biological triplicates and is expressed as mean ± standard error.

<sup>b</sup> Test compound concentration used was 10 µM instead of 20 µM.

Compound **24** showed the highest percentage GSH depletion. Although compound **12** displayed higher apparent percentage depletion as compared to compound **24**, it should be noted that compound **12** was tested at a higher concentration. When tested at 20 µM, compound **24** caused complete cell death at the 6 h time point.

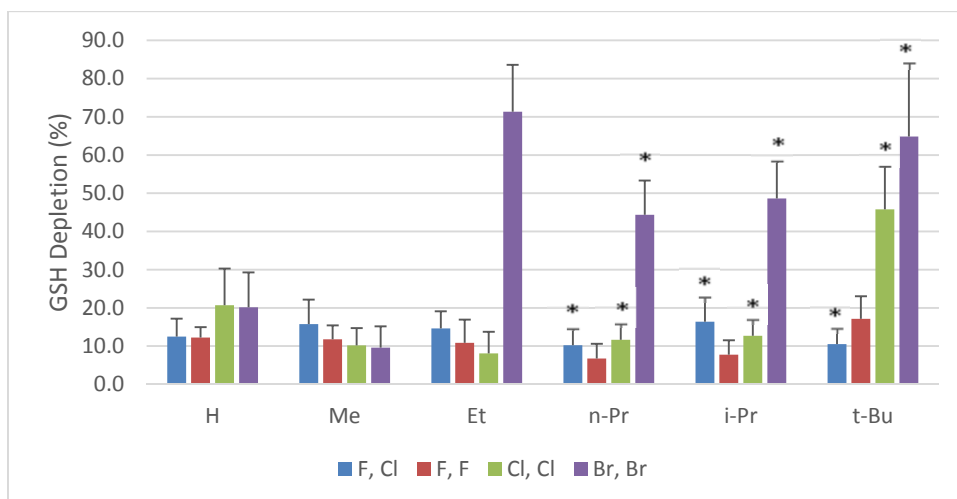


**Figure 5-6** Comparison plot for GSH depletion between halogen substituents at R<sub>2</sub> and R<sub>3</sub> grouped by R<sub>1</sub> substituents. “\*” indicates that test compound concentration used was 10  $\mu$ M instead of 20  $\mu$ M.

The halogen substituents at R<sub>2</sub> and R<sub>3</sub> had an apparent effect on the GSH depletion exhibited by the compounds. A comparison plot (Figure 5-6) across the halogen combinations while keeping alkyl substituents constant showed that Br-Br compounds in general showed more depletion as compared to other halogen combinations, especially when coupled with larger alkyl substituents at R<sub>1</sub> (ethyl, propyls and *tert*-butyl). F-F compounds were observed to have lower GSH depletion as compared to other halogen combinations, especially when coupled with larger alkyl substituents (propyls and *tert*-butyl). F-Cl and Cl-Cl compounds have almost similar trends across all alkyl substituents, with comparable GSH depletion values except in the case of *tert*-butyl substitution whereby Cl-Cl combination saw a significant increase in GSH depletion.

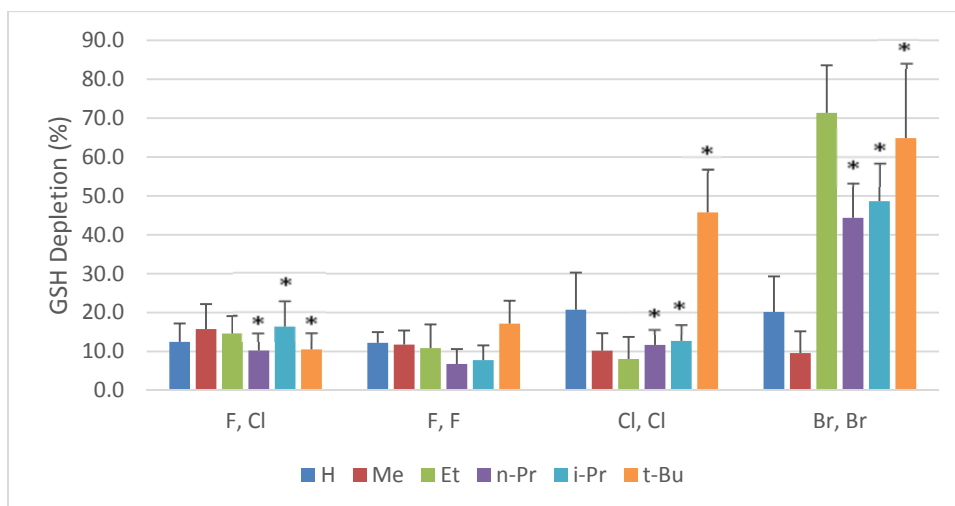


**Figure 5-7** Comparison plot for GSH depletion between alkyl substituents at R<sub>1</sub> and grouped by R<sub>2</sub> and R<sub>3</sub> substituents. “\*” indicates that test compound concentration used was 10 μM instead of 20 μM

Figure 5-7 shows the comparison between alkyl substituents while keeping the halogen combinations constant for GSH depletion. The *n*-propyl, *iso*-propyl and *tert*-butyl substituted compounds of F-Cl, Cl-Cl and Br-Br combinations were tested at a lower concentration due to excessive cell death especially in the case of *tert*-butyl substituted compounds. *tert*-Butyl substituted compounds were observed to have higher GSH depletion as compared to other alkyl substituents. The only exception is compound **21** (*tert*-butyl, F-Cl), where the GSH depletion percentage was observed to be lower than the *iso*-propyl substituted counterpart. For Br-Br compounds, the measured viability of *tert*-butyl substitution was lower than that of ethyl substitution but this is because a lower concentration of 10 μM was used for *tert*-butyl substituted compounds due to excessive cell death at 6 h. *n*-Propyl and *iso*-propyl substituted compounds have similar trends across all halogen combinations. It was observed that the propyl substituted compounds had comparably higher GSH depletion as compared to smaller alkyl substituted or non-alkylated compounds. It is also of importance to note the propyl substituted compounds

were tested at a lower concentration. The only exception was the F-F combination for propyl substituted compounds where GSH depletion was observed to be lower than other alkyl substituted compounds. *iso*-Propyl substituted compounds was shown to have slightly higher GSH depletion as compared to *n*-propyl substituted compounds across all halogen combinations. For non-alkylated and methyl substituted compounds, the GSH depletion percentages were low as compared to larger alkyl substituents across all halogen combinations. Non-alkylated compounds of Cl-Cl and Br-Br combinations were observed to have increased GSH depletion over methyl substituted ones. The compound with the highest GSH depletion was compound **24** (*tert*-butyl, Br-Br) and the lowest was compound **14** (*n*-propyl, F-F).

### 5.3.3. Reactivity of AGs of the compounds towards Phe-Lys

The compounds possess a carboxylic acid group and they are structurally similar to diclofenac. Thus, AGs can play a role in the toxicity caused by the compounds via metabolism. We generated AGs from the compounds using HLM and UDPGA as co-factor. Alamethicin was added as a pore-forming agent to aid in the penetration of the compounds into the membrane bound UGTs. The biosynthesized AGs were then incubated with dipeptide, Phe-Lys, which traps the reactive AGs formed via acyl migration or transacylation. The AG reactivity was calculated as the relative amount of trapped AGs at 24 h divided by total amount of AGs at 0 h.

**Table 5-7** Reactivity of AGs of the twenty-four compounds toward Phe-Lys in a 24 h incubation.

Compound	R <sub>1</sub>	R <sub>2</sub>	R <sub>3</sub>	AG Reactivity – 24 h <sup>a</sup> (%)
<b>1</b>	H	F	Cl	5.36 ± 0.29
<b>2</b>	H	F	F	0.29 ± 0.01
<b>3 (Diclofenac)</b>	H	Cl	Cl	8.67 ± 0.69
<b>4</b>	H	Br	Br	7.02 ± 0.41
<b>5 (Lumiracoxib)</b>	Me	F	Cl	6.04 ± 0.56
<b>6</b>	Me	F	F	0.44 ± 0.06
<b>7</b>	Me	Cl	Cl	9.15 ± 0.96
<b>8</b>	Me	Br	Br	6.28 ± 0.46
<b>9</b>	Et	F	Cl	6.14 ± 0.67
<b>10</b>	Et	F	F	0.56 ± 0.08
<b>11</b>	Et	Cl	Cl	8.72 ± 1.25
<b>12</b>	Et	Br	Br	5.50 ± 0.57
<b>13</b>	<i>n</i> -Pr	F	Cl	4.96 ± 0.24
<b>14</b>	<i>n</i> -Pr	F	F	0.77 ± 0.01
<b>15</b>	<i>n</i> -Pr	Cl	Cl	4.60 ± 0.29
<b>16</b>	<i>n</i> -Pr	Br	Br	3.16 ± 0.12
<b>17</b>	<i>i</i> -Pr	F	Cl	5.47 ± 0.24
<b>18</b>	<i>i</i> -Pr	F	F	0.78 ± 0.01
<b>19</b>	<i>i</i> -Pr	Cl	Cl	5.38 ± 0.12
<b>20</b>	<i>i</i> -Pr	Br	Br	3.66 ± 0.15
<b>21</b>	<i>t</i> -Bu	F	Cl	3.72 ± 0.06
<b>22</b>	<i>t</i> -Bu	F	F	0.74 ± 0.01
<b>23</b>	<i>t</i> -Bu	Cl	Cl	3.86 ± 0.17
<b>24</b>	<i>t</i> -Bu	Br	Br	2.74 ± 0.02

<sup>a</sup> AG reactivity (%) was determined from duplicates and is expressed as mean ± standard deviation.

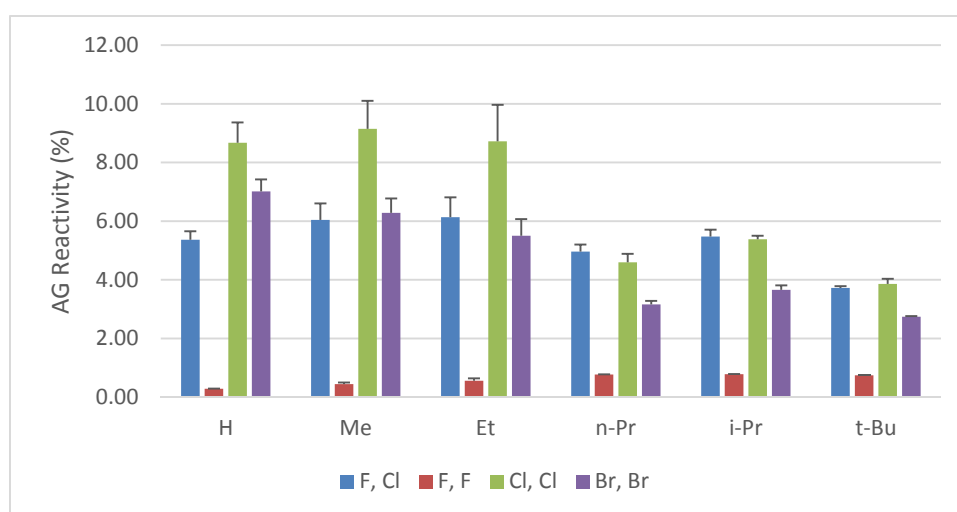


**Figure 5-8** Comparison plot for AG reactivity between halogen substituents at R<sub>2</sub> and R<sub>3</sub> and grouped by R<sub>1</sub> substituents.



The reactivity of the AGs over 24 h were not as high as expected. The reactivity ranged from 0.29% to 9.15% (Table 5-7). The compound with the highest AG reactivity was compound 7 and the lowest was compound 2. The AG reactivity of the F-F compounds (2, 6, 10, 14, 18 and 22) was consistently very much lower than other halogen combinations (Figure 5-8). The reactivity of the AGs of the F-F compounds was consistently below 1%. Compounds that possess at least one chlorine atom had an elevated AG reactivity. The Cl-Cl compounds possess the highest AG reactivity among each alkyl series. Bromine substitution was observed to elevate AG reactivity but to a less extent than chlorine.

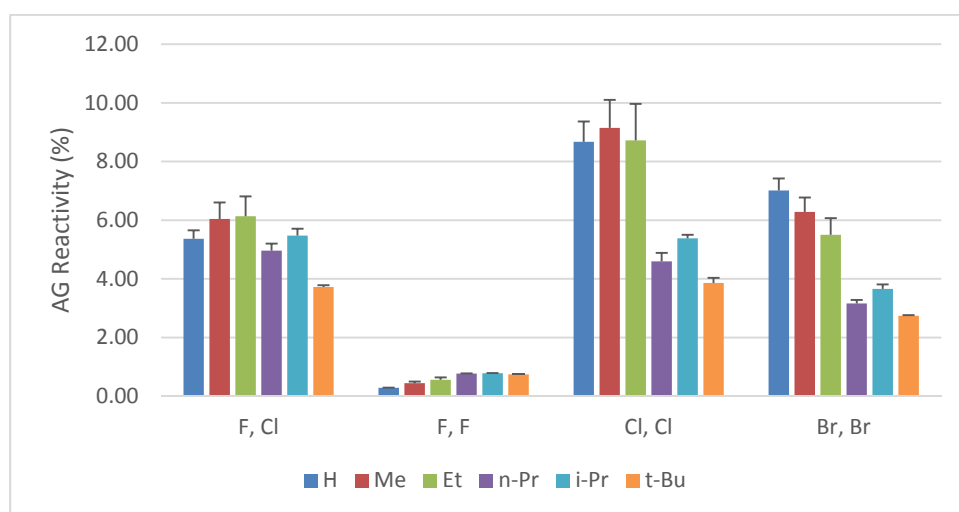


**Figure 5-9** Comparison plot for AG reactivity between alkyl substituents at R<sub>1</sub> and grouped by R<sub>2</sub> and R<sub>3</sub> substituents.

Surprisingly, the increase in alkyl size at R<sub>1</sub> seemed to decrease the reactivity of the AGs. The *n*-propyl, *iso*-propyl and *tert*-butyl substituted compounds were shown to have decreased AG reactivity as compared to the smaller alkylated or non-alkylated compounds. The exception was F-F compounds where we observed a very slight increase in reactivity as alkyl substituent

increased in size. The changes in reactivity contributed by methyl and ethyl were minimum as the AG reactivity values were not that much different as compared to non-alkylated compounds.

#### 5.3.4. Relationship between metabolic stability and metabolite reactivity

To determine the role of metabolism in the toxicity of the compounds, we performed linear regressions to elucidate the relationship between metabolic stability and reactivity for both Phase I and Phase II metabolism. However, the trend was not correlated strongly quantitatively, especially for Phase I metabolism (Appendix 5-4). Thus, we carried out qualitative cross-comparisons of the metabolic stability and reactivity of the compounds for both phases of metabolism. Figure 5-10 shows the cross-comparison for Phase I metabolism (separated into the two concentrations of compounds employed) and Figure 5-11 shows the cross-comparison for Phase II metabolism.

From Figure 5-10, it was observed that there is no visible trend between Phase I metabolic stability and *in vitro* GSH depletion, which was in line with the linear regression performed ( $R^2 = 0.0085$  and  $R^2 = 0.0008$  for 20  $\mu\text{M}$  and 10  $\mu\text{M}$  test concentration respectively). We expected to observe that compounds with high GSH depletion will have short metabolic  $t_{1/2}$  as we assumed that a faster rate of metabolism will result in higher chance of formation of reactive metabolites. However, we observed that short metabolic  $t_{1/2}$  did not correspond to high GSH depletion, indicating that metabolically unstable compounds do not necessarily equate to high reactivity of the metabolites formed. Compounds that followed our expectations were compounds **13**, **15**,

**16**, **20** and **23**, which were observed to have relative short metabolic  $t_{1/2}$  coupled with high GSH depletion. Compounds **7** to **11**, **14**, **18**, **19** and **22**, also followed our expectations of relatively long metabolic  $t_{1/2}$  coupled with low GSH depletion.

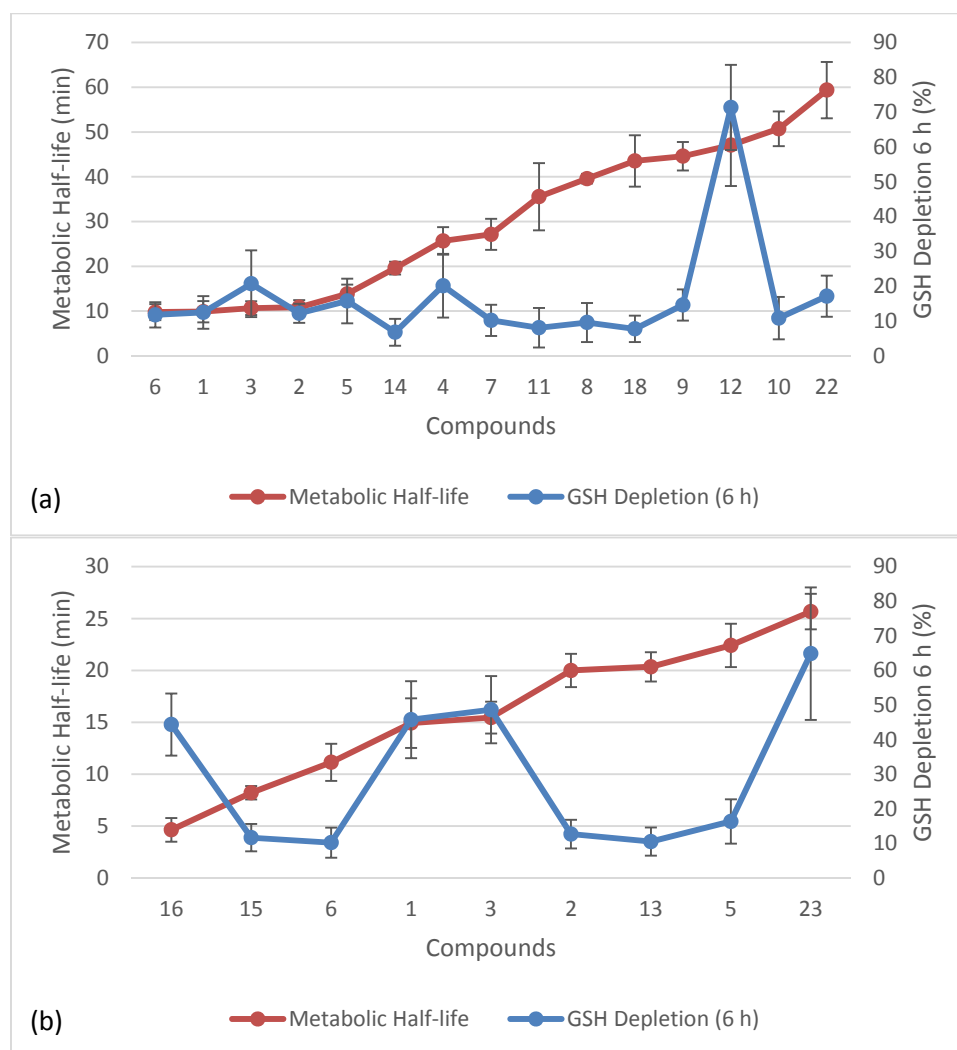


**Figure 5-10** (a) Comparison of Phase I average metabolic  $t_{1/2}$  and *in vitro* GSH depletion tested at 20  $\mu$ M (6 h) and (b) comparison of Phase I average metabolic  $t_{1/2}$  and *in vitro* GSH depletion tested at 10  $\mu$ M (6 h).

The other compounds did not follow our expectations of long metabolic  $t_{1/2}$  and low GSH depletion, vice versa. Compounds **12**, **17** and **24** have relatively long metabolic  $t_{1/2}$ , indicating they were not easily converted to metabolites by metabolic enzymes. However, these three compounds were shown to have

high GSH depletion despite being metabolically stable. On the other hand, compounds **1** to **6** have relatively short metabolic  $t_{1/2}$  but had low GSH depletion instead of high GSH depletion.

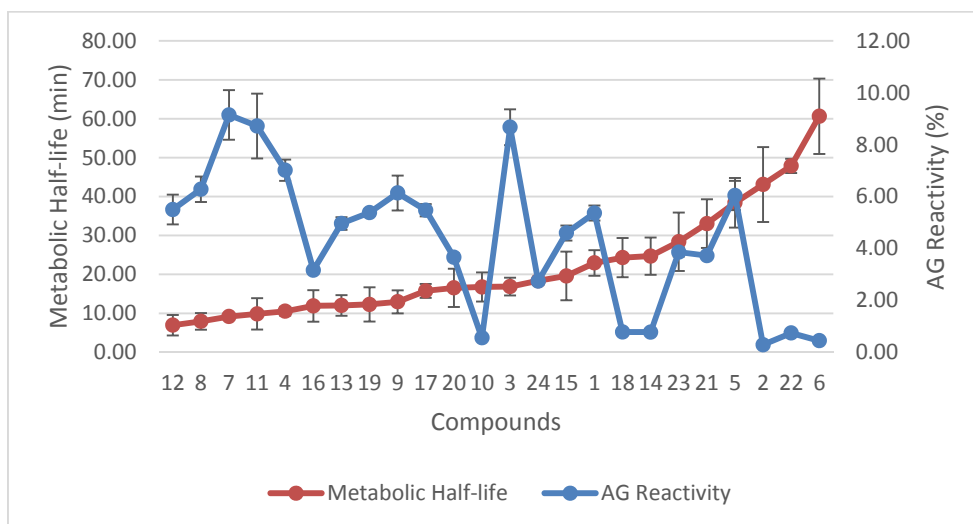


**Figure 5-11** Comparison of Phase II average metabolic  $t_{1/2}$  and AG reactivity (24 h).

For Phase II metabolism, a clearer trend can be seen between metabolic stability and AG reactivity. Similar to Phase I metabolism, we expected short metabolic  $t_{1/2}$  to correspond to high AG reactivity and vice versa. From Figure 5-11, it can be observed that was somewhat a decreasing trend in AG reactivity associated with increase in metabolic  $t_{1/2}$ . This was also observed in the linear regression performed where an inverse relationship was observed between AG reactivity and Phase II metabolic stability (Appendix 5-4). However, there were exceptions and abnormalities which lead to the poor linear regression obtained ( $R^2 = 0.3802$ ). Compound **10** has a relatively shorter  $t_{1/2}$  as compared to other F-F compounds, but has an AG reactivity similar to the more metabolically stable compounds. Compounds **5**, **21** and **23** are relatively metabolically stable on the basis of their long metabolic  $t_{1/2}$  but their

AGs were shown to be as reactive as compounds that are not as stable as them. Similarly, compounds **1**, **3** and **15** have higher or similar AG reactivity as compounds that possess half of their metabolic  $t_{1/2}$ .

### 5.3.5. Relationship between metabolic stability and toxicity

Similar to defining the relationship between metabolic stability and reactivity, we performed linear regression to clarify the relationship between metabolic stability and toxicity. We obtained poor linear regression models (Appendix 5-5) and thus, we performed a qualitative cross-comparison between metabolic stability and toxicity to determine if metabolic stability affects the toxicity of the compound. Similar to the comparison between metabolic stability and metabolite reactivity in Section 5.3.4, we expected compounds with low  $LC_{50}$  values to have less metabolic stability.

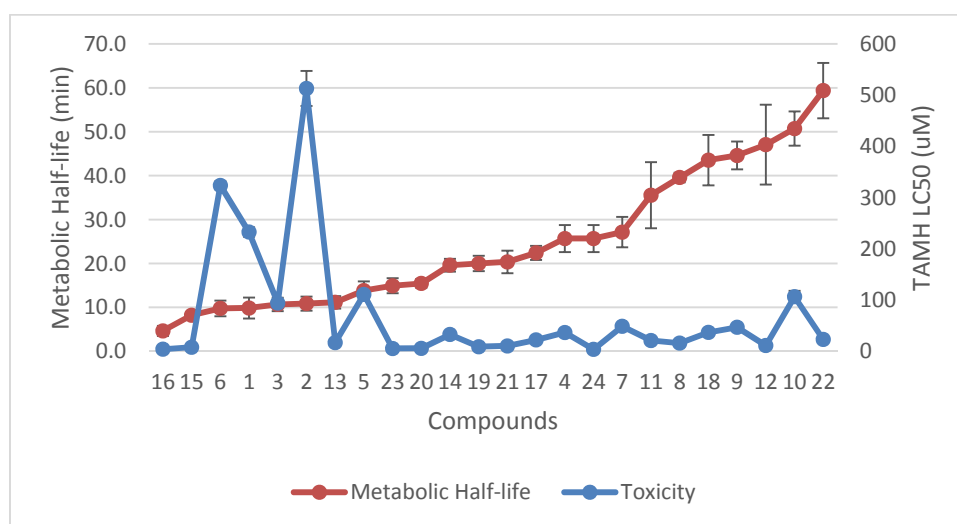


**Figure 5-12** Comparison of Phase I average metabolic  $t_{1/2}$  and *in vitro* toxicity in TAMH.

From Figure 5-12, it can be seen that there is no visible trend between metabolic stability and toxicity for Phase I metabolism, which was mirrored in

the linear regression performed ( $R^2 = 0.08310$ ). Some compounds with low  $LC_{50}$  values were observed to have relatively high metabolic stability while some compounds with high  $LC_{50}$  values were observed to be relatively metabolically unstable. For example, compound **2**, which has the highest  $LC_{50}$  has a relatively short metabolic  $t_{1/2}$  of 10.9 minutes while compound **24**, which has the lowest  $LC_{50}$  value has a moderately long metabolic  $t_{1/2}$  of 25.7 minutes. On the other hand, some compounds were within expectations, with low  $LC_{50}$  values and short metabolic  $t_{1/2}$ , vice versa, such as compounds **10**, **15** and **16**.

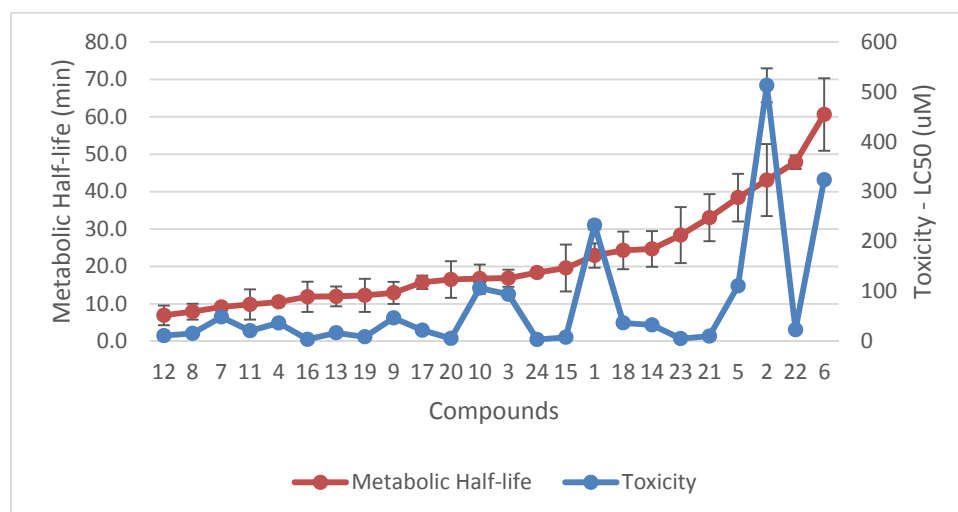


**Figure 5-13** Comparison of Phase II average metabolic  $t_{1/2}$  and *in vitro* toxicity in TAMH.

For Phase II metabolism, we observed an increasing toxicity associated with increase in metabolic  $t_{1/2}$  (Figure 5-13). This was mirrored in the linear regression performed where a positive trend was observed between  $LC_{50}$  values and Phase II metabolic stability (Appendix 5-5). Similar to Phase I metabolism, there were exceptions which resulted in the poor linear regression obtained ( $R_2 = 0.3559$ ). Compounds **4**, **7** and **9** have relatively high  $LC_{50}$  values as compared to other compounds with similar metabolic  $t_{1/2}$ .

Compounds **15** and **20** to **24** have low LC<sub>50</sub> values but moderate to high metabolic stabilities.

#### 5.3.6. Relationship between reactivity and toxicity

As previously mentioned in chapter 3, we postulated that toxicity of the compounds arises from the reactive metabolites formed via metabolism of the compounds. In this section, we initially performed a quantitative linear regression between metabolite reactivity and toxicity but poor models were obtained (Appendix 5-6). Thus, we performed a qualitative cross-comparison between metabolite reactivity and toxicity to investigate the relationship between the two. Figure 5-14 shows the cross-comparison between GSH depletion and toxicity in TAMH cells and Figure 5-15 shows the cross-comparison between AG reactivity and toxicity.

From Figure 5-14 we observed with decrease in LC<sub>50</sub> values, GSH depletion increased for most compounds. This observation was in line with our expectations of low LC<sub>50</sub> corresponding to high GSH depletion. The most toxic (compound **24**) was the compound with the highest relative GSH depletion (tested at a lower concentration of 10 μM). There were exceptions such as compounds **8**, **11**, **14** and **18** which have moderately low LC<sub>50</sub> values but the corresponding GSH depletion percentages were not as high as expected. Due to these exceptions, the correlation between GSH depletion and toxicity was not as strong as expected.

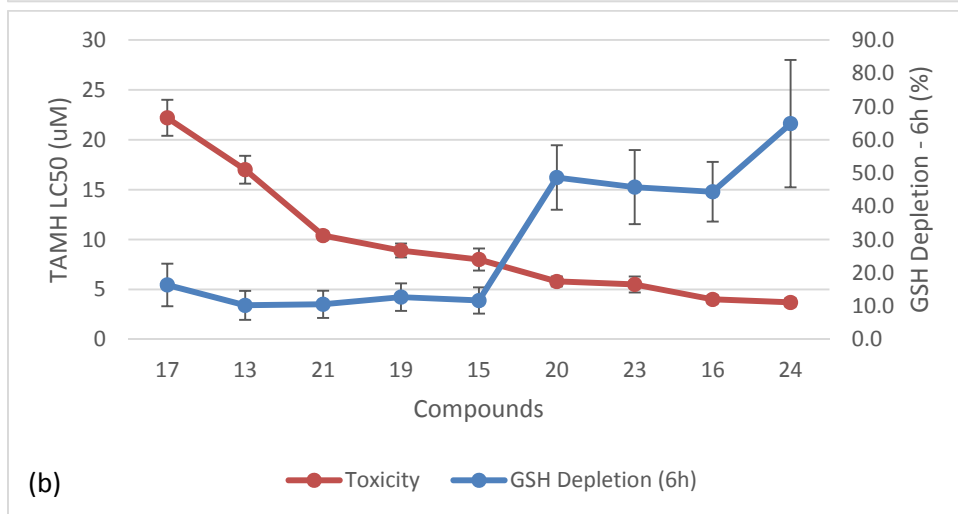
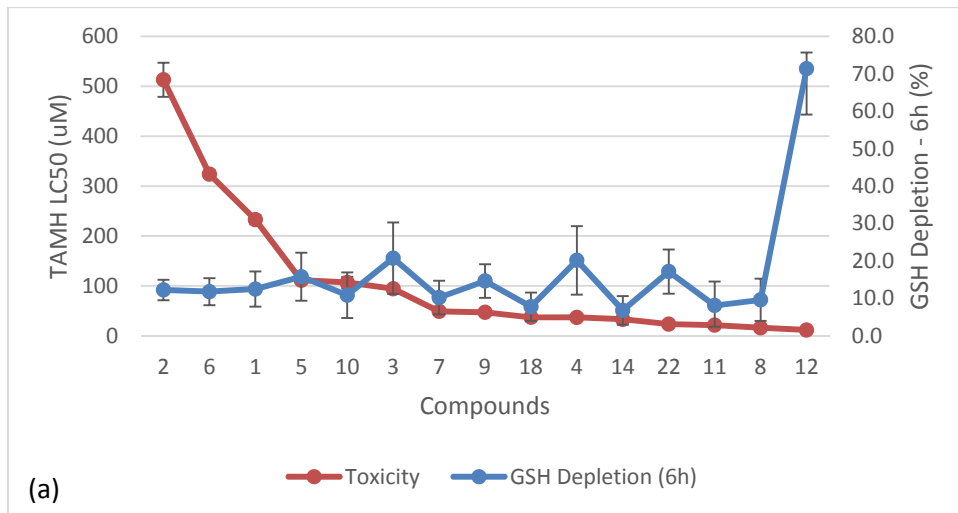


**Figure 5-14** (a) Comparison of *in vitro* GSH depletion tested at 20  $\mu\text{M}$  (6 h) and corresponding *in vitro* toxicity in TAMH and (b) comparison of *in vitro* GSH depletion tested at 10  $\mu\text{M}$  (6 h) and corresponding *in vitro* toxicity in TAMH

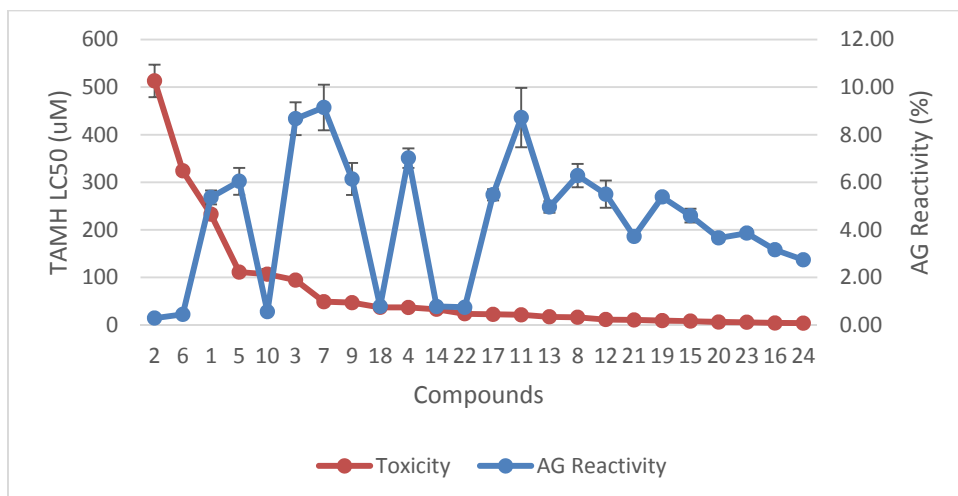


**Figure 5-15** Comparison of AG reactivity and *in vitro* toxicity in TAMH.



On the other hand, we observed that for the cross-comparison for AG reactivity and LC<sub>50</sub> values, there was no discernable trend (Figure 5-15). This was opposite of what we expected between AG reactivity and LC<sub>50</sub> values. For F-F compounds with larger alkyl groups (*n*-propyl, *iso*-propyl and *tert*-butyl), compounds **14**, **18** and **22** have low LC<sub>50</sub> values but their AG reactivity values were significantly lower as compared to other compounds of close LC<sub>50</sub> values. The most toxic compound, compound **24**, was observed to have moderately low AG reactivity. Compounds **3**, **7** and **11** possess toxicity values that fell within the low to moderate region but were observed to have high AG reactivity values.

#### 5.4. Discussion

##### 5.4.1. Phase I and Phase II metabolic stability

Microsomal incubation studies were carried out to investigate the Phase I and Phase II metabolic stability of the compounds separately. We chose to carry out microsomal metabolic stability assays instead of cell-based assays because microsomal assays are faster to carry out and simpler to interpret. Also, results will be reproducible when the same batches of microsomes are used. Comparing our experimental findings and literature findings on the metabolic t<sub>1/2</sub> of diclofenac, we found that our experimental data was not in agreement with literature findings. The values obtained in our experiments were similar to that of previous literature values but it should be noted that a higher concentration of microsomes were used in our case. Thus, it would have been expected that our t<sub>1/2</sub> value for diclofenac be shorter than literature findings. There are many factors accountable these discrepancies. One factor would be

the microsomes used in our study and in literature were from different companies or batches. Commercial microsomes have been shown to differ from company to company and from different batches (Jia and Liu, 2007). Companies prepare their microsomes differently and there is also subject-to-subject differences from which the microsomes were obtained from. The type and amount of organic solvent used in the study will also have effects on the results obtained. It has been shown that type and amount of organic solvent used to dissolve the compounds have inhibitory or inductive effects on *in vitro* activities of metabolic enzymes (Easterbrook *et al.*, 2001). The solvent used in our assays were acetonitrile (0.25% v/v) and have been shown to have the least inhibitory effect on P450s and UGTs activities (Easterbrook *et al.*, 2001). The type and amount of solvents used in literature could have been different and resulted in the discrepancies seen between our findings and literature findings. Therefore, it is of importance to compare the different substituted compounds within the same experimental setup in order to obtain meaningful results.

For Phase I metabolism, we are primarily looking at aromatic hydroxylation of the compounds by P450s as both diclofenac and lumiracoxib are extensively hydroxylated by CYP2C9 (Stierlin *et al.*, 1979; Mangold *et al.*, 2004). As seen in Figure 5-1, F-F compounds were observed to be more metabolically stable as compared to other halogen combinations when the size of the alkyl substituent at R<sub>1</sub> was ethyl and larger. This observation was also seen when comparing between F-Cl and Cl-Cl compounds whereby F-Cl compounds were shown to be slightly more metabolically stable in comparison when alkyl

substituents at R<sub>1</sub> increased in size to ethyl and beyond. This was within our expectations that fluorine substituted compound will show improved metabolic stability. Fluorine has been shown to improve metabolic stability and has been used extensively to improve the biological t<sub>1/2</sub> in drug design. Indeed, a metabolic study done on halogen substituted benzenes have shown that the rate of hydroxylation increases from fluorobenzene to chlorobenzene and furthermore to bromobenzene (Burka *et al.*, 1983). It was postulated that the presence of a fluorine atom adjacent to the site of the metabolic attack could increase or decrease the biotransformation rate depending on whether the metabolic attack is nucleophilic or electrophilic in nature and whether the inductive or resonance effects of the fluorine predominates (Park *et al.*, 2001). Fluorine has been found to decrease the rate of reaction of electrophilic attacks on the  $\pi$  system of the substrate's aromatic ring by the activated heme group in P450s (Cnubben *et al.*, 1994; Koerts *et al.*, 1998). This was due to decreased nucleophilicity of the aromatic ring by fluorine substituents (Koerts *et al.*, 1998). The site of hydroxylation on the halogenated ring of the compounds are *meta* in position to the halogen substituents. From table, the  $\sigma_m$  values for fluorine indicates that it is electron withdrawing to the site of hydroxylation. Coupled with higher electronegativity, fluorine would thus decrease nucleophilicity of the aromatic ring to a greater extent than chlorine or bromine. The higher the number of fluorine atoms substituted into the aromatic ring, the lower the rate of reaction of the aromatic ring with the heme group in P450 enzymes (Cnubben *et al.*, 1994). This could possibly explain the increased metabolic t<sub>1/2</sub> of F-F compounds in our study as compared to other halogen combinations when alkyl group size at R<sub>1</sub> is ethyl or larger.

**Table 5-8** Physicochemical parameters of halogen substituents employed in our study (Allred, 1961; Hansch and Leo, 1979; Batsanov, 2001)

Parameter		F	Cl	Br
Hammett value	$\sigma_m$	0.34	0.37	0.39
	$\sigma_p$	0.06	0.23	0.23
Hansch value, $\pi$		0.14	0.71	0.86
Electronegativity		4.0	3.0	2.8
Van der Waal radii, Å		1.65	2.05	2.10
Taft size, $E_s$		-0.46	-0.97	-1.16

Paradoxically, non-alkylated and methylated F-F compounds, metabolic stability was low, which was reverse of what is expected of fluorinated compounds. We expected bromine-substituted compounds to be less metabolically stable as compared to other halogen substituted compounds but we did not observe such a straightforward trend in our case. As mentioned earlier, F-F compounds were of high metabolic stability when certain alkyl substituents were present. Similar observations with other halogen combinations were seen. Metabolic stability of Br-Br compounds were relatively low in comparison to other halogen combinations when R<sub>1</sub> was substituted with a propyl or *tert*-butyl group. On the other hand, when substituted with ethyl or smaller groups, the metabolic stability increased. Similarly for Cl-Cl and F-Cl compounds where certain alkyl group substitution resulted in decreased or increased metabolic stability as compared other halogen combinations. As seen from table, chlorine and bromine do not have very different Hammett values or electronegativity. Thus, it would be expected that their metabolic stability would not be that different. However, this was not the case and could likely be due to lipophilicity parameters and/or spatial configuration. These will be discussed further in the next few paragraphs.

Other than the halogen substituents affecting the metabolic stability of the compounds, we noticed that the alkyl substituents at R<sub>1</sub> had tremendous effects on the stability of the compounds. Interestingly, we expected *tert*-butyl substituted compounds to have low metabolic stabilities as compared to non-alkylated or other alkylated compounds. Instead, we observed that ethyl substituted compounds were the most metabolically stable regardless of halogen substitutions. Our expectations stemmed from the fact that the Hansch value of *tert*-butyl (Table 5-9) is very high, indicating its significant contribution to the lipophilicity of the compounds. But as seen from Figure 5-5 in section 5.3.1, lipophilicity and metabolic stability did not have any observable relationship across the compounds. This was not as expected as studies have found a positive relationship between lipophilicity and metabolic stability. Metabolism rates have been shown to increase with lipophilicity for both Phase I and Phase II (Siraki *et al.*, 2005; Smith *et al.*, 2006). This is because lipophilic compounds are more likely to interact with both P450s and UGTs (Little and Ryan, 1982; Lewis *et al.*, 1995; Vashishtha *et al.*, 2001).

**Table 5-9** Physicochemical parameters of alkyl substituents employed in our study (Hansch and Leo, 1979).

Parameter	H	Me	Et	<i>n</i> -Pr	<i>i</i> -Pr	<i>t</i> -Bu
Taft size, $E_s$	0.00	-1.24	-1.31	-1.60	-1.71	-2.78
Hansch value, $\pi$	0.00	0.56	1.02	1.55	1.53	1.98

The lack of a relationship between lipophilicity and metabolic stability in our study could be due to the effect of the alkyl substituent on the steric configuration of the compound in the active site of the P450s. In order for hydroxylation to take place, the position to be hydroxylated on the aromatic ring needs to be in contact with the heme group in P450s. Investigative studies

on *in silico* docking of crystal structures of P450s found that in order for a molecule to be effectively hydroxylated, the point of hydroxylation needs to fit into the heme pocket and the molecule needs to be in an optimal configuration within the substrate binding pocket of the enzyme (Williams *et al.*, 2000; Bathelt *et al.*, 2002). Thus, the spatial configuration within the active site is important as just binding to the active site (high binding affinity due to high lipophilicity) does not indicate hydroxylation will occur via the heme group. Looking at the Taft size values ( $E_s$ ) of both halogen and alkyl substituents (Tables 5-8 and 5-9), we can observe a significant differences between each substituent. The steric effect contributed by each different substituent and their combination on the scaffold will result in different spatial configurations. The lack of relationship between Phase I metabolic stability and lipophilicity could possibly be related to the different spatial configurations that arise via different substituent combination on the scaffold. This could also explain why certain non-alkylated and methylated F-F compounds were found to have low metabolic stability yet their other alkylated counterparts were highly metabolically stable.

For Phase II metabolism, we focused on glucuronidation of the carboxylic acid moiety on ring A of the compound, as it is the major metabolic fate for arylacids. Thus, it would seem intuitive that changes in substituents on the more distal ring B ( $R_2$  and  $R_3$ ) of the compound should not affect the Phase II metabolism of the compounds. This was not the case as fluorinated compounds, especially di-fluorinated compounds, of the same alkyl series have remarkably higher metabolic stability as compared to chlorinated or

brominated compounds. This could be due to the lipophilicity of the compounds, with di-fluorinated compounds having the lowest lipophilicity in each alkyl series. The role of glucuronidation in Phase II metabolism is to increase hydrophilicity of the lipophilic xenobiotic so as to aid in excretion. It is thus expected that more lipophilic compounds will be glucuronidated at a higher rate, leading to shorter metabolic  $t_{1/2}$ . However, the relationship between lipophilicity and metabolic stability is not as straight-forward across the series and will be explained later on.

Similar to Phase I metabolism, we observed no relationship between lipophilicity and Phase II metabolic stability across the series. It was found in literature that glucuronidation and lipophilicity follows a positive parabolic trend (Kim, 1991). This trend was not observed in our study due to the narrow range of  $\log P(o/w)$  of the compounds in our series (approximately 3.5 to 6.0) as compared to the *in silico* range calculated in literature (-1.0 to 6.0). Other studies have also found a positive relationship between glucuronidation and lipophilicity and have attributed the relationship to the role of lipophilicity in affecting the compound's ability to recognize the active site of the UGTs (Radomska-Pandya *et al.*, 1999; Smith *et al.*, 2003). In addition, UGTs are bound on the luminal face of the microsomal membrane, which requires the substrates to traverse the endoplasmic reticulum (Radomska-Pandya *et al.*, 1999). Lipophilic compounds will thus have higher penetration rate through the membrane. Such dynamics may not be mimicked from our study because we used alamethicin as a pore forming reagent to aid the compounds to transverse the membrane, which could have changed the relationship between

lipophilicity and Phase II metabolism. In addition, even with increased binding of the compound molecules to the active sites of UGTs due to increased lipophilicity, the configuration of the molecule may not be optimal and could have affected the lipophilicity-glucuronidation relationship

#### 5.4.2. Reactivity of metabolites generated via metabolism

The toxicity of the compounds was postulated to arise from the formation of reactive metabolites. We investigated the reactivity of the possible metabolites formed by two ways. The first was to investigate the ability of the metabolites to conjugate to cellular GSH. In this study, we assumed that the depletion of cellular GSH by the compounds were mainly due to the formation of quinone imines and imine methides intermediates from Phase I metabolism. This assumption was based on studies showing that reactive metabolites of diclofenac such as quinone imines formed adducts with GSH *in vivo* and *in vitro* (Tang *et al.*, 1999a; Tang *et al.*, 1999b; Poon *et al.*, 2001). However, we also accept the fact that Phase II metabolites may also cause some depletion of GSH. However, hard nucleophiles are preferred as binding targets for AGs.

Here, we found the reactivity of the metabolites generated to be altered by changes in substituents. Hence, we examined the lability of hydroxylation at the 4'-position by P450s, its subsequent oxidation to electrophilic quinone imines in Phase I metabolism and the effect of halogen substituents on the aromatic ring (Figure 5-16). The electrophilicity of the quinone imines will be linked to their reactivity towards cellular nucleophiles such as GSH. A relationship between electrophilicity and toxicity of quinones has been



established. The study investigated the effect of different substituents on quinones on their reactivity towards GSH. GSH was used as a nucleophilic trapping agent. It was shown that increasing electrophilicity of a quinone by substituting more electron-withdrawing groups increased its reactivity towards GSH (Chan *et al.*, 2008). Quinones and quinone imines are analogous and thus, this relationship would be seen in quinone imines too. Electron-withdrawing groups on the initial aminophenol will confer stronger electrophilic properties to the quinone imine as the electron density of the aromatic ring decreases. On the other hand, electron-donating groups will confer weaker electrophilic properties.

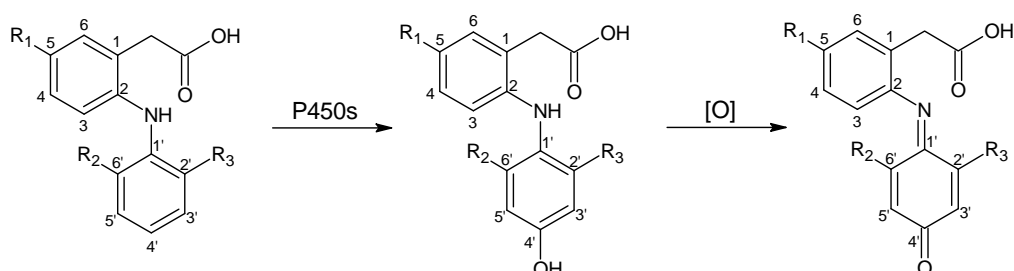


**Figure 5-16** Hydroxylation at 4'-position and subsequent oxidation to a quinone imine.

The main substituents on the compounds that can affect the reactivity of the quinone imines formed via 4'-hydroxylation are fluorine, chlorine and bromine. The possible sites of adduct formation are 3'- and 5'-positions, which is *para* to the halogen substituents. Physicochemical properties of each halogen substituent will thus affect the reactivity of the sites of adduct formation. The Hammett values of fluorine, chlorine and bromine for *para* substituent,  $\sigma_p$ , are 0.06, 0.23 and 0.23 respectively (Table 5-8). From the given Hammett values, fluorine is the least electron-withdrawing substituent

(more negative Hammett value) even though fluorine is more electronegative than chlorine and bromine (Table 5-8). This is because the electron-donating mesomeric effect of fluorine dominates over the electron-withdrawing inductive effect (Neijenesch *et al.*, 1991). The quinone imines of difluoro-substituted compounds at R<sub>2</sub> and R<sub>3</sub> will be the weakest electrophile among the compounds. Weak electrophiles are less reactive towards nucleophiles. The quinone imines of difluoro-substituted compounds will thus be less likely to form covalent adducts with cellular nucleophiles. This effect is reflective of the cellular GSH depletion observed whereby F-F compounds were shown to have low percentage GSH depletion regardless of alkyl substitution at R<sub>1</sub> (Figure 5-6).

Bromine is only slightly more electron-withdrawing than chlorine as a substituent. However, significant differences were observed between the GSH depletion of chlorinated and brominated compounds, with Br-Br compounds observed to have remarkably higher GSH depletion (Figure 5-6). Given the similarity in their electron-withdrawing properties of chlorine and bromine, the lipophilicity contributed by the halogens could have greater effects on toxicity of the compounds as compared to the effects contributed by electrophilicity.

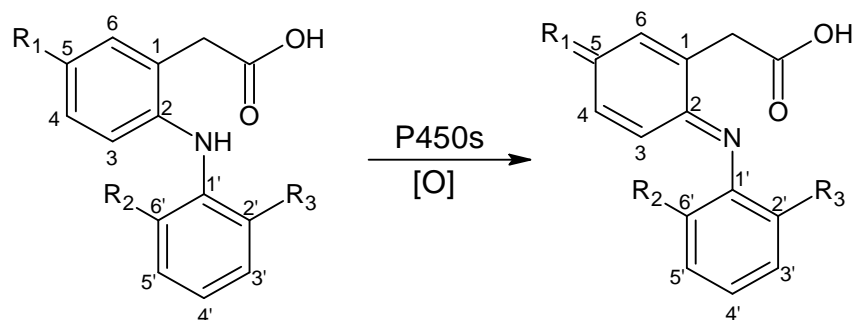


**Figure 5-17** Formation of an imine methide when  $R_1$  is an alkyl group.

Alkyl substituents on the  $R_1$  position can affect the cellular GSH depletion of the compounds too. The compounds possessing an alkyl group *para* to an amine group on an aromatic group have a possibility to be oxidized to imine methides (Figure 5-17). For example, lumiracoxib can be metabolized to an imine methide due to the presence of a methyl group (Kang *et al.*, 2009). On the other hand, diclofenac does not form any imine methides. It is known that imine methides are more reactive than quinone imines due to their highly electrophilic nature, which arises from their decreased propensity to undergo one electron reductions (Thompson *et al.*, 1993). This increased reactivity could be a reason for the increase in toxicity when alkyl groups are substituted at  $R_1$ . Imine methides are analogous to quinone methides, thus, factors affecting the reactivity of quinone methides can be extrapolated to imine methides. One factor that affects the reactivity of imine methides is the type of substitutions on the exocyclic methylene group. Greater steric crowding due to larger substitutions at the exocyclic methylene group decreases the reactivity of the methylene group towards nucleophiles (Thompson *et al.*, 1995). Thus, the reactivity of the methylene group towards nucleophiles decreases as the alkyl group size increases or branching occurs. The reactivity of the methylene group will thus be: methyl > ethyl > *n*-propyl > *iso*-propyl. *tert*-Butyl was

omitted from the list as it is unable to form any imine methides. Our overall trend showed that GSH depletion for propyl substituted compounds were technically higher than methyl and ethyl substituted compounds given propyl-substituted compounds were tested a lower concentration (GSH depletion: *iso*-propyl = *n*-propyl > ethyl > methyl). The exact reason for this anomalous trend is not clear. There could be two reasons as to why this trend was observed, namely the lipophilicity of the compounds and the binding selectivity of the imine methides formed.

A study done on quinone methide formation of eugenol analogues showed that more lipophilic compounds generated more quinone methides (Thompson *et al.*, 1995). Propyl-substituted compounds are more lipophilic as compared to the others, thus, more reactive imine methides could have been formed for propyl-substituted compounds. It was also observed in the study that quinone methides formed from methyl-substituted analogs were so reactive that such quinone methides have little ability to diffuse away from the site of formation to bind with critical cellular nucleophiles and they react readily with the surrounding solvent such as water (Thompson *et al.*, 1995). On the other hand, propyl-substituted analogues formed quinone methides that were of intermediate reactivity and have the ability to diffuse away from the site of formation to bind to cellular nucleophiles (Thompson *et al.*, 1995). This can be applied to the imine methides, whereby in this case, the methyl-substituted compounds at R<sub>1</sub> formed highly reactive imine methides that have little ability to bind to critical cellular nucleophiles as they will non-selectively bind to surrounding nucleophiles such as water in the active site of the enzyme.

Overall, propyl-substituted compounds at the R<sub>1</sub> position have the ability to form reactive imine methides that are of intermediate reactivity. These propyl-substituted imine methides will have lesser tendency to bind to water and can diffuse away from the active site to bind to critical cellular nucleophiles. Thus, the GSH depletion observed with propyl-substituted compounds were higher than ethyl or methyl substituted compounds. All in all, the higher GSH depletion observed with propyl-substituted compounds could be due to their higher lipophilicity and the intermediate reactivity of their imine methides.

As mentioned earlier, it should be noted with interest that *tert*-butyl-substituted compounds do not form imine methides as *tert*-butyl group possesses no extractable hydrogen atom. However, when keeping the halogen-substituents constant, the GSH depletion values of *tert*-butyl-substituted compounds were higher as compared to propyl-substituted compounds, especially for di-chlorinated and di-brominated compounds. *tert*-Butyl substituted compounds could form other reactive metabolites in larger quantities and of higher reactivity. In this case, the formation of imine methides may not be as important a factor in affecting the toxicity of the compounds synthesized. Therefore, we must consider alternative metabolites that can be generated or alternative toxicity pathways as a consequence.

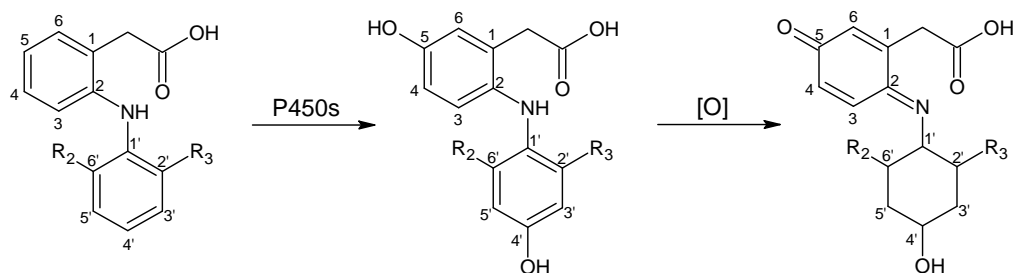


**Figure 5-18** Hydroxylation at 5-position and subsequent oxidation to a quinone imine.

It is also interesting to note that the non-alkylated compounds were shown to have comparable or higher GSH depletion as compared to methylated and in most cases, ethylated compounds (Figure 5-7). Hydroxylation can potentially occur at the 5-position on the arylacetic acid ring via P450s and subsequent oxidation to a quinone imine can occur (Figure). Thus, although lacking the ability to form imine methides, the formation of quinone imines on the arylacetic acid ring could contribute to the depletion of GSH via adduct formation.

AGs formed via Phase II metabolism can bioactivate via two reactive pathways: (1) transacylation, whereby the aglycone moiety conjugates with a nucleophile, releasing the glucuronic acid moiety, and (2) acyl migration, whereby intramolecular rearrangement of the AGs result in ring opening and formation of reactive aldehydes. From what was observed, the halogen substituents at R<sub>2</sub> and R<sub>3</sub> had greater effects on the reactivity of the AGs as compared to the alkyl substituents at R<sub>1</sub>. Di-fluorinated compounds were very non-reactive while di-chlorinated compounds were the most reactive. On the other hand, the larger the alkyl group at R<sub>1</sub>, the less reactive the AGs became.

This is rather interesting as previous studies done on the reactivity of AGs have shown that bulky substituents on the  $\alpha$ -carbon of the acetic acid group affects the reactivity of the AGs due to steric hindrance (Berry *et al.*, 2009). In our study, the  $\alpha$ -carbon was left un-substituted, thus, the steric hindrance on the  $\alpha$ -carbon that affects AG reactivity does not apply. Other studies have found that the reactivity of AGs formed from substituted benzoic acids depended on the Hammett values of the substituents, with electron-donating groups increasing the reactivity of the benzoic acid AGs (Vanderhoeven *et al.*, 2004a; Vanderhoeven *et al.*, 2004b). However, it should be noted that our compounds are arylacetic acids with a more complex structure possessing more than one aromatic ring. In addition, the reactivity of arylacetic acid AGs is more complex and has been postulated to be affected by both steric and electronic factors (Benet *et al.*, 1993; Wang *et al.*, 2004; Berry *et al.*, 2009). Thus, there is no single and straightforward explanation to the phenomenon seen in our study. The effect seen from the alkyl and halogen substituents could be due to the interplay of electronic and steric factors, acting against each other. However, more in-depth investigation needs to be carried out. We propose that further calculations of electronic and steric properties and possible QSAR models may help in the explanation of the results observed for AG reactivity of our compounds.

#### 5.4.3. Role of metabolic stability and metabolite reactivity in toxicity of the compounds

We performed three-way cross-comparisons between metabolic stability, metabolite reactivity and the toxicity of the compounds in terms of *in vitro*

LC<sub>50</sub> data. We observed no direct relationship between metabolic stability and toxicity for Phase I metabolism. This gives an indication that even with greater amount of metabolites formed; it may not mean that the metabolites formed are reactive or toxic in nature. A cross-comparison between GSH depletion and toxicity gave a positive relationship whereby high GSH depletion were shown to relate to high toxicity in many compounds. The results gave an indication that the formation of reactive metabolites and subsequent conjugation with GSH or oxidative stress causing depletion in cellular GSH resulted in the toxicity observed. GSH depletion is a measurement of toxicity in the cell and is a likely indicator of increased chance of binding of reactive metabolites to hepatic proteins.

For compounds with high metabolic stability but yet high GSH depletion, it can be postulated that the amount of reactive metabolites formed, however small, was reactive enough to deplete cellular GSH and perhaps conjugate to other cellular nucleophiles at a relatively high rate to cause significant cell death. Similarly, for compounds with poor metabolic stability but low GSH depletion, it can be postulated that the large amount of metabolites formed were not very reactive in nature, thus resulting in lower cytotoxicity. Thus, metabolic stability may not be a good indicator of toxicity caused by metabolism as highly metabolically stable compounds can be equally or more toxic than metabolically unstable compounds. It is recommended that other assays that determine the actual reactivity of the compounds, for example, GSH depletion assays, be carried out in addition to metabolic stability assays.



For Phase II metabolism, we could observe a positive relationship between metabolic stability and toxicity in general. But there were exceptions whereby compounds with high metabolic stability possess high toxicity. However, a cross-comparison between AG reactivity and toxicity gave no discernable relationship. This could be due to the toxicity of AGs contributing less than the toxicity of the Phase I reactive metabolites. On the other hand, the fluctuating AG reactivity could be due to different rates of transacylation and acyl migration of the AGs depending on the substituent combination on the scaffold. As the reactivity was measured in a controlled trapping environment, it may not clearly reflect on the transacylation or acyl migration rates in a whole cell. Thus, to better elucidate any possible relationships between AG reactivity and toxicity, a cell-based study should be carried out to observe the reactivity of AGs formed as the varying cellular nucleophiles and environment could have a profound effect on the transacylation and acyl migration rate on the AGs as compared to a buffered microsomal incubation used in our study.

### 5.5. Conclusion

The metabolic stabilities of the compounds with respect to Phase I and Phase II pathways were determined via microsomal incubations and LC-MS/MS analysis. The metabolic  $t_{1/2}$  of diclofenac for both phases of metabolism were not similar to that in literature, which we attributed to differences in microsomes batch and experimental procedures. For Phase I metabolism, F-F compounds were shown to be highly metabolically stable, especially when alkyl substituent at  $R_1$  was ethyl and larger. We attributed this to the decreased nucleophilicity of fluorinated compounds and subsequent decreased rate of

reaction with the heme group in P450s for Phase I metabolism. For Phase II metabolism, F-F compounds were observed to be the most metabolically stable regardless of the substituent at R<sub>1</sub>. The decreased lipophilicity of fluorine over chlorine and bromine for the same alkyl series was attributed to the increased metabolic stability observed.

The metabolic stabilities of the compounds across the series (varying alkyl and halogen substituents) were not as we expected and were not correlated to lipophilicity as initially assumed by us. Several exceptions were observed such as high metabolic stability of F-F compounds with ethyl or larger alkyl substituent at R<sub>1</sub> but low metabolic stability with methyl or no alkyl substituent at R<sub>1</sub>. We postulate that this could be due to unfavorable spatial configurations of the compounds within the active site of the P450s for Phase I metabolism. The substituent combination on all three investigated positions is important for spatial configuration given their different steric effect on the molecule. Thus, it is hard to draw a definite conclusion on structure-metabolism relationship with the given experimental data. It is recommended that further *in silico* experiments could aid in determining if spatial configuration plays an important role.

In addition to metabolic stability, we determined both the cellular GSH depletion and AG reactivity of the compounds. We found that GSH depletion increased across the series. We assumed that GSH depletion was mainly due to formation of quinone imines and imine methides via Phase I metabolism of the compounds. We postulated that the electrophilicity of the aromatic ring

affected by the halogen substituents due to electron donating and withdrawing effects could have affected these electrophilic reactive metabolites. The ease of formation of imine methides and the type of imine methides formed could be factors involved in affecting the toxicity of the compounds. However, the question on whether imine methides are truly contributors to toxicity remains as *tert*-butyl substituted compounds at R<sub>1</sub> do not form imine methides yet are considerably toxic. Thus, there is a need to further study the type of reactive metabolites formed in order to determine which reactive metabolite is the major contributor to toxicity.

AG reactivity of our compounds showed that the halogen substituents at R<sub>2</sub> and R<sub>3</sub> affected the reactivity more than the alkyl substituents at R<sub>1</sub>. Literature findings have not yet been able to correlate complex AG structures to reactivity. We postulated that the effect seen from the halogen substituents could be electronic in nature and the effect from the alkyl groups at R<sub>1</sub> could be steric in nature. Further investigation such as calculations of electronic and steric properties and QSAR modelling should be carried out to help in the explanation of the results observed for AG reactivity of our compounds.

The cross-comparisons done between metabolic stability, metabolite reactivity and toxicity gave rise to interesting observations. For Phase I metabolism, we found no relationship between metabolic stability and toxicity. Thus, we conclude metabolic stability may not be a good indicator of toxicity caused by metabolism as highly metabolically stable compounds can be equally or more toxic than metabolically unstable compounds. On the other hand, we found

that metabolite reactivity and toxicity in general have a positive relationship. However, it is important to note that the correlation was not strong. We used GSH depletion as an indicator of metabolite reactivity but one should note that such metabolites could also bind to other cellular nucleophiles, resulting in cell death.

A more complex relationship was seen for Phase II metabolism whereby metabolic stability correlated to toxicity positively while AG reactivity had no correlation to toxicity. Further cell-based AG reactivity assays should be carried out to try and elucidate out a clearer relationship between Phase II metabolism, metabolite reactivity and toxicity.

**Chapter 6. Investigations of the Role of Metabolism in the Toxicity of the Synthesized Compounds: Structure Elucidation of Trapped Reactive Metabolites and Proposition of Possible Bioactivation Pathways**

**6.1. Introduction**

In Chapter 5, we investigated Phase I and II metabolic stability of the compounds and the reactivity of the resulting metabolites. The results supported the hypothesis that toxicity of the compounds arose from formation of reactive metabolites. To crystallize this postulation, it is necessary to confirm the generation of reactive metabolites by identifying and proposing the structures of the possible metabolites formed.

Our work is built upon the previous findings of Phase I reactive metabolites associated with the hepatotoxicity of diclofenac and lumiracoxib. Diclofenac has been found to form quinone imines and subsequent trapping of GSH on both rings (Shen *et al.*, 1999; Tang *et al.*, 1999b; Yu *et al.*, 2005). On the other hand, lumiracoxib has also been found to form quinone imines from the aniline ring (Li *et al.*, 2008; Kang *et al.*, 2009). In addition, imine methides formed from the arylacetic acid ring have been documented (Kang *et al.*, 2009). Since our compounds are structurally similar, we expect to detect similarly trapped reactive metabolites, with the influence of the substituents on this propensity being the object of our study.

In addition, the contribution of Phase II-mediated reactive metabolite formation cannot be undermined. We have shown in Chapter 5 that the AGs

formed from the compounds exhibit measurable reactivity towards a nucleophilic dipeptide consisting of phenylalanine and lysine. Diclofenac has also been documented to form AGs that can undergo transacylation or acyl migration, causing subsequent conjugation to cellular nucleophiles such as GSH and proteins (Kretzrommel and Boelsterli, 1994a; Grillo *et al.*, 2003). Lumiracoxib has been found to form AGs *in vivo* and *in vitro* (Mangold *et al.*, 2004; Kang *et al.*, 2009). However, little to no studies has been carried out to investigate the reactivity of the AGs of lumiracoxib nor to elucidate the structures of the adducted AGs.

Therefore, this chapter is a deliberate effort to explore both Phase I and II metabolic pathways. The first part is the identification and subsequent structure proposition of the Phase I reactive metabolites. Emphasis is placed on investigating the effect of the varying substituents on the compounds and on the structures of the metabolites formed. The metabolites were generated via microsomal incubations and trapped with GSH. LC-MS/MS analysis was carried out to identify the structures of the trapped reactive metabolites. The second part involves the identification of the AGs of diclofenac, lumiracoxib and selected compounds trapped with Phe-Lys using LC-MS/MS analysis. This is to confirm the formation of AGs of lumiracoxib and selected compounds, and that like AGs of diclofenac, are able to undergo transacylation and acyl migrations to form reactive metabolites that contribute to the toxicity of the compounds.

## 6.2 Experimental methods

### 6.2.1. Microsomal incubation for Phase I reactive metabolites trapping with GSH

Stock solutions of compounds were prepared in DMSO at concentrations of 50 mM individually. The stock solutions were further dissolved in acetonitrile to a concentration of 5 mM. Each compound (50  $\mu$ M) was incubated with shaking at 37°C for 1 h in a preparation consisting of 100 mM potassium phosphate buffer (pH 7.4), 1.0 mg/mL HLM, 1.3 mM NADP<sup>+</sup>, 3.3 mM glucose-6-phosphate, 0.4 U/mL glucose-6-phosphate dehydrogenase, 5 mM GSH, 3.3 mM magnesium chloride and 0.05 mM sodium citrate up to a total volume of 1 mL. The final organic solvent concentration was 0.4% v/v. Negative controls were prepared in absence of NADP<sup>+</sup>. The incubation mixture was quenched in 4X v/v ice cold acetonitrile. The mixture was vortexed for 30 s and centrifuged down at 13,000 rpm for 10 min at 4°C. The supernatant was transferred into a clean tube and evaporated under a stream of N<sub>2</sub> at 30°C to dryness. The residue was reconstituted in 200  $\mu$ L of 95/5 water/acetonitrile (v/v) and centrifuged at 13,000 rpm for 10 min at 4°C. The supernatant was collected and injected into an LC-MS/MS for analysis (to be described in a subsequent section).

### 6.2.2. Microsomal incubation for Phase II reactive metabolites trapping with Phe-Lys

The incubation method from elsewhere was carried out with modifications as described below (Wang *et al.*, 2004). Stock solutions of compounds in DMSO were prepared individually. HLM (1.0 mg/mL) and alamethicin (25  $\mu$ g/mg

protein) in 100 mM potassium phosphate buffer were incubated in ice for 15 min. After which, each compound (50  $\mu$ M), 1 mM magnesium chloride and 4 mM UDPGA were added up to a total volume of 120  $\mu$ L and the mixture incubated with shaking at 37°C for 1.5 h. The final organic solvent concentration was 1.0% v/v. The microsomal incubation mixture from was centrifuged at 13,000 rpm and 4°C for 15 min. The supernatant (100  $\mu$ L) was transferred to an equal volume of 20 mM Phe-Lys in 100 mM potassium phosphate buffer (pH 7.4). The mixture was incubated with shaking at 37°C for 24 h. An equal volume of acetonitrile was added to the incubation mixture, followed by vortexing for 1 min. The mixture was centrifuged at 13,000 rpm for 20 min at 4°C. The supernatant was collected and injected into LC-MS/MS for analysis.

### 6.2.3. LC-MS/MS for identification of Phase I GSH trapped metabolites

Samples generated in incubations experiments were analyzed using LC-MS/MS. LC-MS/MS analysis was performed on an Agilent 1290 Infinity LC system connected to a AB Sciex Qtrap® 5500 (AB Sciex, Framingham, MA). The column used was a Waters AQUITY UPLC BEH C18 120Å, 1.7  $\mu$ m, 2.1 mm  $\times$  100 mm column (Waters Corporation, Milford, MA) and the flow rate used was 400  $\mu$ L/min. The column temperature was set at 35°C. The mobile phase used was aqueous 0.1% formic acid, 5 mM ammonium formate and acetonitrile. Gradient elution was used to separate the trapped metabolites in the injection sample. Total run time was 20.5 min for each injected sample. The LC conditions are summarized in Table 6-1.



**Table 6-1** LC conditions for Phase I GSH trapped metabolites identification.

Mobile Phase	A: Aqueous 0.1% formic acid, 5 mM ammonium formate	
	B: Acetonitrile	
Time (min)	% B	Flow ( $\mu\text{L}/\text{min}$ )
0.0	5.0	400
2.0	5.0	400
16.0	90.0	400
17.5	90.0	400
19.0	5.0	400
20.5	5.0	400

Precursor ion followed by enhanced product ion (PI-EPI) analysis was carried out to identify the structures of GSH trapped metabolites in each sample. The PI scan of  $m/z$  272 was run in negative mode at a scan range of  $m/z$  300 to  $m/z$  1000 and a scan rate of 2000 Da/s. Information-dependent acquisition (IDA) was used to trigger the acquisition of EPI spectra for ions greater than 5000 cps with exclusion of ions for 5 s after three occurrences for the two most intense peaks. The EPI scan was run in positive mode for daughter ions from  $m/z$  100 to  $m/z$  1000 at a scan rate of 10,000 Da/s and a LIT fill time of 35 ms. The LC effluent was introduced directly into the MS. Source operation parameters for the LC-MS/MS system are summarized in Table 6-2.

**Table 6-2** MS source parameters for Phase I GSH trapped metabolites identification.

PI scan		EPI scan	
Source parameters		Source parameters	
Temperature ( $^{\circ}\text{C}$ )	500	Temperature ( $^{\circ}\text{C}$ )	500
Curtain gas (psi)	25.0	Curtain gas (psi)	25.0
Gas 1 (psi)	50.0	Gas 1 (psi)	50.0
Gas 2 (psi)	60.0	Gas 2 (psi)	60.0
Collision gas (psi)	Medium	Collision gas (psi)	High
IonSpray voltage (V)	-4500	IonSpray voltage (V)	5500
DP	-75.0	DP	75.0
EP	-10.0	EP	7.0
CE	-30.0	CE	40.0
CXP	-12.0	CES	20.0

### 6.2.3.1. LC-MS/MS for identification of Phase II Phe-Lys trapped metabolites

Samples generated in incubations experiments were analyzed using LC-MS/MS. LC-MS/MS was performed on an Agilent 1290 Infinity LC system connected to a AB Sciex Qtrap® 5500. The column and flow rate used were identical to that of section 6.2.3. The column temperature was set at 35°C. The mobile phase used was constituted of aqueous 5 mM ammonium formate, pH 5.0 and acetonitrile. Gradient elution was used to separate the trapped metabolites in the injection sample. Total run time was 15.0 min for each injected sample. The LC conditions are summarized in Table 6-3.

**Table 6-3** LC conditions for Phase II Phe-Lys trapped metabolites identification.

Mobile Phase	A: Aqueous 5 mM ammonium formate, pH 5.0	
	B: Acetonitrile	
Time (min)	% B	Flow ( $\mu\text{L}/\text{min}$ )
0.0	10.0	400
2.0	10.0	400
10.0	90.0	400
12.0	90.0	400
13.0	10.0	400
15.0	10.0	400

Enhanced mass scan followed by enhanced product ion (EMS-EPI) analysis was carried out to identify the structures of Phe-Lys trapped metabolites in each sample. The EMS scan was run in negative mode at a scan range of  $m/z$  300 to  $m/z$  1000 at a scan rate of 2000 Da/s. IDA was used to trigger the acquisition of EPI spectra for ions greater than 5000 cps for the two most intense peaks. The EPI scan was run in positive mode for daughter ions from  $m/z$  100 to  $m/z$  900 at a scan rate of 10,000 Da/s and a LIT fill time of 35 ms.

The LC effluent was introduced directly into the MS. Source operation parameters for the LC-MS/MS system are summarized in Table 6-4.

**Table 6-4** MS source parameters for Phase II Phe-Lys trapped metabolites identification.

PI scan		EPI scan	
Source parameters		Source parameters	
Temperature (°C)	500	Temperature (°C)	500
Curtain gas (psi)	25.0	Curtain gas (psi)	25.0
Gas 1 (psi)	50.0	Gas 1 (psi)	50.0
Gas 2 (psi)	60.0	Gas 2 (psi)	60.0
Collision gas (psi)	Medium	Collision gas (psi)	High
IonSpray voltage (V)	-4500	IonSpray voltage (V)	4500
DP	-75.0	DP	75.0
EP	-10.0	EP	10.0
CE	-30.0	CE	40.0
CES	0.0	CES	12.0

### 6.3. Results

#### 6.3.1. Structure elucidation of Phase I GSH trapped reactive metabolites for selected compounds

The bio-synthesized GSH trapped reactive metabolites were analyzed using a PI-EPI scan using LC-MS/MS. The initial PI scan detects analytes with the propensity to form a product anion of  $m/z$  272 which corresponds to the glutathionyl moiety (precursor of  $m/z$  272). The detection of the product ion then triggers the acquisition of the EPI scan of the analytes via set IDA parameters. In order to confirm that the formation of the metabolites were due to Phase I metabolism, negative controls were prepared with omission of the required co-factor NADPH. As seen from Figures 6-1a and 6-1b, the total ion chromatogram (TIC) and extracted ion chromatogram (XIC) of the negative control of compound **3** (diclofenac) showed no visible peaks that corresponded to the possible trapped metabolites shown in Figures 6-1c and 6-1d. This

indicated that the peaks observed for the trapped metabolites were not artefacts present in the sample or formed during LC-MS/MS analysis.

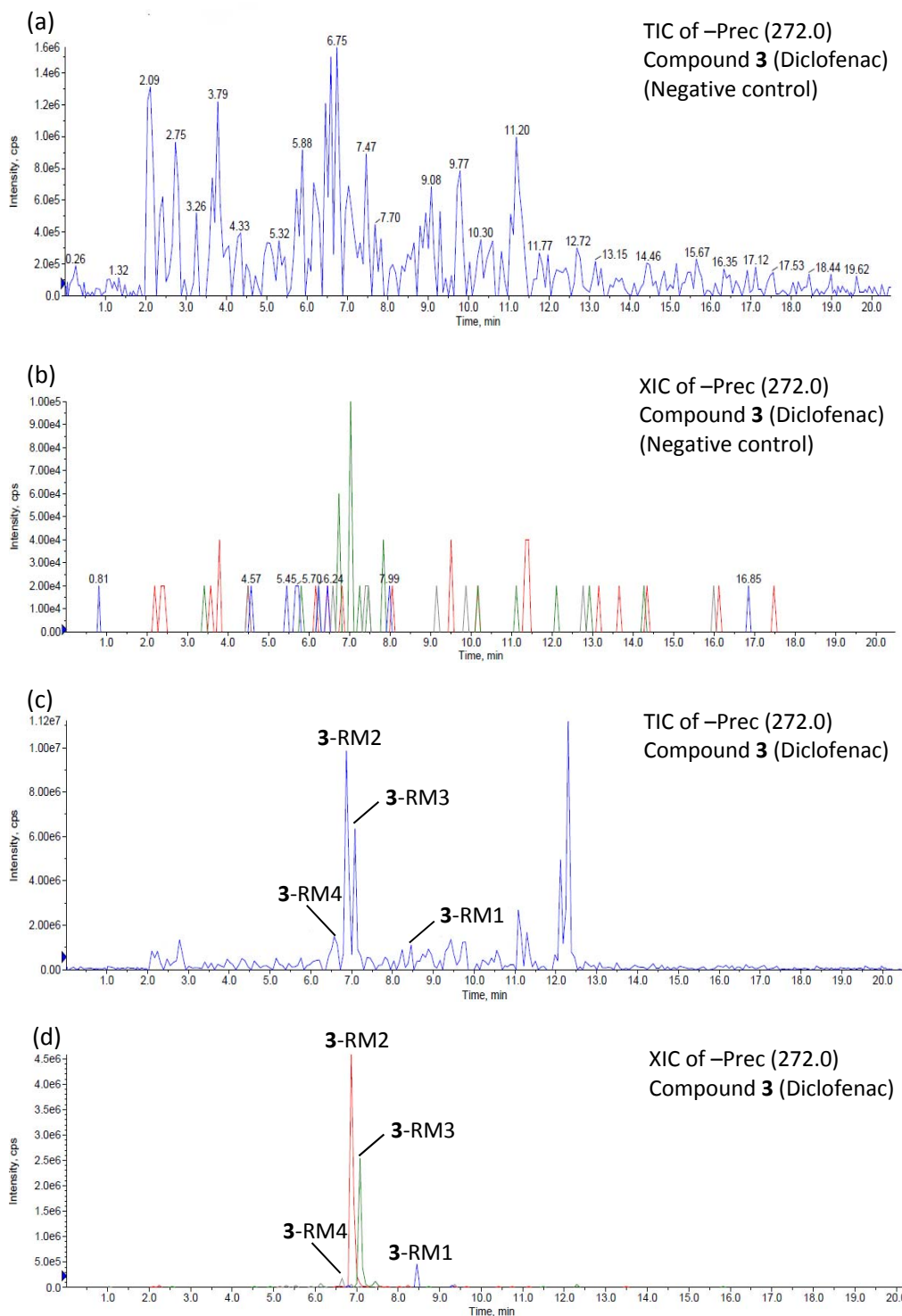


**Figure 6-1** TIC of negative PI scan of  $m/z$  272 and the subsequent XIC trace of the trapped metabolites for compound 3 (diclofenac). (a) TIC of negative control; (b) XIC of negative control; (c) TIC of compound 3 sample and (d) XIC of compound 3 sample.

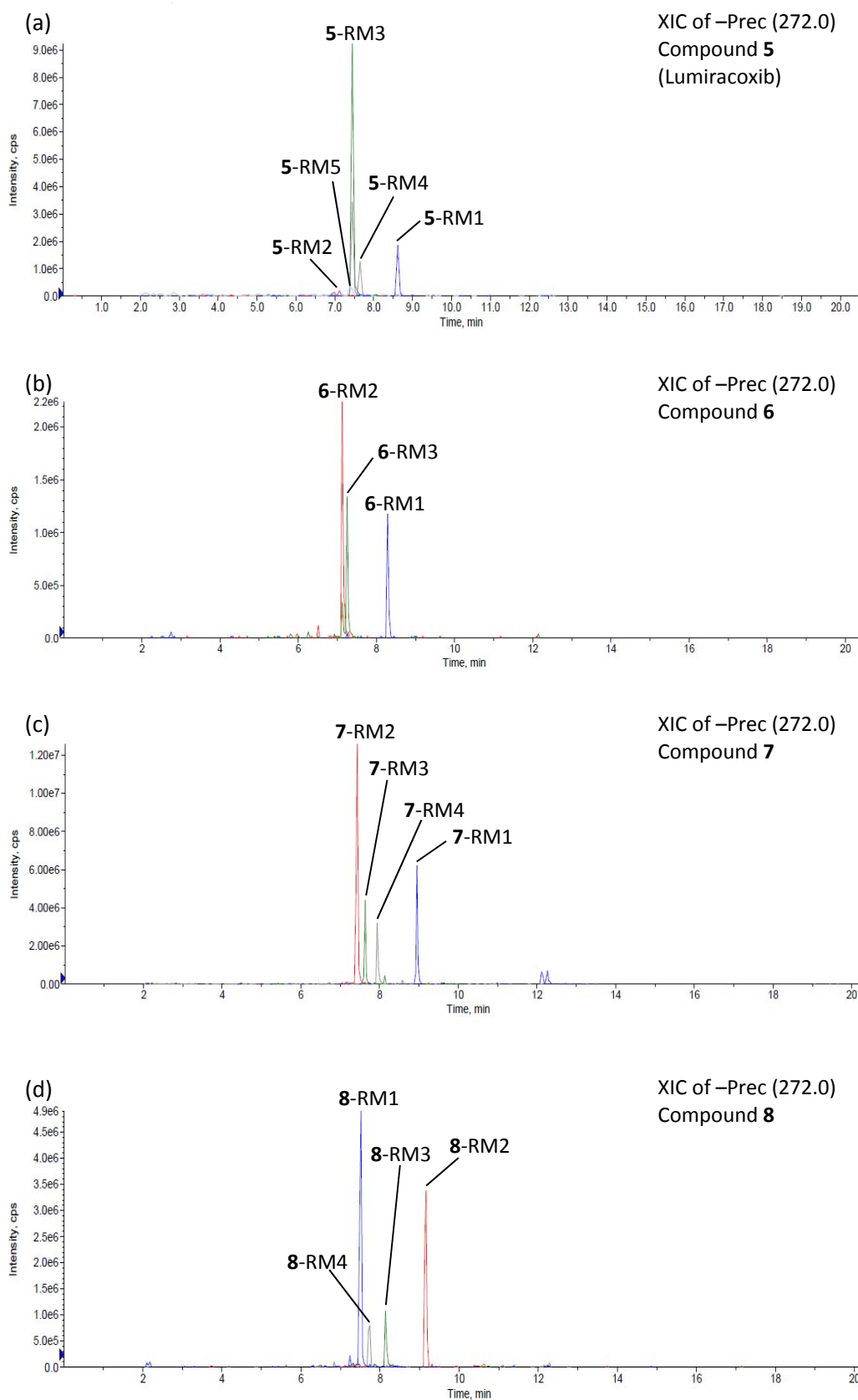


**Figure 6-2** XIC trace of GSH trapped metabolites of (a) compound 5; (b) compound 6; (c) compound 7 and (d) compound 8 of the methyl series.

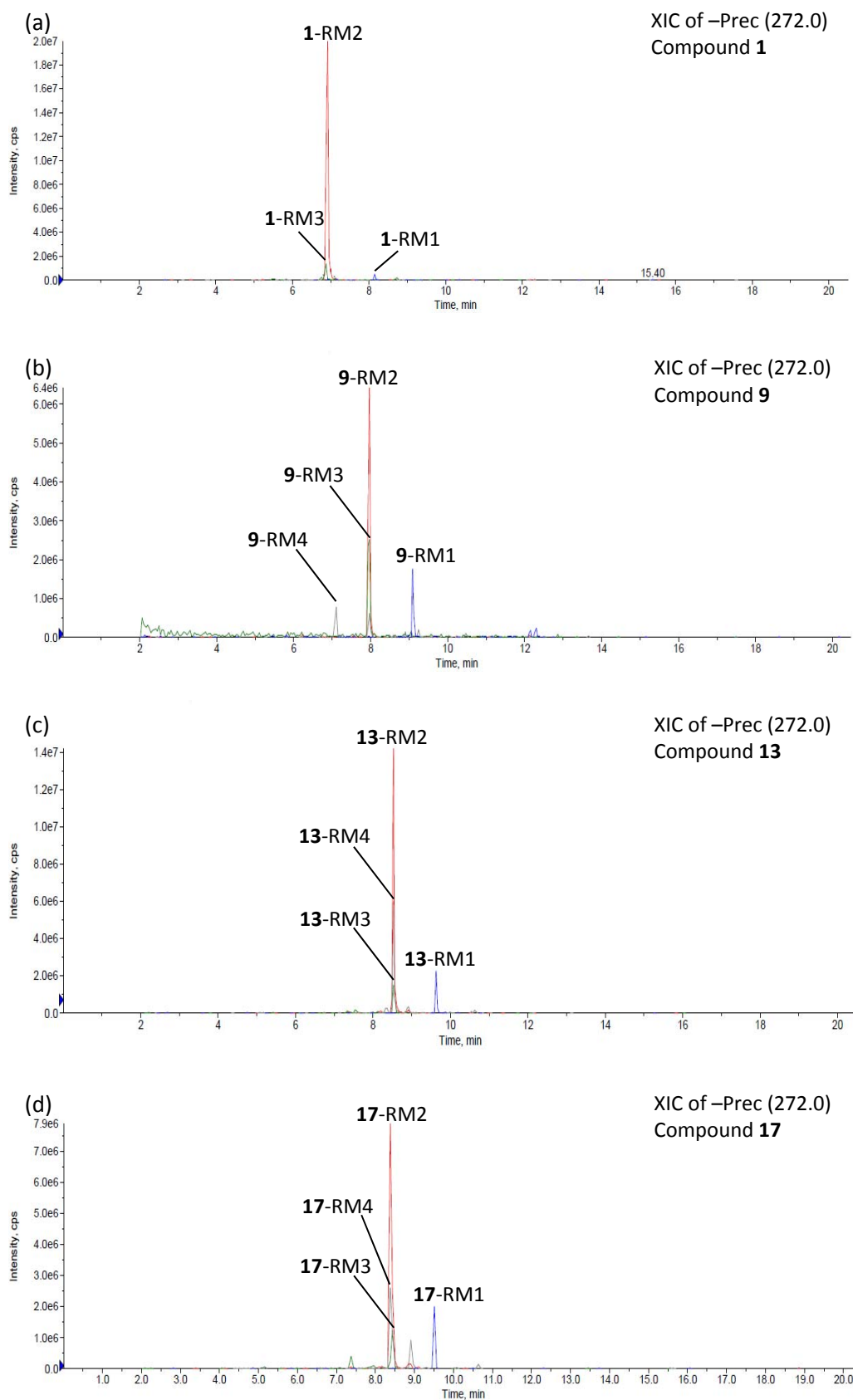


**Figure 6-3** XIC trace of GSH trapped metabolites of (a) compound 1; (b) compound 9; (c) compound 13 and (d) compound 17.

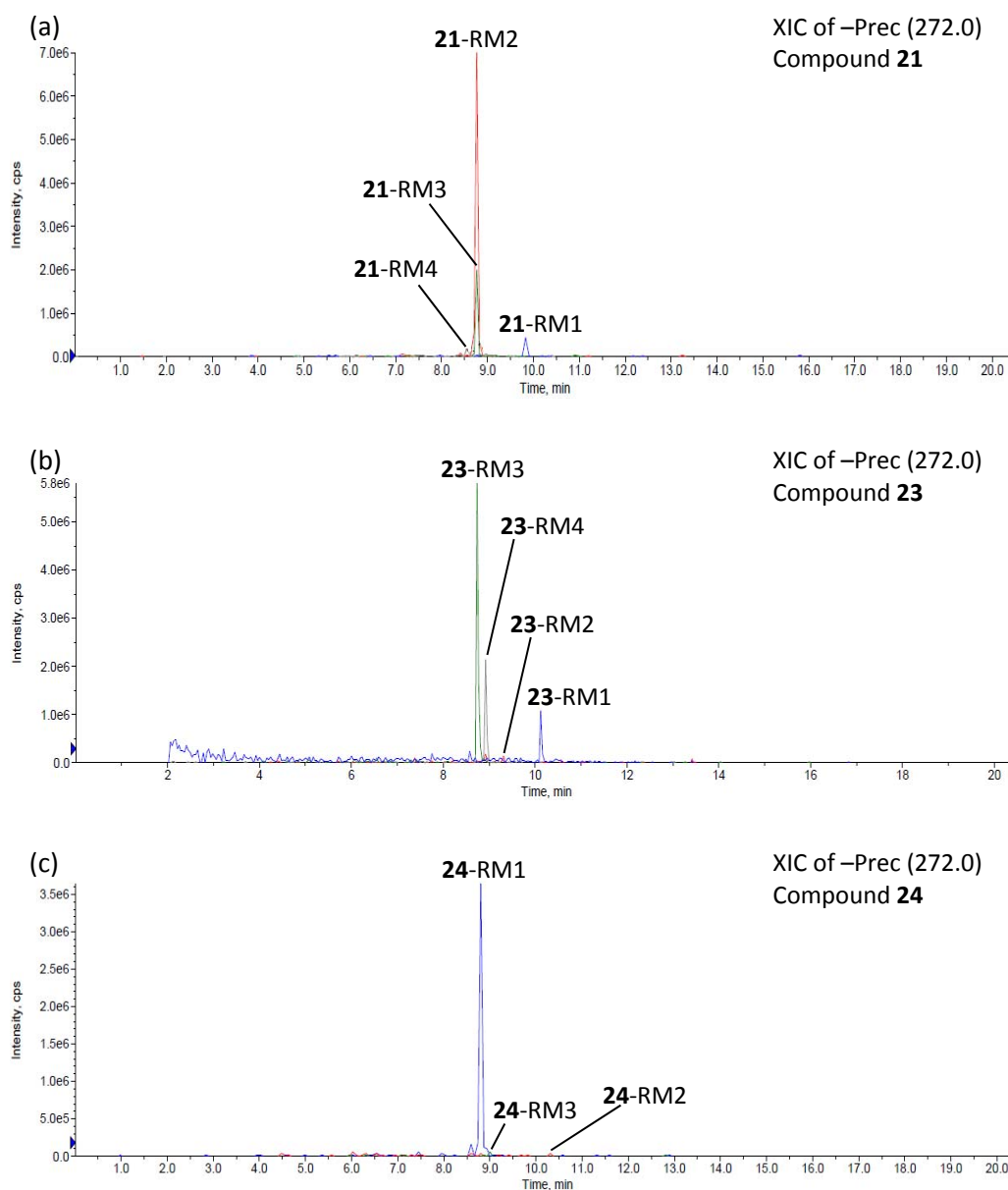


**Figure 6-4** XIC trace of GSH trapped metabolites of (a) compound **21**; (b) compound **23** and (c) compound **24**.

We chose twelve compounds for analysis of their possible reactive metabolites formed via Phase I metabolism. Compound **3** (diclofenac) was chosen as a validation compound to determine if the incubation and LC-MS/MS analysis method is usable. The methyl series (compounds **5** to **8**) were chosen as a comparison set between different halogen substituents at R<sub>2</sub> and R<sub>3</sub>. The F-Cl compounds (**1**, **5**, **9**, **13**, **17** and **21**) were also chosen as a comparison between

different alkyl substituents at R<sub>1</sub>. Figures 6-2 to 6-4 show the XIC of the possible trapped metabolites formed for each analyzed compound.

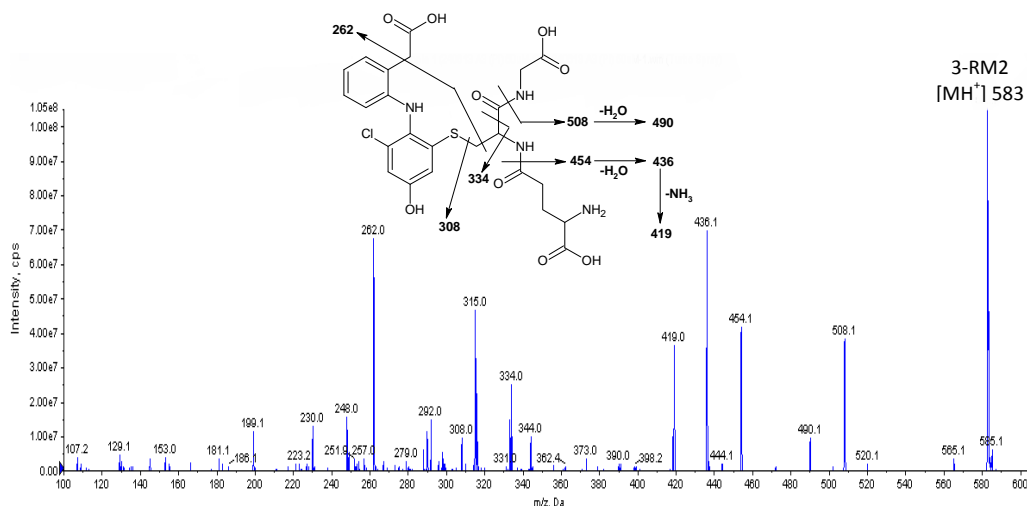


**Figure 6-5** EPI spectra for **3-RM2** ( $m/z$  583). Proposed structure and fragmentation pathway of the structure is shown for **3-RM2**.

Figure 6-5 shows an example of the EPI spectra of a trapped metabolite of compound **3** (**3-RM2**). The EPI spectra list the possible daughter ion fragments from the parent ions analyzed. From this information, the structure of the parent ion can be proposed from the fragmentation pathway shown by the EPI spectra. The main fragments that were observed for each EPI spectra were the neutral loss of the glycine moiety ( $m/z$  75) and the pyroglutamate moiety ( $m/z$  129) from the conjugated GSH chain.

To validate our analysis method used, we compared the proposed structures of diclofenac (compound **3**) in our study with that of literature. **3-RM2** ( $[MH^+]$  583) and **3-RM3s** ( $[MH^+]$  617) are the major metabolites found in our study. **3-RM2** corresponds to the hydroxylation at the 4'-position on the aniline ring followed by dechlorination and subsequent GSH conjugation at the



dechlorinated carbon. **3**-RM3s have two structures; **3**-RM3a was proposed to be hydroxylation at the 4'-position on the aniline ring followed by GSH conjugation on the ring and **3**-RM3b was proposed to be hydroxylation at the 5-position on phenylacetic acid ring followed by GSH conjugation on the ring. These trapped metabolites have been extensively investigated and identified in several microsomal incubation studies, indicating that the analysis method employed in our study is valid for detection of GSH trapped metabolites of our compounds (Tang *et al.*, 1999a; Poon *et al.*, 2001; Yu *et al.*, 2005; Zheng *et al.*, 2007; Wen *et al.*, 2008).

In chapter 5, we investigated the reactivity of the compounds towards cellular GSH after exposure to Phase I metabolism and found that the compounds exhibited some reactivity towards GSH. This work followed-up on that to confirm adduct formation of such reactive species by exogenous GSH and to propose the chemical structures based on signature MS/MS spectra. Tables 6-5 to 6-16 show the proposed structure and fragmentation pathways of the trapped metabolites of the all the compounds analyzed from the EPI spectra scans obtained.

In addition to common metabolites found in literature for diclofenac, we have detected the formation of benzyl-S-GSH metabolite of diclofenac (**3**-RM1) in our study. This was a novel GSH conjugated metabolite of diclofenac detected in studies involving *in vivo* and *in vitro* analysis and proposed to be formed via decarboxylation of the carboxylic acid moiety of ring A (Grillo *et al.*, 2008;

Teffera *et al.*, 2008). Here, we discovered that this benzyl-S-GSH metabolite formation is ubiquitous across all compounds analyzed in our study.

Di-hydroxylated diclofenac metabolites were found to be formed *in vivo* in human (Stierlin *et al.*, 1979) and a di-hydroxylated, dechlorinated GSH trapped diclofenac metabolite formed via *in vitro* microsomal incubations was identified in a separate study (Wen *et al.*, 2008). However, we detected a GSH trapped di-hydroxylated diclofenac metabolites (**3**-RM4s) that did not undergo dechlorination. The peak corresponding to the **3**-RM4s on the XIC of compound **3** was observed to be very small (Figure 6-1d). A further search through literature showed no studies that have identified this GSH trapped di-hydroxylated metabolite.

Comparing across different halogen substituents at R<sub>2</sub> and R<sub>3</sub> on the formation of reactive metabolites for the methylated compounds, we observed some interesting findings. Firstly, the major metabolite formed for each halogen combination was the mono-hydroxylated, dehalogenated GSH adduct (Figures 6-1 to 6-4). Defluorination, dechlorination and debromination has been found to be able to occur in halogenated aromatic compounds during Phase I metabolism (Park *et al.*, 2001; Hakk and Letcher, 2003; Isin and Guengerich, 2007). For the symmetrical F-F, Cl-Cl and Br-Br compounds (**6**, **7** and **8**), the dehalogenation involves either one of the halogen substituent. When an asymmetrical halogenated ring (F-Cl) is involved (e.g. compound **5**, lumiracoxib), we observed that defluorination took priority over dechlorination. This was in line with literature findings whereby compound **5**

(lumiracoxib) was found to form the mono-hydroxylated and defluorinated GSH adduct instead of the dechlorinated GSH adduct (Li *et al.*, 2008; Kang *et al.*, 2009). That said, a mono-hydroxylated and dechlorinated GSH adduct (**5-RM2**) was observed for compound **5** but the amount of this metabolite formed was very small as compared to the defluorinated GSH adduct (**5-RM3**) as seen from Figure 6-2a. **5-RM2** has not been found in prior studies. A study found instead that for dechlorination to occur, defluorination needs to have taken place, resulting in the formation of an adduct with double conjugated GSH (Kang *et al.*, 2009). The preference towards defluorination was observed for all the F-Cl compounds analyzed in this study (compounds **1**, **5**, **9**, **13**, **17** and **21**).

Comparing across the alkyl series for F-Cl compounds, we observed that the major metabolite formed was the mono-hydroxylated, defluorinated GSH adduct regardless of the alkyl substituent at R<sub>1</sub>. With methyl, ethyl, *n*-propyl and *iso*-propyl substituted compounds, a direct GSH adduct with the alkyl group at R<sub>1</sub> was formed. This is in line with literature findings whereby lumiracoxib was observed to form such an adduct (Kang *et al.*, 2009) and quinone methides with methyl, ethyl and propyl substituents were observed to form GSH adducts (Thompson *et al.*, 1995). We confirmed that the *tert*-butyl substituted compounds (**21**, **23** and **24**) were observed to be unable to form a direct GSH adduct with the *tert*-butyl group at R<sub>1</sub>. This was as expected as *tert*-butyl substituted compounds are unable to form imine methides.

Given that *tert*-butyl substituted compounds could not form imine methides and yet was the most toxic compounds of the series, we decided to investigate the two most toxic compounds, **23** and **24**. From the LC-MS/MS analysis data, we observed that for compound **23**, the type of metabolites formed were similar to other compounds. The only exception was the detection of a direct GSH adduct formed through the removal of a chlorine substituent (**23**-RM2) (Table 6-15). This indicated that compound **23**, in its non-hydroxylated state has the ability to form adducts with GSH. On the other hand, for the most toxic compound (**24**), we observed no such direct GSH adduct formation. Instead, we observed that the formation of the mono-hydroxylated, debrominated GSH adduct was very much in dominance over the other two metabolites detected (Figure 6-4c).

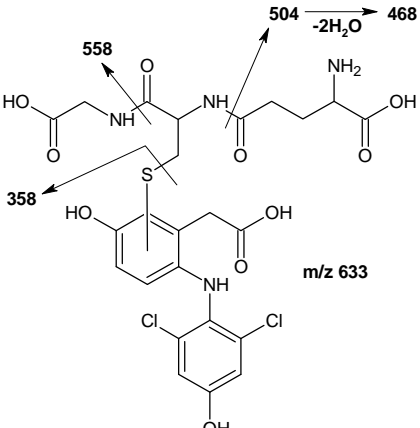
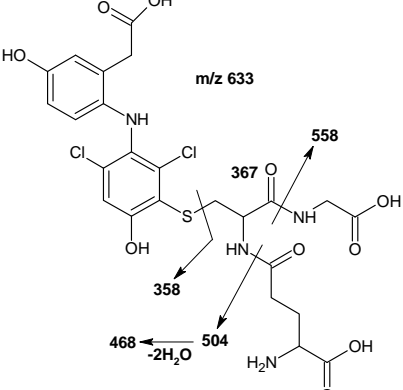
**Table 6-5** Proposed structures and fragmentation pathways for GSH-trapped metabolites of compound 1.

Metabolites	Proposed structure and fragmentation pathway	MH <sup>+</sup>	Fragment ion
1-RM1	<p>Fragmentation pathways for 1-RM1:</p> <ul style="list-style-type: none"> <li><math>m/z\ 541 \xrightarrow{-H_2O} 523</math></li> <li><math>308 \xrightarrow{-pyroGlu} 179</math></li> <li><math>412 \rightarrow 466</math></li> <li><math>234 \xrightarrow{-Cl} 214</math></li> <li><math>308 \rightarrow 308</math></li> </ul>	541	523, 466, 412, 308, 234, 214, 179
1-RM2	<p>Fragmentation pathways for 1-RM2:</p> <ul style="list-style-type: none"> <li><math>m/z\ 583 \rightarrow 308</math></li> <li><math>334 \rightarrow 508 \xrightarrow{-H_2O} 490</math></li> <li><math>454 \xrightarrow{-H_2O} 436 \xrightarrow{-NH_3} 419</math></li> <li><math>308 \rightarrow 262</math></li> </ul>	583	508, 490, 454, 436, 419, 334, 308, 262
1-RM3a	<p>Fragmentation pathways for 1-RM3a:</p> <ul style="list-style-type: none"> <li><math>m/z\ 601 \xrightarrow{-H_2O} 583</math></li> <li><math>526 \xrightarrow{-H_2O} 508</math></li> <li><math>472 \xrightarrow{-H_2O} 454 \xrightarrow{-H_2O} 436</math></li> <li><math>351 \rightarrow 326</math></li> </ul>	601	583, 526, 508, 472, 454, 436, 351, 326
1-RM3b	<p>Fragmentation pathways for 1-RM3b:</p> <ul style="list-style-type: none"> <li><math>m/z\ 601 \xrightarrow{-H_2O} 583</math></li> <li><math>472 \xrightarrow{-H_2O} 454 \xrightarrow{-H_2O} 436</math></li> <li><math>526 \xrightarrow{-H_2O} 508</math></li> <li><math>351 \rightarrow 326</math></li> </ul>	601	583, 526, 508, 472, 454, 436, 351, 326

**Table 6-6** Proposed structures and fragmentation pathways for GSH-trapped metabolites of compound **3** (diclofenac).

Metabolites	Proposed structure and fragmentation pathway	MH <sup>+</sup>	Fragment ion
<b>3-RM1</b>	<p>215 ← 250 (-Cl) 308 → 179 (-pyroGlu) m/z 557 → 539 (-H<sub>2</sub>O) 428</p>	557	539, 482, 428, 308, 250, 215, 179
<b>3-RM2</b>	<p>262 308 334 508 (-H<sub>2</sub>O) → 490 454 (-H<sub>2</sub>O) → 436 436 (-NH<sub>3</sub>) → 419 m/z 583</p>	583	508, 490, 454, 436, 419, 334, 308, 262
<b>3-RM3a</b>	<p>296 m/z 617 367 542 342 452 (-H<sub>2</sub>O) ← 470 (-H<sub>2</sub>O) 488</p>	617	542, 488, 470, 452, 367, 342, 296
<b>3-RM3b</b>	<p>542 488 (-H<sub>2</sub>O) → 470 (-H<sub>2</sub>O) → 452 367 342 296 m/z 617</p>	617	542, 488, 470, 452, 367, 342, 296

**Table 6-6 (Cont.)** Proposed structures and fragmentation pathways for GSH-trapped metabolites of compound **3** (diclofenac).

Metabolites	Proposed structure and fragmentation pathway	$MH^+$	Fragment ion
<b>3-RM4a</b>	 <p style="text-align: center;"><math>m/z</math> 633</p>	633	558, 504, 468, 358
<b>3-RM4b</b>	 <p style="text-align: center;"><math>m/z</math> 633</p>	633	558, 504, 468, 358

**Table 6-7** Proposed structures and fragmentation pathways for GSH-trapped metabolites of compound **5** (lumiracoxib).

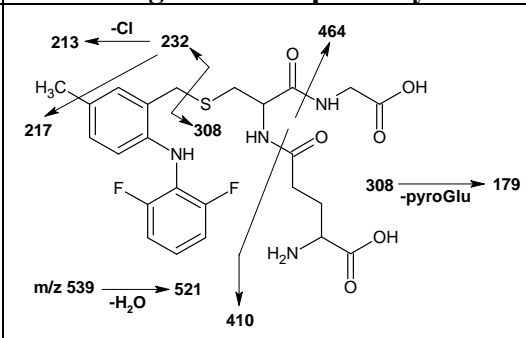
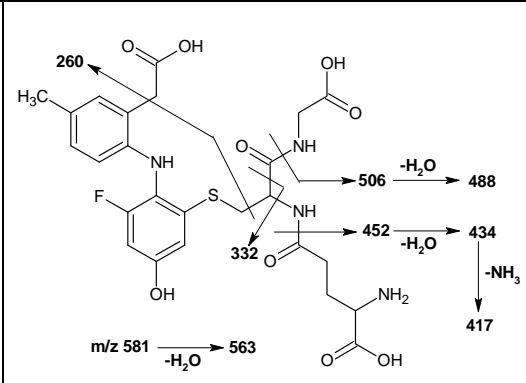
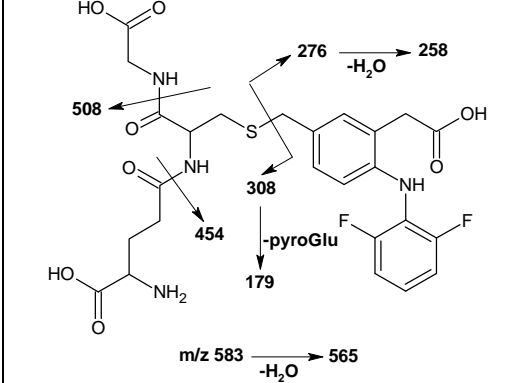
Metabolites	Proposed structure and fragmentation pathway	MH <sup>+</sup>	Fragment ion
<b>5-RM1</b>		555	537, 480, 426, 308, 248, 233, 212, 179
<b>5-RM2</b>		581	563, 506, 454, 432, 417, 347, 322, 276
<b>5-RM3</b>		597	579, 522, 504, 468, 450, 433, 347, 322, 276
<b>5-RM4</b>		599	581, 524, 470, 308, 292, 274, 179



**Table 6-7 (Cont.)** Proposed structures and fragmentation pathways for GSH-trapped metabolites of compound **5** (lumiracoxib).

Metabolites	Proposed structure and fragmentation pathway	$MH^+$	Fragment ion
5-RM5	<p>The diagram illustrates the proposed structure of a GSH-trapped metabolite of lumiracoxib. The structure features a central glutathione (GSH) molecule with a lumiracoxib moiety attached to the gamma-glutamyl group. The lumiracoxib moiety consists of a benzamide ring substituted with a chlorine atom, a fluorine atom, and a hydroxyl group, and a thiophene ring. Fragmentation pathways are indicated by arrows showing the loss of water (<math>-H_2O</math>) from various m/z values: <math>m/z</math> 615 to 597, 540 to 522, 486 to 468, and 468 to 450. Other labeled m/z values include 294, 340, 365, and 486.</p>	615	597, 540, 522, 486, 468, 450, 365, 340, 294

**Table 6-8** Proposed structures and fragmentation pathways for GSH-trapped metabolites of compound 6.

Metabolites	Proposed structure and fragmentation pathway	MH <sup>+</sup>	Fragment ion
<b>6-RM1</b>		539	521, 464, 410, 308, 232, 217, 213, 179
<b>6-RM2</b>		581	563, 506, 488, 452, 434, 417, 332, 260
<b>6-RM3</b>		583	565, 508, 454, 308, 276, 258, 179

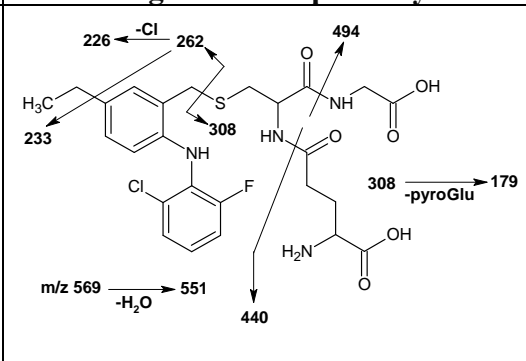
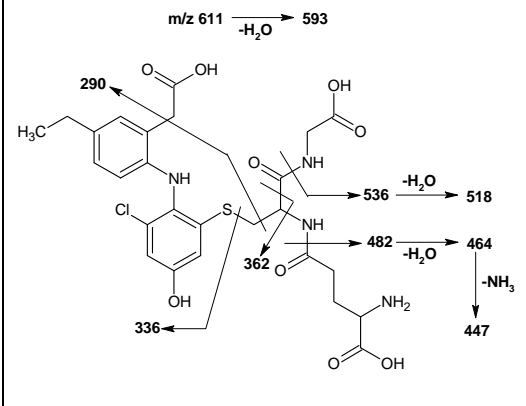
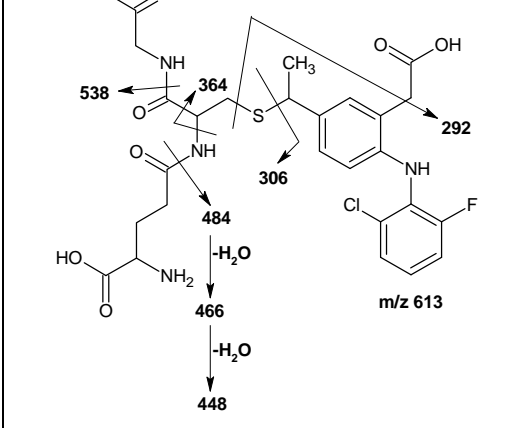
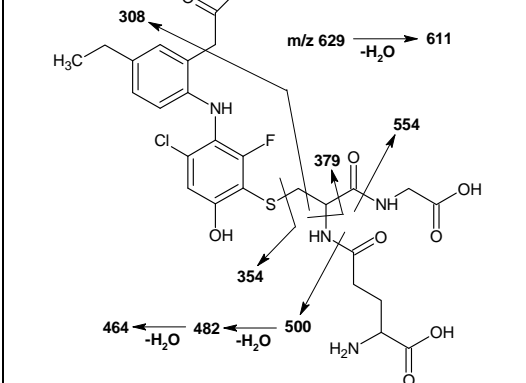
**Table 6-9** Proposed structures and fragmentation pathways for GSH-trapped metabolites of compound 7.

Metabolites	Proposed structure and fragmentation pathway	MH <sup>+</sup>	Fragment ion
7-RM1		571	553, 496, 442, 308, 264, 229, 179
7-RM2		597	579, 522, 504, 468, 450, 433, 347, 333, 276
7-RM3		631	613, 556, 538, 502, 484, 466, 381, 356, 310
7-RM4		615	597, 540, 486, 308, 290, 179

**Table 6-10** Proposed structures and fragmentation pathways for GSH-trapped metabolites of compound **8**.

Metabolites	Proposed structure and fragmentation pathway	MH <sup>+</sup>	Fragment ion
<b>8-RM1</b>	<p>m/z 641 <math>\xrightarrow{-H_2O}</math> 623</p> <p>320, 348, 366, 373, 391, 512, 548, 556, 494, 477</p>	641	623, 566, 548, 512, 494, 477, 391, 373, 366, 348, 320
<b>8-RM2</b>	<p>m/z 659</p> <p>274, 308, 530, 179, 574</p>	659	584, 530, 308, 274, 179
<b>8-RM3</b>	<p>m/z 703 <math>\xrightarrow{-H_2O}</math> 685</p> <p>628, 574, 396, 378, 308, 179</p>	703	685, 628, 574, 396, 378, 308, 179
<b>8-RM4</b>	<p>m/z 719 <math>\xrightarrow{-H_2O}</math> 701</p> <p>311, 469, 644, 626, 444, 572, 590, 70</p>	719	701, 644, 626, 590, 572, 469, 444, 311

**Table 6-11** Proposed structures and fragmentation pathways for GSH-trapped metabolites of compound **9**.

Metabolites	Proposed structure and fragmentation pathway	MH <sup>+</sup>	Fragment ion
<b>9-RM1</b>		569	551, 494, 440, 308, 262, 233, 226, 179
<b>9-RM2</b>		611	593, 536, 518, 482, 464, 447, 362, 336, 290
<b>9-RM3</b>		613	538, 484, 466, 448, 364, 306, 292
<b>9-RM4</b>		629	611, 554, 500, 482, 464, 379, 354, 308

**Table 6-12** Proposed structures and fragmentation pathways for GSH-trapped metabolites of compound **13**.

Metabolites	Proposed structure and fragmentation pathway	MH <sup>+</sup>	Fragment ion
<b>13-RM1</b>		583	565, 508, 454, 308, 276, 240, 234, 179
<b>13-RM2</b>		625	550, 532, 496, 478, 460, 375, 350, 304
<b>13-RM3</b>		643	625, 568, 550, 514, 496, 478, 393, 368
<b>13-RM4</b>		627	609, 552, 534, 498, 480, 352, 334, 320, 306, 302

**Table 6-13** Proposed structures and fragmentation pathways for GSH-trapped metabolites of compound 17.

Metabolites	Proposed structure and fragmentation pathway	MH <sup>+</sup>	Fragment ion
17-RM1		583	508, 454, 308, 276, 240, 234, 179
17-RM2		625	550, 532, 496, 478, 461, 376, 304
17-RM3		643	568, 514, 496, 478, 393, 322
17-RM4		627	552, 534, 498, 480, 378, 359, 352, 321, 306

**Table 6-14** Proposed structures and fragmentation pathways for GSH-trapped metabolites of compound **21**.

Metabolites	Proposed structure and fragmentation pathway	MH <sup>+</sup>	Fragment ion
<b>21-RM1</b>		597	579, 522, 468, 348, 308, 290, 255, 234, 179
<b>21-RM2</b>		639	564, 546, 510, 492, 475, 390
<b>21-RM3</b>		657	639, 582, 564, 528, 510, 492, 407, 382, 336
<b>21-RM4</b>		623	605, 548, 530, 494, 476, 373



**Table 6-15** Proposed structures and fragmentation pathways for GSH-trapped metabolites of compound **23**.

Metabolites	Proposed structure and fragmentation pathway	MH <sup>+</sup>	Fragment ion
<b>23-RM1</b>		613	595, 538, 484, 308, 306, 271, 250
<b>23-RM2</b>		623	605, 548, 530, 494, 476, 458, 374
<b>23-RM3</b>		639	621, 564, 546, 510, 492, 475, 390, 364
<b>23-RM4</b>		673	655, 598, 580, 544, 526, 508, 423, 398

**Table 6-16** Proposed structures and fragmentation pathways for GSH-trapped metabolites of compound **24**.

Metabolites	Proposed structure and fragmentation pathway	MH <sup>+</sup>	Fragment ion
24-RM1		683	665, 608, 590, 554, 536, 518, 306
24-RM2		701	683, 572, 394, 315, 338, 308, 179
24-RM3		761	743, 686, 668, 632, 614, 511, 455

### 6.3.2. Structure elucidation of Phase II Phe-Lys trapped reactive metabolites for selected compounds

The bio-synthesized Phe-Lys trapped reactive metabolites from Phase II metabolism were analyzed using an EMS-EPI scan using LC-MS/MS. The initial EMS scan detects for analytes and the acquisition of the EPI scan was triggered via set IDA parameters when a peak is detected from the EMS scan.

As seen from Figure 6-6a, the TIC of compound **3** (diclofenac) shows several peaks, of which three corresponded to the Phe-Lys trapped AGs formed from compound **3** as seen from the XIC trace (Figure 6-6b). Two peaks were observed for **3**-rAG1 due to the formation of isomeric derivatives.

Further EPI spectra showed that the reactivity of the AGs towards Phe-Lys arose from both acyl migration (**3**-rAG1) and transacylation (**3**-rAG2) (Figures 6-6c and 6-6d). This was in line with literature findings whereby AGs of diclofenac were found to undergo acyl migration and subsequently conjugate to cellular nucleophiles with retention of the glucuronic acid moiety (Kretzrommel and Boelsterli, 1994a; Wang *et al.*, 2004). Also, AGs of diclofenac were found to undergo direct transacylation whereby the glucuronic acid moiety was lost and replaced by a cellular nucleophile (Grillo *et al.*, 2003). The mechanisms of transacylation and acyl migration will be further explained in the section 6.4.2. We also observed that the peak corresponding to transacylation in the XIC trace was very much smaller than the peak corresponding to acyl migration (Figure 6-6b).

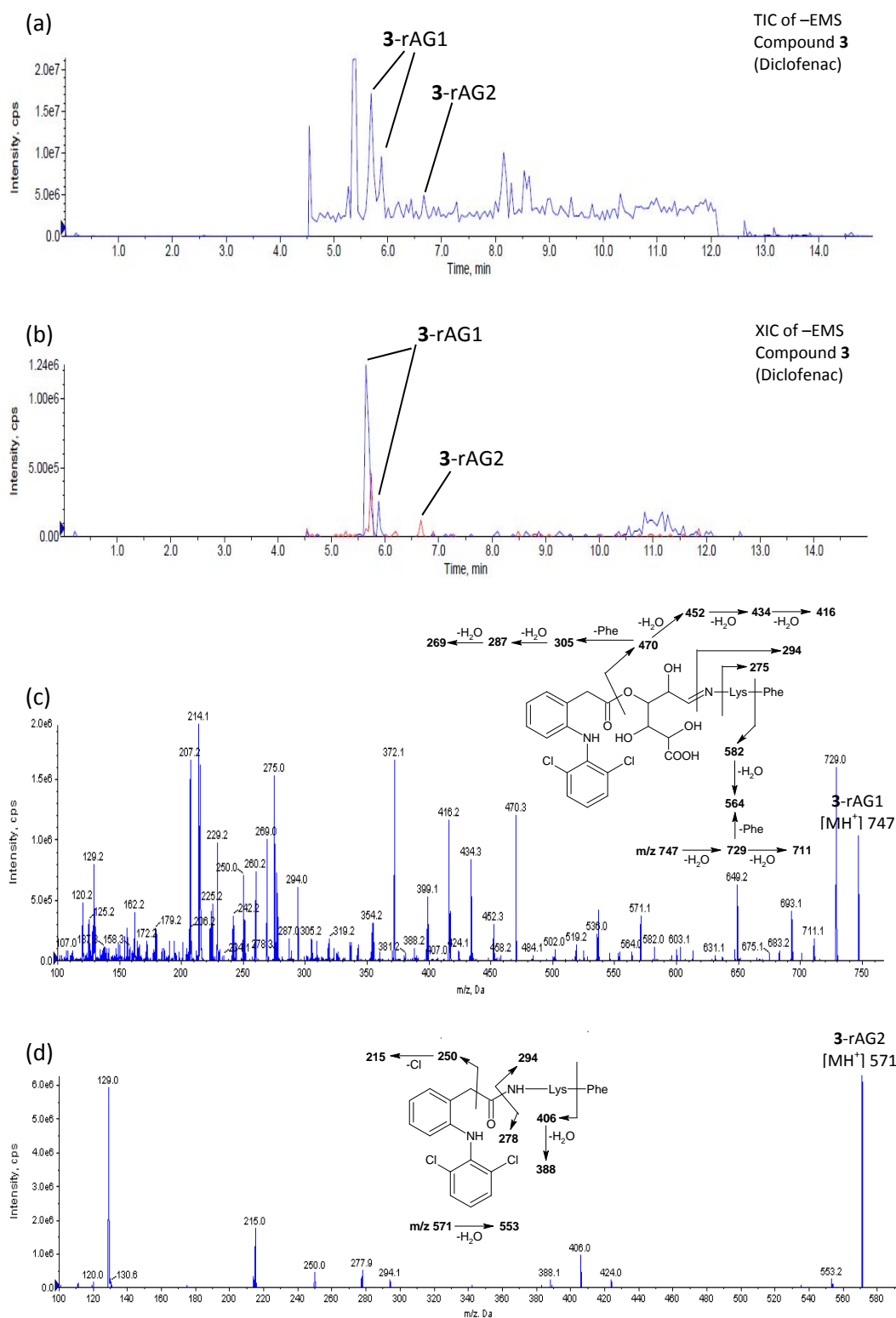


**Figure 6-6** (a) TIC of negative EMS full scan of compound 3 (diclofenac) reactive AGs trapped with Phe-Lys; (b) XIC of negative EMS full scan, showing the peaks corresponding to the two reactive AGs trapped with Phe-Lys; (c) Positive EPI spectra of 3-rAG1 that underwent acyl migration and the fragmentation pathway involved and (d) Positive EPI spectra of 3-rAG2 that underwent transacylation and the fragmentation pathway involved.

To confirm that AGs of lumiracoxib, like diclofenac can undergo acyl migration and transacylation, we carried out the EMS-EPI scan on Phe-Lys trapped lumiracoxib AGs samples. As seen from Figure 6-7a, we found three peaks that corresponded to the trapped AGs of lumiracoxib (compound **5**), two of which corresponded to isomeric derivatives of **5-rAG1** and one of which corresponded to **5-rAG2**. Similar to diclofenac, we found Phe-Lys derivatives that underwent acyl migration (**5-rAG1**) and transacylation (**5-rAG2**). Further EPI spectra scans gave the fragmentation pathway of the derivatives, which clearly indicated that **5-rAG1** retained the glucuronic acid moiety and **5-rAG2** lost the glucuronic acid moiety. Thus, we have proposed the structure of reactive AGs of lumiracoxib and have shown that like diclofenac, it can form conjugates with cellular nucleophiles via acyl migration or transacylation. Also observed for diclofenac, we found that the peak corresponding to transacylation in the XIC trace for lumiracoxib was very much smaller than the peak corresponding to acyl migration (Figure 6-7b).

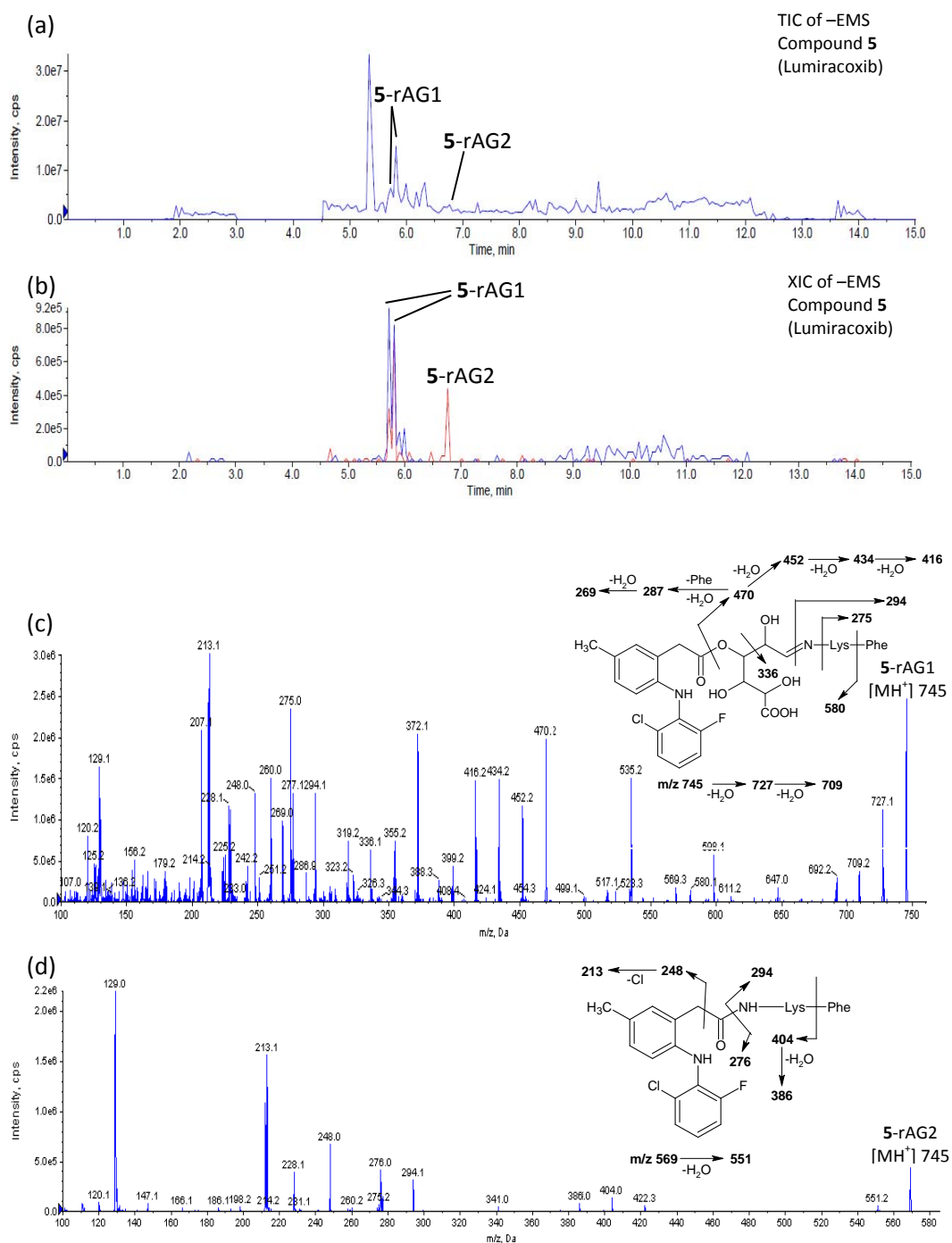


**Figure 6-7** (a) TIC of negative EMS full scan of compound **5** (lumiracoxib) reactive AGs trapped with Phe-Lys; (b) XIC of negative EMS full scan, showing the peaks corresponding to the two reactive AGs trapped with Phe-Lys; (c) Positive EPI spectra of **5-rAG1** that underwent acyl migration and the fragmentation pathway involved and (d) Positive EPI spectra of **5-rAG2** that underwent transacylation and the fragmentation pathway involved.

Five compounds of the F-Cl series (**1**, **9**, **13**, **17** and **21**) were selected to investigate the ability of their AGs to undergo acyl migration and

transacylation, congruent to the phenomenon seen with diclofenac. Similar to diclofenac and lumiracoxib, we found that all five compounds can undergo acyl migration and transacylation with subsequent adduct formation with Phe-Lys (Table 6-17). Similar to both diclofenac and lumiracoxib, we observed that the peak corresponding to transacylation in the XIC trace was very much smaller than the peak corresponding to acyl migration (Appendix 6-1). From data obtained from this sub-set of compounds, we propose that all the AGs of the compounds in our series can undergo the same acyl migration and transacylation transformations, contributing to the formation of reactive metabolites.

**Table 6-17** Proposed structures and fragmentation pathways for Phe-Lys-trapped metabolites of five selected compounds.

Metabolites	Proposed structure and fragmentation pathway	MH <sup>+</sup>	Fragment ion
<b>1-rAG1</b>		731	713, 695, 566, 548, 470, 452, 434, 416, 305, 294, 287, 275, 269
<b>1-rAG2</b>		555	537, 390, 372, 294, 262, 234, 199

**Table 6-17 (Cont.)** Proposed structures and fragmentation pathways for Phe-Lys-trapped metabolites of five selected compounds.

Metabolites	Proposed structure and fragmentation pathway	MH <sup>+</sup>	Fragment ion
<b>9-rAG1</b>	<p>m/z 759 <math>\xrightarrow{-H_2O}</math> 741 <math>\xrightarrow{-H_2O}</math> 723</p>	759	741, 723, 594, 470, 452, 434, 416, 305, 294, 287, 275, 269
<b>9-rAG2</b>	<p>m/z 583 <math>\xrightarrow{-H_2O}</math> 565</p>	583	565, 418, 400, 294, 290, 262, 227
<b>13-rAG1</b>	<p>m/z 773 <math>\xrightarrow{-H_2O}</math> 755</p>	773	755, 608, 470, 452, 434, 416, 305, 294, 287, 275, 269
<b>13-rAG2</b>	<p>m/z 597 <math>\xrightarrow{-H_2O}</math> 579</p>	597	579, 432, 304, 294, 276, 241
<b>17-rAG1</b>	<p>m/z 773 <math>\xrightarrow{-H_2O}</math> 755 <math>\xrightarrow{-H_2O}</math> 737</p>	773	755, 737, 608, 470, 452, 434, 416, 305, 294, 287, 275, 269



**Table 6-17 (Cont.)** Proposed structures and fragmentation pathways for Phe-Lys-trapped metabolites of five selected compounds.

Metabolites	Proposed structure and fragmentation pathway	MH <sup>+</sup>	Fragment ion
17-rAG2	<p>m/z 597 <math>\xrightarrow{-H_2O}</math> 579</p>	597	579, 432, 304, 294, 276, 241
21-rAG1	<p>m/z 787 <math>\xrightarrow{-H_2O}</math> 769</p>	787	769, 622, 470, 452, 434, 416, 305, 294, 287, 275, 269
21-rAG2	<p>m/z 611 <math>\xrightarrow{-H_2O}</math> 593</p>	611	593, 294, 290, 255

## 6.4. Discussion

### 6.4.1. Structure elucidation and possible bioactivation pathways of Phase I GSH trapped reactive metabolites for selected compounds

The LC-MS/MS analyses for the structure elucidation of the twelve selected compounds have confirmed the formation of several reactive metabolites, consistent with the role expected in the depletion of cellular GSH and subsequent toxicity expressed by the compounds. Collectively, the compounds

have generated several distinct reactive metabolites that are also associated with diclofenac and lumiracoxib metabolism.

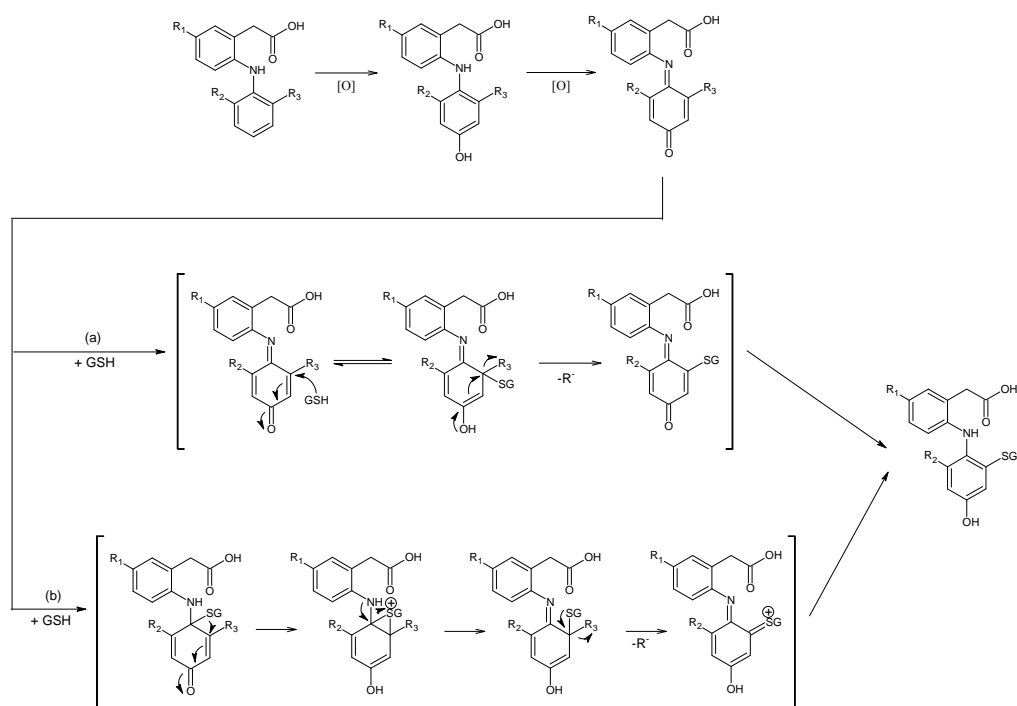


**Figure 6-8** Possible pathways for dehalogenation of quinone imines formed with subsequent conjugation of GSH via (a) direct attack on chlorinated atom or (b) *ipso* GSH addition.

The most common reactive metabolite detected for all the compounds was the mono-hydroxylated and dehalogenated GSH adduct. Like fluorine and chlorine substituents which can undergo dechlorination and defluorination in previous studies for diclofenac and lumiracoxib, bromine substituents can also undergo debromination in our series of compounds (Yu *et al.*, 2005; Kang *et al.*, 2009). This metabolite had been proposed to be formed via the quinone imine intermediate derived from the aniline ring (Yu *et al.*, 2005). The GSH molecule attacks the halogenated carbon on the quinone imine followed by removal of the halogen ion (Figure 6-8a). Another study proposed that formation of such dehalogenated GSH adduct could be via an *ipso* GSH

addition to a halogenated quinone imine at the *ortho* position (Figure 6-8b) (Zhang *et al.*, 2011). Thus, we postulate that generic dehalogenation, including debromination, for the series of compounds could be due to either pathway proposed in literature.

We made an interesting observation with F-Cl compounds, where defluorination prevailed over dechlorination during GSH adduct formation. While unexpected, this observation was also made by studies done on lumiracoxib whereby defluorination occurred instead of or before dechlorination (Li *et al.*, 2008; Kang *et al.*, 2009). Li *et al.* (2008) postulated that the preference towards defluorination could be due the small size of fluorine allowing easier access of the GSH to attack the site and stronger electron-withdrawing effect of fluorine rendering the fluorinated carbon a preferred target for attack by nucleophilic GSH. For some compounds such as lumiracoxib (compound **5**) and compound **21**, we detected a mono-hydroxylated, dechlorinated GSH adduct (**5**-RM2 and **21**-RM4). This type of adduct had not been previously found for compounds with such chemical scaffold. A possible reason could be that the amount of the mono-hydroxylated, dechlorinated adducts detected was very small as shown by the extremely low peak height in the XICs (Figures 6-1d and 6-4a) and could have gone undetected in previous studies.

There were no previous studies done on the metabolism of brominated 2-phenylaminophenylacetic acid derived compounds. We have mentioned that metabolic debromination was observed with our brominated compounds.

Metabolic debromination have been extensively studied in brominated flame retardants (Hakk and Letcher, 2003). It is less commonly studied in pharmaceutical drugs due to the fact that brominated drugs are uncommon (Hernandes *et al.*, 2010). From what was observed from our results, debromination, like defluorination and dechlorination serves as a mechanistic pathway to adduct formation. The higher toxicity observed with brominated compounds over other halogenated compounds could likely be due to other factors that affect the reactivity of the metabolites (Chapter 3 and Chapter 5).

Mono-hydroxylated GSH adduct were detected for each compound in addition to their dehalogenated counterpart. However, this adduct was not as significant as their dehalogenated counterpart. Similar to the mono-hydroxylated, dehalogenated GSH adducts, it had been proposed that the formation of such adducts was via the formation of a quinone imine and subsequent conjugation of GSH to an un-substituted carbon on the aromatic ring (Figure 6-9) (Tang *et al.*, 1999b; Li *et al.*, 2008). For hydroxylation to occur on Ring A, the substituent at R<sub>1</sub> can only be hydrogen as that is the point of hydroxylation. Thus, no mono-hydroxylated, GSH conjugated adducts on Ring A will be observed for compounds possessing an alkyl group on Ring A as shown in the proposed fragmentation pathways for alkylated compounds.

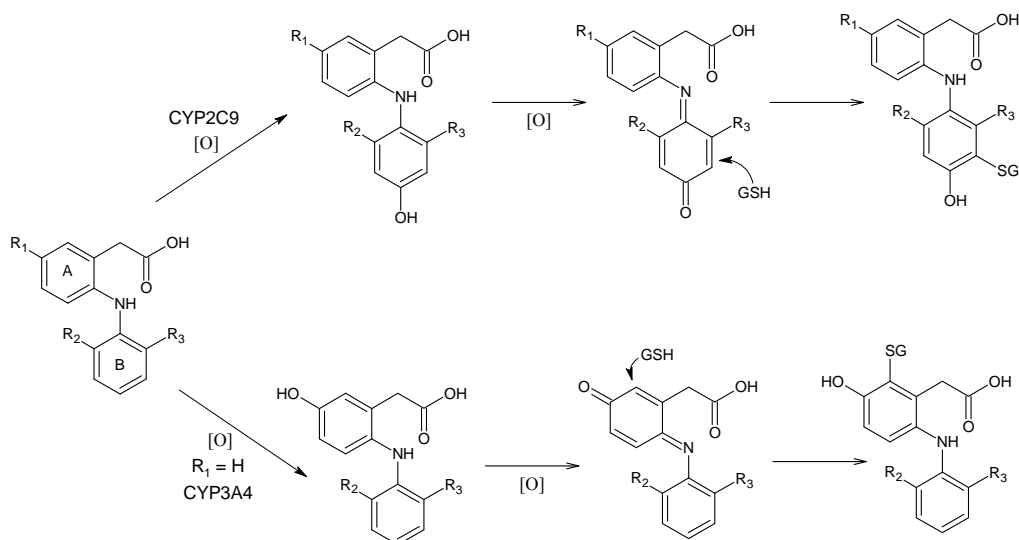


**Figure 6-9** Possible pathways for GSH adduct formation from quinone imines formed from the phenylacetic acid (Ring A) or the aniline ring (Ring B).

For the compounds substituted with methyl, ethyl, *n*-propyl and *iso*-propyl at  $R_1$  in our study, we detected the formation of a direct GSH adduct to the alkyl group of the compounds (**5-RM4**, **6-RM3**, **7-RM4**, **8-RM3**, **9-RM3**, **13-RM4**, **17-RM4**). This direct GSH adduct was also detected for lumiracoxib (**5-RM4**) in literature and was proposed to be formed via an imine methide (Figure 6-10) (Kang *et al.*, 2009). Imine methides can be formed as long as extractable hydrogens are available on the alkyl group involved. Thus, *tert*-butyl substituted compounds do not have the ability to form imine methides. This is confirmed by the absence of the direct GSH adducts observed with *tert*-butyl substituted compounds **21**, **23** and **24**.

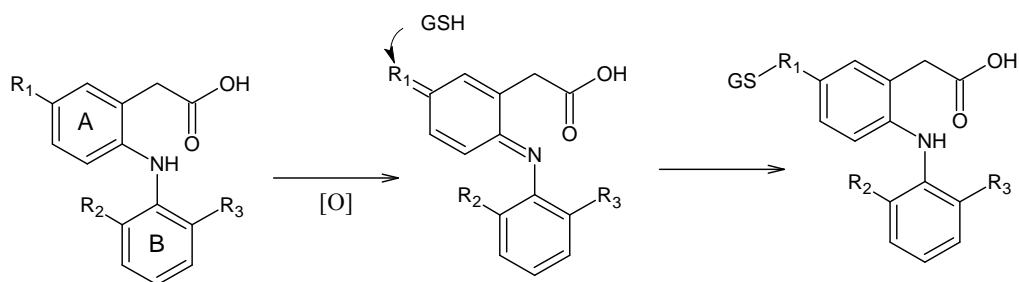


**Figure 6-10** Possible pathways for GSH adduct formation from imine methides formed from alkyl groups with an extractable hydrogen ( $R_1$  = methyl, ethyl, *n*-propyl and *iso*-propyl).

A GSH adduct formed via decarboxylation of the carboxylic acid group and subsequent conjugation with GSH was detected for all the compounds assayed. This GSH adduct was previously found in literature and was proposed to be formed via oxidative decarboxylation and formation of an *ortho*-imine methide (Figure 6-11) (Grillo *et al.*, 2008; Teffera *et al.*, 2008). Grillo *et al.* (2008) found that the P450 responsible for the oxidative decarboxylation was CYP3A4. Previously, lumiracoxib was proposed to be metabolized only by CYP2C9 (Mangold *et al.*, 2004). We found that lumiracoxib has the propensity to form this decarboxylated GSH adduct (**5-RM1**), thus, indicating that perhaps lumiracoxib can be metabolized by CYP3A4 via the oxidative decarboxylation pathway. This applies to our other compounds too as the decarboxylated GSH adduct was observed for all the compounds analyzed.

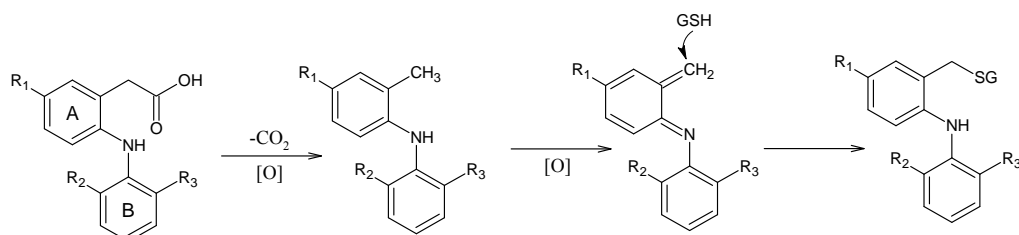


**Figure 6-11** Possible pathways for GSH adduct formation from *ortho*-imine methides formed oxidative decarboxylation.

It is of interest to note that the two most toxic compounds could not form imine methides. As a result, it is reasonable to propose that although the formation of imine methides may contribute to the toxicity of the compounds, it may not be a major determinant. On the other hand, Compound **23** was found to be able to form direct GSH adducts via dechlorination without prior hydroxylation on the aromatic ring (**23**-RM2), as an alternative metabolic pathway towards nucleophile addition. However, the peak corresponding to this GSH adduct is extremely small and its role as a major contributing factor to the toxicity of the compound remains questionable (Figure 6-4b). A possible mechanism for the formation of such a metabolite could be an *ipso* GSH addition to a dihalogenated aniline ring (Ring B) (Figure 6-12). This mechanism was proposed for dihalogenated anilines at the *ortho*- and *para*-positions but could likely be applied to double *ortho*-halogenated anilines (Zhang *et al.*, 2011).

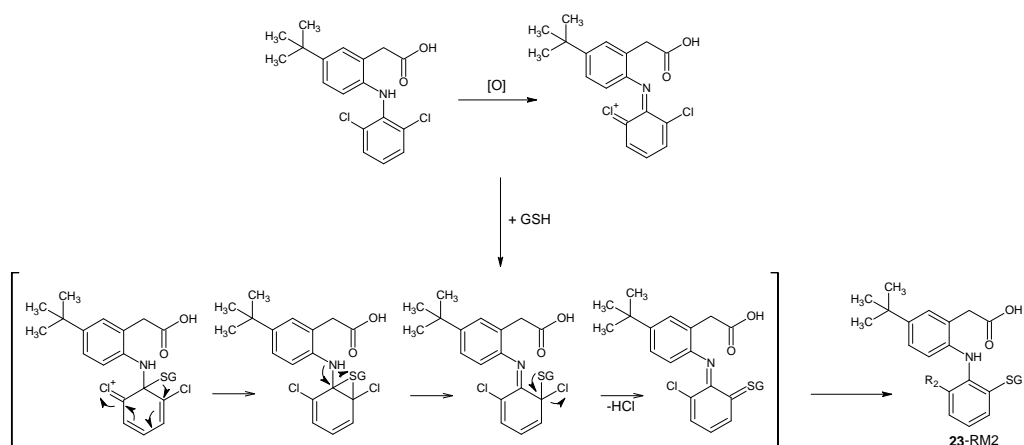


**Figure 6-12** Possible pathway for formation of **23**-RM2 from dechlorination followed by direct GSH conjugation via an *ipso* GSH addition mechanism.

For both compounds **23** and **24**, the major GSH adduct observed was the mono-hydroxylated, dehalogenated adduct (**23**-RM3 and **24**-RM1), especially

in the case of compound **24** where the other GSH adducts detected were very much lower than **24**-RM1. This GSH adduct could be more harmful than other adducts as the reactive metabolite precursor seems to be more reactive than other metabolites with its abundant formation. Given that **24**-RM1 is an abundant metabolite of compound **24**, it is no surprise compound **24** is highly toxic. Overall, we observed that common adducts were formed for each compound. The different substituents on them affect the quantity of each type of adduct formed when qualitatively comparing the peaks in each XIC trace. However, there seems to be no deducible trend on the effect of individual substituents on the structures of adducts formed as cross-compound comparison cannot be carried out. In order to investigate further, studies to quantify each GSH adduct formed for each compound would be needed for cross-compound comparison to elucidate the effect of substituents on the type and amount of adduct formed.

#### 6.4.2. Structure elucidation and possible bioactivation pathways of Phase II

##### Phe-Lys trapped reactive metabolites for selected compounds

AGs have been extensively studied and were found to be reactive when acyl migration or transacylation occurs and subsequent glycation of cellular nucleophiles such as proteins and DNA. Transacylation involves an intermolecular exchange of the glucuronic acid moiety for a cellular nucleophile such as GSH or protein (Faed, 1984; Stachulski *et al.*, 2006). The adduct forms consist of the parent aglycone and the conjugated nucleophile with the loss of the glucuronic acid moiety (Figure 6-13). Acyl migration occurs when the parent aglycone moiety migrate from the 1-position to the 2-



or 3-position to form 2-*O*- $\beta$  or 3-*O*- $\beta$ -AG followed by ring opening and formation of an aldehyde at the anomeric carbon (Faed, 1984; Langguth and Benet, 1992). Glycation of the amine group on cellular nucleophiles to the reactive aldehyde can form an imine known as a Schiff Base (Figure 6-13) (Smith *et al.*, 1990; Ding *et al.*, 1993).

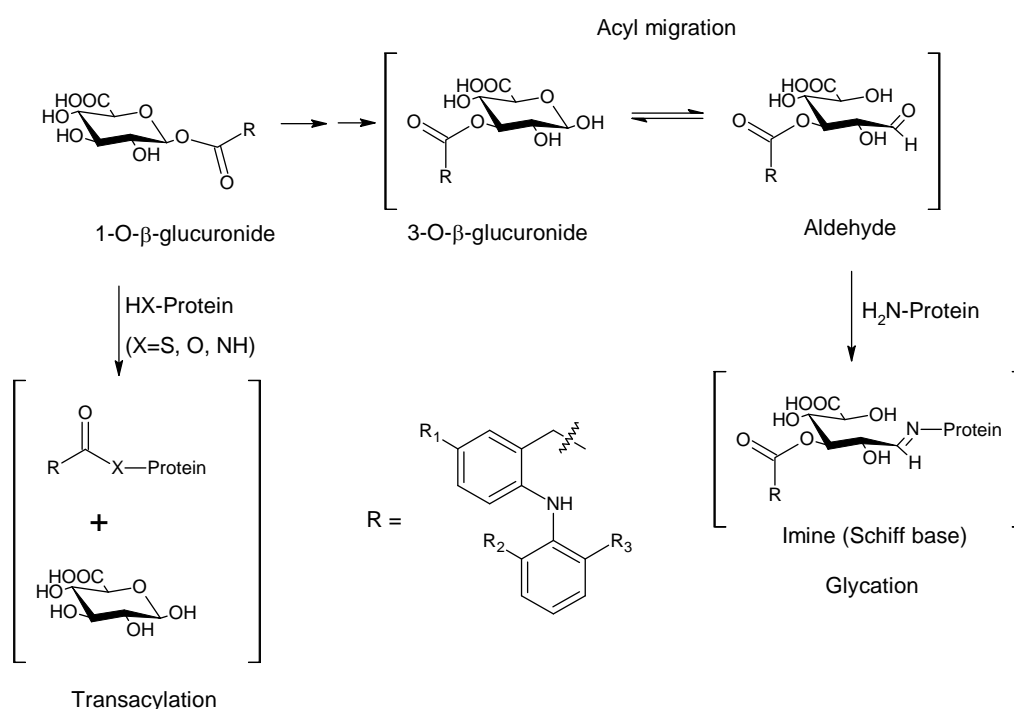


**Figure 6-13** Pathways involved in formation of AG adducts for the synthesized compounds. Transacylation involves replacement of the glucuronic acid moiety with a nucleophile. Acyl migration involves intramolecular rearrangement of aglycone. Here, a 3-*O*- $\beta$ -glucuronide is shown and subsequent ring opening to form an aldehyde and glycation to form a Schiff base. 2-*O*- $\beta$ -glucuronides and 4-*O*- $\beta$ -glucuronides are able to undergo ring opening to form reactive aldehydes.

The AGs of diclofenac have been shown to be reactive towards cellular protein and GSH via both acyl migration and transacylation and have been proposed to be a contributor to the hepatotoxicity associated with diclofenac (Kretzrommel and Boelsterli, 1993; Kretzrommel and Boelsterli, 1994a; Grillo *et al.*, 2003). We have shown in our study that our analysis method could

detect the trapped AGs that had undergone acyl migration and transacylation. Lumiracoxib have been shown to form AGs *in vivo*, albeit as a minor metabolite and *in vitro* (Mangold *et al.*, 2004; Kang *et al.*, 2009). However, no studies have investigated the reactivity of AGs of lumiracoxib either via acyl migration or transacylation. In Chapter 5, we have shown that the AGs biosynthesized from lumiracoxib have a degree of reactivity that is slightly lower as compared to diclofenac. Further LC-MS/MS analysis of the Phe-Lys trapped AGs of lumiracoxib showed that the AGs can undergo acyl migration (**5-rAG1**) and transacylation (**5-rAG2**) as shown by the proposed fragmentation pathways seen in Figures 6-7c and 6-7d. Thus, we propose that like diclofenac, the AGs of lumiracoxib may contribute to the hepatotoxicity associated with the drug due to the reactivity seen with its AGs and the ability to form acyl migrated and transacylated glycation adducts.

Similar to diclofenac and lumiracoxib, we observed acyl migration and transacylation occurring for the AGs of five selected compounds (**1**, **9**, **13**, **17** and **21**) in our series of compounds. This reflects a high possibility that the compounds in our series can form AGs which can further undergo acyl migration and transacylation. This may play a role in the toxicity observed with the compounds. This is supported by the AG reactivity results shown in Chapter 5 whereby we found that all the AGs of all the compounds in our series had certain degrees of reactivity towards the trapping agent, Phe-Lys. Judging from the reactive AGs identified and proposed, the substituents at R<sub>1</sub>, R<sub>2</sub> and R<sub>3</sub> had no effect on the structures of the trapped AGs but instead had some effects on the reactivity of the AGs as shown in Chapter 5.

Comparing the peaks corresponding to the different trapped AGs for each compound, the peak corresponding to transacylation was consistently smaller than that of acyl migration for all of the assayed compounds. This difference in peak heights could be due acyl migration being the major pathway in which AGs bioactivates. However, we also cannot rule out that this difference could be due to the different reactivity of the acyl migrated AGs and AGs undergoing transacylation towards the trapping agent used.

### 6.5. Conclusion

The bioactivation of the synthesized compounds via Phase I and Phase II metabolism were associated with the toxicity observed in Chapter 5. In order to further confirm that bioactivated reactive metabolites were responsible for the toxicity of the compounds and to investigate the possible structures of the reactive metabolites, we carried out LC-MS/MS analysis for structure elucidation on twelve selected compounds. GSH trapped metabolites were detected for each compound analyzed, which indicates that the presence of trapped metabolites supports a role for formation of reactive metabolites in the toxicity observed with the synthesized compounds.

We found that for Phase I metabolism, the major reactive metabolite was the mono-hydroxylated, dehalogenated metabolite for all the compounds tested. For F-Cl compounds, there was a preference for defluorination over dechlorination. The reactivity of the hydroxylated metabolites was proposed to arise from the formation of quinone imines, which are electrophilic in nature

and is susceptible towards attack by cellular nucleophiles such as GSH or protein. The compounds that possess an alkyl substituent at R<sub>1</sub> (methyl, ethyl, *n*-propyl, *iso*-propyl) were able to directly conjugate to GSH at the alkyl substituent. The formation of these GSH adducts at the alkyl group was proposed to be due to the formation of imine methides. *tert*-Butyl substituted compounds were unable to form such a GSH adduct due to the absence of an extractable hydrogen at the site of attack.

In addition to hydroxylated, dehalogenated and direct GSH adducts of our compounds, we also detected benzyl-S-GSH adducts for all the compounds. Benzyl-S-GSH adducts were proposed to be formed via oxidative decarboxylation by CYP3A4. This adduct was previously detected for diclofenac but was not detected for lumiracoxib. Thus, lumiracoxib benzyl-S-GSH adduct is a novel metabolite detected in our study. With the detection of this GSH adduct, we propose that lumiracoxib and our synthesized compounds, like diclofenac, can be metabolized by both CYP2C9 and CYP3A4. A summary of all the possible Phase I metabolites proposed for our synthesized compounds are illustrated in Figure 14.

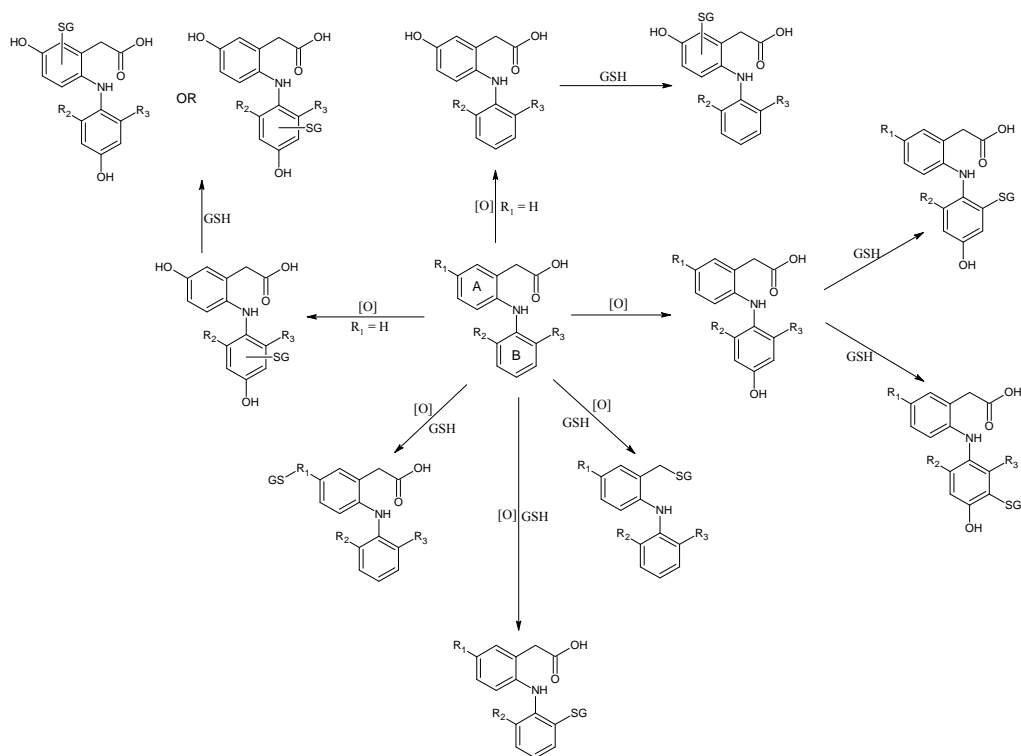


**Figure 6-14** Possible reactive metabolites and their GSH conjugates proposed for our synthesized compounds. It should be noted that individual compounds have their own signature reactive metabolites and not every reactive metabolites illustrated will be found for a single compound.

We have confirmed that lumiracoxib, like diclofenac, can form adducts with amine groups on proteins via acyl migration and transacylation from the fragmentation spectras of the Phe-Lys trapped AGs. Although AGs of lumiracoxib have been found to a minor metabolite *in vivo*, the ability of the AGs to bind to cellular nucleophiles can contribute to the hepatotoxicity associated with the drug. In addition, from the proposed pathways of Phase II reactive metabolites of five selected compounds, we propose that all the compounds in our series can form AGs that have the ability to undergo acyl migration and transacylation, which in turn could play a role in the toxicity observed with the compounds.

All in all, we have shown that our compounds can form reactive metabolites via both Phase I and Phase II metabolism *in vitro*. Together with the Phase I and Phase II metabolite reactivity results in Chapter 5, we conclude that the formation of reactive metabolites may have a role in toxicity observed with our compounds. From what was observed from our reactive metabolite trapping results, the most common pathway for formation of reactive metabolites for Phase I metabolism was hydroxylation with dehalogenation. For Phase II metabolism, the most common pathway was acyl migration. However, we should carry out absolute quantification of the individual trapped metabolites in order to confirm on the importance of the pathways involved and to carry out cross-compound comparisons in order to determine the effect of substituents on the type and amount of adducts formed. On the other hand, we cannot conclude on which phase of metabolism contributes more to the toxicity of the compounds as both phases of metabolism were measured separately from each other. In order to investigate whether Phase I and Phase II metabolism has a more critical role, both phases of metabolism should be carried out for the compounds concurrently and the reactive metabolites formed individually quantitated.

## **Chapter 7. Conclusion and Future Work**

The aim of the thesis is to investigate the effects of substituent on toxicity and pharmacological properties, specifically using the 2-phenylaminophenylacetic acid scaffold that brought about drugs like diclofenac and lumiracoxib. Although there have been several individual studies on the toxicity and pharmacology of said drugs, there have been few to no studies to compare the toxicity on its own or with pharmacological properties of such structurally similar drugs. Several studies have shown the undeniable link between bioactivation and hepatotoxicity of diclofenac and lumiracoxib. However, the relative contribution of the diverse mechanisms described thus far, and the influence of key substituents that may perturb this process remains elusive. Thus, we hypothesized that the varying substituents on the 2-phenylaminophenylacetic acid scaffold will affect bioactivation and subsequently, toxicity to a significant degree. We also hypothesized that the substituents will affect the intricate link between toxicity and pharmacological properties.

In order to investigate our hypotheses, we designed and synthesized twenty-four 2-phenylaminophenylacetic acid analogs that were structurally similar to diclofenac and lumiracoxib with varying substituents at three positions on the said chemical backbone (Chapter 2). The *in vitro* toxicity of the synthesized compounds were determined on two liver cell-lines in Chapter 3 with differentiating metabolic capabilities using MTT assay in order to determine their toxicity and subsequently, the effect of substituents on the toxicity

expressed by the compounds on liver cells and the possible role of metabolism in toxicity of the compounds. The cytotoxicity profile of the compounds showed that metabolism could play an important role in the toxicity of the compounds, given that  $LC_{50}$  values were lower in the more metabolically capable cell line (TAMH) as compared to the less metabolically capable cell line (HuH-7). Substituents on both phenyl rings were observed to affect the toxicity of the compounds significantly. It was observed that increasing the alkyl group size at  $R_1$  resulted in an increase in toxicity (indicated by a decrease in  $LC_{50}$  values). Increasing the halogen group size at  $R_2$  and  $R_3$  also increased the toxicity. Taken together, fluoro-substituted compounds are the least toxic while bromo-substituted compounds are the most toxic. Further comparative structure-toxicity relationships were carried out via a QSTR model. A linear relationship between lipophilicity and toxicity was elucidated, with increase in lipophilicity contributing to toxicity. However, with only the cytotoxicity data, we cannot attribute metabolism to reactive metabolites as the major cause.

The initial data from Chapter 3 enabled us to postulate a possible role of metabolism and bioactivation in the toxicity observed by the compounds. With that in mind, we decided carry out more in-depth investigations of the role of metabolism and bioactivation in the toxicity observed for the compounds in Chapter 5. *In vitro* bioactivation assays such as metabolic stabilities, GSH depletion assay and AG reactivity determination were thus performed. From observations made from our QSTR models in Chapter 3, we initially expected that lipophilicity, toxicity of the compounds and Phase I and Phase II



metabolic stability to exhibit an inverse relationship. However, the metabolic stability of the compounds across the series (varying alkyl and halogen substituents) was not correlated to lipophilicity. We postulate that this could be due to unfavourable spatial configurations of the compounds within the active site of the P450s for Phase I metabolism. The usage of alamethicin as a pore forming reagent to aid penetration the compounds across cell membranes could have changed the relationship between lipophilicity and Phase II metabolism. A cross-comparison between toxicity and metabolic stability showed that no relationship between metabolic stability and toxicity was observed for Phase I metabolism. On the other hand, for Phase II metabolism, metabolic stability correlated to toxicity positively. This gives an indication that metabolic stability of a compound may not be a predictor of bioactivation even though metabolism itself is a pre-requisite. Instead, the reactivity of the metabolites generated in the process could possibly play a more important role in the manifestation of toxicity for the compounds.

In addition to metabolic stability, we determined both the cellular GSH depletion and AG reactivity of the compounds. We found that GSH depletion increased across the series. On the other hand, AG reactivity decreased across the series. The effect of substituents on GSH depletion and AG reactivity was clearly observed from our experimental data. Larger substituents (either alkyl or halogen) generally increased the GSH depletion of the compound, with some exceptions. This was as what we expected, which was GSH depletion increasing with increase in size of the compounds. On the other hand, the reverse was seen for AG reactivity, which was not as expected. Difluorinated

compounds were observed to have absolutely low AG reactivity regardless of which alkyl substituent were present on the scaffold. A cross-comparison between metabolite reactivity and toxicity gave rise to a proportional relationship between GSH depletion and toxicity. However, the correlation was not strong due to exceptions. This supports the possible role of bioactivation in the toxicity exhibited by our compounds towards liver cells. On the other hand, AG reactivity was found to correlate to toxicity inversely, albeit to a slight degree. A possible explanation could be that the toxicity of the compounds may be less dependent on Phase II metabolism. We postulate that the effect of substituents on AG reactivity from the halogen substituents could be electronic in nature and the effect from the alkyl groups at R<sub>1</sub> could be steric in nature.

We have thus far shown that bioactivation may play an important role in the toxicity of the compounds and that substituents on the compounds in turn could affect the bioactivation process and subsequently, the toxicity of the compounds. In Chapter 6, we looked further into the possible pathways and structures of the Phase I and Phase II reactive metabolites of the compounds that could potentially contribute to the toxicity of the compounds. One reason for carrying out the identification was to confirm the formation of reactive metabolites via their trapped counterparts. GSH trapped (Phase I) and Phe-Lys trapped (Phase II) metabolites were detected for each compound analyzed, which indicated that the formation of reactive metabolites do have a role in toxicity observed with the synthesized compounds.

The proposed reactive metabolites for both Phase I and Phase II metabolism are summarized in Figure 7-1. Mono-hydroxylated metabolites for all the compounds tested were found to be able to undergo dehalogenation during GSH adduct formation, including brominated compounds of this chemical scaffold that were not previously studied. For F-Cl unsymmetrical compounds, there was a preference for defluorination over dechlorination. The compounds that possess an alkyl substituent at R<sub>1</sub> (methyl, ethyl, n-propyl, iso-propyl) were able to directly conjugate to GSH at the alkyl substituent via formation of imine methides. *tert*-Butyl substituted compounds were unable to form such an GSH adduct due to the absence of an extractable hydrogen at the site of attack. This is rather interesting as *tert*-butyl compounds were shown to be the most toxic of all the alkyl substituted compounds. This could indicate that the formation of imine methide may not be a major bioactivation pathway. Benzyl-S-GSH adducts were detected for all the compounds formed and its formation was proposed to be via oxidative decarboxylation. Lumiracoxib benzyl-S-GSH adduct is a novel metabolite not previously detected in bioactivation studies of lumiracoxib. From the data obtained, we observed that the varying substituents do affect the structures and amount of reactive metabolites formed. However, due to the limitations of the study done on Phase I metabolism, we are unable to firmly conclude any trends or effects of the substituents on structures and amount of reactive metabolites formed.

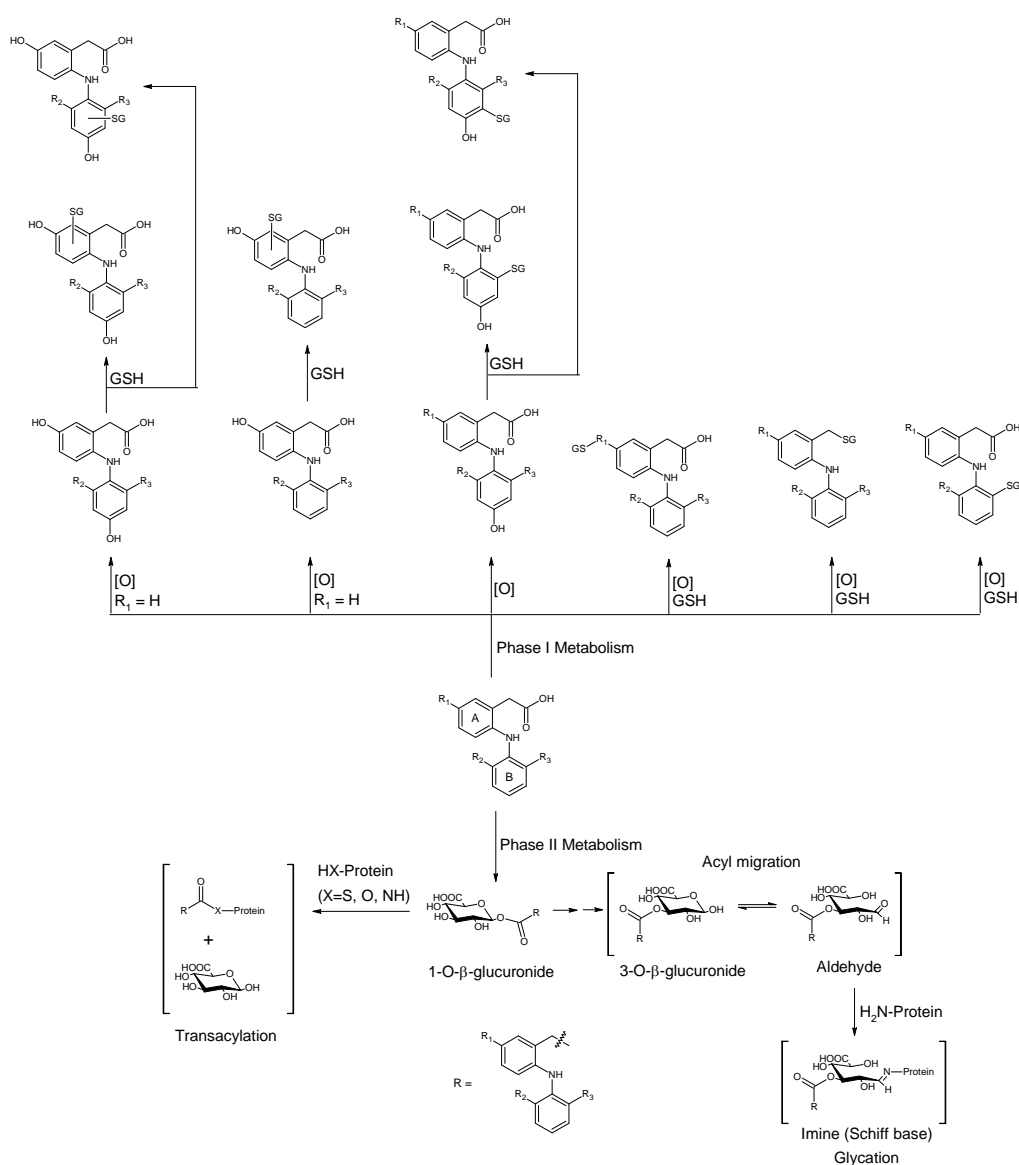


**Figure 7-1** Possible reactive metabolites and their trapped conjugates proposed for our synthesized compounds for both Phase I and Phase II metabolism. For Phase I metabolism, it should be noted that individual compounds have their own signature reactive metabolites and not every reactive metabolites illustrated will be found for a single compound. For Phase II metabolism, every compound will potentially form only the transacylated or acyl migrated- glycated adduct.

For Phase II metabolism, our compounds were shown to be able to undergo either transacylation and/ or acyl migration and subsequent adduct formation with Phe-Lys. This vindicates the AG reactivity data from Chapter 5, indicating that the metabolite reactivity observed was due to transacylation and/or acyl migration. Judging from the reactive AGs identified and proposed,

the substituents at R<sub>1</sub>, R<sub>2</sub> and R<sub>3</sub> had no effect on the structures of the trapped AGs but instead had some effects on the reactivity of the AGs as shown in Chapter 5.

In addition to toxicity, the pharmacological aspect of the compounds in terms of their inhibitory effects on COX-1 and COX-2 was determined using whole cell assay in Chapter 4. In terms of absolute activity, diclofenac (compound **3**) was found to be the most potent in both COX isoforms. In general, the addition of an alkyl group at R<sub>1</sub> on ring A of the compound and the increase in size of the alkyl group were observed to decrease potency. The halogen substituents at R<sub>2</sub> and R<sub>3</sub> on ring B were found to affect the activity in addition to the alkyl group at R<sub>1</sub>, with improvement to potency via the presence of a chlorine substituent. In terms of selectivity, lumiracoxib (compound **5**) was found to be the most selective of all the compounds. The selectivity arises from the addition of the methyl or ethyl group at R<sub>1</sub>. However, further increase in alkyl chain length decreased selectivity in general. An increase in selectivity was observed to occur with a decrease in absolute potency for certain cases. Thus, it can be concluded that the right combination of substituents at R<sub>1</sub>, R<sub>2</sub> and R<sub>3</sub> are required for good selectivity and potency.

A safety index was generated to link toxicity to pharmacology and to show the effect of substituents on the toxicity-pharmacology relationship. Diclofenac (compound **3**) was found to be the safest among all the compounds and is not selective to COX-2. Lumiracoxib (compounds **5**), which is selective towards COX-2 had a 3.8 times lower safety index as compared to diclofenac. From this, we can conclude that selectivity (due to changes in substituents) may

come at the expense of compound safety (increased toxicity) in the case of diclofenac and lumiracoxib.

Taken together, the findings of this thesis supported the hypothesis that varying substituents on the 2-phenylaminophenylacetic acid scaffold will alter bioactivation and subsequently, toxicity to a significant degree. Although the metabolic stability of the compounds provided no indication that the extent of metabolism influenced toxicity of the compounds, further metabolite reactivity studies and reactive metabolite identification allowed us to conclude that the formation of reactive metabolites via metabolism may have a major role in the toxic observed with our compounds. However, other toxicity pathways cannot be excluded and could also play an important role in the toxicity observed with the compounds. In addition, the link between toxicity and pharmacology was elucidated in this thesis for our series of compounds, providing a better understanding in the balance between toxicity and activity and presents the possibility to associate the two biological outcomes.

The present work has raised questions and issues that could be pursued in future investigations. Firstly, we postulated that the effect of substituents on AG reactivity from the halogen substituents could be due electronic in nature and the effect from the alkyl groups at R<sub>1</sub> could be due steric in nature. Further investigation such as calculations of electronic and steric properties and QSAR modelling should be carried out to help in the explanation of the results observed for AG reactivity of our compounds. Secondly, we could not conclude on the trends and effects of the substituents on structures and amount

of reactive metabolites formed for Phase I metabolism. Absolute quantification of the individual trapped metabolites could be carried out in order to confirm on the importance of the pathways involved and to carry out cross-compound comparisons in order to determine the effect of substituents on the type and amount of adducts formed. Thirdly, while we have characterized the involvement of both Phase I and II metabolism to toxicity, we were unable to determine their relative contribution as both phases of metabolism were measured separately from each other. In order to investigate whether Phase I and Phase II metabolism has a more critical role, both phases of metabolism should be carried out for the compounds concurrently and the reactive metabolites formed individually quantitated. Fourthly, further synthesis of compounds with other types of substituents such as  $-CF_3$  or a halogen at  $R_1$ , alkyl groups at  $R_2$  and  $R_3$  and substituents at other positions such as key sites for metabolism will enable a broader and more complete insight on the effect of substituents on structure-toxicity-bioactivation relationships and on the structure-toxicity-activity relationships. Last but not least, other toxicity pathways such as direct toxicity of the parent compound should be further investigated.

In conclusion, the results presented in this thesis have contributed to a better understanding on the structure-toxicity-bioactivation relationships and on the structure-toxicity-activity relationships for 2-phenylaminophenylacetic acid derived compounds. Several more questions were raised with regards to the initial investigative questions, allowing more room for improvement and further investigations. Overall, the rigors of this process have led to the

development of a set of approaches that bears witness to the differential influence of substituents on both toxicity and pharmacological activity. Such process could be refined and broadened for other drug studies in the days ahead.



## **Bibliography**

- Acemoglu, M., Allmendinger, T., Calienni, J., Cercus, J., Loiseleur, O., Sedelmeier, G.H., Xu, D., 2004. Synthesis of new N-aryl oxindoles as intermediates for pharmacologically active compounds. *Tetrahedron* **60**, 11571-11586.
- Agundez, J.A., Lucena, M.I., Martinez, C., Andrade, R.J., Blanca, M., Ayuso, P., Garcia-Martin, E., 2011. Assessment of nonsteroidal anti-inflammatory drug-induced hepatotoxicity. *Expert Opinion on Drug Metabolism & Toxicology* **7**, 817-828.
- Allred, A.L., 1961. Electronegativity values from thermochemical data. *Journal of Inorganic and Nuclear Chemistry* **17**, 215-221.
- Attia, S.M., 2010. Deleterious Effects of Reactive Metabolites. *Oxidative Medicine and Cellular Longevity* **3**, 238-253.
- Bannwarth, B., Berenbaum, F., 2007. Lumiracoxib in the management of osteoarthritis and acute pain. *Expert Opinion on Pharmacotherapy* **8**, 1551-1564.
- Barbato, F., LaRotonda, M.I., Quaglia, F., 1997. Interactions of nonsteroidal antiinflammatory drugs with phospholipids: Comparison between octanol/buffer partition coefficients and chromatographic indexes on immobilized artificial membranes. *Journal of Pharmaceutical Sciences* **86**, 225-229.
- Barnard, S., Kelly, D.F., Storr, R.C., Park, B.K., 1993. The effect of fluorine substitution on the hepatotoxicity and metabolism of paracetamol in the mouse. *Biochemical Pharmacology* **46**, 841-849.
- Bathelt, C., Schmid, R.D., Pleiss, J., 2002. Regioselectivity of CYP2B6: homology modeling, molecular dynamics simulation, docking. *Journal of Molecular Modeling* **8**, 327-335.
- Batsanov, S.S., 2001. Van der Waals Radii of Elements. *Inorganic Materials* **37**, 871-885.
- Benet, L.Z., Spahnlanguth, H., Iwakawa, S., Volland, C., Mizuma, T., Mayer, S., Mutschler, E., Lin, E.T., 1993. Predictability of the covalent binding of acidic drugs in man. *Life Sciences* **53**, PL141-PL146.
- Berg, J., Christoph, T., Widerna, M., Bodenteich, A., 1997. Isoenzyme-specific cyclooxygenase inhibitors: A whole cell assay system using the human erythroleukemic cell line HEL and the human monocytic cell line Mono Mac 6. *Journal of Pharmacological and Toxicological Methods* **37**, 179-186.

- Berry, N.G., Iddon, L., Iqbal, M., Meng, X.L., Jayapal, P., Johnson, C.H., Nicholson, J.K., Lindon, J.C., Harding, J.R., Wilson, I.D., Stachulski, A.V., 2009. Synthesis, transacylation kinetics and computational chemistry of a set of arylacetic acid 1 beta-O-acyl glucuronides. *Organic & Biomolecular Chemistry* **7**, 2525-2533.
- Bessems, J.G.M., Gaisser, H.D., Koppele, J.M.T., VanBennekom, W.P., Commandeur, J.N.M., Vermeulen, N.P.E., 1995. 3,5-disubstituted analogues of paracetamol. Synthesis, analgesic activity and cytotoxicity. *Chemico-Biological Interactions* **98**, 237-250.
- Bessone, F., 2010. Non-steroidal anti-inflammatory drugs: What is the actual risk of liver damage? *World Journal of Gastroenterology* **16**, 5651-5661.
- Blobaum, A.L., Marnett, L.J., 2007. Molecular determinants for the selective inhibition of cyclooxygenase-2 by lumiracoxib. *Journal of Biological Chemistry* **282**, 16379-16390.
- Boelsterli, U.A., 2003. Diclofenac-induced liver injury: a paradigm of idiosyncratic drug toxicity. *Toxicology and Applied Pharmacology* **192**, 307-322.
- Bolton, J.L., Trush, M.A., Penning, T.M., Dryhurst, G., Monks, T.J., 2000. Role of quinones in toxicology. *Chemical Research in Toxicology* **13**, 135-160.
- Bruggemann, R., Bartel, H.G., 1999. A theoretical concept to rank environmentally significant chemicals. *Journal of Chemical Information and Computer Sciences* **39**, 211-217.
- Bruggemann, R., Bucherl, C., Pudenz, S., Steinberg, C.E.W., 1999. Application of the concept of partial order on comparative evaluation of environmental chemicals. *Acta Hydrochimica Et Hydrobiologica* **27**, 170-178.
- Burka, L.T., Plucinski, T.M., Macdonald, T.L., 1983. Mechanisms of hydroxylation by cytochrome-P450 – Metabolism of monohalobenzenes by phenobarbital-induced microsomes. *Proceedings of the National Academy of Sciences of the United States of America-Biological Sciences* **80**, 6680-6684.
- Carlsen, L., 2008. Assessment of Chemicals Applying Partial Order Ranking Techniques. *Combinatorial Chemistry & High Throughput Screening* **11**, 794-805.
- Chakraborti, A.K., Garg, S.K., Kumar, R., Motiwala, H.F., Jadhavar, P.S., 2010. Progress in COX-2 Inhibitors: A Journey So Far. *Current Medicinal Chemistry* **17**, 1563-1593.

- Chan, K., Jensen, N., O'Brien, P.J., 2008. Structure–activity relationships for thiol reactivity and rat or human hepatocyte toxicity induced by substituted p-benzoquinone compounds. *Journal of Applied Toxicology* **28**, 608-620.
- Chan, K., Jensen, N.S., Silber, P.A., O'Brien, P.J., 2007. Structure-activity relationships for halobenzene induced cytotoxicity in rat and human hepatocytes. *Chemico-Biological Interactions* **165**, 165-174.
- Cnubben, N.H.P., Peelen, S., Borst, J.W., Vervoort, J., Veeger, C., Rietjens, I., 1994. Molecular orbital-based quantitative structure-activity relationship for the cytochrome P450-catalyzed 4-hydroxylation of halogenated anilines. *Chemical Research in Toxicology* **7**, 590-598.
- Coe, K.J., Jia, Y., Ho, H.K., Rademacher, P., Bammler, T.K., Beyer, R.P., Farin, F.M., Woodke, L., Plymate, S.R., Fausto, N., Nelson, S.D., 2007. Comparison of the cytotoxicity of the nitroaromatic drug flutamide to its cyano analogue in the hepatocyte cell line TAMH: Evidence for complex I inhibition and mitochondrial dysfunction using toxicogenomic screening. *Chemical Research in Toxicology* **20**, 1277-1290.
- Cronin, M.T.D., Schultz, T.W., 1996. Structure-toxicity relationships for phenols to *Tetrahymena pyriformis*. *Chemosphere* **32**, 1453-1468.
- Davies, N.M., Skjodt, N.M., 2000. Choosing the Right Nonsteroidal Anti-Inflammatory Drug for the Right Patient: A Pharmacokinetic Approach. *Clinical Pharmacokinetics* **38**, 377-392.
- Ding, A., Ojingwa, J.C., McDonagh, A.F., Burlingame, A.L., Benet, L.Z., 1993. Evidence for covalent binding of acyl glucuronides to serum-albumin via an imine mechanism as revealed by tandem mass-spectroscopy. *Proceedings of the National Academy of Sciences of the United States of America* **90**, 3797-3801.
- Easterbrook, J., Lu, C., Sakai, Y., Li, A.P., 2001. Effects of organic solvents on the activities of cytochrome P450 isoforms, UDP-dependent glucuronyl transferase, and phenol sulfotransferase in human hepatocytes. *Drug Metabolism and Disposition* **29**, 141-144.
- Faed, E.M., 1984. Properties of Acyl Glucuronides: Implications for Studies of the Pharmacokinetics and Metabolism of Acidic Drugs. *Drug Metabolism Reviews* **15**, 1213-1249.
- FitzGerald, G.A., Patrono, C., 2001. The Coxibs, Selective Inhibitors of Cyclooxygenase-2. *New England Journal of Medicine* **345**, 433-442.
- Fratello, G., Marchini, S., Zucco, F., Saporà, O., Stamatì, A., 1997. Cytotoxicity of halogenated benzenes and its relationship with logP. *Toxicology in Vitro* **11**, 673-677.

- Gan, T.J., 2010. Diclofenac: an update on its mechanism of action and safety profile. *Current Medical Research and Opinion* **26**, 1715-1731.
- Ganey, P.E., Kauffman, F.C., Thurman, R.G., 1988. Oxygen-dependent hepatotoxicity due to doxorubicin – Role of reducing equivalent supply in perfused rat-liver. *Molecular Pharmacology* **34**, 695-701.
- Giri, S., Nieber, K., Bader, A., 2010. Hepatotoxicity and hepatic metabolism of available drugs: current problems and possible solutions in preclinical stages. *Expert Opinion on Drug Metabolism & Toxicology* **6**, 895-917.
- Grillo, M.P., Knutson, C.G., Sanders, P.E., Waldon, D.J., Hua, F.M., Ware, J.A., 2003. Studies on the chemical reactivity of diclofenac acyl glucuronide with glutathione: Identification of diclofenac-S-acyl-glutathione in rat bile. *Drug Metabolism and Disposition* **31**, 1327-1336.
- Grillo, M.P., Ma, J., Teffera, Y., Waldon, D.J., 2008. A novel bioactivation pathway for 2- 2-(2,6-dichlorophenyl)aminophenyl ethanoic acid (diclofenac) initiated by cytochrome P450-mediated oxidative decarboxylation. *Drug Metabolism and Disposition* **36**, 1740-1744.
- Grosser, T., 2006. The pharmacology of selective inhibition of COX-2. *Thrombosis and Haemostasis* **96**, 393-400.
- Guo, L., Dial, S., Shi, L.M., Branham, W., Liu, J., Fang, J.L., Green, B., Deng, H., Kaput, J., Ning, B.T., 2011. Similarities and Differences in the Expression of Drug-Metabolizing Enzymes between Human Hepatic Cell Lines and Primary Human Hepatocytes. *Drug Metabolism and Disposition* **39**, 528-538.
- Hacker, M., 2009. Adverse Drug Reactions. In Hacker, M., Messer, W., Bachmann, K., (Eds.), *Pharmacology: principles and practice*. Academic Press/Elsevier, Boston, pp. 327-352.
- Hakk, H., Letcher, R.J., 2003. Metabolism in the toxicokinetics and fate of brominated flame retardants - a review. *Environment International* **29**, 801-828.
- Halfon, E., Reggiani, M.G., 1986. ON RANKING CHEMICALS FOR ENVIRONMENTAL-HAZARD. *Environmental Science & Technology* **20**, 1173-1179.
- Hansch, C., Leo, A., 1979. *Substituent Constants for Correlation Analysis in Chemistry and Biology*. Wiley, New York.
- Hernandes, M.Z., Cavalcanti, S.M.T., Moreira, D.R.M., de Azevedo, W.F., Leite, A.C.L., 2010. Halogen Atoms in the Modern Medicinal

Chemistry: Hints for the Drug Design. *Current Drug Targets* **11**, 303-314.

- Ionescu, C., Caira, M.R., 2005a. Pathways of Biotransformation - Phase I Reactions. In Ionescu, C., Caira, M.R., (Eds.), *Drug Metabolism: Current Concepts*. Springer, Dordrecht, pp. 41-128.
- Ionescu, C., Caira, M.R., 2005b. Pathways of Biotransformation - Phase II Reactions. In Ionescu, C., Caira, M.R., (Eds.), *Drug Metabolism: Current Concepts*. Springer, Dordrecht, pp. 129-170.
- Isin, E.M., Guengerich, F.P., 2007. Complex reactions catalyzed by cytochrome P450 enzymes. *Biochimica Et Biophysica Acta-General Subjects* **1770**, 314-329.
- Jia, L., Liu, X.D., 2007. The conduct of drug metabolism studies considered good practice (II): In vitro experiments. *Current Drug Metabolism* **8**, 822-829.
- Kang, P., Dalvie, D., Smith, E., Renner, M., 2009. Bioactivation of Lumiracoxib by Peroxidases and Human Liver Microsomes: Identification of Multiple Quinone Imine Intermediates and GSH Adducts. *Chemical Research in Toxicology* **22**, 106-117.
- Kenny, J.R., Maggs, J.L., Meng, X.L., Sinnott, D., Clarke, S.E., Park, B.K., Stachulski, A.V., 2004. Syntheses and characterization of the acyl glucuronide and hydroxy metabolites of diclofenac. *Journal of Medicinal Chemistry* **47**, 2816-2825.
- Khojasteh, C., Wong, H., Hop, C.E.C.A., 2010. *Drug Metabolizing Enzymes, The Drug Metabolism and Pharmacokinetics Quick Guide*. Springer, London, pp. 17-46.
- Kim, K.H., 1991. Quantitative structure-activity relationships of the metabolism of drugs by uridine-diphosphate glucuronosyltransferase. *Journal of Pharmaceutical Sciences* **80**, 966-970.
- Koerts, J., Soffers, A., Vervoort, J., De Jager, A., Rietjens, I., 1998. Occurrence of the NIH shift upon the cytochrome P450-catalyzed in vivo and in vitro aromatic ring hydroxylation of fluorobenzenes. *Chemical Research in Toxicology* **11**, 503-512.
- Kretzrommel, A., Boelsterli, U.A., 1993. Diclofenac covalent protein-binding is dependent on acyl glucuronide formation and is inversely related to P450-mediated acute cell injury in cultured rat hepatocytes. *Toxicology and Applied Pharmacology* **120**, 155-161.
- Kretzrommel, A., Boelsterli, U.A., 1994a. Mechanism of covalent adduct formation of diclofenac to rat hepatic-microsomal proteins – Retention

- of the glucuronic-acid moiety in the adduct. *Drug Metabolism and Disposition* **22**, 956-961.
- Kretzrommel, A., Boelsterli, U.A., 1994b. Selective protein adducts to membrane-proteins in cultured rat hepatocytes exposed to diclofenac – Radiochemical and immunochemical analysis. *Molecular Pharmacology* **45**, 237-244.
- Langguth, H.S., Benet, L.Z., 1992. Acyl Glucuronides Revisited: Is the Glucuronidation Process a Toxication as Well as a Detoxification Mechanism? *Drug Metabolism Reviews* **24**, 5-47.
- Lee, K.S., Oh, S.J., Kim, H.M., Lee, K.H., Kim, S.K., 2011. Assessment of Reactive Metabolites in Drug-Induced Liver Injury. *Archives of Pharmacal Research* **34**, 1879-1886.
- Lee, W.M., 2003. Medical progress: Drug-induced hepatotoxicity. *New England Journal of Medicine* **349**, 474-485.
- Leemann, T., Transon, C., Dayer, P., 1993. Cytochrome-P450TB (CYP2C) – A major monooxygenase catalyzing diclofenac 4'-hydroxylation in human liver. *Life Sciences* **52**, 29-34.
- Lerche, D., Bruggemann, R., Sorensen, P., Carlsen, L., Nielsen, O.J., 2002. A comparison of partial order technique with three methods of multi-criteria analysis for ranking of chemical substances. *Journal of Chemical Information and Computer Sciences* **42**, 1086-1098.
- Leung, L., Kalgutkar, A.S., Obach, R.S., 2011. Metabolic activation in drug-induced injury. *Drug Metabolism Reviews*, 1-16.
- Lewis, D.F.V., Ioannides, C., Parke, D.V., 1995. A quantitative structure-activity relationship study on a series of 10 parasubstituted toluenes binding to cytochrome P450B4 (CYP2B4), and their hydroxylation rates. *Biochemical Pharmacology* **50**, 619-625.
- Li, J.J., 2009. *Name Reactions: A Collection of Detailed Reaction Mechanisms and Synthetic Applications*. Springer-Verlag Berlin Heidelberg, Germany.
- Li, Y., Slatter, J.G., Zhang, Z.P., Doss, G.A., Braun, M.P., Stearns, R.A., Dean, D.C., Baillie, T.A., Tang, W., 2008. In vitro metabolic activation of lumiracoxib in rat and human liver preparations. *Drug Metabolism and Disposition* **36**, 469-473.
- Lipinski, C.A., 2000. Drug-like properties and the causes of poor solubility and poor permeability. *Journal of Pharmacological and Toxicological Methods* **44**, 235-249.

- Lipinski, C.A., Lombardo, F., Dominy, B.W., Feeney, P.J., 2001. Experimental and computational approaches to estimate solubility and permeability in drug discovery and development settings. *Advanced Drug Delivery Reviews* **46**, 3-26.
- Little, P.J., Ryan, A.J., 1982. Inhibitors of hepatic mixed-function oxidases .4. Effects of benzimidazole and related-compounds on aryl-hydrocarbon hydroxylase-activity from phenobarbitone and 3-methylcholanthrene induced rats. *Journal of Medicinal Chemistry* **25**, 622-626.
- Mangold, J.B., Gu, H., Rodriguez, L.C., Bonner, J., Dickson, J., Rordorf, C., 2004. Pharmacokinetics and metabolism of lumiracoxib in healthy male subjects. *Drug Metabolism and Disposition* **32**, 566-571.
- Masferrer, J.L., Zweifel, B.S., Seibert, K., Needleman, P., 1990. Selective regulation of cellular cyclooxygenase by dexamethasone and endotoxin in mice. *Journal of Clinical Investigation* **86**, 1375-1379.
- McDonald, M.G., Rettie, A.E., 2007. Sequential metabolism and bioactivation of the hepatotoxin benzbromarone: Formation of glutathione adducts from a catechol intermediate. *Chemical Research in Toxicology* **20**, 1833-1842.
- McLaughlin, L.A., Dickmann, L.J., Wolf, C.R., Henderson, C.J., 2008. Functional expression and comparative characterization of nine murine cytochromes P450 by fluorescent inhibition screening. *Drug Metabolism and Disposition* **36**, 1322-1331.
- Mitchell, J.A., Akarasereenont, P., Thiemermann, C., Flower, R.J., Vane, J.R., 1993. Selectivity of nonsteroidal antiinflammatory drugs as inhibitors of constitutive and inducible cyclooxygenase. *Proceedings of the National Academy of Sciences of the United States of America* **90**, 11693-11697.
- Monks, T.J., Hinson, J.A., Gillette, J.R., 1982. Bromobenzene and para-bromophenol toxicity and covalent binding invivo. *Life Sciences* **30**, 841-848.
- Monks, T.J., Jones, D.C., 2002. The Metabolism and Toxicity of Quinones, Quinonimines, Quinone Methides, and Quinone-Thioethers. *Current Drug Metabolism* **3**, 425-438.
- Moser, P., Sallmann, A., Wiesenberg, I., 1990. Synthesis and quantitative structure-activity-relationships of diclofenac analogs. *Journal of Medicinal Chemistry* **33**, 2358-2368.
- Neijenesch, H.A., Deruiter, R., Ridderikhoff, E.J., Vandenende, J.O., Laarhoven, L.J., Vanputten, L.J.W., Cornelisse, J., 1991. Intramolecular meta photocycloaddition of 6-arylhex-2-enes .2. *Journal of Photochemistry and Photobiology a-Chemistry* **60**, 325-343.

- Nelson, S.D., 2001. Structure toxicity relationships - How useful are they in predicting toxicities of new drugs? *Biological Reactive Intermediates Vi: Chemical and Biological Mechanisms in Susceptibility to and Prevention of Environmental Diseases* **500**, 33-43.
- Obach, R.S., 1999. Prediction of human clearance of twenty-nine drugs from hepatic microsomal intrinsic clearance data: An examination of in vitro half-life approach and nonspecific binding to microsomes. *Drug Metabolism and Disposition* **27**, 1350-1359.
- O'Neill, P.M., Harrison, A.C., Storr, R.C., Hawley, S.R., Ward, S.A., Park, B.K., 1994. The effect of fluorine substitution on the metabolism and antimalarial activity of amodiaquine. *Journal of Medicinal Chemistry* **37**, 1362-1370.
- Park, B.K., Kitteringham, N.R., O'Neill, P.M., 2001. Metabolism of fluorine-containing drugs. *Annual Review of Pharmacology and Toxicology* **41**, 443-470.
- Patel, R.N., Attur, M.G., Dave, M.N., Patel, I.V., Stuchin, S.A., Abramson, S.B., Amin, A.R., 1999. A Novel Mechanism of Action of Chemically Modified Tetracyclines: Inhibition of COX-2-Mediated Prostaglandin E2 Production. *The Journal of Immunology* **163**, 3459-3467.
- Perloft, E.S., Crocker, R.M., Dandeneau, A.A., Morgan, L., Crespi, C.L., Stresser, D.M., 2006. Validation of a Phase I and Phase II Metabolic Stability Assay in Subcellular Fractions, Woburn, MA, United States of America, pp.
- Pierce, R.H., Franklin, C.C., Campbell, J.S., Tonge, R.P., Chen, W.C., Fausto, N., Nelson, S.D., Bruschi, S.A., 2002. Cell culture model for acetaminophen-induced hepatocyte death in vivo. *Biochemical Pharmacology* **64**, 413-424.
- Plumb, J.A., Milroy, R., Kaye, S.B., 1989. Effects of the pH Dependence of 3-(4,5-Dimethylthiazol-2-yl)-2,5-diphenyltetrazolium Bromide-Formazan Absorption on Chemosensitivity Determined by a Novel Tetrazolium-based Assay. *Cancer Research* **49**, 4435-4440.
- Poon, G.K., Chen, Q., Teffera, Y., Ngui, J.S., Griffin, P.R., Braun, M.P., Doss, G.A., Freedman, C., Stearns, R.A., Evans, D.C., Baillie, T.A., Tang, W., 2001. Bioactivation of diclofenac via benzoquinone imine intermediates-identification of urinary mercapturic acid derivatives in rats and humans. *Drug Metabolism and Disposition* **29**, 1608-1613.
- Prasanna, S., Manivannan, E., Chaturvedi, S.C., 2005. QSAR studies on structurally similar 2-(4-methanesulfonylphenyl)pyran-4-ones as selective COX-2 inhibitors: a Hansch approach. *Bioorganic & Medicinal Chemistry Letters* **15**, 313-320.



- Prins, B., Dartee, W.P., Verboom, W., Reinhoudt, D.N., Koster, A.S., 1994. Quantitative structure-activity relationships for the acute cytotoxicity of 13(bis)aziridiny-benzoquinones – Relation to cellular ATP depletion. *Archives of Toxicology* **68**, 255-260.
- Radominska-Pandya, A., Czernik, P.J., Little, J.M., Battaglia, E., Mackenzie, P.I., 1999. Structural and functional studies of UDP-glucuronosyltransferases1\*. *Drug Metabolism Reviews* **31**, 817-899.
- Regan, S.L., Maggs, J.L., Hammond, T.G., Lambert, C., Williams, D.P., Park, B.K., 2010. Acyl Glucuronides: The Good, The Bad and The Ugly. *Biopharmaceutics & Drug Disposition* **31**, 367-395.
- Rice, G.C., Bump, E.A., Shrieve, D.C., Lee, W., Kovacs, M., 1986. Quantitative-analysis of cellular glutathione by flow-cytometry utilizing monochlorobimane – Some applications to radiation and drug-resistance invitro and invivo. *Cancer Research* **46**, 6105-6110.
- Rowlinson, S.W., Kiefer, J.R., Prusakiewicz, J.J., Pawlitz, J.L., Kozak, K.R., Kalgutkar, A.S., Stallings, W.C., Kurumbail, R.G., Marnett, L.J., 2003. A novel mechanism of cyclooxygenase-2 inhibition involving interactions with Ser-530 and Tyr-385. *Journal of Biological Chemistry* **278**, 45763-45769.
- Russo, M.W., Galanko, J.A., Shrestha, R., Fried, M.W., Watkins, P., 2004. Liver transplantation for acute liver failure from drug induced liver injury in the United States. *Liver Transplantation* **10**, 1018-1023.
- Sangster, 2006. LOGKOW Database, Montreal, Quebec, Canada, pp.
- Schultz, T.W., Cajinaquezada, M., Wesley, S.K., 1989. Structure toxicity relationships for mono alkyl-substituted or halogen-substituted anilines. *Bulletin of Environmental Contamination and Toxicology* **43**, 564-569.
- Selassie, C.D., 2003. History of Quantitative Structure-Activity Relationship. In Abraham, D.J., (Ed.), *Burger's Medicinal Chemistry and Drug Discovery*. John Wiley & Sons, Inc., New York, pp. 1-48.
- Shen, S.J., Marchick, M.R., Davis, M.R., Doss, G.A., Pohl, L.R., 1999. Metabolic activation of diclofenac by human cytochrome P450 3A4: Role of 5-hydroxydiclofenac. *Chemical Research in Toxicology* **12**, 214-222.
- Siraki, A.G., Chevaldina, T., O'Brien, P.J., 2005. Application of quantitative structure-toxicity relationships for acute NSAID cytotoxicity in rat hepatocytes. *Chemico-Biological Interactions* **151**, 177-191.
- Sivertsson, L., Ek, M., Darnell, M., Edebert, I., Ingelman-Sundberg, M., Neve, E.P.A., 2010. CYP3A4 Catalytic Activity Is Induced in Confluent

- Huh7 Hepatoma Cells. *Drug Metabolism and Disposition* **38**, 995-1002.
- Smith, D.A., Waterbeemd, H.v.d., Walker, D.K., 2006. *Pharmacokinetics and Metabolism in Drug Design*. WILEY-VCH Verlag GmbH & Co. KGaA, Weinheim.
- Smith, P.A., Sorich, M.J., McKinnon, R.A., Miners, J.O., 2003. In silico insights: Chemical and structural characteristics associated with uridine diphosphate-glucuronosyltransferase substrate selectivity. *Clinical and Experimental Pharmacology and Physiology* **30**, 836-840.
- Smith, P.C., Benet, L.Z., McDonagh, A.F., 1990. Covalent binding of zomepirac glucuronide to proteins – Evidence for a Schiff-base mechanism. *Drug Metabolism and Disposition* **18**, 639-644.
- Srivastava, A., Maggs, J.L., Antoine, D.J., Williams, D.P., Smith, D.A., Park, B.K., 2010. Role of Reactive Metabolites in Drug-Induced Hepatotoxicity. In Uetrecht, J., (Ed.), *Adverse Drug Reactions*. Springer-Verlag Berlin Heidelberg, London, pp. 165-194.
- Stachulski, A.V., Harding, J.R., Lindon, J.C., Maggs, J.L., Park, B.K., Wilson, I.D., 2006. Acyl glucuronides: Biological activity, chemical reactivity, and chemical synthesis. *Journal of Medicinal Chemistry* **49**, 6931-6945.
- Stepan, A.F., Walker, D.P., Bauman, J., Price, D.A., Baillie, T.A., Kalgutkar, A.S., Aleo, M.D., 2011. Structural Alert/Reactive Metabolite Concept as Applied in Medicinal Chemistry to Mitigate the Risk of Idiosyncratic Drug Toxicity: A Perspective Based on the Critical Examination of Trends in the Top 200 Drugs Marketed in the United States. *Chemical Research in Toxicology* **24**, 1345-1410.
- Stierlin, H., Faigle, J.W., Sallmann, A., Kung, W., Richter, W.J., Kriemler, H.P., Alt, K.O., Winkler, T., 1979. Biotransformation of diclofenac sodium (Voltaren) in animals and in man .1. Isolation and identification of principal metabolites. *Xenobiotica* **9**, 601-610.
- Stirnemann, G., Kessebohm, K., Lauterburg, B., 2010. Liver injury caused by drugs: an update. *Swiss Medical Weekly* **140**, 18-24.
- Tang, W., 2003. The metabolism of diclofenac - Enzymology and toxicology perspectives. *Current Drug Metabolism* **4**, 319-329.
- Tang, W., Stearns, R.A., Bandiera, S.M., Zhang, Y., Raab, C., Braun, M.P., Dean, D.C., Pang, J.M., Leung, K.H., Doss, G.A., Strauss, J.R., Kwei, G.Y., Rushmore, T.H., Chiu, S.H.L., Baillie, T.A., 1999a. Studies on cytochrome P-450-mediated bioactivation of diclofenac in rats and in human hepatocytes: Identification of glutathione conjugated metabolites. *Drug Metabolism and Disposition* **27**, 365-372.

- Tang, W., Stearns, R.A., Wang, R.W., Chiu, S.H.L., Baillie, T.A., 1999b. Roles of human hepatic cytochrome P450s 2C9 and 3A4 in the metabolic activation of diclofenac. *Chemical Research in Toxicology* **12**, 192-199.
- Teffera, Y., Waldon, D.J., Colletti, A.E., Albrecht, B.K., Zhao, Z., 2008. Identification of a Novel Glutathione Conjugate of Diclofenac by LTQOrbitrap. *Drug Metabolism Letters* **2**, 35-40.
- Thompson, D.C., Perera, K., Krol, E.S., Bolton, J.L., 1995. o-Methoxy-4-alkylphenols that form quinone methides of intermediate reactivity are the most toxic in rat liver slices. *Chemical Research in Toxicology* **8**, 323-327.
- Thompson, D.C., Thompson, J.A., Sugumaran, M., Moldeus, P., 1993. Biological and toxicological consequences of quinone methide formation. *Chemico-Biological Interactions* **86**, 129-162.
- Tran, T., Lee, W., 2013. DILI: New Insights into Diagnosis and Management. *Current Hepatitis Reports* **12**, 53-58.
- Trott, O., Olson, A.J., 2010. Software News and Update AutoDock Vina: Improving the Speed and Accuracy of Docking with a New Scoring Function, Efficient Optimization, and Multithreading. *Journal of Computational Chemistry* **31**, 455-461.
- United-Nations, 2005a. Consolidated List of products whose consumption and/or sale have been banned, withdrawn, severely restricted or not approved by governments. In Nations, U., (Ed.), *Pharmaceuticals: restrictions in use and availability*. United Nations Publications, New York, pp.
- United-Nations, 2005b. Consolidated List of products whose consumption and/or sale have been banned, withdrawn, severely restricted or not approved by governments. In Nations, U., (Ed.), *Pharmaceuticals: restrictions in use and availability*. United Nations Publication, New York, pp.
- Vanderhoeven, S.J., Lindon, J.C., Troke, J., Tranter, G.E., Wilson, I.D., Nicholson, J.K., 2004a. NMR and QSAR studies on the transacylation reactivity of model 1 $\beta$ -O-acyl glucuronides. I: design, synthesis and degradation rate measurement. *Xenobiotica* **34**, 73-85.
- Vanderhoeven, S.J., Troke, J., Tranter, G.E., Wilson, I.D., Nicholson, J.K., Lindon, J.C., 2004b. Nuclear magnetic resonance (NMR) and quantitative structure–activity relationship (QSAR) studies on the transacylation reactivity of model 1 $\beta$ -O-acyl glucuronides. II: QSAR modelling of the reaction using both computational and experimental NMR parameters. *Xenobiotica* **34**, 889-900.

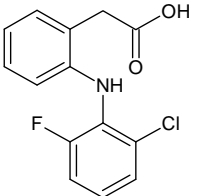
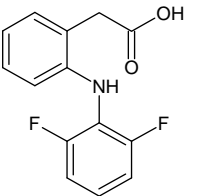
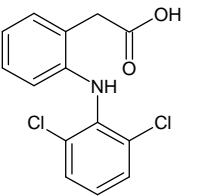
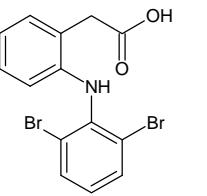
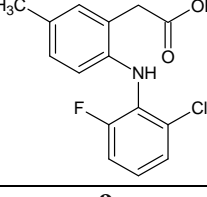
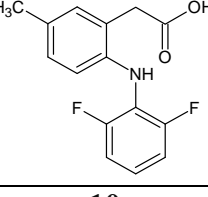
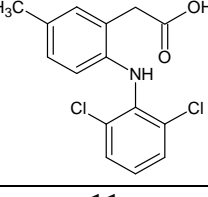
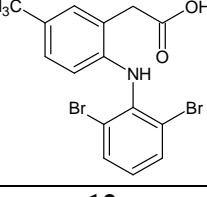
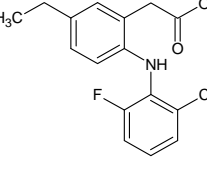
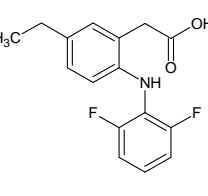
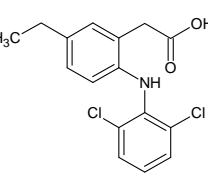
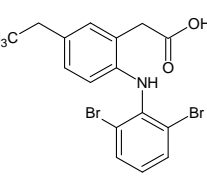
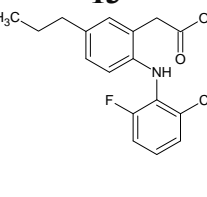
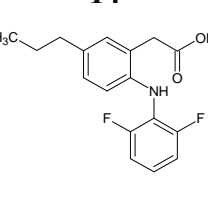
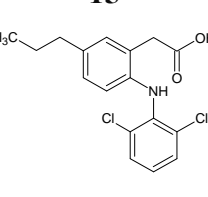
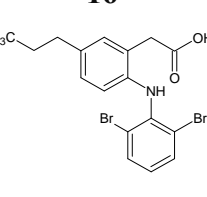
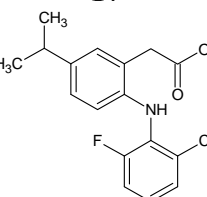
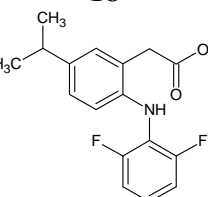
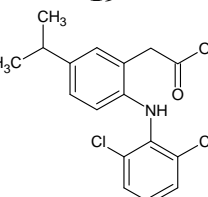
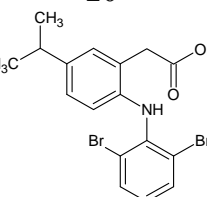
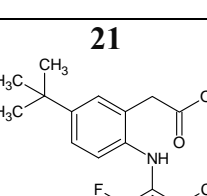
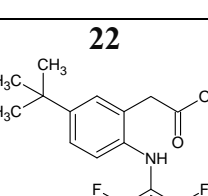
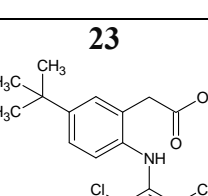
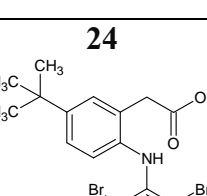
- Vashishtha, S.C., Hawes, E.M., McKay, G., McCann, D.J., 2001. Quaternary ammonium-linked glucuronidation of 1-substituted imidazoles: Studies of human UDP-glucuronosyltransferases involved and substrate specificities. *Drug Metabolism and Disposition* **29**, 1290-1295.
- Vasquezvivar, J., Augusto, O., 1992. Hydroxylated metabolites of the antimalarial drug primaquine – Oxidation and redox cycling. *Journal of Biological Chemistry* **267**, 6848-6854.
- Vogel, A.I., 1989. *A Textbook of Practical Organic Chemistry*. Longman Scientific & Technical, London.
- Vonkeman, H.E., van de Laar, M., 2010. Nonsteroidal Anti-Inflammatory Drugs: Adverse Effects and Their Prevention. *Seminars in Arthritis and Rheumatism* **39**, 294-312.
- Wang, J.Y., Davis, M., Li, F.B., Azam, F., Scatina, J., Talaat, R., 2004. A novel approach for predicting acyl glucuromide reactivity via Schiff base formation. Development of rapidly formed peptide adducts for LC/MS/MS measurements. *Chemical Research in Toxicology* **17**, 1206-1216.
- Warne, M.A., Osborn, D., Lindon, J.C., Nicholson, J.K., 1999. Quantitative structure-toxicity relationships for halogenated substituted-benzenes to *Vibrio fischeri*, using atom-based semi-empirical molecular-orbital descriptors. *Chemosphere* **38**, 3357-3382.
- Wen, B., Ma, L., Nelson, S.D., Zhu, M., 2008. High-throughput screening and characterization of reactive metabolites using polarity switching of hybrid triplequadrupole linear ion trap mass spectrometry. *Analytical Chemistry* **80**, 1788-1799.
- Wilcken, R., Zimmermann, M.O., Lange, A., Joerger, A.C., Boeckler, F.M., 2013. Principles and Applications of Halogen Bonding in Medicinal Chemistry and Chemical Biology. *Journal of Medicinal Chemistry* **56**, 1363-1388.
- Wilkerson, W.W., Copeland, R.A., Covington, M., Trzaskos, J.M., 1995. Antiinflammatory 4,5-diarylpyrroles .2. Activity as a function of cyclooxygenase-2 inhibition. *Journal of Medicinal Chemistry* **38**, 3895-3901.
- Williams, D.P., Kitteringham, N.R., Naisbitt, D.J., Pirmohamed, M., Smith, D.A., Park, B.K., 2002. Are Chemically Reactive Metabolites Responsible for Adverse Reactions to Drugs? *Current Drug Metabolism* **3**, 351-366.
- Williams, J.A., Hyland, R., Jones, B.C., Smith, D.A., Hurst, S., Goosen, T.C., Peterkin, V., Koup, J.R., Ball, S.E., 2004. Drug-drug interactions for UDP-glucuronosyltransferase substrates: A pharmacokinetic

explanation for typically observed low exposure (AUC(i)/AUC) ratios. *Drug Metabolism and Disposition* **32**, 1201-1208.

- Williams, P.A., Cosme, J., Sridhar, V., Johnson, E.F., McRee, D.E., 2000. Mammalian microsomal cytochrome P450 monooxygenase: Structural adaptations for membrane binding and functional diversity. *Molecular Cell* **5**, 121-131.
- Wold, S., Eriksson, L., Clementi, S., 1995. Statistical Validation of QSAR Results. In Waterbeemd, H.v.d., (Ed.), *Chemometric Methods in Molecular Design*. Wiley-VCH Verlag GmbH, Weinheim, Germany, pp.
- Wolfe, J.P., Buchwald, S.L., 2000. Scope and limitations of the Pd/BINAP-catalyzed amination of aryl bromides. *Journal of Organic Chemistry* **65**, 1144-1157.
- Wu, J.C., Merlino, G., Cveklova, K., Mosinger, B., Fausto, N., 1994. Autonomous growth in serum-free medium and production of hepatocellular carcinomas by differentiated hepatocyte lines that overexpress transforming growth-factor-alpha. *Cancer Research* **54**, 5964-5973.
- Yu, L.J., Chen, Y., DeNinno, M.P., O'Connell, T.N., Hop, C., 2005. Identification of a novel glutathione adduct of diclofenac, 4'-hydroxy-2'-glutathion-deschloro-diclofenac, upon incubation with human liver microsomes. *Drug Metabolism and Disposition* **33**, 484-488.
- Zhang, C.H., Kenny, J.R., Le, H., Deese, A., Ford, K.A., Lightning, L.K., Fan, P.W., Driscoll, J.P., Halladay, J.S., Hop, C., Khojasteh, S.C., 2011. Novel Mechanism for Dehalogenation and Glutathione Conjugation of Dihalogenated Anilines in Human Liver Microsomes: Evidence for ipso Glutathione Addition. *Chemical Research in Toxicology* **24**, 1668-1677.
- Zheng, J., Ma, L., Xin, B.M., Olah, T., Humphreys, W.G., Zhu, M.S., 2007. Screening and identification of GSH-trapped reactive metabolites using hybrid triple quadrupole linear ion trap mass spectrometry. *Chemical Research in Toxicology* **20**, 757-766.
- Zhou, S.F., Liu, J.P., Chowbay, B., 2009. Polymorphism of human cytochrome P450 enzymes and its clinical impact. *Drug Metabolism Reviews* **41**, 89-295.

## Appendix

**Appendix 2-1: Complete structures of all twenty-four synthesized compounds**

<p style="text-align: center;"><b>1</b></p> 	<p style="text-align: center;"><b>2</b></p> 	<p style="text-align: center;"><b>3</b></p> 	<p style="text-align: center;"><b>4</b></p> 
<p style="text-align: center;"><b>5</b></p> 	<p style="text-align: center;"><b>6</b></p> 	<p style="text-align: center;"><b>7</b></p> 	<p style="text-align: center;"><b>8</b></p> 
<p style="text-align: center;"><b>9</b></p> 	<p style="text-align: center;"><b>10</b></p> 	<p style="text-align: center;"><b>11</b></p> 	<p style="text-align: center;"><b>12</b></p> 
<p style="text-align: center;"><b>13</b></p> 	<p style="text-align: center;"><b>14</b></p> 	<p style="text-align: center;"><b>15</b></p> 	<p style="text-align: center;"><b>16</b></p> 
<p style="text-align: center;"><b>17</b></p> 	<p style="text-align: center;"><b>18</b></p> 	<p style="text-align: center;"><b>19</b></p> 	<p style="text-align: center;"><b>20</b></p> 
<p style="text-align: center;"><b>21</b></p> 	<p style="text-align: center;"><b>22</b></p> 	<p style="text-align: center;"><b>23</b></p> 	<p style="text-align: center;"><b>24</b></p> 

**Appendix 2-2:** Characterization of synthesized compounds (**1** – **24**) and intermediates (**25** – **72**)

**{2-[(2-Chloro-6-fluorophenyl)amino]phenyl}acetic acid (1)**

Off-white powder. Yield: 64.5%. M.p.: 150.3 – 151.4 °C. <sup>1</sup>H NMR (300 MHz, *DMSO-d*<sub>6</sub>) δ 7.36 (d, *J* = 7.9 Hz, 1H), 7.28 – 7.06 (m, 5H), 6.86 (t, *J* = 7.3 Hz, 1H), 6.47 (d, *J* = 7.6 Hz, 1H), 3.68 (s, 2H); <sup>13</sup>C NMR (75 MHz, *DMSO-d*<sub>6</sub>) δ 173.59 (s, 1C), 156.12 (d, *J*<sub>C-F</sub> = 247.5 Hz, 1C), 142.59 (s, 1C), 130.95 (s, 1C), 128.58 (d, *J*<sub>C-F</sub> = 14.0 Hz, 1C), 128.24 (d, *J*<sub>C-F</sub> = 4.0 Hz, 1C), 127.69 (s, 1C), 125.95 (s, 1C), 124.22 (d, *J*<sub>C-F</sub> = 8.7 Hz, 1C), 124.02 (s, 1C), 121.04 (s, 1C), 116.13 (s, 1C), 115.43 (d, *J*<sub>C-F</sub> = 20 Hz, 1C), 37.93 (s, 1C); MS-ESI: [M+H]<sup>+</sup>: 280.0, 282.0 m/z.

**{2-[(2,6-Difluorophenyl)amino]phenyl}acetic acid (2)**

White powder. Yield: 61.3%. M.p.: 131.8 – 132.8 °C. <sup>1</sup>H NMR (300 MHz, *DMSO-d*<sub>6</sub>) δ 7.20 – 7.11 (m, 5H), 7.10 (t, *J* = 7.4 Hz, 1H), 6.85 (t, *J* = 7.3 Hz, 1H), 6.54 (d, *J* = 7.9 Hz, 1H), 3.69 (s, 2H); <sup>13</sup>C NMR (75 MHz, *DMSO-d*<sub>6</sub>) δ 173.39 (s, 1C), 156.12 (d, *J*<sub>C-F</sub> = 245.5 Hz, 1C), 156.04 (d, *J*<sub>C-F</sub> = 245.2 Hz, 1C), 142.60 (s, 1C), 130.82 (s, 1C), 127.59 (s, 1C), 123.63 (s, 1C), 123.17 (t, *J*<sub>C-F</sub> = 9.7 Hz, 1C), 120.54 (s, 1C), 119.76 (t, *J*<sub>C-F</sub> = 15.4 Hz, 1C), 115.51 (s, 1C), 112.21 (d, *J*<sub>C-F</sub> = 16.1 Hz, 1C), 112.12 (d, *J*<sub>C-F</sub> = 16.2 Hz, 1C), 37.49 (s, 1C); MS-ESI [M+H]<sup>+</sup>: 264.0 m/z.

**{2-[(2,6-Dichlorophenyl)amino]phenyl}acetic acid (3)**

White powder. M.p.: 155.8 – 157.4 °C. <sup>1</sup>H NMR (300 MHz, *CDCl*<sub>3</sub>) δ 7.34 (d, *J* = 8.1 Hz, 2H), 7.25 (d, *J* = 6.7 Hz, 1H), 7.15 (t, *J* = 7.7 Hz, 1H), 6.98 (t, *J* = 8.1 Hz, 1H), 6.96 (t, *J* = 6.7 Hz, 1H), 6.80 (s, 1H), 6.56 (d, *J* = 8.0 Hz, 1H), 3.86 (s, 2H); <sup>13</sup>C NMR (75 MHz, *CDCl*<sub>3</sub>) δ 178.10 (s, 1C), 142.65 (s, 1C), 137.73 (s, 1C), 130.97 (s, 1C), 129.43 (s, 2C), 128.87 (s, 2C), 128.26 (s, 1C), 124.07 (s, 1C), 123.63 (s, 1C), 122.20 (s, 1C), 118.43 (s, 1C), 38.23 (s, 1C); MS-ESI [M+H]<sup>+</sup>: 296.0, 298.0, 300.0 m/z.

**{2-[(2,6-Dibromophenyl)amino]phenyl}acetic acid (4)**

White powder. Yield: 25.6%. M.p.: 152.4 – 153.6 °C. <sup>1</sup>H NMR (300 MHz, CDCl<sub>3</sub>) δ ppm 7.35 (d, *J* = 8.0 Hz, 2H), 7.25 (d, *J* = 4.7 Hz, 1H), 7.13 (t, *J* = 7.6 Hz, 1H), 6.97 (t, *J* = 7.4 Hz, 1H), 6.85 (t, *J* = 8.0 Hz, 1H), 6.70 (s, 1H), 6.52 (d, *J* = 7.9 Hz, 1H), 3.85 (s, 2H); <sup>13</sup>C NMR (75 MHz, CDCl<sub>3</sub>) δ 178.17 (s, 1C), 142.91 (s, 1C), 140.16 (s, 1C), 132.85 (s, 2C), 131.04 (s, 1C), 128.35 (s, 1C), 125.51 (s, 1C), 123.91 (s, 1C), 122.24 (s, 1C), 119.94 (s, 2C), 118.59 (s, 1C), 38.28 (s, 1C); MS-ESI [M+H]<sup>+</sup>: 383.8, 385.8, 387.8 m/z. HRMS-ESI [M-H]<sup>-</sup>: Calcd 381.9084 m/z Found 381.9070 m/z.

**{2-[(2-Chloro-6-fluorophenyl)amino]-5-methylphenyl}acetic acid (5)**

Pale yellow powder. Yield: 89.2%. M.p.: 137.5 – 139.5 °C. <sup>1</sup>H NMR (300 MHz, DMSO-*d*<sub>6</sub>) δ 7.34 (d, *J* = 7.8 Hz, 1H), 7.21 (dd, *J* = 9.0 Hz, *J*<sub>H-F</sub> = 9.8 Hz, 1H), 7.14-6.98 (m, 3H), 6.91 (d, *J* = 7.7 Hz, 1H), 6.43 (d, *J* = 6.6 Hz, 1H), 3.65 (s, 2H), 2.21 (s, 3H); <sup>13</sup>C NMR (75 MHz, DMSO-*d*<sub>6</sub>) δ 173.38 (s, 1C), 155.50 (d, *J*<sub>C-F</sub> = 247.1 Hz, 1C), 139.86 (s, 1C), 131.24 (s, 1C), 130.01 (s, 1C), 128.95 (d, *J*<sub>C-F</sub> = 13.8 Hz, 1C), 127.87 (s, 1C), 127.28 (d, *J*<sub>C-F</sub> = 4.1 Hz, 1C), 125.68 (s, 1C), 124.29 (s, 1C), 123.28 (d, *J*<sub>C-F</sub> = 8.7 Hz, 1C), 116.69 (s, 1C), 115.24 (d, *J*<sub>C-F</sub> = 20.1 Hz, 1C), 37.69 (s, 1C), 20.07 (s, 1C); [M+H]<sup>+</sup>: 293.9, 295.8 m/z.

**{2-[(2,6-Difluorophenyl)amino]-5-methylphenyl}acetic acid (6)**

Off-white crystals. Yield: 74.5%. M.p.: 136.4 – 137.4 °C. <sup>1</sup>H NMR (300 MHz, DMSO-*d*<sub>6</sub>) δ 7.16-7.01 (m, 4H), 6.99 (s, 1H), 6.91 (d, *J* = 8.2 Hz, 1H), 6.49 (d, *J* = 8.1 Hz, 1H), 3.65 (s, 2H), 2.20 (s, 3H); <sup>13</sup>C NMR (75 MHz, DMSO-*d*<sub>6</sub>) δ 173.39 (s, 1C), 155.61 (d, *J*<sub>C-F</sub> = 245.0 Hz, 1C), 155.53 (d, *J*<sub>C-F</sub> = 245.0, 1C), 139.96 (s, 1C), 131.23 (s, 1C), 129.64 (s, 1C), 127.90 (s, 1C), 124.10 (s, 1C), 122.25 (t, *J*<sub>C-F</sub> = 9.6 Hz, 1C), 120.33 (t, *J*<sub>C-F</sub> = 15.1 Hz, 1C), 116.26 (s, 1H), 112.10 (d, *J*<sub>C-F</sub> = 16.0 Hz, 1C), 112.00 (d, *J*<sub>C-F</sub> = 16.3 Hz, 1C), 37.48 (s, 1C), 20.07 (s, 1C); MS-ESI [M+H]<sup>+</sup>: 278.0 m/z.

**{2-[(2,6-Dichlorophenyl)amino]-5-methylphenyl}acetic acid (7)**

Off-white fluffy crystals. Yield: 82.6%. M.p.: 146.6 – 148.2 °C. <sup>1</sup>H NMR (300 MHz, DMSO-*d*<sub>6</sub>) δ 7.49 (d, *J* = 8.0 Hz, 2H), 7.19-7.01 (m, 3H), 6.87 (d, *J* =



8.0 Hz, 1H), 6.23 (d,  $J = 8.1$  Hz, 1H), 3.66 (s, 2H), 2.20 (s, 3H);  $^{13}\text{C}$  NMR (75 MHz,  $\text{DMSO-}d_6$ )  $\delta$  173.37 (s, 1C), 140.06 (s, 1C), 137.50 (s, 1C), 131.36 (s, 1C), 129.96 (s, 1C), 129.19 (s, 2C), 129.11 (s, 2C), 127.86 (s, 1C), 124.90 (s, 1C), 124.37 (s, 1C), 116.67 (s, 1C), 37.76 (s, 1C), 20.09 (s, 1C);  $[\text{M}+\text{H}]^+$ : 309.9, 312.0, 314.0 m/z.

**{2-[(2,6-Dibromophenyl)amino]-5-methylphenyl}acetic acid (8)**

Pale yellow crystals. Yield: 42.3%. M.p.: 133.0 – 135.0 °C.  $^1\text{H}$  NMR (300 MHz,  $\text{DMSO-}d_6$ )  $\delta$  7.69 (d,  $J = 8.0$  Hz, 2H), 7.07-6.96 (m, 2H), 6.92 (s, 1H), 6.86 (d,  $J = 8.0$  Hz, 1H), 6.17 (d,  $J = 8.1$  Hz, 1H), 3.65 (s, 2H), 2.20 (s, 3H);  $^{13}\text{C}$  NMR (75 MHz,  $\text{DMSO-}d_6$ )  $\delta$  173.00 (s, 1C), 140.08 (s, 1C), 139.61 (s, 1C), 132.68 (s, 2C), 131.11 (s, 1C), 129.56 (s, 1C), 127.64 (s, 1C), 126.20 (s, 1C), 124.16 (s, 1C), 120.03 (s, 2C), 116.36 (s, 1C), 37.53 (s, 1C), 19.82 (s, 1C); MS-ESI  $[\text{M}+\text{H}]^+$ : 397.8, 399.6, 401.7 m/z. HRMS-ESI  $[\text{M}-\text{H}]^-$ : Calcd 395.9240 m/z Found 395.9231 m/z.

**{2-[(2-Chloro-6-fluorophenyl)amino]-5-ethylphenyl}acetic acid (9)**

White fluffy crystals. Yield: 52.8%. M.p.: 141.0 – 142.0 °C.  $^1\text{H}$  NMR (400 MHz,  $\text{DMSO-}d_6$ )  $\delta$  7.35 (dt,  $J = 8.1$  Hz, 1.2 Hz,  $J_{\text{H-F}} = 1.2$  Hz, 1H), 7.23 (ddd,  $J = 8.3$  Hz, 1.3 Hz,  $J_{\text{H-F}} = 9.7$  Hz, 1H), 7.03 – 6.89 (m 3H), 6.94 (dd,  $J = 8.2$  Hz, 2.0 Hz, 1H), 6.44 (dd,  $J = 8.1$  Hz,  $J_{\text{H-F}} = 3.0$  Hz, 1H), 3.66 (s, 2H), 2.51 (q,  $J = 7.6$  Hz, 2H), 1.13 (t,  $J = 7.6$  Hz, 3H);  $^{13}\text{C}$  NMR (101 MHz,  $\text{DMSO-}d_6$ )  $\delta$  173.50 (s, 1C), 155.59 (d,  $J_{\text{C-F}} = 247.3$  Hz, 1C), 140.12 (s, 1C), 136.58 (s, 1C), 130.14 (s, 1C), 128.94 (d,  $J_{\text{C-F}} = 13.7$  Hz, 1C), 127.40 (d,  $J_{\text{C-F}} = 4.3$  Hz, 1C), 126.75 (s, 1C), 125.76 (d,  $J_{\text{C-F}} = 3.0$  Hz, 1C), 124.24 (s, 1C), 123.45 (d,  $J_{\text{C-F}} = 8.9$  Hz, 1C), 116.67 (s, 1C), 115.30 (d,  $J_{\text{C-F}} = 20.1$  Hz, 1C), 37.85 (s, 1C), 27.33 (s, 1C), 15.69 (s, 1C); MS-ESI  $[\text{M}+\text{H}]^+$ : 307.9, 309.9 m/z.

**{2-[(2,6-Difluorophenyl)amino]-5-ethylphenyl}acetic acid (10)**

White powder. Yield: 32.4%. M.p.: 120.4 – 121.8 °C.  $^1\text{H}$  NMR (400 MHz,  $\text{CDCl}_3$ )  $\delta$  7.03 (ddd,  $J = 8.2$  Hz, 2.1 Hz,  $J_{\text{H-F}} = 10.3$  Hz, 2H), 6.94-6.91 (m, 3H), 6.74 (dt,  $J = 8.2$  Hz, 2.3 Hz,  $J_{\text{H-F}} = 2.3$  Hz, 1H), 3.79 (s, 2H), 2.59 (q,  $J = 7.6$  Hz, 2H), 1.22 (t,  $J = 7.6$  Hz, 3H);  $^{13}\text{C}$  NMR (101 MHz,  $\text{DMSO-}d_6$ )  $\delta$  173.51 (s, 1C), 155.71 (d,  $J_{\text{C-F}} = 244.93$  Hz, 1C), 155.65 (d,  $J_{\text{C-F}} = 244.9$  Hz,

1C), 140.24 (s, 1C), 136.22 (s, 1C), 130.13 (s, 1C), 126.77 (s, 1C), 124.03 (s, 1C), 122.45 (t,  $J_{C-F} = 9.5$  Hz, 1C), 120.30 (t,  $J_{C-F} = 15.2$  Hz, 1C), 116.20 (s, 1C), 112.21 (d,  $J_{C-F} = 6.3$  Hz, 1C), 112.04 (d,  $J_{C-F} = 6.1$  Hz, 1C), 37.64 (s, 1C), 27.34 (s, 1C), 15.75 (s, 1C); MS-ESI  $[M+H]^+$ : 292.0 m/z.

### **{2-[(2,6-Dichlorophenyl)amino]-5-ethylphenyl}acetic acid (11)**

White fluffy crystals. Yield: 68.8%. M.p.: 123.5 – 125.1 °C.  $^1H$  NMR (400 MHz, *DMSO-d*<sub>6</sub>)  $\delta$  7.49 (d,  $J = 8.1$  Hz, 2H), 7.14 (t,  $J = 8.0$  Hz, 1H), 7.06 (s, 1H), 7.05 (s, 1H), 6.91 (d,  $J = 8.1$  Hz, 1H), 6.24 (d,  $J = 8.1$  Hz, 1H), 3.67 (s, 2H), 2.50 (q,  $J = 7.7$  Hz, 2H), 1.13 (t,  $J = 7.6$  Hz, 3H);  $^{13}C$  NMR (101 MHz, *DMSO-d*<sub>6</sub>)  $\delta$  173.47 (s, 1C), 140.33 (s, 1C), 137.52 (s, 1C), 136.50 (s, 1C), 130.25 (s, 1C), 129.33 (s, 2C), 129.17 (s, 2C), 126.72 (s, 1C), 125.07 (s, 1C), 124.33 (s, 1C), 116.64 (s, 1C), 37.92 (s, 1C), 27.33 (s, 1C), 15.64 (s, 1C); MS-ESI  $[M+H]^+$ : 324.0, 326.1, 327.0 m/z.

### **{2-[(2,6-Dibromophenyl)amino]-5-ethylphenyl}acetic acid (12)**

Off-white crystals. Yield: 39.3%. M.p.: 118.9 – 121.1 °C.  $^1H$  NMR (400 MHz, *CDCl*<sub>3</sub>)  $\delta$  7.69 (d,  $J = 8.0$  Hz, 2H), 7.05 (s, 1H), 7.01 (t,  $J = 8.0$  Hz, 1H), 6.92 (s, 1H), 6.70 (d,  $J = 8.1$  Hz, 1H), 6.18 (d,  $J = 8.1$  Hz, 1H), 3.67 (s, 2H), 2.5 (q,  $J = 7.6$  Hz, 2H), 1.13 (t,  $J = 7.5$  Hz, 3H);  $^{13}C$  NMR (101 MHz, *DMSO-d*<sub>6</sub>)  $\delta$  173.36 (s, 1C), 140.61 (s, 1C), 139.90 (s, 1C), 136.31 (s, 1C), 133.00 (s, 2C), 130.24 (s, 1C), 126.74 (s, 1C), 126.60 (s, 1C), 124.37 (s, 1C), 120.42 (s, 2C), 116.58 (s, 1C), 37.94 (s, 1C), 27.31 (s, 1C), 15.60 (s, 1C); MS-ESI  $[M+H]^+$ : 411.7, 413.7, 415.7 m/z. HRMS-ESI  $[M-H]^-$ : Calcd 409.9397 m/z Found 409.9393 m/z.

### **{2-[(2-Chloro-6-fluorophenyl)amino]-5-propylphenyl}acetic acid (13)**

White fluffy crystals. Yield: 39.4%. M.p.: 123.9 – 125.8 °C.  $^1H$  NMR (400 MHz, *DMSO-d*<sub>6</sub>)  $\delta$  7.34 (d,  $J = 8.1$  Hz), 7.22 (ddd,  $J = 8.4$  Hz, 1.3 Hz,  $J_{H-F} = 9.6$  Hz, 1H), 7.11 – 7.07 (m, 2H), 7.01 (s, 1H), 6.91 (dd,  $J = 8.2$  Hz, 1.7 Hz, 1H), 6.43 (dd,  $J = 8.1$  Hz,  $J_{H-F} = 2.9$  Hz, 1H), 3.65 (s, 2H), 2.45 (t,  $J = 7.4$  Hz, 2H), 1.53 (sext,  $J = 7.4$  Hz, 2H), 0.87 (t,  $J = 7.3$  Hz, 3H);  $^{13}C$  NMR (101 MHz, *DMSO-d*<sub>6</sub>)  $\delta$  173.56 (s, 1C), 155.61 (d,  $J_{C-F} = 247.3$  Hz, 1C), 140.17 (s, 1C), 135.04 (s, 1C), 130.73 (s, 1C), 128.97 (d,  $J_{C-F} = 13.7$  Hz, 1C), 127.40 (d,  $J_{C-F}$

= 6.0 Hz, 1C), 127.38 (s, 1C), 125.80 (d,  $J_{C-F} = 3.0$  Hz, 1C), 124.22 (s, 1C), 123.48 (d,  $J_{C-F} = 8.8$  Hz, 1C), 116.65 (s, 1C), 115.34 (d,  $J_{C-F} = 20.2$  Hz, 1C), 37.89 (s, 1C), 36.50 (s, 1C), 24.22 (s, 1C), 13.70 (s, 1C); MS-ESI  $[M+H]^+$ : 321.9, 323.9 m/z. HRMS-ESI  $[M-H]^-$ : Calcd 320.0859 m/z Found 320.0852 m/z.

#### **{2-[(2,6-Difluorophenyl)amino]-5-propylphenyl}acetic acid (14)**

White powder. Yield: 37.9%. M.p.: 120.4 – 121.3 °C.  $^1H$  NMR (400 MHz,  $CDCl_3$ )  $\delta$  7.14 – 7.04 (m, 4H), 7.0 (s, 1H), 6.92 (dd,  $J = 8.2$  Hz, 2.0 Hz, 1H), 6.49 (dt,  $J = 8.1, 21.9$  Hz,  $J_{H-F} = 1.9$  Hz, 1H), 3.65 (s, 2H), 2.45 (t,  $J = 7.6$  Hz, 2H), 1.53 (sext,  $J = 7.6$  Hz, 2H), 0.87 (t,  $J = 7.3$  Hz, 3H);  $^{13}C$  NMR (101 MHz,  $DMSO-d_6$ )  $\delta$  173.48 (s, 1C), 155.71 (d,  $J_{C-F} = 245.0$  Hz, 1C), 155.64 (d,  $J_{C-F} = 245.0$ , 1C), 140.24 (s, 1C), 134.57 (s, 1C), 130.66 (s, 1C), 127.33 (s, 1C), 123.92 (s, 1C), 122.45 (t,  $J_{C-F} = 9.5$  Hz, 1C), 120.27 (t,  $J_{C-F} = 15.2$  Hz, 1C), 116.07 (s, 1C), 112.20 (d,  $J_{C-F} = 6.2$  Hz, 1C), 112.03 (d,  $J_{C-F} = 6.1$  Hz, 1C), 37.61 (s, 1C), 36.46 (s, 1C), 24.20 (s, 1C), 13.66 (s, 1C); MS-ESI  $[M+H]^+$ : 306.0 m/z. HRMS-ESI  $[M-H]^-$ : Calcd 304.1155 m/z Found 304.1147 m/z.

#### **{2-[(2,6-Dichlorophenyl)amino]-5-propylphenyl}acetic acid (15)**

White fluffy crystals. Yield: 52.1%. M.p.: 119.2 – 121.0 °C.  $^1H$  NMR (400 MHz,  $DMSO-d_6$ )  $\delta$  7.49 (d,  $J = 8.1$  Hz, 2H), 7.14 (d,  $J = 8.1$  Hz, 1H), 7.09 (s, 1H), 7.03 (s, 1H), 6.89 (dd,  $J = 8.1$  Hz, 1.6 Hz, 1H), 6.24 (d,  $J = 8.1$  Hz, 1H), 3.67 (s, 2H), 2.45 (t,  $J = 7.6$  Hz, 2H), 1.54 (sext,  $J = 7.5$  Hz, 2H), 0.88 (t,  $J = 7.3$  Hz, 3H);  $^{13}C$  NMR (101 MHz,  $DMSO-d_6$ )  $\delta$  173.36 (s, 1C), 140.25 (s, 1C), 137.46 (s, 1C), 134.78 (s, 1C), 130.67 (s, 1C), 129.20 (s, 2C), 129.07 (s, 2C), 127.17 (s, 1C), 124.89 (s, 1C), 124.21 (s, 1C), 116.52 (s, 1C), 37.81 (s, 1C), 36.41 (s, 1C), 24.07 (s, 1C), 13.61 (s, 1C); MS-ESI  $[M+H]^+$ : 337.9, 339.9, 341.7 m/z. HRMS-ESI  $[M-H]^-$ : Calcd 336.0564 m/z Found 336.0558 m/z.

#### **{2-[(2,6-Dibromophenyl)amino]-5-propylphenyl}acetic acid (16)**

Off-white powder. Yield: 39.9%. M.p.: 119.2 – 121.5 °C.  $^1H$  NMR (400 MHz,  $DMSO-d_6$ )  $\delta$  7.69 (d,  $J = 8.0$  Hz, 2H), 7.03 (s, 1H), 7.01 (t,  $J = 8.0$  Hz, 1H), 6.94 (s, 1H), 6.89 (dd,  $J = 8.0$  Hz, 1.8 Hz, 1H), 6.18 (d,  $J = 8.1$  Hz, 1H), 3.66 (s, 2H), 2.45 (t,  $J = 7.4$  Hz, 2H), 1.54 (sext,  $J = 7.5$  Hz, 2H), 0.88 (t,  $J = 7.3$

Hz, 3H);  $^{13}\text{C}$  NMR (101 MHz, *DMSO-d*<sub>6</sub>)  $\delta$  173.47 (s, 1C), 140.76 (s, 1C), 140.07 (s, 1C), 134.87 (s, 1C), 133.13(s, 1C), 130.90 (s, 2C), 127.44 (s, 1C), 126.66 (s, 1C), 124.50 (s, 1C), 120.51 (s, 2C), 116.71 (s, 1C), 38.05 (s, 1C), 36.63 (s, 1C), 24.26 (s, 1C), 13.84 (s, 1C); MS-ESI  $[\text{M}+\text{H}]^+$ : 425.7, 427.7, 429.7 m/z. HRMS-ESI  $[\text{M}-\text{H}]^-$ : Calcd 423.9553 m/z Found 423.9550 m/z.

**{2-[(2-Chloro-6-fluorophenyl)amino]-5-(propan-2-yl)phenyl}acetic acid (17)**

Off-white powder. Yield: 35.1%. M.p.: 130.3 – 131.6 °C.  $^1\text{H}$  NMR (400 MHz, *DMSO-d*<sub>6</sub>)  $\delta$  7.35 (d,  $J$  = 8.1 Hz, 1H), 7.23 (ddd,  $J$  = 8.3 Hz, 1.2 Hz,  $J_{\text{H-F}}$  = 10.1 Hz, 1H), 7.12-7.07 (m, 3H), 6.97 (dd,  $J$  = 8.2, 1.9 Hz, 1H), 6.45 (dd,  $J$  = 8.2,  $J_{\text{H-F}}$  = 3.0 Hz, 1H), 3.67 (s, 2H), 2.79 (sept,  $J$  = 6.9 Hz, 1H), 1.16 (d,  $J$  = 6.9 Hz, 6H);  $^{13}\text{C}$  NMR (101 MHz, *DMSO-d*<sub>6</sub>)  $\delta$  173.50 (s, 1C), 155.56 (d,  $J_{\text{C-F}}$  = 247.35 Hz, 1C), 141.17 (s, 1C), 140.16 (s, 1C), 128.88 (d,  $J_{\text{C-F}}$  = 13.8 Hz, 1C), 128.68 (s, 1C), 127.39 (d,  $J_{\text{C-F}}$  = 4.3 Hz, 1C), 125.70 (d,  $J_{\text{C-F}}$  = 2.9 Hz, 1C), 125.19 (s, 1C), 124.06 (s, 1C), 123.42 (d,  $J_{\text{C-F}}$  = 8.8 Hz, 1C), 116.44 (s, 1C), 115.27 (d,  $J_{\text{C-F}}$  = 20.1 Hz, 1C), 37.92 (s, 1C), 32.61 (s, 1C), 23.99 (s, 2C); MS-ESI  $[\text{M}+\text{H}]^+$ : 321.9, 323.9 m/z. HRMS-ESI  $[\text{M}-\text{H}]^-$ : Calcd 320.0859 m/z Found 320.0851 m/z.

**{2-[(2,6-Difluorophenyl)amino]-5-(propan-2-yl)phenyl}acetic acid (18)**

Off-white powder. Yield: 38.6%. M.p.: 117.1 – 119.2 °C.  $^1\text{H}$  NMR (400 MHz, *DMSO-d*<sub>6</sub>)  $\delta$  7.13-7.05 (m, 5H), 6.98 (dd,  $J$  = 8.2, 1.6 Hz, 1H), 6.51 (d,  $J$  = 8.2 Hz, 1H), 3.67 (s, 2H), 2.79 (sept,  $J$  = 6.9 Hz, 1H), 1.16 (d,  $J$  = 6.9 Hz, 6H);  $^{13}\text{C}$  NMR (101 MHz, *DMSO-d*<sub>6</sub>)  $\delta$  173.42 (s, 1C), 155.65 (d,  $J_{\text{C-F}}$  = 244.96 Hz, 1C), 155.59 (d,  $J_{\text{C-F}}$  = 244.96 Hz, 1C), 140.74 (s, 1C), 140.23 (s, 1C), 128.60 (s, 1C), 125.13 (s, 1C), 123.79 (s, 1C), 122.37 (t,  $J_{\text{C-F}}$  = 9.5 Hz, 1C), 120.17 (t,  $J_{\text{C-F}}$  = 15.2 Hz, 1C), 115.94 (s, 1C), 112.10 (d,  $J_{\text{C-F}}$  = 6.3 Hz, 1C), 111.93 (d,  $J_{\text{C-F}}$  = 6.1 Hz, 1C), 37.65 (s, 1C), 32.55 (s, 1C), 23.96 (s, 2C); MS-ESI  $[\text{M}+\text{H}]^+$ : 306.0 m/z. HRMS-ESI  $[\text{M}-\text{H}]^-$ : Calcd 304.1155 m/z Found 304.1147 m/z.

**{2-[(2,6-Dichlorophenyl)amino]-5-(propan-2-yl)phenyl}acetic acid (19)**

White fluffy crystals. Yield: 59.6%. M.p.: 134.8 – 136.7 °C. <sup>1</sup>H NMR (400 MHz, *DMSO-d*<sub>6</sub>) δ 7.50 (d, *J* = 8.1 Hz, 2H), 7.14 (t, *J* = 8.0 Hz, 1H), 7.09 (s, 2H), 6.94 (dd, *J* = 8.2 Hz, 2.1 Hz, 1H), 6.25 (d, *J* = 8.2 Hz, 1H), 3.68 (s, 2H), 2.79 (sept, *J* = 6.9 Hz, 1H), 1.16 (d, *J* = 6.9 Hz, 6H); <sup>13</sup>C NMR (101 MHz, *DMSO-d*<sub>6</sub>) δ 173.37 (s, 1C), 140.97 (s, 1C), 140.30 (s, 1C), 137.40 (s, 1C), 129.29 (s, 2C), 129.04 (s, 2C), 128.69 (s, 1C), 125.08 (s, 1C), 124.96 (s, 1C), 124.06 (s, 1C), 116.39 (s, 1C), 37.91 (s, 1C), 32.52 (s, 1C), 23.91 (s, 2C); MS-ESI [M+H]<sup>+</sup>: 337.8, 339.9, 340.7 m/z. HRMS-ESI [M-H]<sup>-</sup>: Calcd 336.0564 m/z Found 336.0566 m/z.

**{2-[(2,6-Dibromophenyl)amino]-5-(propan-2-yl)phenyl}acetic acid (20)**

White fluffy crystals. Yield: 45.2%. M.p.: 127.8 – 130.0 °C. <sup>1</sup>H NMR (400 MHz, *DMSO-d*<sub>6</sub>) δ 7.69 (d, *J* = 8.0 Hz, 2H), 7.09 (s, 1H), 7.02 (t, *J* = 8.0 Hz, 1H), 6.94 (s, 1H), 6.93 (dd, *J* = 8.0 Hz, 2.0 Hz, 1H), 6.19 (d, *J* = 8.2 Hz, 1H), 3.67 (s, 2H), 2.78 (sept, *J* = 7.2 Hz, 1H), 1.16 (d, *J* = 6.9 Hz, 6H); <sup>13</sup>C NMR (101 MHz, *DMSO-d*<sub>6</sub>) δ 173.33 (s, 1C), 140.87 (s, 1C), 140.64 (s, 1C), 139.84 (s, 1C), 132.93 (s, 2C), 128.74 (s, 1C), 126.56 (s, 1C), 125.19 (s, 1C), 124.17 (s, 1C), 120.44 (s, 2C), 116.41 (s, 1C), 37.99 (s, 1C), 32.54 (s, 1C), 23.95 (s, 2C); MS-ESI [M+H]<sup>+</sup>: 425.7, 427.6, 429.7 m/z. HRMS-ESI [M-H]<sup>-</sup>: Calcd 423.9553 m/z Found 423.9555 m/z.

**{5-*tert*-Butyl-2-[(2-chloro-6-fluorophenyl)amino]phenyl}acetic acid (21)**

White crystals. Yield: 31.4%. M.p.: 131.3 – 133.2 °C. <sup>1</sup>H NMR (400 MHz, *DMSO-d*<sub>6</sub>) δ 7.36 (d, *J* = 8.1 Hz, 1H), 7.27-7.21 (m, 2H), 7.15-7.08 (m, 3H), 6.45 (dd, *J* = 8.4, *J*<sub>H-F</sub> = 2.9 Hz, 1H), 3.69 (s, 2H), 1.24 (s, 9H); <sup>13</sup>C NMR (101 MHz, *DMSO-d*<sub>6</sub>) δ 173.51 (s, 1C), 155.55 (d, *J*<sub>C-F</sub> = 247.35, 1C), 143.35 (s, 1C), 139.81 (s, 1C), 128.78 (d, *J*<sub>C-F</sub> = 13.8 Hz, 1C), 127.51 (s, 1C), 127.42 (d, *J*<sub>C-F</sub> = 4.3 Hz, 1C), 125.65 (d, *J*<sub>C-F</sub> = 3.0 Hz, 1C), 124.15 (s, 1C), 123.56 (s, 1C), 123.43 (d, *J*<sub>C-F</sub> = 8.9 Hz, 1C), 116.04 (s, 1C), 115.21 (d, *J*<sub>C-F</sub> = 20.2 Hz, 1C), 38.04 (s, 1C), 33.69 (s, 1C), 31.11 (s, 3C); MS-ESI [M+H]<sup>+</sup>: 335.9, 337.9 m/z. HRMS-ESI [M-H]<sup>-</sup>: Calcd 334.1016 m/z Found 334.1011 m/z.

**{5-*tert*-Butyl-2-[(2,6-difluorophenyl)amino]phenyl}acetic acid (22)**

White crystals. Yield: 50.3%. M.p.: 121.9 – 123.9 °C. <sup>1</sup>H NMR (400 MHz, *DMSO-d*<sub>6</sub>) δ 7.20 (s, 1H), 7.14-7.09 (m, 4H), 7.08 (s, 1H), 6.50 (dt, *J* = 8.4 Hz, *J*<sub>H-F</sub> = 1.9 Hz, 1H), 3.69 (s, 2H), 1.24 (s, 9H); <sup>13</sup>C NMR (101 MHz, *DMSO-d*<sub>6</sub>) δ 173.49 (s, 1C), 155.70 (d, *J*<sub>C-F</sub> = 245.1 Hz, 1C), 155.64 (d, *J*<sub>C-F</sub> = 245.0 Hz, 1C), 142.97 (s, 1C), 139.92 (s, 1C), 127.47 (s, 1C), 124.16 (s, 1C), 123.33 (s, 1C), 122.47 (t, *J*<sub>C-F</sub> = 9.5 Hz, 1C), 120.11 (t, *J*<sub>C-F</sub> = 15.2 Hz, 1C), 115.54 (s, 1C), 112.11 (d, *J*<sub>C-F</sub> = 6.2 Hz, 1C), 111.9 (d, *J*<sub>C-F</sub> = 6.2 Hz, 1C), 37.82 (s, 1C), 33.66 (s, 1C), 31.22 (s, 3C); MS-ESI [M+H]<sup>+</sup>: 319.9 m/z. HRMS-ESI [M-H]<sup>-</sup>: Calcd 318.1311 m/z Found 318.1302 m/z.

**{5-*tert*-Butyl-2-[(2,6-dichlorophenyl)amino]phenyl}acetic acid (23)**

White fluffy crystals. Yield: 43.6%. M.p.: 134.9 – 136.7 °C. <sup>1</sup>H NMR (400 MHz, *DMSO-d*<sub>6</sub>) δ 7.50 (d, *J* = 8.1 Hz, 2H), 7.23 (s, 1H), 7.15 (t, *J* = 8.1 Hz, 1H), 7.09 (s, 1H), 7.08 (dd, *J* = 8.3 Hz, 2.2 Hz, 1H), 6.24 (d, *J* = 8.4 Hz, 1H), 3.69 (s, 2H), 1.23 (s, 9H); <sup>13</sup>C NMR (101 MHz, *DMSO-d*<sub>6</sub>) δ 173.48 (s, 1C), 143.23 (s, 1C), 140.03 (s, 1C), 137.38 (s, 1C), 129.41 (s, 2C), 129.06 (s, 2C), 127.61 (s, 1C), 125.07 (s, 1C), 124.10 (s, 1C), 123.61 (s, 1C), 116.00 (s, 1C), 38.10 (s, 1C), 33.69 (s, 1C), 31.22 (s, 3C); MS-ESI [M+H]<sup>+</sup>: 351.9, 353.8, 354.9 m/z. HRMS-ESI [M-H]<sup>-</sup>: Calcd 350.0720 m/z Found 350.0715 m/z.

**{5-*tert*-Butyl-2-[(2,6-dibromophenyl)amino]phenyl}acetic acid (24)**

White crystals. Yield: 25.7%. M.p.: 138.7 – 140.5 °C. <sup>1</sup>H NMR (400 MHz, *DMSO-d*<sub>6</sub>) δ 7.70 (d, *J* = 8.0 Hz, 2H), 7.23 (s, 1H), 7.08 (dd, *J* = 8.4, 2.2 Hz, 1H), 7.03 (t, *J* = 8.0 Hz, 1H), 6.94 (s, 1H), 6.18 (d, *J* = 8.4 Hz, 1H), 3.69 (s, 2H), 1.24 (s, 9H); <sup>13</sup>C NMR (101 MHz, *DMSO-d*<sub>6</sub>) δ 173.38, 143.11, 140.33, 139.81, 132.92, 127.63, 126.65, 124.18, 123.67, 120.56, 116.01, 38.13, 33.70, 31.24; MS-ESI [M+H]<sup>+</sup>: 439.7, 441.7, 443.6 m/z. HRMS-ESI [M-H]<sup>-</sup>: Calcd 437.9710 m/z Found 437.9710 m/z.

**2-(2-Iodophenyl)-*N,N*-dimethylacetamide (25)**

Colorless oil. Yield: 95.0%. <sup>1</sup>H NMR (300 MHz, *CDCl*<sub>3</sub>) δ 7.84 (d, *J* = 7.8 Hz, 1H), 7.31 (t, *J* = 7.6 Hz, 1H), 7.26 (t, *J* = 7.1 Hz, 1H), 6.94 (td, *J* = 7.9 Hz, 1.8 Hz, 1H), 3.80 (s, 2H), 3.02 (s, 6H).

**2-{2-[(2-Chloro-6-fluorophenyl)amino]phenyl}-*N,N*-dimethylacetamide (26)**

Orange crystals. Yield: 90.5%. <sup>1</sup>H NMR (300 MHz, CDCl<sub>3</sub>) δ 7.22 (d, *J* = 7.9 Hz, 1H), 7.18-7.08 (m, 2H), 7.05-6.85 (m, 3H), 6.69 (dd, *J* = 7.8, *J*<sub>H-F</sub> = 2.9 Hz, 1H), 3.84 (s, 2H), 3.21 (s, 3H), 3.00 (s, 3H).

**2-{2-[(2,6-Difluorophenyl)amino]phenyl}-*N,N*-dimethylacetamide (27)**

Orange crystals. Yield: 81.3%. <sup>1</sup>H NMR (300 MHz, CDCl<sub>3</sub>) δ 7.13 (m, 2H), 6.95-6.84 (m, 4H), 6.74 (d, *J* = 7.8 Hz, 1H), 3.84 (s, 2H), 3.22 (s, 3H), 2.99 (s, 3H).

**2-{2-[(2,6-Dibromophenyl)amino]phenyl}-*N,N*-dimethylacetamide (28)**

Purple crystals. Yield: 97.6%. <sup>1</sup>H NMR (300 MHz, CDCl<sub>3</sub>) δ 7.56 (d, *J* = 8.0 Hz, 2H), 7.16 (d, *J* = 7.4 Hz, 1H), 7.08 (t, *J* = 7.7 Hz, 1H), 6.92 (t, *J* = 7.2 Hz, 1H), 6.84 (t, *J* = 8.0, 1H), 6.47 (d, *J* = 7.9 Hz, 1H), 3.85 (s, 2H), 3.20 (s, 3H), 3.00 (s, 3H).

**2-Bromo-*N*-(2-chloro-6-fluorophenyl)-*N*-(4-methylphenyl)acetamide (49)**

Yellow residue. Yield: 74.5%. <sup>1</sup>H NMR (300 MHz, CDCl<sub>3</sub>) δ 7.48 (d, *J* = 7.7 Hz, 1H), 7.36 – 7.04 (m, 6H), 3.91 – 3.80 (m, 2H), 2.35 (d, *J* = 14.4 Hz, 3H).

**2-Bromo-*N*-(2,6-difluorophenyl)-*N*-(4-methylphenyl)acetamide (50)**

Red oil. Yield: 99.5%. <sup>1</sup>H NMR (300 MHz, CDCl<sub>3</sub>) δ 7.41 (d, *J* = 7.8 Hz, 1H), 7.28 – 7.18 (m, 3H), 6.93 (t, *J* = 8.1 Hz, 1H), 3.85 (d, *J* = 6.9 Hz, 2H), 2.35 (d, *J* = 13.5 Hz, 3H).

**2-Bromo-*N*-(2,6-dichlorophenyl)-*N*-(4-methylphenyl)acetamide (51)**

Synthesis carried out as stated in general method. Purification carried out by recrystallization from ethanol. White crystals. Yield: 73.9%. <sup>1</sup>H NMR (300 MHz, CDCl<sub>3</sub>) δ 7.67 – 7.08 (m, 7H), 4.00 (s, 1H), 3.80 (s, 1H), 2.34 (d, *J* = 15.2 Hz, 3H).

**2-Bromo-*N*-(2,6-dibromophenyl)-*N*-(4-methylphenyl)acetamide (52)**

Synthesis carried out as stated in general method. Purification carried out by chromatography (eluting with EtOAc:hexane, 1:9 to 1:4). Pale orange crystals. Yield: 59.8%. <sup>1</sup>H NMR (300 MHz, CDCl<sub>3</sub>) δ 7.72 – 7.69 (m, 3H), 7.28 – 7.04 (m, 4H), 4.06 (s, 1H), 3.81 (s, 1H), 2.34 (d, *J* = 15.0 Hz, 3H).

**1-(2-Chloro-6-fluorophenyl)-5-methyl-1,3-dihydro-2*H*-indol-2-one (53)**

Pale yellow crystals. Yield: 37.3%. <sup>1</sup>H NMR (300 MHz, CDCl<sub>3</sub>) δ 7.42 (ddd, *J* = 8.4 Hz, 6.1 Hz, *J*<sub>H-F</sub> = 14.7 Hz, 1H), 7.18-7.00 (m, 4H), 6.46 (d, *J* = 7.9 Hz, 1H), 3.72 (s, 2H), 2.35 (s, 3H).

**1-(2,6-Difluorophenyl)-5-methyl-1,3-dihydro-2*H*-indol-2-one (54)**

Bright yellow crystals. Yield: 74.5%. <sup>1</sup>H NMR (300 MHz, CDCl<sub>3</sub>) δ 7.48-7.34 (m, 2H), 7.25-7.13 (m, 2H), 7.01 (d, *J* = 7.9 Hz, 1H), 6.37 (d, *J* = 8.0 Hz, 1H), 3.74 (s, 2H), 2.35 (s, 3H).

**1-(2,6-Dichlorophenyl)-5-methyl-1,3-dihydro-2*H*-indol-2-one (55)**

Yellow crystals. Yield: 53.9%. <sup>1</sup>H NMR (300 MHz, CDCl<sub>3</sub>) δ 7.50 (d, *J* = 8.0 Hz, 2H), 7.38 (d, *J* = 7.5 Hz, 1H), 7.17 (s, 1H), 7.01 (d, *J* = 7.6 Hz, 1H), 6.30 (d, *J* = 7.8 Hz, 1H), 3.74 (s, 2H), 2.35 (s, 3H).

**1-(2,6-Dibromophenyl)-5-methyl-1,3-dihydro-2*H*-indol-2-one (56)**

Synthesis carried out as stated in general method. Purification carried out by chromatography (eluting with DCM:hexane, 7:3 to 4:1). Light brown crystals. <sup>1</sup>H NMR (300 MHz, CDCl<sub>3</sub>) δ 7.71 (d, *J* = 8.1 Hz, 2H), 7.22 (t, *J* = 8.1 Hz, 1H), 7.17 (s, 1H), 7.01 (d, *J* = 7.9 Hz, 1H), 6.29 (d, *J* = 8.0 Hz, 1H), 3.73 (s, 2H), 2.35 (s, 3H).

**1-(2-Chloro-6-fluorophenyl)-5-ethyl-1*H*-indole-2,3-dione (57)**

Orange-red residue. Yield: 61.5%. <sup>1</sup>H NMR (300 MHz, CDCl<sub>3</sub>) δ 7.58 (s, 1H), 7.49-7.36 (m, 4H), 7.26-7.20 (m, 1H), 6.48 (d, *J* = 8.1 Hz, 1H), 2.66 (q, *J* = 7.6 Hz, 2H), 1.25 (t, *J* = 7.6 Hz, 3H).



**1-(2,6-Difluorophenyl)-5-ethyl-1*H*-indole-2,3-dione (58)**

Orange-red residue. Yield: 60.7%. <sup>1</sup>H NMR (300 MHz, CDCl<sub>3</sub>) δ 7.56 (s, 1H), 7.47 (tt, *J* = 8.5, *J*<sub>H-F</sub> = 6.1 Hz, 1H), 7.40 (dd, *J* = 8.1 Hz, *J*<sub>H-F</sub> = 1.8 Hz, 1H), 7.13 (dd, *J* = 7.7 Hz, *J*<sub>H-F</sub> = 8.0 Hz, 2H), 6.58 (d, *J* = 8.1 Hz, 1H), 2.66 (q, *J* = 7.6 Hz, 2H), 1.24 (t, *J* = 7.6 Hz, 3H).

**1-(2,6-Dichlorophenyl)-5-ethyl-1*H*-indole-2,3-dione (59)**

Orange-red residue. Yield: 65.3%. <sup>1</sup>H NMR (300 MHz, CDCl<sub>3</sub>) δ 7.61-7.50 (m, 3H), 7.45-7.36 (m, 2H), 6.41 (d, *J* = 8.1 Hz, 1H), 2.66 (q, *J* = 7.6 Hz, 2H), 1.25 (t, *J* = 7.6 Hz, 3H).

**1-(2,6-Dibromophenyl)-5-ethyl-1*H*-indole-2,3-dione (60)**

Orange-yellow residue. Yield: 63.0%. <sup>1</sup>H NMR (400 MHz, CDCl<sub>3</sub>) δ 7.72 (d, *J* = 8.1 Hz, 2H), 7.58 (s, 1H), 7.38 (d, *J* = 8.1 Hz, 1H), 7.26 (t, *J* = 8.1 Hz, 1H), 6.39 (d, *J* = 8.1 Hz, 1H), 2.66 (q, *J* = 7.6 Hz, 2H), 1.25 (t, *J* = 7.6 Hz, 3H).

**1-(2-Chloro-6-fluorophenyl)-5-propyl-1*H*-indole-2,3-dione (61)**

Orange-red residue. Yield: 67.1%. <sup>1</sup>H NMR (400 MHz, CDCl<sub>3</sub>) δ 7.54 (s, 1H), 7.48-7.40 (m, 2H), 7.36 (dd, *J* = 8.1, *J*<sub>H-F</sub> = 1.6 Hz, 1H), 7.23 (td, *J* = 8.6 Hz, *J*<sub>H-F</sub> = 1.6 Hz, 1H), 6.48 (d, *J* = 8.1 Hz, 1H), 2.59 (t, *J* = 7.6 Hz, 2H), 1.64 (sext, *J* = 7.6 Hz, 2H), 0.95 (t, *J* = 7.3 Hz, 3H).

**1-(2,6-Difluorophenyl)-5-propyl-1*H*-indole-2,3-dione (62)**

Orange-red residue. Yield: 70.6%. <sup>1</sup>H NMR (400 MHz, CDCl<sub>3</sub>) δ 7.54 (s, 1H), 7.48 (tt, *J* = 8.6, *J*<sub>H-F</sub> = 6.1 Hz, 1H), 7.38 (dd, *J* = 8.1, *J*<sub>H-F</sub> = 1.8 Hz, 1H), 7.13 (dd, *J* = 7.7 Hz, *J*<sub>H-F</sub> = 8.5 Hz, 2H), 6.57 (d, *J* = 8.1 Hz, 1H), 2.59 (t, *J* = 7.6 Hz, 2H), 1.64 (sext, *J* = 7.7 Hz, 2H), 0.95 (t, *J* = 7.3 Hz, 3H).

**1-(2,6-Dichlorophenyl)-5-propyl-1*H*-indole-2,3-dione (63)**

Orange-red residue. Yield: 62.5%. <sup>1</sup>H NMR (400 MHz, CDCl<sub>3</sub>) δ 7.54 (s, 1H), 7.51 (d, *J* = 7.7 Hz, 2H), 7.41 (t, *J* = 7.4 Hz, 1H), 7.35 (dd, *J* = 8.1, 1.3 Hz, 1H), 6.40 (d, *J* = 8.1 Hz, 1H), 2.58 (t, *J* = 7.6 Hz, 2H), 1.63 (sext, *J* = 7.5 Hz, 2H), 0.95 (t, *J* = 7.3 Hz, 3H).

**1-(2,6-Dibromophenyl)-5-propyl-1*H*-indole-2,3-dione (64)**

Orange-red residue. Yield: 53.5%. <sup>1</sup>H NMR (400 MHz, CDCl<sub>3</sub>) δ 7.72 (d, *J* = 8.1 Hz, 2H), 7.55 (s, 1H), 7.35 (dd, *J* = 8.1, 1.8 Hz, 1H), 7.26 (t, *J* = 8.1 Hz, 1H), 6.39 (d, *J* = 8.1 Hz, 1H), 2.59 (t, *J* = 7.6 Hz, 2H), 1.65 (sext, *J* = 7.6 Hz, 2H), 0.95 (t, *J* = 7.3 Hz, 3H).

**1-(2-Dihloro-6-fluorophenyl)-5-(propan-2-yl)-1*H*-indole-2,3-dione (65)**

Orange-red residue. Yield: 83.2%. <sup>1</sup>H NMR (400 MHz, CDCl<sub>3</sub>) δ 7.60 (s, 1H), 7.46-7.39 (m, 3H), 7.22 (td, *J* = 8.5, *J*<sub>H-F</sub> = 1.5 Hz, 1H), 6.48 (d, *J* = 8.2 Hz, 1H), 2.91 (sept, *J* = 6.9 Hz, 1H), 1.24 (d, *J* = 6.9 Hz, 6H).

**1-(2,6-Difluorophenyl)-5-(propan-2-yl)-1*H*-indole-2,3-dione (66)**

Orange-red residue. Yield: 93.0%. <sup>1</sup>H NMR (400 MHz, CDCl<sub>3</sub>) δ 7.60 (s, 1H), 7.51-7.45 (m, 1H), 7.43 (*J* = 8.2 Hz, *J*<sub>H-F</sub> = 1.9 Hz, 1H), 7.12 (dd, *J* = 7.5 Hz, *J*<sub>H-F</sub> = 8.8 Hz, 2H), 6.58 (d, *J* = 8.2 Hz, 1H), 2.91 (sept, *J* = 6.9 Hz, 1H), 1.24 (dd, *J* = 6.9, 1.6 Hz, 6H).

**1-(2,6-Dichlorophenyl)-5-(propan-2-yl)-1*H*-indole-2,3-dione (67)**

Orange-red residue. Yield: 87.7%. <sup>1</sup>H NMR (400 MHz, CDCl<sub>3</sub>) δ 7.62 (s, 1H), 7.53 (d, *J* = 7.8 Hz, 2H), 7.42 (t, *J* = 7.6 Hz, 1H), 7.40 (d, *J* = 8.8 Hz, 1H), 6.41 (d, *J* = 8.1 Hz, 1H), 2.92 (sept, *J* = 6.9 Hz, 1H), 1.26 (d, *J* = 6.9 Hz, 6H).

**1-(2,6-Dibromophenyl)-5-(propan-2-yl)-1*H*-indole-2,3-dione (68)**

Orange-red residue. Yield: 47.6%. <sup>1</sup>H NMR (400 MHz, CDCl<sub>3</sub>) δ 7.73 (d, *J* = 8.1 Hz, 2H), 7.62 (s, 1H), 7.40 (dd, *J* = 8.3, 1.7 Hz, 1H), 7.26 (t, *J* = 8.1 Hz, 1H), 6.40 (d, *J* = 8.1 Hz, 1H), 2.92 (sept, *J* = 6.9 Hz, 1H), 1.26 (d, *J* = 7.0 Hz, 6H).

**5-*tert*-Butyl-1-(2-chloro-6-fluorophenyl)-1*H*-indole-2,3-dione (69)**

Orange-red residue. Yield: 41.4%. <sup>1</sup>H NMR (400 MHz, CDCl<sub>3</sub>) δ 7.67 (s, 1H), 7.49 (dd, *J* = 8.3, *J*<sub>H-F</sub> = 2.1 Hz, 1H), 7.38-7.29 (m, 2H), 7.12 (td, *J* = 8.2 Hz, *J*<sub>H-F</sub> = 1.7 Hz, 1H), 6.40 (d, *J* = 8.3 Hz, 1H), 1.21 (s, 9H).

**5-tert-Butyl-1-(2,6-difluorophenyl)-1H-indole-2,3-dione (70)**

Orange-red residue. Yield: 54.0%. <sup>1</sup>H NMR (400 MHz, CDCl<sub>3</sub>) δ ppm 7.76 (s, 1H), 7.61 (dd, *J* = 8.4, *J*<sub>H-F</sub> = 2.1 Hz, 1H), 7.47 (tt, *J* = 8.5, *J*<sub>H-F</sub> = 6.1 Hz, 1H), 7.12 dd, *J* = 7.7 Hz, *J*<sub>H-F</sub> = 8.4 Hz, 2H), 6.60 (d, *J* = 8.4 Hz, 1H), 1.31 (s, 9H).

**5-tert-Butyl-1-(2,6-dichlorophenyl)-1H-indole-2,3-dione (71)**

Orange-red residue. Yield: 44.1%. <sup>1</sup>H NMR (400 MHz, CDCl<sub>3</sub>) δ ppm 7.62 (s, 1H), 7.43 (dd, *J* = 8.3, 2.1 Hz, 1H), 7.36 (d, *J* = 8.0 Hz, 2H), 7.26 (t, *J* = 8.1 Hz, 1H), 6.28 (d, *J* = 8.3 Hz, 1H), 1.17 (s, 9H).

**5-tert-Butyl-1-(2,6-dibromophenyl)-1H-indole-2,3-dione (72)**

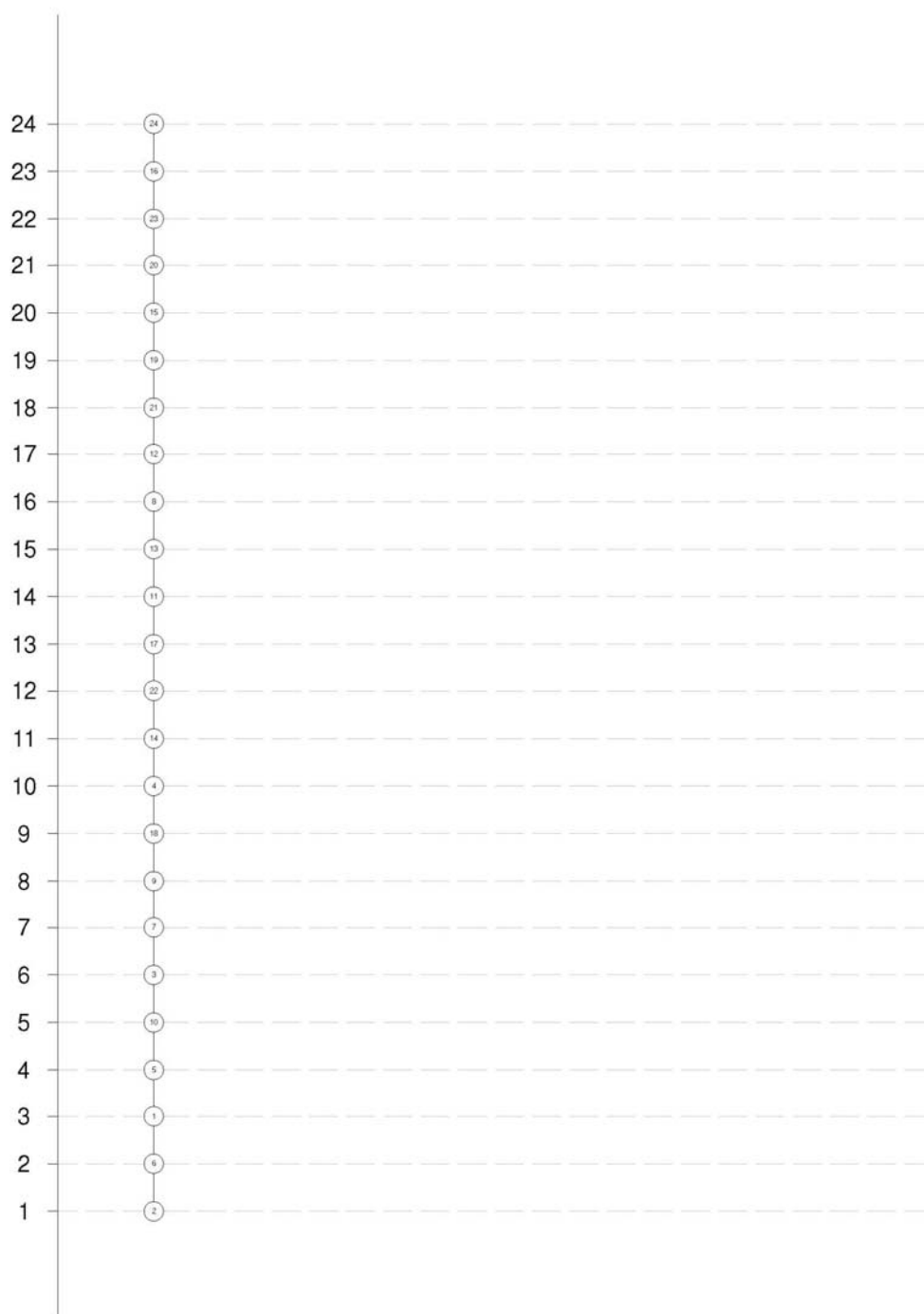
Orange-red residue. Yield: 29.4%. <sup>1</sup>H NMR (400 MHz, CDCl<sub>3</sub>) δ ppm 7.79 (s, 1H), 7.73 (d, *J* = 8.1 Hz, 2H), 7.58 (dd, *J* = 8.3, 2.1 Hz, 1H), 7.27 (t, *J* = 8.1 Hz, 1H), 6.41 (d, *J* = 8.3 Hz, 1H), 1.33 (s, 9H).

**Appendix 2-3:** Purities of compounds **1 – 24** as determined by HPLC at 280 nm (two gradients)

$$\text{Area \%} = [\text{Area of Major Peak} / \text{Area of All Peaks observed during run}] \times 100$$

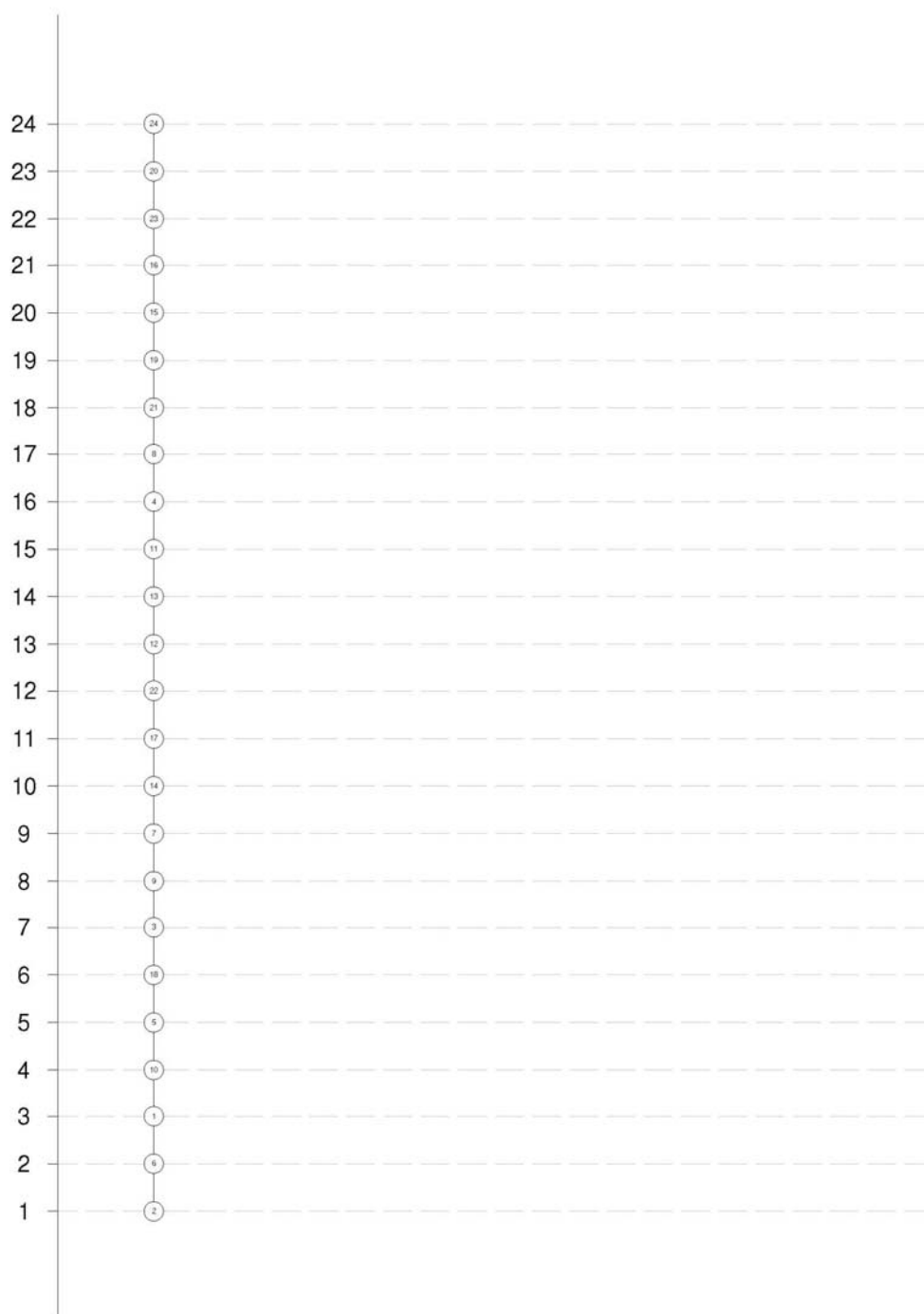
Compound No.	Gradient A		Gradient B	
	Retention Time (min)	Area (%)	Retention Time (min)	Area (%)
1	7.527	100.0	9.616	98.5
2	7.188	100.0	9.213	100.0
3	7.895	100.0	10.030	100.0
4	8.101	100.0	10.167	100.0
5	8.013	97.1	8.298	97.1
6	7.683	98.4	8.000	98.2
7	8.410	98.5	8.631	97.4
8	8.616	100.0	8.793	100.0
9	6.901	100.0	8.655	100.0
10	6.608	100.0	8.380	100.0
11	7.270	100.0	8.941	100.0
12	7.453	100.0	9.070	98.2
13	7.382	100.0	8.969	98.3
14	7.083	100.0	8.732	100.0
15	7.757	100.0	9.223	98.8
16	7.943	99.2	9.340	98.3
17	7.234	100.0	8.867	100.0
18	6.931	100.0	8.628	100.0
19	7.568	100.0	9.117	100.0
20	7.746	100.0	9.236	100.0
21	7.468	100.0	9.043	100.0
22	7.187	100.0	8.822	100.0
23	7.858	100.0	9.274	100.0
24	8.029	97.5	9.383	97.0

**Appendix 3-1a:** Partial ranking (Hasse diagram) of the twenty-four compounds in TAMH cells



The numbers in the circles are the compound numbers. The numbers in the left margin are the levels that the compounds are assigned to according to partial order ranking based on the TAMH cell line.

**Appendix 3-1b:** Partial ranking (Hasse diagram) of the twenty-four compounds in HuH-7 cells



The numbers in the circles are the compound numbers. The numbers in the left margin are the levels that the compounds are assigned to according to partial order ranking based on the HuH-7 cell line.

**Appendix 3-2a:** QSTR regression statistics for TAMH cells

QSAR regression model obtained for the TAMH cell line was:

$$-\log(\text{TAMH IC}_{50}) = 0.801 \times \log P(o/w) - 0.568$$

**Regression Statistics for TAMH**

<i>Regression Statistics</i>	
R	0.990658145
R Square	0.98140356
Adjusted R Square	0.980558267
Standard Error	0.083060887
Observations	24

**ANOVA for TAMH**

	<i>df</i>	<i>SS</i>	<i>MS</i>	<i>F</i>	<i>Significance F</i>
Regression	1	8.01002055	8.01002055	1161.02214	1.56048E-20
Residual	22	0.15178044	0.00689911		
Total	23	8.16180099			

Statistical significance of coefficients and intercepts of QSTR equation for TAMH

	<i>Coefficients</i>	<i>Standard Error</i>	<i>t Stat</i>	<i>P-value</i>
Intercept	0.567965311	0.11820142	4.805063365	8.45554E-05
logP(o/w)	0.800720504	0.023499612	34.07377491	1.56048E-20

### Appendix 3-2b: QSTR regression statistics for HuH-7

QSAR regression model obtained for the HUH-7 cell line was:

$$-\log(\text{HUH-7 IC}_{50}) = 14.485 \times \text{FASA\_H} - 8.913$$

#### Regression Statistics for HuH-7

<i>Regression Statistics</i>	
R	0.910480327
R Square	0.828974427
Adjusted R Square	0.821200537
Standard Error	0.103188421
Observations	24

#### ANOVA for HuH-7

	<i>df</i>	<i>SS</i>	<i>MS</i>	<i>F</i>	<i>Significance F</i>
Regression	1	1.13544131	1.13544131	106.635733	6.70708E-10
Residual	22	0.234252704	0.01064785		
Total	23	1.369694015			

Statistical significance of coefficients and intercepts of QSTR equation for HuH-7

	<i>Coefficients</i>	<i>Standard Error</i>	<i>t Stat</i>	<i>P-value</i>
Intercept	-8.912674809	1.204923456	-7.396880494	2.11449E-07
FASA_H	14.48485412	1.402693377	10.32645791	6.70708E-10



#### Appendix 4-1: Recipes for Western-Blot buffers and gels

##### Cell lysis buffer

Reagents	Volume (mL)	Final Concentration
1M Hydroxyethyl piperazineethanesulfonic acid (HEPES), pH 7.5	10	50 mM
5M Sodium Chloride	6	150 mM
0.5M Ethylenediaminetetraacetic acid (EDTA)	0.4	1 mM
100% Glycerol	20	10%
100% Triton-X	2	1%
0.2M Sodium pyrophosphate	10	10 mM
Deionized water	151.6	-

##### Complete lysis buffer

Reagents	Volume (mL)
Cell lysis buffer	950
0.5 M Sodium fluoride	20
100 mM Sodium orthovanadate	20
100 mM Phenylmethylsulfonyl fluoride (PMSF)	10
200 µg/mL Aprotinin	0.5

##### 6X Laemmli SDS protein sample buffer

Reagents	Amount
4X Tris-Cl/SDS (pH 6.8)	7 mL
Glycerol	3.8 g
SDS	1 g
Bromophenol blue	1.2 mg

##### 5X PBS-T

Reagents	Amount
Sodium chloride	40 g
Potassium chloride	1 g
Na <sub>2</sub> HPO <sub>4</sub> • 7H <sub>2</sub> O	13.6 g
KH <sub>2</sub> PO <sub>4</sub>	1.2 g
Tween-20	2.5 mL
Deionized water	Make up to 1 L

##### 10X Wet transfer buffer, pH 8.3

Reagents	Amount
Tris-base	60.6 g
Glycine	288 g
Deionized water	Make up to 2 L

#### 5X Running buffer

<b>Reagents</b>	<b>Amount</b>
Tris-base	15.1 g
Glycine	72 g
10% SDS	50 mL
Deionized water	Make up to 1 L

#### 5% SDS-PAGE stacking gel

<b>Reagents</b>	<b>Amount (mL)</b>
30% Acrylamide	0.335
4X Tris-Cl/SDS, pH 6.8	0.625
Deionized water	1.525
10% (w/v) APS	0.02
TEMED	0.004

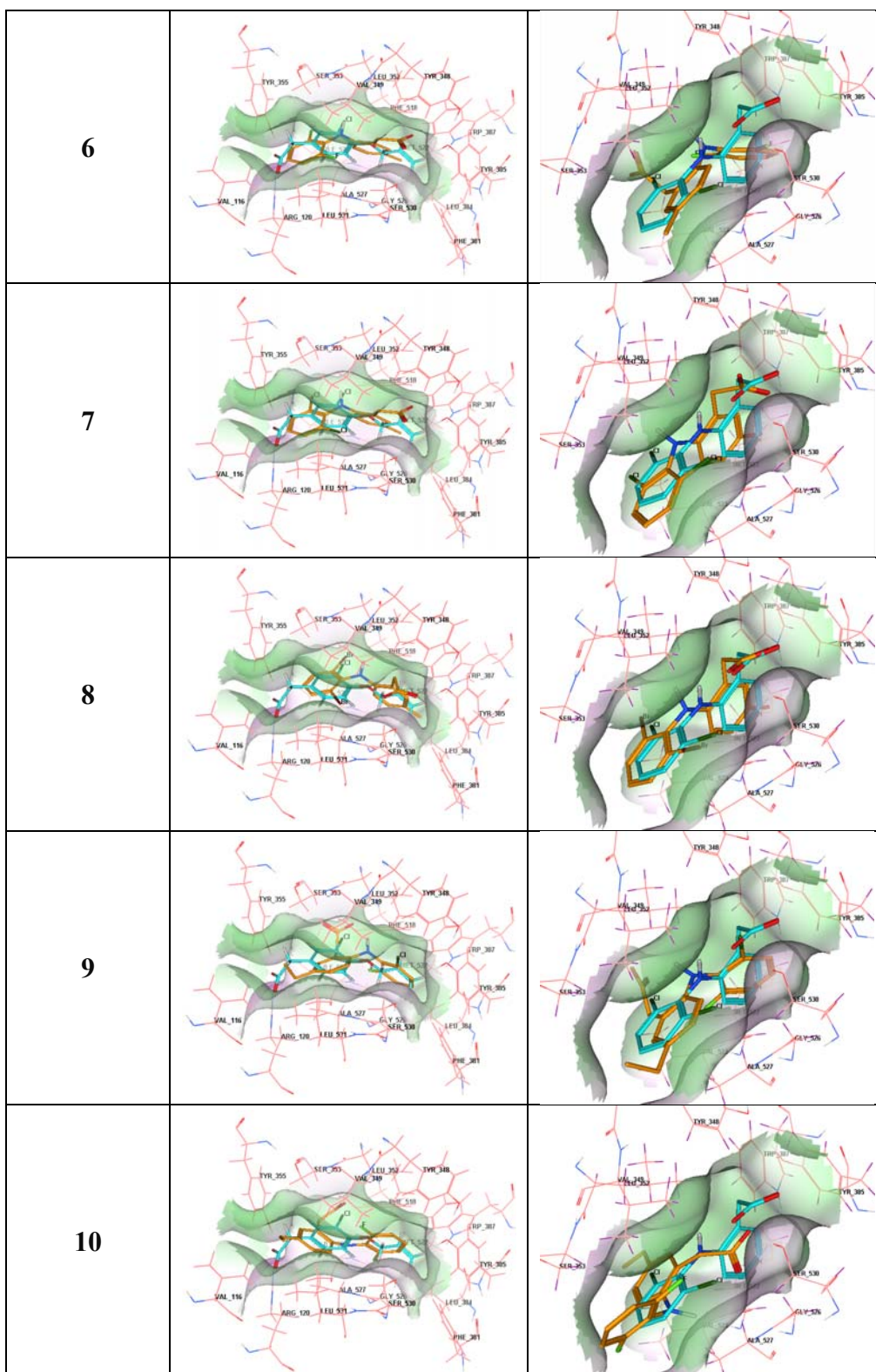
#### 10% SDS-PAGE resolving gel

<b>Reagents</b>	<b>Amount (mL)</b>
30% Acrylamide	3.30
4X Tris-Cl/SDS, pH 6.8	2.50
Deionized water	4.20
10% (w/v) APS	0.05
TEMED	0.007

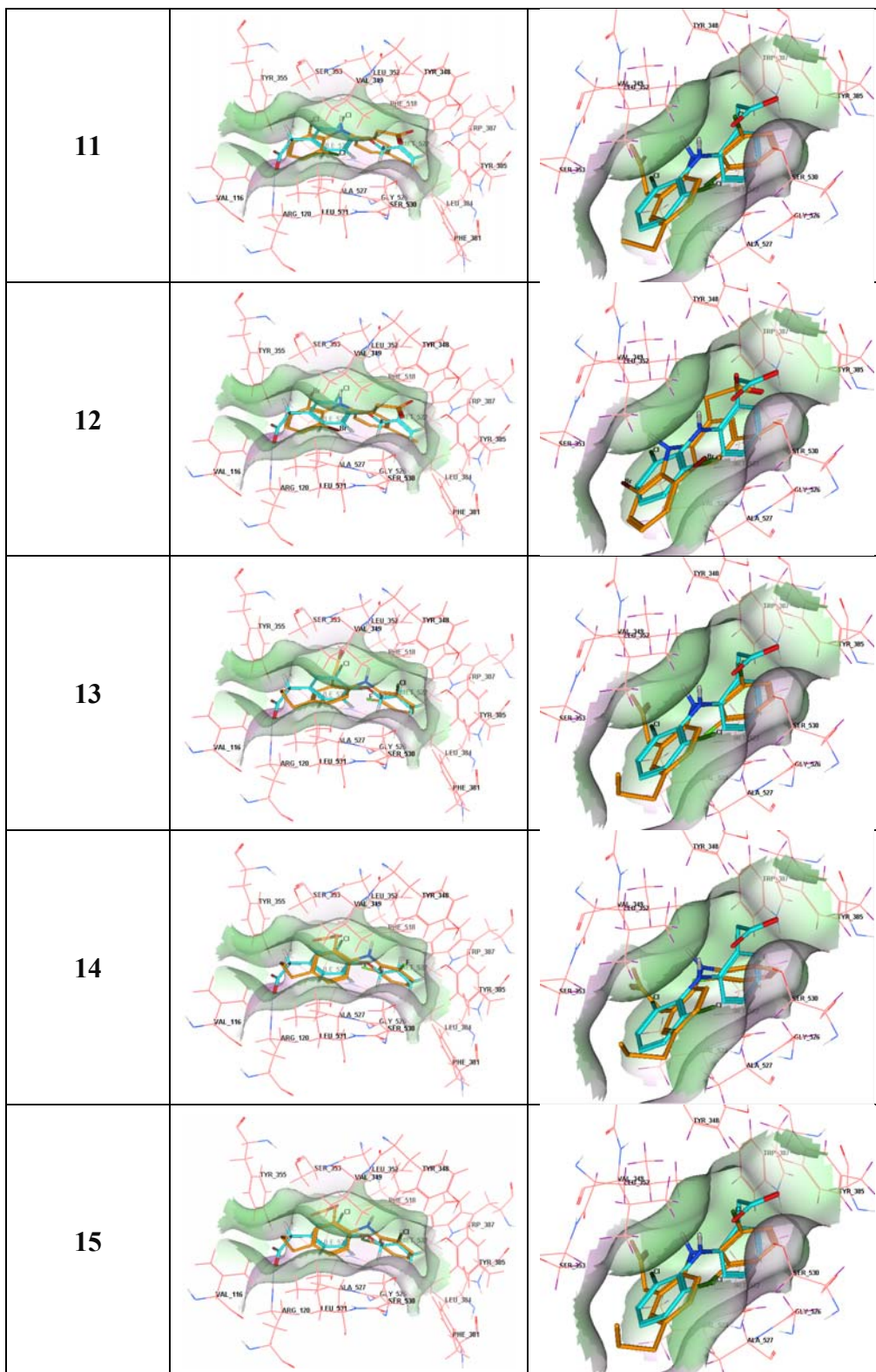
**Appendix 4-2: Docking poses of all twenty-four compounds in COX-1 and COX-2**

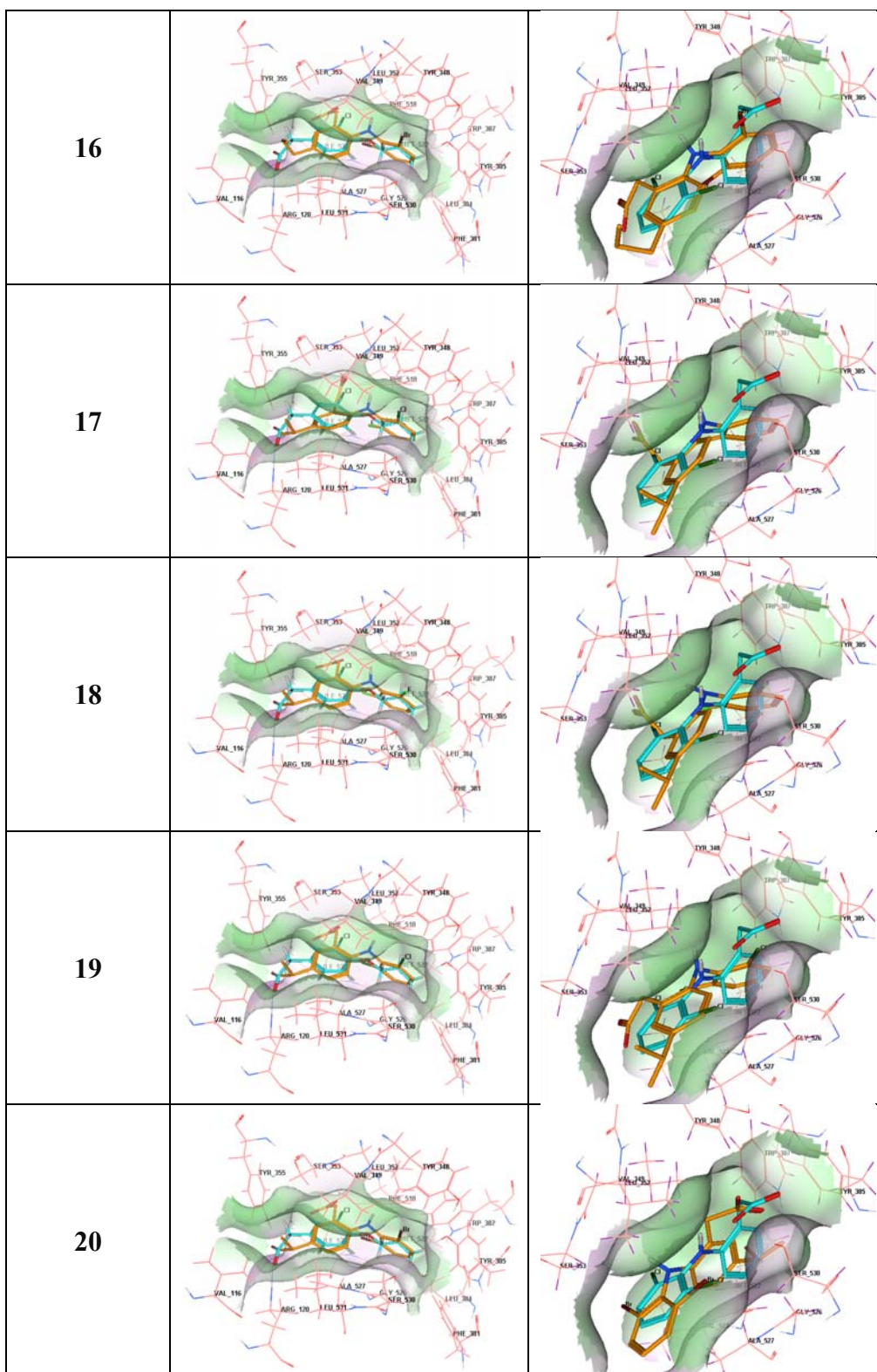
Orange = docked molecule; blue = existing ligand.

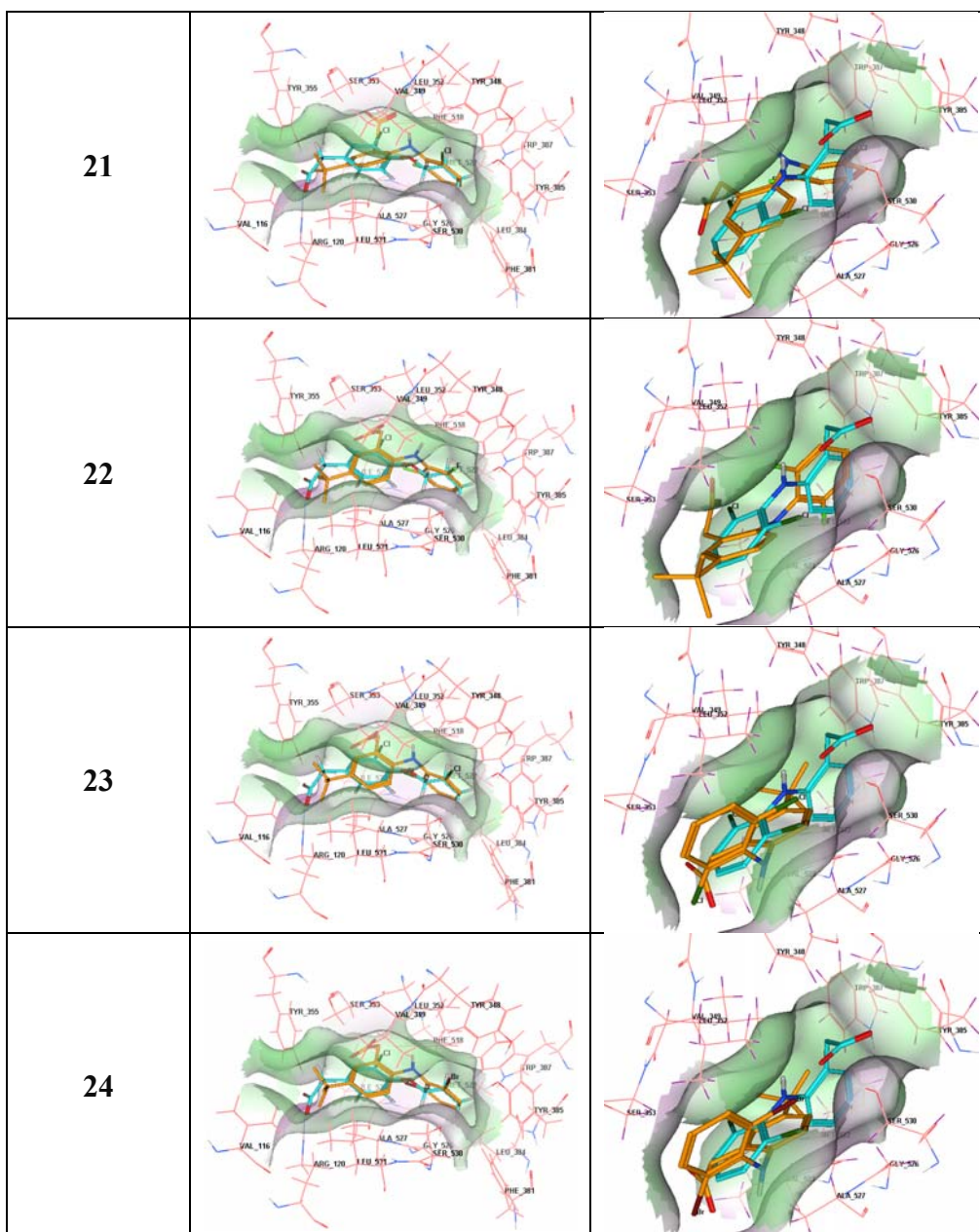
Compound	COX-1	COX-2
1		
2		
3		
4		
5		











**Appendix 4-3:** Log D(o/w) value calculated using online ACD/I-Lab prediction engine

<b>Compound</b>	<b>Log D(o/w)</b>
1	0.98
2	0.46
3	1.57
4	1.73
5	1.35
6	0.83
7	1.92
8	2.20
9	1.64
10	1.11
11	2.2
12	2.44
13	1.90
14	1.37
15	2.46
16	2.70
17	1.89
18	1.40
19	2.46
20	2.72
21	2.28
22	1.73
23	2.75
24	3.03



**Appendix 5-1:** Precursor and product ions utilized for MRM analysis in determination of Phase I and Phase II metabolic stability.

**Compounds 1 to 12**

Compound	Precursor ion, m/z (Q1)	Product ion, m/z (Q3)	Retention time (min)
<b>1</b>	278.2	234.1 197.9	2.89
<b>2</b>	262.1	218.0 197.9	2.77
<b>3</b>	294.1	250.0 213.8	3.04
<b>4</b>	383.8	339.9 257.8	3.12
<b>5</b>	291.8	247.8 211.8	3.08
<b>6</b>	276.2	231.8 211.9	2.95
<b>7</b>	307.9	263.9 228.0	3.24
<b>8</b>	397.8	353.9 274.1	3.31
<b>9</b>	306.0	261.9 210.7	3.25
<b>10</b>	290.0	246.0 225.9	3.12
<b>11</b>	321.8	278.1 242.1	3.40
<b>12</b>	411.9	367.8 288.0	3.47

Compounds **13** to **24**

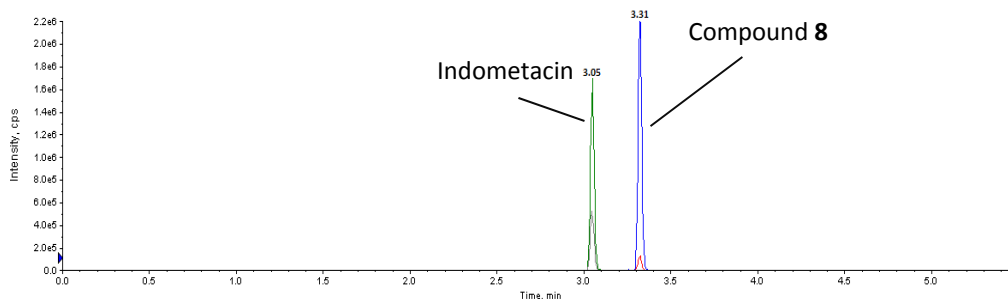
Compound	Precursor ion, m/z (Q1)	Product ion, m/z (Q3)	Retention time (min)
<b>13</b>	320.1	275.9 210.9	3.43
<b>14</b>	303.9	259.8 240.2	3.30
<b>15</b>	335.9	291.9 227.1	3.58
<b>16</b>	425.6	381.9 301.9	3.65
<b>17</b>	320.1	275.9 223.9	3.38
<b>18</b>	303.8	260.3 240.1	3.26
<b>19</b>	335.9	291.9 256.2	3.53
<b>20</b>	425.6	381.9 301.9	3.60
<b>21</b>	334.0	290.0 237.8	3.48
<b>22</b>	318.0	274.0 254.1	3.36
<b>23</b>	350.0	306.1 270.0	3.62
<b>24</b>	439.9	395.8 316.0	3.69

**Appendix 5-2:** List of masses used for SIM analysis. Selection was based on nominal mass and tailored for negative ESI mode.

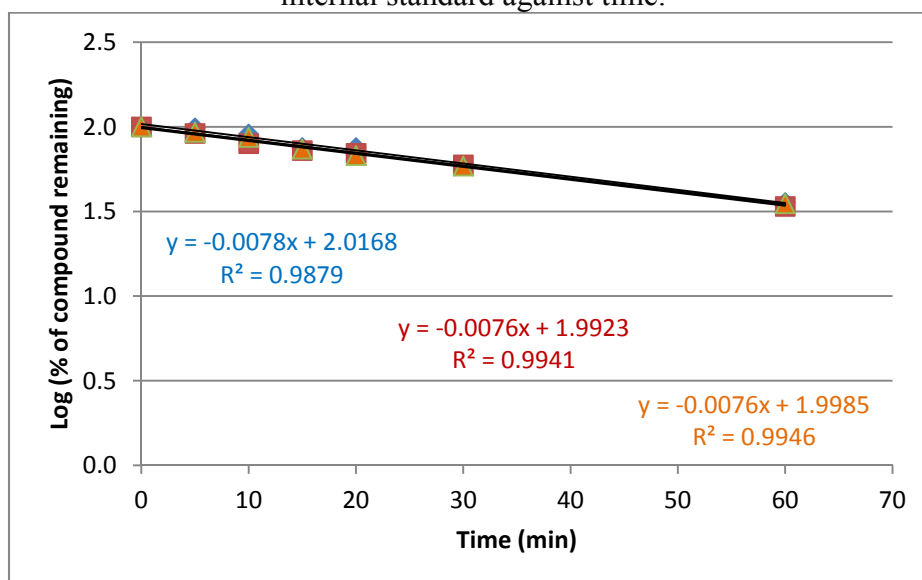
Compound	Mass of AG (Da)	Compound	Mass of AG-Phe-Lys (Da)
1	454	1	729
2	438	2	713
3	470	3	745
4	558	4	833
5	468	5	743
6	452	6	727
7	484	7	759
8	572	8	847
9	482	9	757
10	466	10	741
11	498	11	773
12	586	12	861
13	496	13	771
14	480	14	755
15	512	15	787
16	600	16	875
17	496	17	771
18	480	18	755
19	512	19	787
20	600	20	875
21	510	21	785
22	494	22	769
23	526	23	801
24	614	24	889

**Appendix 5-3:** Representative mass spectrum and linear regression model for determination of Phase I and Phase II metabolic stability.

MRM spectrum of compound **8** and indomethacin (internal standard)



Linear regression model of relative ratio of peak area of compound **8** to internal standard against time.

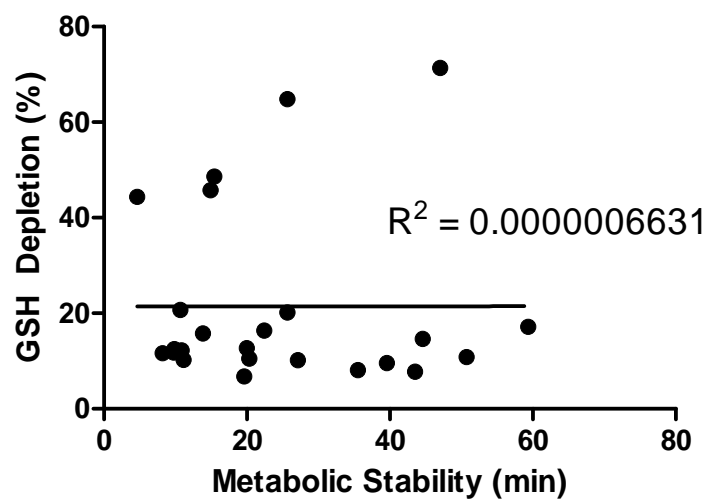


Calculation of  $t_{1/2}$  from linear regression model equations

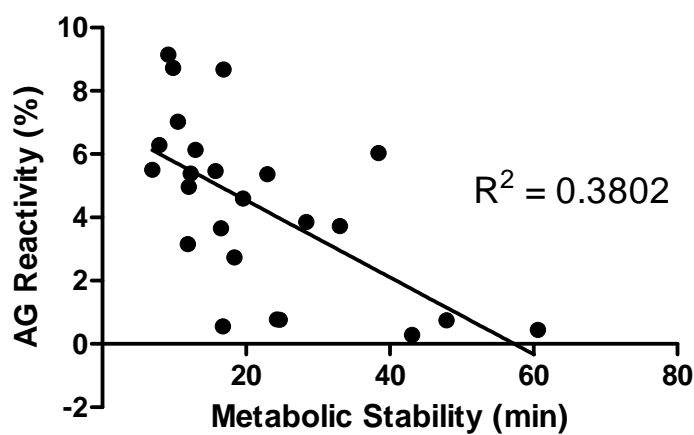
Log 50%	1.7		
$t_{1/2}$ (as calculated from regression equation)	1	2	3
Average $t_{1/2}$ (min)	40.7	38.6	39.4
Standard deviation	1.1		
% CV	2.7		

**Appendix 5-4:** Linear regression models for metabolite reactivity and metabolic stability relationships for Phase I and Phase II metabolism.

### GSH Depletion vs Phase I Metabolic Stability

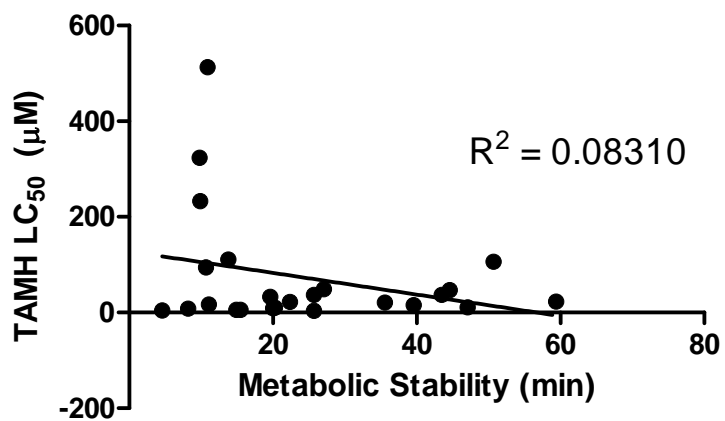


### AG Reactivity vs Phase II Metabolic Stability

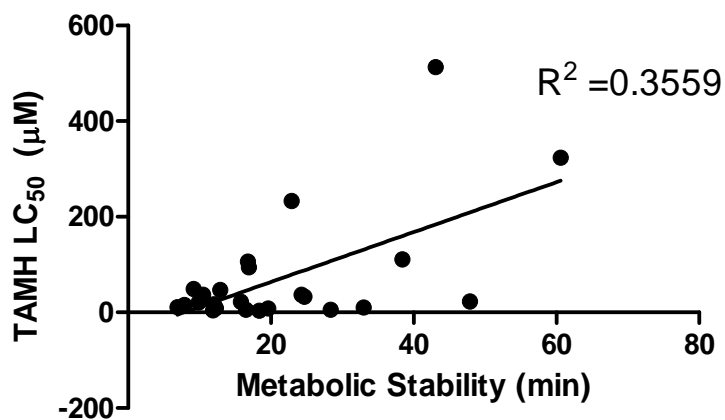


**Appendix 5-5:** Linear regression models for toxicity and metabolic stability relationships for Phase I and Phase II metabolism

**TAMH LC<sub>50</sub> vs Phase I Metabolic Stability**

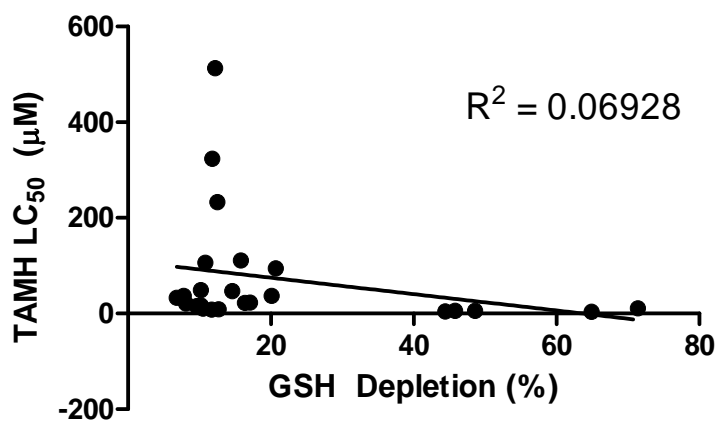


**TAMH LC<sub>50</sub> vs Phase II Metabolic Stability**

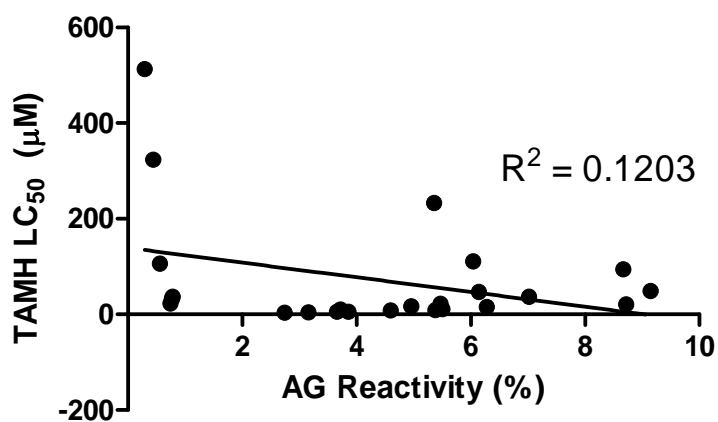


**Appendix 5-6:** Linear regression models for toxicity and metabolite reactivity relationships for Phase I and Phase II metabolism

**TAMH LC<sub>50</sub> vs GSH Depletion**



**TAMH LC<sub>50</sub> vs AG reactivity**



## Appendix 6-1: Phase II reactive metabolite trapping - XIC traces of selected compounds

